Newton-Krylov Dual-Primal Methods

for Implicit Time Discretizations

in Cardiac Electrophysiology

Advisors:
Prof. Simone SCACCHI
Prof. Luca F. PAVARINO

PhD Dissertation of:
Ngoc Mai Monica HUYNH
matr. 469013

Newton-Krylov Dual-Primal Methods
for Implicit Time Discretizations
in Cardiac Electrophysiology

Ngoc Mai Monica Huynh
Dipartimento di Matematica, Università degli Studi di Pavia
via Ferrata 5, 27100 Pavia (Italy)

September 24$^{\text{th}}$, 2021

Abstract

The description of the functioning mechanisms of the heart has always attracted many researchers. Thanks to modern computing resources, many interdisciplinary studies in this field involving clinicians, biologists, physicists, engineers and mathematicians have emerged. This cross-curricular interest has given birth to many mathematical models of cardiac physiological events, as well as tools to computationally study and predict dysfunctions such as heart failure and arrhythmias. As a result, most interactions between different physical models as well as possible outcomes of medical therapies can be studied without invasive procedures or human testing.

However, mathematical modelling involves several challenges, ranging from the coupling of the different physics to the design of efficient implementations. Simulation of these models requires huge computational effort, both in terms of memory and of speed, and this motivates the employment of large scale system architectures for numerical calculations.

One of the most effective ways to solve large algebraic systems arising from the discretization of Partial Differential Equations (PDEs), which usually model these biological phenomena, is provided by Domain Decomposition (DD) methods (DDMs).

The main idea underlying these methods is the subdivision of the problem into smaller local subproblems, either at the continuous, discrete or algebraic levels. Each of these subproblems is solved independently from the others, but their algorithms ensure global continuity of the solution. These algorithms provide powerful tools for avoiding dealing with ill-conditioned problems as well as for ensuring fast convergence. When solving a linear system of the type $Ax = b$ of large dimensions, the inverse A^{-1} is never computed, since it requires a huge computational effort. Moreover, if A is sparse, this property may not hold for its inverse A^{-1}. Direct factorizations may not be viable either, due to the large dimension of A.

DDMs are suitable for parallelization, which is an appealing feature given the increasing growth of supercomputers.

In the following work, we will refer to DDMs as iterative algorithms for the solution of large algebraic systems. In particular, we consider the class of non-overlapping DDMs (often referred to as iterative substructuring methods), focusing on Balancing Domain Decomposition with Constraints (BDDC) and Dual-Primal Finite Element Tearing and Interconnecting (FETI-DP) methods. In these methods, variables are divided into three groups: internal, which belong to the internal part of the subdomains; dual and primal, which, taken together, form the interface set of variables. In general, the primal set of variables coincides with the vertices of the subdomains in two dimensions, while in 3D this coarse space can be chosen suitably with the problem.

In this Thesis we study efficient, scalable and robust DD solvers for the solution of the Bidomain model, which describes the propagation of the electric signal in the cardiac tissue by means of parabolic reaction-diffusion PDEs.

We derive the algebraic formulation of the Bidomain model by discretizing with Q_1 finite elements in space and the Backward Euler method in time. In particular, by applying a fully implicit time discretization, the resulting algebraic system is nonlinear and we propose two strategies for

its solution.

The first strategy we investigate relies on a decoupling (or segregated) approach, where at each time step we split the solution of the ionic model and the Bidomain system. We wrap the nonlinear system within a Newton method and we linearize the algebraic system, resulting in a symmetric problem. We construct and theoretically analyze BDDC and FETI-DP algorithms for the Jacobian linear system in order to accelerate the convergence of the Preconditioned Conjugate Gradient method. We prove a novel theoretical bound for the projection operator, using both ρ and deluxe scaling. This bound is then employed in the proofs of the upper bound for the condition number of the preconditioned operator showing a theoretical quasi-optimality property.

In the second strategy, we explore a coupled (or monolithic) solution, where the ionic model is solved at the same time as the Bidomain system. In this case, the arising Jacobian system is non-symmetric and we employ the Generalized Minimal Residual (GMRES) method for its solution. We provide a tailored theoretical analysis for the convergence of the solver. This analysis exploits a classical result for the upper bound of the residual of GMRES iterations, together with a proof technique recently proposed for BDDC applied to advection-diffusion problems.

We numerically validate both these quasi-optimality properties through extensive parallel tests. We also test the robustness of proposed solvers in case of realistic human ionic models, such as Luo-Rudy (1991) and Ten Tusscher-Panfilov (2006), as well as in presence of an ischemic transmural region, modeled by jumps in the diffusion coefficients. The results indicate scalability and robustness of the solvers, as well as their quasi-optimality.

Future works should be devoted to the optimization of the codes in order to reduce the computational workload and to the employ of quasi-Newton methods for the improvement of the numerical performance.

Other appealing future works are the design, theoretical analysis and numerical implementation of nonlinear dual-primal DD solvers for this system, as a numerical comparison of the performances between the two nonlinear approaches, for both solution strategies.

Advisors:

Prof. Simone Scacchi

Prof. Luca F. Pavarino

Acknowledgments

When I concluded my Master thesis, I thought it would have been the first and last Acknowledgments I would ever write in my life. How naive I was.
So here we are again (hopefully for the last time).

First and foremost, I would like to express my sincere gratitude to my advisors and mentors prof. Simone Scacchi and prof. Luca Pavarino for welcoming me in their research group, being very patient and always encouraging. I really appreciated your guidance through these years with many fatherly advises (both mathematical and non-mathematical) and all the opportunities you offered me. Thank you for always pushing me to believe in myself.

I would like to thank again Dr. Lorenzo Mascotto for all the smiles and laughs, even from another country: his non-conforming way of thinking (and speaking) enlightened various moments of this journey.

In these three years many people have crossed my path, each of whom left a sign of their passage in my heart. Agnese, for many sleepovers and for sharing a bit of your lightheartedness; Anderson, loyal and honest friend. Claudio, collegue and friend, who shared up-and-down moments and danger drivings home; thank you for lightening many existential crises with your non-stop talking. Federico, Eleonora, Irene and Silvia, for many chit-chats and feedbacks; Meda and Signo, for being witty and funny friends; my little academic sister, Silvia, for being always so kind and caring.
A special mention goes to Elena, Chiara and Nicola, who shared the same path and burdens.
I would like to thank also all the PhD fellows of *Gabbia DiMat* for their friendship and support.
I am honored to have met you all.

I am really lucky for still counting on Bea, Co, Fra, Luca, Minuti, Palu, Porotti, Riccelen: thank you for all the breakfasts, brunches, lunches, tea breaks, dinners, sleepovers, board games, nights out, kittens and the gossiping. We may not meet so often anymore, but we have found a way to keep the *Tavoli del primo piano* and the *Minuters* alive.
A piece of my heart goes to my lifetime friend Giulia, who is always there ready to listen (even when the topic is off her interests) and to face happy and difficult moments together. Thank you for all the distractions and for being a daydreamer with me.

I honestly do not know how to express my thankfulness to my husband, my parents and my brother. You have supported all my personal and career choices, expressing your doubts whenever there were any but always rooting for me. So, *cảm ơn* Ba và Mẹ, *cảm ơn* Tam and *cảm ơn* Mattia. I dedicate this achievement to you.

Lastly, *cảm ơn* Bà Nội và Bà Ngoại: I know you are always by my side.

If you can keep your head when all about you
Are losing theirs and blaming it on you,
If you can trust yourself when all men doubt you,
But make allowance for their doubting too;
If you can wait and not be tired of waiting,
Or being lied about, don't deal in lies,
Or being hated, don't give way to hating,
And yet don't look too good, nor talk to wise.

If you can dream – and not make dreams your master;
If you can think – and not make thoughts your aim;
If you can meet with Triumph and Disaster
And treat those two impostors just the same;
If you can bear to hear the truth you've spoken
Twisted by knaves to make a trap for fools,
Or watch the things you gave your life to, broken
And stoop and build'em up with worn-out tools;

If you can make one heap of all your winnings
And risk it on one turn of pitch-and-toss,
And lose, and start again at your beginnings
And never breathe a word about your loss;
If you can force your heart and nerve and sinew
To serve your turn long after they are gone,
And so hold on when there is nothing in you
Except the Will which says to them: 'Hold on!'

If you can talk with crowds and keep your virtue,
Or walk with Kings – nor lose the common touch,
If neither foes nor loving friends can hurt you,
If all men count with you, but none too much;
If you can fill the unforgiving minute
With sixty seconds' worth of distance run,
Yours is the Earth and everything that's in it,
And – which is more – you'll be a Man, my son!

$\sim$ R. Kipling, *If.*

Contents

List of Figures

List of Tables

Chapter 1

Introduction

Can we simulate and predict complex biophysical phenomena, such as functions and dysfunctions of the cardiac electrical activity, without invasive procedures?

Although this target seems to be ambitious, since it requires synergy between apparently distant fields, it has been tackled with huge effort by the scientific community in the last decade. While recent improvements in medical therapies have extended patients' life expectancy, the growth of collaborations between clinicians, biologists, engineers, physicists and mathematicians has resulted in the development of many multi-disciplinary studies. The description of the functioning mechanisms of the heart has always fascinated many researchers and this cross-curricular trend has given opportunity to translate physiological events into mathematical models, as well as tools to computationally study and predict dysfunctions. For examples, References [18, 32, 91, 117], based on experiments and clinical data, provide mathematical models and workflows for the study of cardiac phenomena, also in patient-specific cases.

The advantage of this computational approach is the possibility of performing realistic investigations in a non-invasive way: dysfunctions of the heart which would require clinical inspection for an in-depth analysis can be carried out through numerical simulations instead, exploring all the interactions between cardiac bio-electrical and mechanical phenomena, as in Refs. [21, 24, 30, 31, 86, 100].

However, the mathematical modelling of these biophysical events involves several challenges. Indeed, the estimate of the parameters of the models (see for example References [34, 54, 55]) or the coupling of different physics (Refs. [92, 103, 118]) are research topics in the scientific community. An other important issue to deal with is the need of efficient implementations: as a matter of fact, the simulation of these models require huge computational efforts, both in terms of memory and speed. This motivates the employment of large scale system architectures for the numerical calculations: for example, in the field of cardiac mechanics, References [11, 26, 67, 71] explore the performances of huge supercomputers in solving and simulating cardiac electro-mechanical systems.

In this Thesis, we focus on the development and analysis of efficient preconditioned solvers for fully implicit time discretizations of the Bidomain model.

This system of Partial Differential Equations (PDEs) describes the propagation of electric impulses in the cardiac tissue, by means of two degenerate parabolic reaction-diffusion equations (see Refs. [27, 98, 102]). This model provides an accurate and rich description of the evolution of the transmembrane potential $v = u_i - u_e$, where u_i and u_e are the intra- and extracellular electric potentials respectively: due to its accuracy, it is usually employed in numerical studies concerning pathological conditions (Refs. [19, 30]), but its (potentially) high computational cost impedes the easy coupling with other models, such as the mechanical or the vascular ones. For this reason, by assuming equal anisotropy between the intra- and extracellular diffusion coefficients, the reduced Monodomain model is widely employed in various numerical studies (eg. [21, 53, 99, 125]).

In order to take into account the electrochemical reactions that occur at a cellular level, the Bidomain system is coupled through the reaction term to a system of Ordinary Differential Equa-

tions (ODEs), modelling the inward and outward flow of ionic currents across the cell membrane. Indeed, the electric impulse is originated in the sino-atrial node and then is transmitted to the ventricle myocardium, causing a quick depolarization of the tissue: this means that the trans-membrane potential changes sign in few milliseconds. This potential drop drives a change in the concentration of different ionic species inside and outside each cell, which in turn condition the slow repolarization of the cell. In this work, we will consider mainly the Rogers-McCulloch ionic model [105], a phenomenological model where the gating and the concentration variables are represented by only one unknown: this model reproduces macroscopically the main action potential features, but it neglects several sub-cellular processes. However, reduced models like this one are usually employed in large time and space simulations, as well as in numerical studies that do not need to accurately represent the ionic processes. Other two models that will be considered here are the Luo-Rudy phase 1 [80, 81] and the Ten Tusscher-Panfilov [114, 115] ionic models, which have been developed more recently and describe mammalian and human ventricular ionic currents respectively.

As already mentioned, the simulations and numerical studies of the cardiac activities require enormous computational resources: in order to develop efficient and optimal codes, it is necessary to define successful solution strategies, from the discretization choices to the solvers to be employed.

Lot of attention has to be paid to the time discretization, especially when coupling different models (electrical and mechanical models), as the time scales involved are very different. Concerning the Bidomain model, the numerical time step needs to be small enough to capture the tiny but fast-propagating wavefront, without incurring in stability issues of the numerical scheme or slowing down the computational speed. In the literature, many works take in consideration semi-implicit time discretizations, such as in References [20, 26, 28, 96, 108, 127, 128], where the diffusion term is treated implicitly while the reaction term explicitly. Other works have been focused on the splitting of the differential operator, like Refs. [22, 23, 111, 112], applying different numerical schemes for the diffusion and the reaction terms. However, operator splittings and decoupling techniques introduce additional errors which increase the time finite difference errors. Possible alternatives consider fully implicit time discretizations (which can be computationally more expensive) as in Ref. [90] or decoupling strategies based on segregated implicit time discretizations as in References [36, 88, 89, 109].

This Thesis deals with fully implicit time discretizations, where the solution strategy is presented in two variants: since the discretized Bidomain system is nonlinear, due to the implicit treatment of the reaction term, a classic Newton scheme wraps the nonlinear algebraic system which can include or not the ionic system. In case the ODEs are not included in the non-linear system (segregated or *decoupled* approach), the Jacobian linear system to be solved at each Newton step is symmetric, thus allowing an easy application of the Preconditioned Conjugate Gradient for its solution. Conversely, if the ODEs are not included (monolithic or *coupled* strategy), the resulting linearized problem is non-symmetric, requiring to adopt the Generalized Minimal Residual (GMRES) method or the stabilized BiConjugate Gradient (BiCGS) method.

In general, when working with linear systems with potentially millions of degrees of freedom (dofs), it is necessary to define a preconditioning procedure, in order to avoid dealing with ill-conditioned problems as well as to ensure fast convergence. Indeed, when solving a linear system of the type $Ax = b$ of large dimensions, the inverse A^{-1} is never computed, since it requires a huge computational effort; moreover, if A is sparse, this property could not hold for its inverse A^{-1}. Also direct factorizations may not be viable: if the matrix is dense of order n, then Gaussian elimination will need $O(n^3)$ operations. On the other hand, iterative methods can suffer from slow convergence. In this framework, Domain Decomposition (DD) methods (DDMs) provide powerful tools to solve these issues.

Modern DDMs originate in the 80s and generally refer to parallel and scalable methods for the iterative solution of PDEs, based on the decomposition of the problems into smaller subproblems. Thanks to this basic idea, DDMs are widely applied in large-scale problems arising from applied mathematics, computer and life sciences, engineering, etc. The subdivision can enter at different levels: at the continuous level, by defining several physical models on different parts of the domain;

at the discrete level, where different discretization techniques are employed in order to preserve physical properties of the original problem. Lastly, the decomposition can be performed at the level of the algebraic system arising from the discretization. From now on, we will refer to DDMs as iterative algorithms for the solution of algebraic systems, like in Reference [116].

In this perspective, the computational domain is decomposed into smaller subdomain, on each of which a restriction of the original problem is defined. The partitioning can be either performed with *overlapping* (Schwarz methods) or *non-overlapping* subdomains. Each smaller problem is then solved independently, i.e. in parallel, which is essential for the development of efficient and optimized codes. With the ever increasing growth of modern supercomputers, it is necessary to design and implement efficient solvers that are able to take advantage of the available computational resources. Several parallel numerical libraries are available, such as the Portable Extensive Toolkit for Scientific Computation (PETSc) from the Argonne National Laboratory [3] or Trilinos from Sandia National Laboratories [113].

This Thesis focuses mainly on the design, numerical analysis and parallel implementation of dual-primal DD preconditioners for the Jacobian linear system arising within each Newton iteration for the solution of fully implicit time discretization of the Bidomain model. Dual-primal methods belong to the class of iterative substructuring (non-overlapping) DD methods. In dual-primal algorithms, the unknowns are divided into three groups: the internal ones, which belong to the internal part of the subdomains; the dual and the primal ones, which altogether form the interface set of variables. In general, the primal set of variables coincides with the vertices of the subdomains in 2D, while in 3D the primal set must be chosen appropriately. The two preconditioners considered here are the Dual-Primal Finite Element Tearing and Interconnecting (FETI-DP) and the Balancing Domain Decomposition with Constraints (BDDC) preconditioners.

The Finite Element Tearing and Interconnecting (FETI) methods are a family of DD algorithms, which have been developed in the 90s, see References [42, 43, 45–47]. In these methods, continuity condition is reached only at convergence. The first numerical evidence of the convergence properties of FETI methods applied to second-order elliptic problems is reported in Ref. [45], whereas the first theoretical estimates on the condition number of FETI are proved in Reference [84]. FETI-DP methods are derived from the one-level and two-level FETI methods. They differ from standard FETI methods, as in this case the primal degrees of freedom are required to be continuous across the subdomains. They are introduced in Ref. [48] with vertex constraints and then extended to 3D in [46]. A 2D convergence bound is proved in Ref. [85], while a complete 3D study of both algorithms is provided in Refs. [69, 72–74]. In FETI-DP methods the continuity of the solution across the subdomain boundaries is enforced by Lagrange multipliers. The basic idea is to form a Schur complement by eliminating the primal variables and solve the arising linear system in the Lagrange variables with an iterative method, usually in combination with a preconditioner. Scaling of the preconditioner is an important step in order to guarantee convergence results, independent of jumps in the coefficients of the partial differential equation. FETI-DP methods have been applied in several contexts, from three-dimensional elliptic problems with heterogeneous coefficients in Ref. [73] to linear elasticity problems ([72, 104]) and structural mechanics ([44, 69–71]). In the biomechanics field, we find evidences of robustness of this preconditioner in the works [2, 13, 71, 127].

Balancing Domain Decomposition with Constraints (BDDC) have been introduced more recently in [37] and theoretically analyzed in [82, 83]. BDDC are a two-level preconditioners, where local and coarse problems are treated additively; moreover, a proper choice of the set of primal constraints across the interface of the subdomains is needed. These primal constraints can be vertex points as well as averages over edges and/or faces of the subdomains and this set can influence the rate of convergence. BDDC have been also applied to a wide range of problems, from incompressible Stokes equations in [77] to isogeometric analysis in [5–7], as well as in [38] for H-curl problems. BDDC have been extended also to the solution of Navier-Stokes equations and to multilevel approaches in [56, 57]. BDDC for advection-diffusion problems have been studied in the works [97, 121–123]. In the cardiac field, we find application of BDDC in [127, 128] for the solution of the linearized semi-implicit Bidomain problem, and in [26, 95] for cardiac mechanics.

As we mentioned, this Thesis deals with fully implicit time discretizations of the Bidomain model, decoupled from or coupled to the ionic model. In both cases, the resulting algebraic system turns out to be a nonlinear problem. In such cases, two DD approaches are possible. a) The linearization is performed after the geometric decomposition, leading to face the solution of (weakly coupled) nonlinear problems on the subdomains. In the literature, this step has been denoted as *nonlinear localization.* Nonlinear FETI-DP and nonlinear BDDC have been studied for example in [75], while more generally, nonlinear preconditioning has been analyzed in [79]. b) As in traditional DD approaches, a geometric decomposition is performed after linearization, where the nonlinear problem $A(u) = 0$ is solved by using a Newton-type method. In this way, we first linearize the problem using an iterative method $u^{(k+1)} = u^{(k)} + \alpha^{(k)}\delta u^{(k)}$, with a suitable steplength $\alpha^{(k)}$. The increment $\delta u^{(k)}$ is obtained by solving the Jacobian linear system $DA(u^{(k)})\delta u^{(k)} = -A(u^{(k)})$, by using a DD method in order to decrease the problem dimension and improve the convergence. These are commonly known as Newton-Krylov (NK) DD methods and they provide the basis for the design of the preconditioned solvers we propose and analyze throughout this work. They were originally designed for the solution of problems arising in computational fluid dynamics ([16, 17, 126]). So far, NK solvers have been developed for implicit time discretizations of the Bidomain model in [88, 89, 109], with overlapping one-level and multilevel Schwarz preconditioners, while NK-BDDC solvers have been proposed for the nonlinear elasticity equations modeling the cardiac mechanics in [26, 95]. One advantage of dual-primal preconditioners is the easy extension to unstructured meshes, since they do not need inter-grid operators.

The goal of this Thesis is to design, theoretical analyze and validate numerically dual-primal Newton-Krylov solvers for implicit time discretization of the Bidomain system, both through decoupled and coupled solution strategies. Thanks to the results of [78, 83], showing that FETI-DP and BDDC shares the same spectrum in case the same coarse space is chosen, we carry out a unique convergence rate analysis that hold for both preconditioner. In the decoupled approach, we prove in Theorem 4.1 a bound for the condition number of the preconditioned operator, both in case the standard ρ-scaling and the recently introduced *deluxe*-scaling (see [38]) are applied. For the coupled strategy instead, since the resulting Jacobian system is non-symmetric, we extend the analysis of [40, 121], providing an upper bound in Theorem 5.1 for the residual at the m-*th* iteration of the GMRES algorithm, preconditioned with BDDC.

The Thesis is structured as follows.

- In Chapter 2, we briefly review the principles of cell membrane, moving from a biological description of the intra- and extracellular exchanges to the mathematical formulations of the corresponding models, introducing the Goldman-Hodgkin-Katz (GHK) current equation and the Nernst equilibrium potential. Then we show how the cell membrane can be modeled as an electrical circuit, presenting the notion of channel gating. Afterwards, we introduce the concept of cardiac action potential and the milestone Hodgkin-Huxley ionic model, which provides the basis for the development of human ventricular ionic models (such as the Luo-Rudy and Ten Tusscher-Panfilov models) presented next in the Chapter. Additionally, we give an insight into two simpler phenomenological models, namely the FitzHugh-Nagumo and the Rogers-McCulloch models, which are easier to implement and facilitate preliminary tests of the solver we propose. Successively, we finally introduce the cardiac Bidomain model for the description of the electrical impulse in the cardiac tissue and its numerical discretization prior to the definition of the solver. In particular, we present two solution strategies for the time discretization. The Chapter is ended by the theoretical study of continuity and coercivity of the bilinear forms associated to the Jacobian linear problems arising from the Newton schemes, which will be needed for the theoretical convergence analysis of the proposed solvers in the next Chapters.

- In order to introduce the preconditioners chosen for our solver, we review in Chap. 3 the basic ideas of DD methods, focusing on non-overlapping dual-primal algorithms. In particular, after a short presentation of the idea of subdivision of the problem into smaller local

subproblems, we give an overview of the main ingredients needed for the definition of the preconditioners, such as restriction operators and scaling procedures. Next, FETI-DP and BDDC preconditioners are presented through an algebraic formulation, following [72, 104, 127]. Eventually, we report classic technical tools from functional analysis and DD which will be employed in the proofs of the convergence rate bounds.

- The theoretical convergence analysis for the decoupled solution strategy is presented in Chapter 4, where we first prove a bound for the projection operator (Lemma 4.1), for both cases of ρ and deluxe scalings. This Lemma holds for both preconditioners, as they have been proven to be spectrally equivalent in [78, 83].Then we provide an upper bound for the preconditioned operator (Theorem 4.1) that holds for both FETI-DP and BDDC preconditioners, each with a separate proof.

- Chapter 5 contains the theoretical study of the convergence rate for the coupled - or monolithic solution strategy. As the Jacobian linear system is non-symmetric, we are forced to employ iterative solvers such as GMRES. Consequently, the theoretical analysis is based on the work of Eistentat [40], which provides a bound for the residual of GMRES iterations, and on the work of Tu and Li [121], where BDDC preconditioner has been applied to the solution of non-symmetric problems. In this perspective, while Lemma 5.1 is quite similar to the analogous for the decoupled case, the construction of the proof of Theorem 5.1 requires different steps in order to achieve the final bound.

- Chapter 6 presents extensive parallel numerical experiments that validate the theoretical analysis of the previous Chapters. We first give an overview of our computational setting (parallel architectures, computational domains, parameters tuning and employed parallel library); next, we provide scalability and optimality tests for the Monodomain and Bidomain equations, using both decoupled and coupled solution strategies. Furthermore, we test the robustness, scalability and optimality of the Bidomain decoupled solver in the presence of an ischemic transmural region.

- Chapter 7 ends this Thesis with some remarks on the advantages and limitations of the proposed solvers, listing possible future developments and improvements.

Chapter 2

Cardiac reaction-diffusion models and numerical settings

In this Chapter, we briefly review some principles of cell membrane physiology, from its biological structure to the governing equations of the ionic currents. We introduce the notion of cardiac action potential and a milestone in the field of mathematical physiology, the Hodgkin-Huxley model for ionic currents; then, we review some of the most used ventricular models, such as the Beeler-Reuter, the Luo-Rudy phase one, and Ten Tusscher-Panfilov models. We also present a couple of phenomenological ionic models, which will be considered as benchmark for the theoretical convergence analysis and its preliminary numerical validation.

Afterwards we introduce the cardiac Bidomain model, which describes the propagation of electric signals in the cardiac tissue, and its reduced formulation, the Monodomain model.
We close the Chapter by discussing the properties of the bilinear forms associated with the linear problem arising from a finite element discretization in space and the Backward Euler method in time.

2.1 Membrane ionic models

2.1.1 Principles of cell membrane

The cell membrane is a biological separator between the interior of the cell (*intracellular* space) from the outside environment (*extracellular* space). The basic function of the cell membrane is to protect the cell from its external surroundings: it regulates the passage of substances in and out the cell, by being selectively permeable to ions and organic molecules.

It consists of a double layer (or *bilayer*) of phospholipid molecules about 7.5 nm thick, with the nonpolar hydrophobic tails (impermeable to charged ions and molecules) pointing toward the inside of the membrane and the polar hydrophilic heads forming the inner and outer faces of the membrane (Fig. 2.1). Proteins and cholesterol molecules are scattered throughout the flexible phospholipid membrane. Proteins may attach loosely to the inner or outer surface of the plasma membrane (*peripheral proteins*), or they may lie across the membrane, extending from inside to outside (*integral proteins*).

The intracellular and extracellular environments mainly consist of a dilute aqueous solution of dissolved salts, primarily NaCl and KCl, which dissociate into Na^+, K^+ and Cl^- ions. Typical concentrations can be found in Table 2.1. The cell membrane acts as a barrier to the free flow of these ions and maintains their concentration differences.

Even though the cell membrane itself is impermeable to ions, there exists a number of water-filled pores with diameters of about 0.8 nm, as well as protein-lined pores, called *channels proteins*, which allow passage of specific molecules. Ions can be transported across the cell membrane by passive or active processes, where an active process requires the expenditure of energy (by using

the concentration gradient of a different ion, called *exchanger* or by consuming chemically stored energy in the form of ATP), while a passive process results solely from the inherent and random movement of molecules, driven by concentration gradients and electric fields.
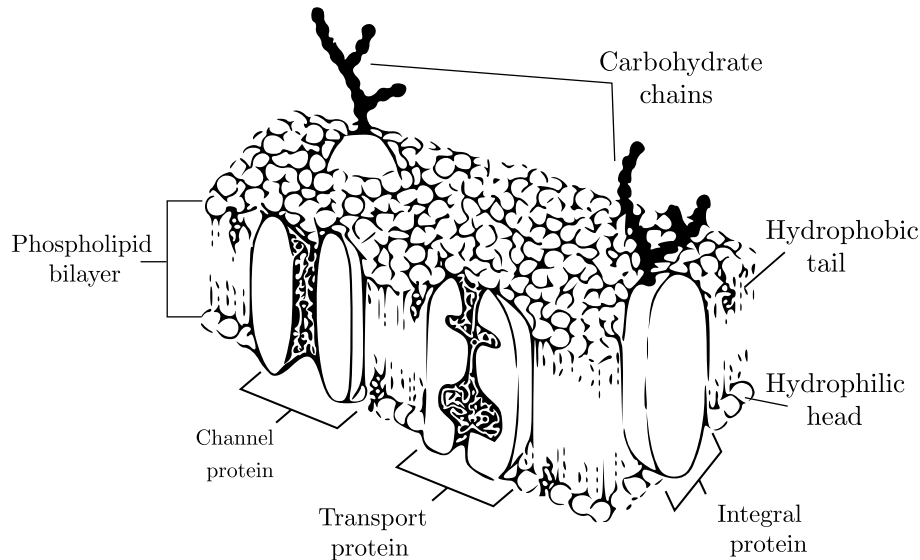
Figure 2.1: Schematic diagram of cell membrane.

In the literature passive processes are divided into three main categories [68].
Osmosis is the process that transports water through the cell membrane; *simple diffusion* accounts for the passage of small molecules through pores and of lipid-soluble molecules through the bilipid layer, as it happens for water, urea (a nitrogenous waste product of metabolism), and hydrated chloride ions, for example. *Carrier-mediated diffusion* occurs when a molecule is bound to a carrier molecule that moves readily through the membrane (for example, the transport of glucose and amino acids).

On the other hand, concentration differences are set up and maintained by active mechanisms that use energy to pump ions against their concentration gradient. This process is made by *transport proteins* that spend energy to transfer material across the membrane. Differences in ionic concentrations create a potential difference across the cell membrane that drives ionic currents.

The most important example of active (energy-consuming) transport is the sodium-potassium pump. This pump acts as an antiport, actively pumping sodium ions out of the cell against its steep electrochemical gradient and pumping potassium ions in. In general, the principal function of the active transport processes is to regulate the intracellular ionic composition of the cell. In this way the operation of sodium-potassium pump results in high intracellular K^+ concentrations and low intracellular Na^+ concentrations.

For more details and additional topics, see Ref. [68].

	Squid Giant Axon		Human Red Blood Cell	
	Intra	Extra	Intra	Extra
Na^+	50	437	19	155
K^+	397	20	136	5
Cl^-	40	556	78	112

Table 2.1: Typical values for intracellular and extracellular ionic concentrations, from two different cell types. Concentrations are given in units of mM.

2.1.2 The membrane potential

As already stated, each ionic channel permits the passage of specific ions and this specificity generates a potential difference. For example, consider two compartments i and e filled with a solution of NaCl separated by a thin membrane. Suppose to add a concentration of NaCl of 100 mM in compartment i and only 10 mM in compartment e. If the membrane had been completely permeable to all ions, the diffusion would drive the ions from compartment i to e until the concentrations were equal. Assume that the membrane is permeable only to Na^+ ions instead: in this case, diffusive forces would drive the ions over compartment e where the concentration is low, creating a surplus of negative Cl^- ions in compartment i and positive Na^+ ions in compartment e. This charge difference sets up an electric field across the membrane which tends to drive back Na^+ ions to compartment i: the point of equilibrium is reached when the Na^+ flux caused by the electric field is equal to and in opposite direction to the flux caused by diffusion.

We briefly introduce the basic equations needed for the construction of a membrane model; for more detailed studies, see Refs. [27, 68, 111].

The Nernst-Planck Equation. One of the most important equations in electrophysiology is the Nernst-Planck equation [27, 68, 111], the constitutive law describing the total flux of a ion across the membrane.

Suppose we are in the same situation as previously described, where we have two compartments (separated by a semipermeable membrane) filled with the same ion, for example the potassium ion Na^+, but at different concentrations $[Na^+]_i \neq [Na^+]_e$, as shown in Fig 2.2. The solutions on each side of the membrane are assumed to be electrically neutral (at least initially), and thus each ion Na^+ is balanced by another ion with opposite sign (for example, Cl^-). We denote *inside* the left part of the membrane and *outside* the right part.
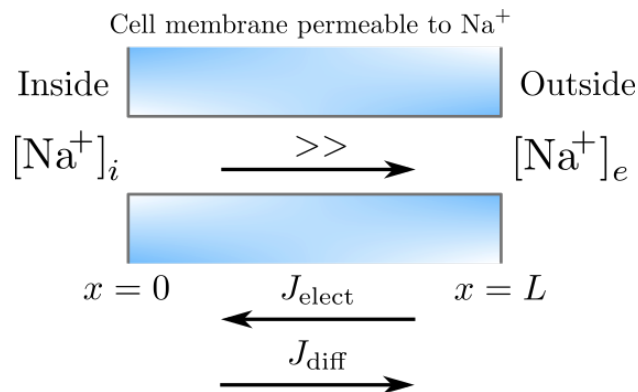
Figure 2.2: A schematic diagram of the electrodiffusion model for current through an ionic channel. Each side of the channel is electrically neutral, and both ion types can diffuse through the channel.

If the membrane is permeable to Na^+ but not to Cl^-, the concentration difference of the membrane results in a flow of Na^+ from the higher concentration space to the lower one. However, as Cl^- cannot diffuse through the membrane, the diffusion of Na^+ causes an increase of charge across the membrane. This charge imbalance (in turn) sets up an electric field that opposes the further diffusion of Na^+ through the membrane and the equilibrium is reached when the electric field exactly balances the diffusion of Na^+. Note that at steady state there will be more Na^+ ions on one side than on the other, and thus neither side of the membrane is exactly electrically neutral.

The total flux of Na^+ can be described by the following laws:

- *Fick's Law.*. If we denote by c (mol cm^{-3}) the concentration of the ion Na^+, then the ionic diffusion flux is given by

$$J_{\text{diff}} = -D\nabla c,$$

  where ∇c indicates the gradient of c and D is a diffusion coefficient (cm^2 s^{-1}).

- *Planck's equation.* The flow of ions through the membrane is driven by concentrations gradients and also by electric field. So the contribution to the flow from the electric field is given by

$$J_{\text{elect}} = -\mu \, \frac{z}{|z|} \, c \, \nabla u,$$

  where

  - μ is the mobility of the ion (cm^2 V^{-1} s^{-1}), defined as the velocity of the ion under a constant unit electric field;
  - z is the valence of the ion, so that $z/|z|$ is the sign of the force on the ion;
  - u is the electrical potential (V), so that $-\nabla u$ is the electrical field.

The ionic mobility μ and the Fick's diffusion constant are linked by the Einstein's relation

$$D = \mu \frac{RT}{|z|F},$$

where $R = 8.3143$ J K^{-1} mol^{-1} is the universal gas constant, $T = 310$ K is the absolute temperature and $F = 96.4867$ C / mmol is the Faraday's constant. When the effects of concentration and electrical gradients are combined, we obtain the *Nernst-Planck equation*

$$J = -D \left(\nabla c + \frac{zF}{RT} c \, \nabla u \right).$$

If the flow of ions and the electric field are transverse to the membrane, we can write a one-dimensional relation

$$J = -D \left(\frac{dc}{dx} + \frac{zF}{RT} c \frac{du}{dx} \right).$$

In general, the electric potential u is determined by the local charge density and so J must be found by solving a coupled system of equations.

Suppose now that the membrane has thickness L, such that the potential across the membrane is $v = u(0) - u(L) = u_i - u_e$, where the indexes i, e denote intra- and extracellular quantities; as boundary condition we suppose in the inside the concentration $c(0) = c_i$, while in the outside $c(L) = c_e$. Furthermore we assume that the electric field is constant through the membrane, such that $du/dx = -v/L$.

At a steady state with no production of ions, the flux J must be constant, leading to the equation

$$\frac{dc}{dx} - \frac{zF}{RT} \frac{v}{L} c + \frac{J}{D} = 0,$$

whose solution is

$$J = \frac{D}{L} \frac{zF}{RT} \frac{c_i - c_e \, e^{-\frac{zF}{RT} v}}{1 - e^{-\frac{zF}{RT} v}},$$

by imposing the boundary conditions. This flux density becomes an electrical current density (current per unity area) when multiplied by zF (the amount of charge carried per mole) and thus the ion current (A cm^{-2}) is given by

$$I = \frac{D}{L} \frac{z^2 F^2}{RT} \frac{c_i - c_e \, e^{-\frac{zF}{RT} v}}{1 - e^{-\frac{zF}{RT} v}},$$

known as *Goldman-Hodgkin-Katz* (GHK) current equation, where $D/L =: P$ is the permeability of the membrane. This current is zero if the diffusively driven flow and the electrical driven flow are in balance, i.e. $I = 0$, yielding the *Nernst equilibrium potential*

$$v = -\frac{RT}{zF} \log \frac{c_i}{c_e}. \tag{2.1}$$

Another common approach, widely used in the description of cardiac ionic currents, describes the ionic current I as a linear function of the membrane potential. Suppose that the potential drop across the membrane has two components: the first potential drop v_S is given by the Nernst equation (2.1) and the second potential drop is due to an electrical current, given by rI_S, being r the channel resistance and I_S is the membrane current of a generic ion S. Summing these two contributions we find

$$v = rI_S + v_S,$$

and solving for the current, we get the current-voltage relationship

$$I_S = G\left(v - v_S\right),$$

where $G = 1/r$ is the *membrane conductance*. We note that the current I_S and the conductance G are usually specified per unit area of membrane, being the product of the single channel conductance times the number of channels per unit area of membrane.

The linear current-voltage relation is also denoted *long-channel* or *high-concentration* and it derives from the Poisson-Nernst-Planck (PNP) equation.

Nernst equation can be considered as a "universal" law, as it is independent of how the ions move through the membrane, but depends only on the concentration difference. Moreover, any equation that expresses the transmembrane current of a ion in terms of the membrane potential must have a reversal potential v_{ion}, i.e. the current must be zero at the Nernst potential $v = v_{\text{ion}}$. However, although this is true in the case we are considering the movement of a single ion species, it could be more complicated when more than one type of ion species can cross the membrane: in this case, the membrane potential that generates zero total current does not necessarily have zero net current for each individual ion, so the phases are not, in general, at equilibrium, even when there is no total current. Therefore, the arguments of chemical equilibrium used to derive the Nernst equation cannot be used, and there is no universal expression for the reversal potential in the multiple ion case. In this case, the reversal potential depends on the model used to describe the individual transmembrane ionic flows.

2.1.3 Electrical circuit model of the cell membrane

Since the cell membrane separates charge, it can be viewed as a capacitor that acts in parallel with a resistor, which represents the ionic channels. A simple electrical circuit model of the cell membrane is shown in Fig. 2.3.

The capacitive current is given by $I_{\text{cap}} = C_m \dfrac{dv}{dt}$, where C_m is the capacitance of the capacitor (assumed to be constant) and v is the transmembrane potential. The membrane potential can be described by the following relation, thanks to the conservation law for the current, where the transmembrane current is given by the sum of the capacitative and ionic currents must be equal to the applied current I_{app},

$$C_m \frac{dv}{dt} + I_{\text{ion}}(v) = I_{\text{app}}.$$

Channel gating. As already mentioned in this Chapter, ionic channels can either open or close in response to voltage. In general, the current through a population of channels can be written as

$$I_{\text{ion}} = g(v,t)\ \phi(v),$$

where $g(v,t)$ is the proportion of open channels in the population per unity area, while $\phi(v)$ is the current-voltage relationship of a single open channel (GHK or linear model). So, if we suppose to have

- $\phi(v) = G(v - v_{\text{eq}})$ in linear form, being v_{eq} the equilibrium potential,

- $g(v,t) = \frac{N}{S}$, where N is the number of open channels and S is the area,

Outside

Inside
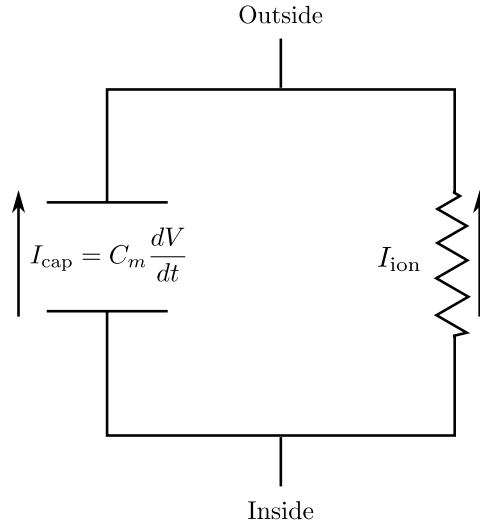
Figure 2.3: Electrical circuit model of the cell membrane.

then we can write

$$I_{\mathrm{ion}}(v) = G_{\max} w(v - v_{\mathrm{eq}}),$$

where $G_{\max} := N_{\mathrm{tot}} G/S$ is the maximum conductance and $w := N/N_{\mathrm{tot}}$ is the gating variable, representing the percentage of open channels.

The modeling of w depends on the structure of the channels: we briefly present two simple models for the K$^+$ and the Na$^+$ channels and we refer to [27, 68] for a more detailed discussion.

One or two unit protein, two states. The simplest model for the K$^+$ channel assumes that the channel can exist in either a closed state S_0 or an open state S_1, and the rate of conversion from one state to another is dependent to the voltage ($\alpha(v)$ and $\beta(v)$); thus

$$S_0 \underset{\beta(v)}{\overset{\alpha(v)}{\rightleftarrows}} S_1.$$
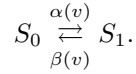
Let w denote the proportion of channels in the open state: it is possible to derive from the law of mass action a differential equation for the rate change of w as

$$\frac{dw}{dt} = \alpha(v)(1 - w) - \beta(v)w, \qquad w(0) = 0,$$

where we used the fact that, thanks to the conservation of channels, the proportion of closed channels is $1 - w$. It is often convenient to rewrite the equation as

$$\begin{cases} \dfrac{dw}{dt} = \dfrac{w_\infty - w}{\tau_\infty} \\ w(0) = 0 \end{cases},$$

where $w_\infty := \dfrac{\alpha(v)}{\alpha(v) + \beta(v)}$ is the equilibrium state and $\tau_\infty := \dfrac{1}{\alpha(v) + \beta(v)}$ is the time constant.

An important generalization of the two-state model occurs when the channel is assumed to consist of multiple identical subunits, each of which can be in either the closed or open state (as in the case of the potassium ion K$^+$). Let's denote by S_i the group of channels with exactly i open subunits. Then, the conversions between channel groups are governed by the reaction scheme

$$S_0 \underset{\beta}{\overset{2\alpha}{\rightleftarrows}} S_1 \underset{2\beta}{\overset{\alpha}{\rightleftarrows}} S_2.$$
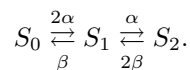
By denoting with n the proportion of channels in the open state, from the law of mass action we obtain

$$\frac{dn}{dt} = \alpha(1 - n) - \beta n, \tag{2.2}$$

and the current that flows through the channel is given by

$$I_{\text{ion}} = G_{\max} n^2 (v - v_{\text{eq}}).$$

This argument generalizes to the case of k identical independent binding sites, where the channel conductance is proportional to n^k, so for the potassium K^+ channels it holds

$$I_{K^+} = G_{\max} n^4 (v - v_{\text{eq}}).$$

The opening or closing state of the subunits modules the conductance of the channel, which can be increased or decreased depending on the proportion of open or closed subunits.

k subunits, two states. A more complex model is needed to explain the behavior of the Na^+ channel, which both activates and inactivates. The simplest approach is to extend the previous analysis to the case of multiple subunits (let's say three subunits) of two different types, m and h, where each subunit can be either closed or open.

Suppose we are in the case of two m subunits and one h subunit. Let S_{ij} denote the channel with i m-subunits open and j h subunit open. We want to determine a differential equation for S_{21} (i.e. when the channel is entirely open). The law of mass action and a substitution yield

$$\begin{cases} \dfrac{dm}{dt} = \alpha(1 - m) - \beta m \\ \dfrac{dh}{dt} = \gamma(1 - h) - \delta h \end{cases},$$

and

$$I_{\text{ion}} = G_{\max} m^2 h \ (V - V_{\text{eq}}).$$

As the sodium channel consists of four subunits, three of which are identical, the current equation will be

$$I_{Na^+} = G_{\max} m^3 h \ (V - V_{\text{eq}}).$$

2.1.4 Cardiac ionic current models

So far we have seen that the potential difference across the cell membrane causes ionic currents to flow through channels. The regulation of this activity is one of the most important cellular function. Many cells, such as neurons and muscle cells, use the transmembrane potential as a signal, and thus the functioning of the nervous system and muscle contraction are both dependent on the generation and propagation of electrical signals [68]. To understand this process it is helpful to divide cell types in two groups: excitable and nonexcitable cells.

- *Nonexcitable cell*: if currents are applied to the cell for a short period of time, the potential returns directly to its equilibrium value after the applied stimulus is removed. Typical examples are epithelial and photoreceptors cells.

- *Excitable cell*: if the applied current is sufficiently strong, the transmembrane potential goes through a large excursion (called *action potential*, AP) before returning to rest. Cardiac cells, skeletal muscle cells, secretory cell and most neurons belongs to this category. An excitable cell either respond to a stimulus or not at all, and thus a stimulus of sufficient amplitude may be reliably distinguished from background noise.

The most important landmark in the study of generation and propagation of signals is the work of Alan Hodgkin and Andrew Huxley [59–63], who developed the first quantitative model of the propagation of an electrical signal along a squid giant axon. Their ideas have since been extended and applied to a wide variety of excitable cells.

Cardiac action potential. Let us first remark what an action potential is. As already stated, it represents a large transmembrane potential excursion before returning to rest, due to a sufficiently strong applied stimulus. We can notice two main features.

- *Threshold potential v_S*: it is the critical value for which the action potential takes place. In this way, the cell reacts to the applied stimulus only if $v > v_S$.

- *Refractory phase*: in this time interval, no stimulus can produce another AP until the transmembrane potential returns to rest.
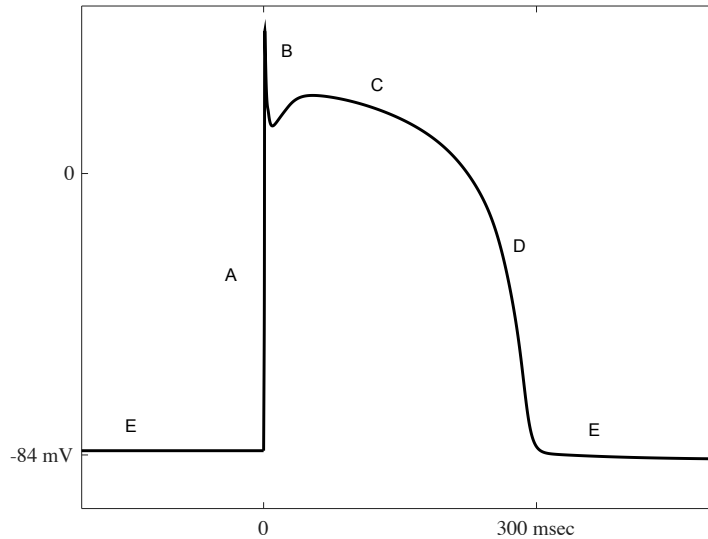
Figure 2.4: Evolution of the cardiac transmembrane potential in time during the AP. The letters correspond to the different phases of the AP.

We can identify five phases of cardiac AP (see Fig. 2.4).

In phase A (depolarization), fast Na$^+$ channels open, allowing a rapid inflow of positive ions into the cell (I$_{Na}$ current). Consequently, the transmembrane potential passes from a negative resting value to positive values. When the fast Na$^+$ channels inactivate, phase B occurs: the outward flows of K$^+$ and Cl$^-$ ions (I$_{to1}$ and I$_{to2}$ currents respectively) cause a rapid decrease of the action potential. Phase C is characterized by an inward current of Ca^{2+} (I$_{Ca}$) and an outward movement of K$^+$ (slow delayed rectifier potassium current I$_{Ks}$). This balance maintains the potential almost constant; usually, this phase is referred to with the term "plateau". This phase is sustained at a lower rate by the sodium-calcium exchanger current I$_{Na,Ca}$ and by the sodium-potassium pump current I$_{Na,K}$. The rapid repolarization of the cell – phase D – is a consequence of the closing of the Ca^{2+} channels and while K$^+$ channels are still open. This net outward current, corresponding to a negative change in the membrane potential which returns to negative values, causes more K$^+$ channels to open (I$_{Kr}$ current and the inwardly rectifying current I$_{K1}$). Then, the cell repolarize due to this net outward positive current. During phase E the potential is kept constant. Some of the K$^+$ ionic channels remain open, in order to guarantee the correct concentrations of ions outside and inside the cell.

The Hodgkin-Huxley model. We now want to introduce the Hodgkin-Huxley (HH) model for the membrane potential [59–63]. Hodgkin and Huxley carried their studies on the squid giant axon, where the principal ionic currents are the sodium and the potassium current, as in many neural cells. Although there are other ionic currents, primarily the chloride current, in the Hodgkin-Huxley theory they are small and lumped together into one current called the *leakage current*.

We already described in Sec. 2.1.3 how the membrane can be modeled as a capacitor in parallel with an ionic current, resulting in the equation $C_m \dfrac{dv}{dt} + I_{ion}(v,t) = 0$, where v denotes the

transmembrane potential, which is the difference between the internal and the external potentials and C_m is the capacitance of the capacitor. In the HH model, the sodium and potassium currents are both gated, while the leakage current is time independent and is formulated as a linear function of the transmembrane potential. This circuit (Fig. 2.5) is described by the following system of equations

$$
\begin{cases}
C_m \dfrac{dv}{dt} + I_{\text{ion}}(v, m, h, n) = I_{\text{app}} \\[2mm]
\dfrac{dm}{dt} = \alpha_m(1 - m) - \beta_m m \\[2mm]
\dfrac{dh}{dt} = \alpha_h(1 - h) - \beta_h h \\[2mm]
\dfrac{dn}{dt} = \alpha_n(1 - n) - \beta_n n
\end{cases}
$$

where we denote with $I_{\text{ion}} = I_{\text{Na}^+} + I_{\text{K}^+} + I_{\text{L}}$ sum of the sodium, potassium and leakage currents; I_{app} is the applied current. The specific rate functions α and β proposed by Hodgkin and Huxley
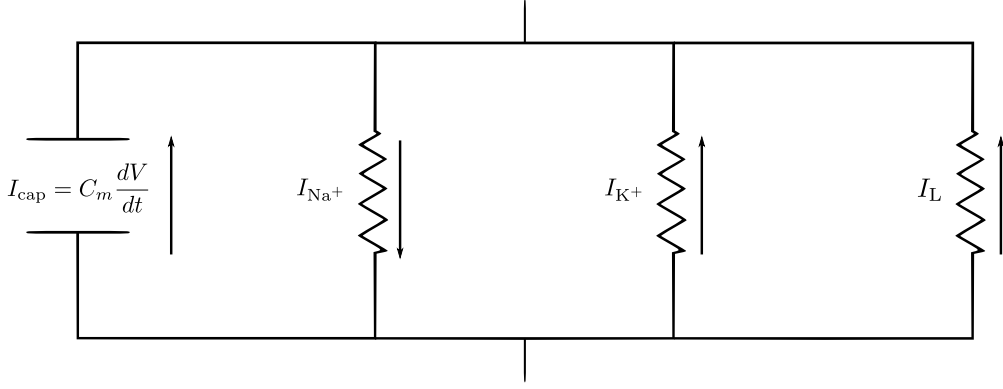
Figure 2.5: Schematic diagram of the electrical circuit of the HH membrane model.

are, in units of $(\text{ms})^{-1}$ [68],

$$
\alpha_m = 0.1 \frac{25 - v}{\exp\left(\frac{25-v}{10}\right) - 1}, \qquad \beta_m = 4 \exp\left(\frac{-v}{18}\right),
$$

$$
\alpha_h = 0.07 \exp\left(\frac{-v}{20}\right), \qquad \beta_h = \frac{1}{\exp\left(\frac{30-v}{10}\right) + 1},
$$

$$
\alpha_n = 0.01 \frac{10 - v}{\exp\left(\frac{10-v}{10}\right) - 1}, \quad \beta_n = 0.125 \exp\left(\frac{-v}{80}\right).
$$

and the currents reads

$$
I_{\text{Na}^+} = G_{\text{Na}} m^3 h (v - v_{\text{Na}})
$$
$$
I_{\text{K}^+} = G_{\text{K}} n^4 (v - v_{\text{K}})
$$
$$
I_{\text{L}} = G_{\text{L}} (v - v_{\text{L}})
$$

where the maximal conductances are $G_{\text{Na}} = 120$, $G_{\text{K}} = 36$ and $G_{\text{L}} = 0.3$, and the (adjusted) equilibrium potentials are $v_{\text{Na}} = 115$, $v_{\text{K}} = -12$ and $v_{\text{L}} = 10.6$.

If the potential v is raised slightly by a small stimulating current, the system returns to its stable equilibrium. However, if the stimulating current is large enough to raise the potential, see Fig. 2.6, the potential rises, m continues to rise and the inward sodium current is increased. This causes the depolarization phase.
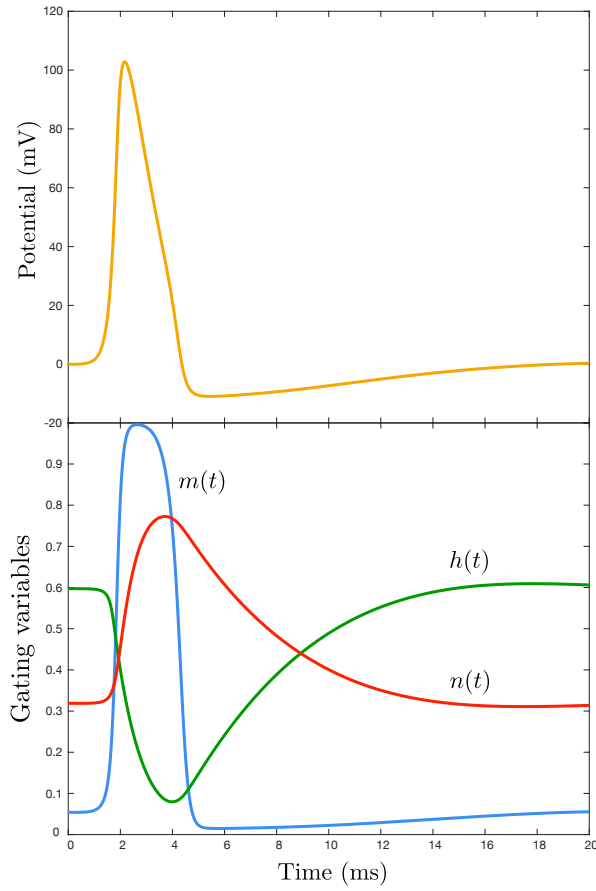
Figure 2.6: Top: action potential of the Hodgkin-Huxley equations. Bottom: the gating variables m, n and h during an action potential.

When the potential is at rest, the sodium inactivation h is positive, at about 0.6. As the potential increases, h approaches zero, so that sodium channels begin to close and the inward sodium current decreases.

At about the same time that the sodium current is inactivated, the outward potassium current is activated: this drives the potential below rest toward $v_\mathrm{K} = -12$. When v is negative, n declines and the potential eventually returns to rest, and the whole process can start again.

Of course the shape of the HH action potential (Fig. (2.6)) is substantially different respect to the cardiac one reported in Fig. 2.4, as they describe different types of cells. Therefore, when plugged into the bidomain equations, we would be able to reproduce both the depolarization and repolarization of the tissue, but both the propagation velocity and the time interval between those two phases would be incorrect. Thus, in order to obtain physiologically reliable models for the transmembrane potentials, it is necessary to consider a more detailed representation of the underlying cellular physiology.

Although this model is not directly relevant for studies of the heart, its ideas and mathematical formalism have been widely used as building bricks for a number of models describing cardiac action potentials. Indeed, it is possible to generalize the HH formalism by considering the following general structure for the ionic current:

$$I_\mathrm{ion}(v, w, c) = \sum_{k=1}^{N_\mathrm{ion}} G_k(v, c) \prod_{j=1}^{M} w_j^{p_{j_k}} (v - v_k(c)) + I_n(v, w, c)$$

where N_ion is the number of ionic currents, G_k is the k-th membrane maximal conductance and

v_k the reversal potential for the k-th current, p_{j_k} are integers and I_n represents time independent ionic currents.

By coupling the systems of ODEs accounting the dynamics of the gating variables $w := (w_1, \dots, w_M)$ and the dynamics of the ionic concentration variables $c := (c_1, \dots, c_S)$, the time evolution of the transmembrane potential of a single cell is given by the system

$$\begin{cases} C_m \, \dfrac{dv}{dt} + I_{\text{ion}}(v, w, c) = I_{\text{app}} \\ \dfrac{dw}{dt} - R(v, w) = 0, \qquad \dfrac{dc}{dt} - C(v, w, c) = 0, \\ v(0) = v_0, \qquad w(0) = w_0, \qquad c(0) = c_0, \end{cases}$$

with C_m the surface capacitance and I_{app} is the applied current per unit area of the membrane surface. For more details and a qualitative study of the HH model, we refer to Refs. [27, 68].

Ventricular models. The first model to describe the ventricular action potential was proposed by Beeler and Reuter in 1977 [4], based on the HH formalism.

This model is based on experimental data from the guinea pig and, as an improvement with respect to the Hodgkin-Huxley model, it takes into account the role of Ca^{2+}: indeed, the entry of calcium produces a significant change in the calcium intracellular concentration $[Ca^{2+}]_i$, mainly by triggering the Ca^{2+} release from the sarcoplasmic reticulum (SR) via a calcium-induced calcium-release (CICR) process. Thus it adequately reproduces characteristic experimental phenomena such as the slow recovery of the sodium system from inactivation and membrane oscillations. In this model, the ionic current is given as the sum of four currents $I_{\text{ion}} = I_{\text{Na}} + I_s + I_{K1} + I_{x_1}$ for a total of six gating variables and one equation for the Ca^{2+} dynamics. More extensive explanations on this model can be found in [27, 68, 111].

This model is quite simple, but still widely used: recent models are more physiologically accurate when describing the behaviour of a single cell, but the computational efficiency can be relevant when simulating the electrical activity of the complete heart.

Another classical model for ventricular cells is the Luo-Rudy (LR) model, originally formulated in 1991 [80] and then revised in 1994 [81] in order to give a detailed description of CICR, intracellular calcium cycling and calcium buffering.

The first model (often referred to as Luo-Rudy phase one model, LR1) is a development of the Beeler-Reuter model and it includes six ionic currents: I_{Na} a fast sodium current; I_{si} a slow inward current; I_K and I_{K1} time-dependent and a time-independent potassium currents; I_{Kp} a plateau potassium current and I_b a time-independent background current. In addition, the reversal potential E_{si} depends on the intracellular concentration $[Ca^{2+}]_i$, whose dynamics is described by a ODE.

On the other hand, the second model (referred to as Luo-Rudy phase two, LR2) [81] provides a much more detailed description of the specific ionic currents across the membrane: it includes twelve membrane currents, in addition to the Ca^{2+} dynamics. This model also describes a number of internal fluxes, including the Ca^{2+} flux in and out of the SR as well as buffering of calcium. The SR is a network inside the cell that takes up calcium from the myoplasm and later release it back in response to the activation of the cell: in this way, the concentration of calcium inside the myoplasm varies and this variation is important for the contractile ability of the muscle cells. For a detailed discussion, we refer to Refs. [9, 68]. In order to describe the calcium dynamics of the SR, the Luo-Rudy phase two model proposes three different intracellular calcium concentrations, the myoplasm calcium concentration $[Ca^{2+}]_i$ and two SR calcium concentrations $[Ca]_{\text{NSR}}$ and $[Ca]_{\text{JSR}}$; moreover, four ionic currents are related to the uptake and the release of calcium from the SR.

The last model we would like to review is the human ventricular tissue model proposed by ten Tusscher et al. in 2004 [114] and revised by ten Tusscher and Panfilov in 2006 [115]. This formulation can reproduce human epicardial, endocardial and M cell action potential by modifying the transient outward and slow delayed rectifier currents. Moreover, it accurately reproduces the

experimentally observed data on action potential duration (APD) restitution (APDR), which is an important feature for reentry phenomena, and some proprierties of wave propagation in human ventricular tissue, such as the conduction velocity (CV) restitution (CVR), which is involved in the generation of arrhythmias. The APD is defined as the interval in which the cardiac cell is in an excited state, as a function of the diastolic interval (DI) (the time interval when the cardiac cell is in an unexcited state), while the CV property of a propagating electric impulse in the cardiac tissue depends on the APD and on one or several previous diastolic or interbeat intervals [27, Sections 2.9.6 and 3.1.4], [111, Sec. 2.2], [68].

The total ionic current I_{ion} is the sum of all transmembrane ionic currents

$$I_{\mathrm{ion}} = I_{\mathrm{Na}} + I_{\mathrm{K1}} + I_{\mathrm{to}} + I_{\mathrm{Kr}} + I_{\mathrm{Ks}} + I_{\mathrm{CaL}} + I_{\mathrm{NaCa}} + I_{\mathrm{NaK}} + I_{\mathrm{pCa}} + I_{\mathrm{pK}} + I_{\mathrm{bCa}} + I_{\mathrm{bNa}}.$$

The fast Na^+ current I_{Na} presents three gating variables (m is the activation gate, h the inactivation and j is the slow inactivation gate), each of whom is governed by a HH-type equation and characterized by a steady-state value and a time constant for reaching this steady-state value. The time constant τ_j differs from the one in LR1 as here a more gradual CV restitution is granted. The L-type calcium current I_{CaL} is made up of a voltage-dependent activation gate d, a voltage-dependent inactivation gate f and an intracellular calcium-dependent inactivation gate f_{Ca}. In the original formulation [114], the activation times curve of this current is taken from the LR2 model, due to limited experimental data. However, in the updated model [115] from 2006, modifications are made to include the injection of calcium into the subspace and its inactivation by the $\mathrm{Ca}_{\mathrm{SS}}$ via the inactivation gate f_{cass}. Moreover, voltage-clamp experiments induce the incorporation of both a slow voltage inactivation gate f and a fast voltage inacivation gate f_2. A single formulation for the steady-state activation curve r_∞ is used for the transient outward current I_{to}, as no significant differences between activation in epicardial and endocardial cells were recorded; on the other hand the steady-state inactivation curve s_∞ presents two different formulations for epicardial and endocardial cells, in order to fit experimental data. This current is not included in the LR model, neither in phase one nor in phase two. Two other currents that are not included in Luo-Rudy formulations are the slow and rapid delayed rectifier current I_{Ks} and I_{Kr}: these two currents are in charge of the rapid repolarization phase of the action potential (phase D in Fig. 2.4), as the L-type Ca^{2+} channels close while the slow delayed rectifier K^+ channels are still open. The inward rectification is modeled as a time-dependent inactivation gate. The formulation of the $\mathrm{Na}^+/\mathrm{Ca}^{2+}$ exchanger current is similar to the one used in LR model, with an additional α factor that accounts for the higher concentration of calcium in the subspace close to the sarcolemmal membrane, where this exchanger is operating. Also the $\mathrm{Na}^+/\mathrm{K}^+$ pump current (I_{NaK}), the plateau (I_{pCa} and I_{pK}) and background (I_{bNa} and I_{bCa}) currents formulation resemble the one in the LR model. In the calcium dynamics, three currents describe the movements of calcium ions inside the cell: I_{leak} is a leakage current form the sarcoplasmic reticulum to the cytoplasm, I_{up} represent the pump current raising calcium in the SR and I_{rel} is the CICR current. In the model from 2006, a description of calcium dynamics in the subspace ($\mathrm{Ca}_{\mathrm{SS}}$), in the cytoplasm ($\mathrm{Ca}_i$) and in the sarcoplasmic reticulum ($\mathrm{Ca}_{\mathrm{SR}}$) is given. In addition, two differential equations are provided to describe the changes in the intracellular sodium Na_i and potassium K_i concentrations, where the external stimulus current I_{stim} and the axial current flow I_{ax} are accounted.

An important feature in this model is that all the major currents are fitted to experimental data on human ventricular myocites, while being relatively computational simple, thus easily allowing the simulation of reentrant spiral waves in a 2-dimensional sheet of epicardial tissue for the investigation of reentrant arrhythmias.

For all the mentioned models, we refer to the original papers for the Equations of ionic currents and gating variables [4, 80, 81] and to Appendix A.

Several ionic models are available at the CellML Physiome Model Repository in different programming languages (https://models.physiomeproject.org/).

Phenomenological models. Despite the accuracy of the ventricular models presented in the previous paragraph, several models have been developed in order to investigate phenomena on larger spatial and temporal scales, where the sub-cellular processes are ignored and only an action potential is provided. We mention here the FitzHugh-Nagumo model [51, 52], the Rogers-McCulloch [105] model, the Morris-Lecar model [87], the Aliev-Panfilov model [1] and the Fenton-Karma model [49]. We give a brief insight of the first two models, as the Rogers-McCulloch model is then employed in most of the numerical tests in Chapter 6.

The FitzHugh-Nagumo model. The FitzHugh-Nagumo model extracts the essential behavior of the Hodgkin-Huxley model and presents it in a simplified form [51, 52]. Thus, the FitzHugh-Nagumo model has two variables: the first (v) is called the excitation variable, while the second (w) is called the recovery variable.

The FitzHugh-Nagumo model can be derived from a simplified circuital model of the cell membrane (Fig. 2.7). Here the cell consists of three components in parallel:

- a capacitor representing the membrane capacitance, with current i_c;

- a nonlinear current-voltage device for the excitation variable, with a current $j = F(v)$ with F a cubic function in v;

- a resistor (with resistance R), inductor (L) and battery (with potential v_0) in series for the recovery current i.

Using Kirchhoff's law $i_c + i + j = I_{app}$ and noticing that the total potential difference is given by $v = v_0 + Ldi/dt + Ri$, we can write the equations for the behavior of this membrane circuit diagram:

$$\begin{cases} C_m \dfrac{\partial v}{\partial t} = -i + F(v) + I_{app}, \\ L \dfrac{\partial i}{\partial t} = v - v_0 - Ri, \end{cases}$$

where I_{app} is the applied external current.
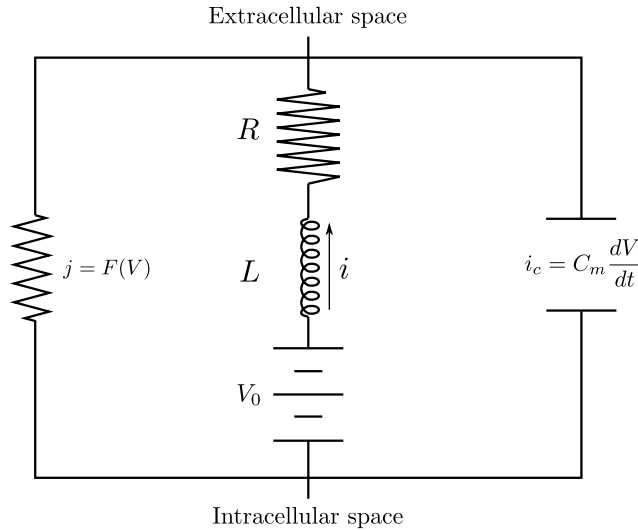
Figure 2.7: Schematic diagram of the electrical circuit of the FHN membrane model.

We notice that the current i in this model plays the role of the potassium current in the HH model, that's why it is called recovery current. The function $F(v)$ is assumed to be of cubic shape.

The FitzHugh-Nagumo equations [51] can be written in the following form:

$$\begin{cases} \dfrac{\partial v}{\partial t} - f(v, w) = I_{\text{app}} \\ \dfrac{\partial w}{\partial t} = g(v, w), \end{cases}$$

with Neumann boundary conditions $v_{|\partial\Omega} = 0$, where $\partial\Omega$ is the boundary of the domain Ω considered. The function f has a cubic form and it is often written as:

$$f(v, w) = c_1 v(v - a)(1 - v) - c_2 w,$$

while g is a linear function of v and w

$$g(v, w) = b(v - c_3 w),$$

see for example [111]. In this ODEs system u is the excitation variable, which can be identified with the transmembrane potential, and w is the recovery variable. Here, a, b, c_1, c_2 and c_3 are given parameters, which may be adjusted to simulate different cell types. This parameter choice (reported in the caption of Fig. 2.8) gives a normalized action potential, with the resting potential being zero and the peak potential approximately 0.9. Plots of v and w are shown in the left panel of Figure 2.8. The action potential shown in the figure results from applying a stimulus current I_{app} of strength 0.05 mA/cm^2, lasting from $t = 50$ to $t = 60$ ms.
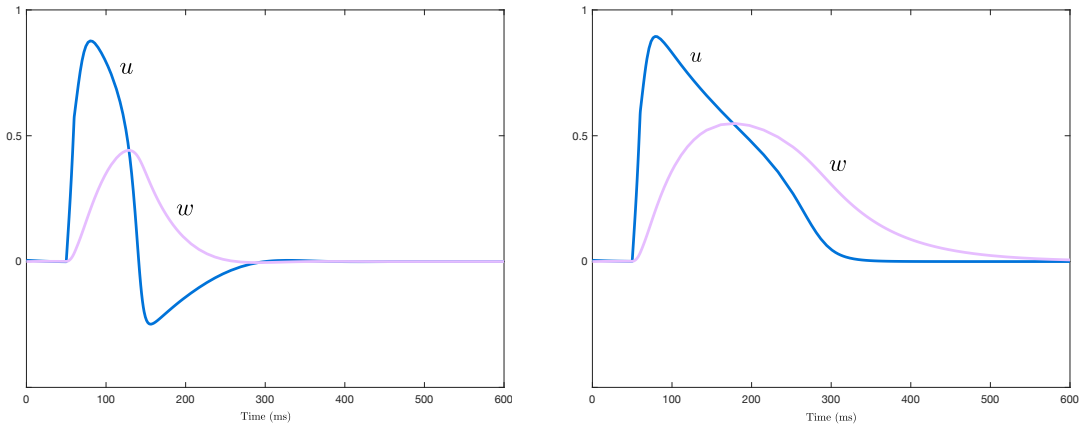
Figure 2.8: Transmembrane potential v (blue) and recovery variable w (lilac) computed using the FHN model (left panel) and the Rogers-McCulloch model (right panel). Membrane parameters are taken from [111]: $a = 0.13$, $b = 0.013$, $c_1 = 0.26$, $c_2 = 0.1$ and $c_3 = 1$. The external applied current I_{app} has strength 0.05 mA/cm^2 lasting from 50 ms to 60 ms. Note the hyperpolarization of v in the recovery phase.

The Rogers-McCulloch Model One detail of the original formulation by FitzHugh-Nagumo that does not match well with physiological data is that the cell hyperpolarizes in the repolarization phase: as a matter of fact, the waveform solution of the FHN system presents a negative excursion of v during the refractory part of the wave (left panel of Fig. 2.8). A modification of the equations to overcome this problem was suggested by Rogers and McCulloch [105], by modifying the last term in the first equation:

$$\begin{cases} \dfrac{\partial v}{\partial t} = c_1 v(v - a)(1 - v) - c_2 vw + I_{\text{app}}, \\ \dfrac{\partial w}{\partial t} = b(v - c_3 w), \end{cases}$$

The right panel of Fig. 2.8 shows the action potential computed with the modified model. We see that the undershoot in the transmembrane potential is eliminated, giving a more physiologically realistic solution.

2.2   The Bidomain model

So far we have reviewed a number of ionic models describing the dynamics of action potential within a single cell. In order to describe the propagation of the electric signal in the heart, a model for the cardiac tissue must be provided. Moreover, the mathematical model should be able to describe the potential difference across the membrane: a natural approach would be to model each cell as a single unit, thus enabling complete control of all facets in the intracellular and extracellular potentials. However, this strategy would lead to a very complex and computational inefficient model, due to the large number of cells in the heart. This motivates the continuous approximation of the cardiac tissue as follows [27, 111].

At a cellular level, the structure of the cardiac tissue can be viewed as composed by two ohmic conducting media, the *intracellular* space Ω_i inside the cell and the *extracellular* space Ω_e outside, separated by the active membrane Γ (which also acts as an insulator between the two domains, as otherwise there would be no potential difference across the domain). In each point of the two domains the electric potential is defined as a quantity averaged over a small volume: consequently, every point of the cardiac tissue is assumed to be both the intracellular and the extracellular spaces, thus being assigned both an intracellular and an extracellular potential. From now on, we will denote by Ω the cardiac tissue volume represented by the superposition of the intra- and extracellular spaces.

A very common assumption is that the domains are continuous and fill the complete volume of the heart, and that the membrane is a distributed continuum that fills the complete tissue volume. Structural inhomogeneities in the intra- or extracellular spaces due to the presence of gap junctions, blood vessels and collagen are generally included in the conductivity tensors D_i and D_e as inhomogeneous functions of space.

The cardiac tissue is composed of elongated cardiac cells, with roughly a cylidrical shape of diameter $d_c \sim 10\ \mu$m and length $l_c \sim 100\ \mu$m. These cells are coupled together mainly end-to-end and side-to-side by *gap junctions*, which are small channels embedded in the cell membrane providing direct intercellular communication between the internal compartments of two neighbouring cells. Thanks to these gap junctions, ions and other molecules can pass directly from one cell to another without entering in the extracellular space.

The cells are arranged in fibers set as laminar sheets running counterclockwise from the epicardium to the endocardium [27, 76, 98]. In this way, at each point $\mathbf{x}$ of the cardiac domain Ω it is possible to define an orthonormal triplet of vectors $\mathbf{a}_l(\mathbf{x})$, $\mathbf{a}_t(\mathbf{x})$ and $\mathbf{a}_n(\mathbf{x})$ parallel to the local fiber direction, tangent and orthogonal to the laminar sheets respectively.

To be able to formulate a mathematical model, we define the anisotropic conductivity tensors D_i and D_e of the two media as

$$D_{i,e}(\mathbf{x}) = \sum_{\bullet = \{l,t,n\}} \sigma_\bullet^{i,e} \mathbf{a}_\bullet(\mathbf{x}) \mathbf{a}_\bullet^T(\mathbf{x}),$$

where $\sigma_\bullet^{i,e}$ are conductivity coefficients in the intra- and extracellular domain along the corresponding direction $\mathbf{a}_\bullet$, with $\bullet = l, t, n$. For our theoretical purpose, we assume here that these coefficients are constant in space.

We denote by $\mathbf{J}_i(\mathbf{x},t)$ and $\mathbf{J}_e(\mathbf{x},t)$ the local average current densities per unit area in the intra- and extracellular domains, and by i_m the transmembrane current per unit volume flowing across the membrane surface Γ. If we consider a volume V enclosing $\mathbf{x}$ and we denote by $|V|$ its volume, ∂V its smooth surface and by $\mathbf{n}$ the outward normal on ∂V, we can write the current conservation law as

$$\frac{1}{|V|} \int_{\partial V} \mathbf{J}_e \cdot \mathbf{n}\ d\sigma = -\frac{1}{|V|} \int_{\partial V} \mathbf{J}_i \cdot \mathbf{n}\ d\sigma = C_m \frac{1}{|V|} \int_V i_m dx,$$

where C_m is the surface capacitance. The equation above means that the flux flowing in the extracellular volume must be equal and opposite to the one exiting from the intracellular volume, and both must equal the transmembrane current across the membrane. By the divergence theorem, it follows

$$\text{div}\mathbf{J}_e(x,t) = -\text{div}\mathbf{J}_i(x,t) = C_m i_m.$$

As we made the assumption that the intra- and extracellular media are ohmic, the following relations hold

$$\mathbf{J}_i = -D_i \nabla u_i, \qquad \mathbf{J}_e = -D_e \nabla u_e,$$

which lead to the parabolic-parabolic formulation of the Bidomain system.

Parabolic-parabolic formulation. Find the intra- and extracellular potentials $u_{i,e}$: $\Omega \times (0,T) \to \mathbb{R}$, the transmembrane potential $v = u_i - u_e$: $\Omega \times (0,T) \to \mathbb{R}$, the gating variables $\mathbf{w}$: $\Omega \times (0,T) \to \mathbb{R}^M$, the ionic concentration variables $\mathbf{c}$: $\Omega \times (0,T) \to \mathbb{R}^S$, such that

$$
\begin{cases}
\chi C_m \dfrac{\partial v}{\partial t} - \text{div}\,(D_i \nabla u_i) + I_{\text{ion}}(v, \mathbf{w}, \mathbf{c}) = I_{\text{app}}^i & \text{in } \Omega \times (0,T), \\[2mm]
-\chi C_m \dfrac{\partial v}{\partial t} - \text{div}\,(D_e \nabla u_e) - I_{\text{ion}}(v, \mathbf{w}, \mathbf{c}) = I_{\text{app}}^e & \text{in } \Omega \times (0,T), \\[2mm]
\dfrac{\partial \mathbf{w}}{\partial t} - \mathbf{R}(v, \mathbf{w}) = 0 & \text{in } \Omega \times (0,T), \\[2mm]
\dfrac{\partial \mathbf{c}}{dt} - \mathbf{C}(v, \mathbf{w}, \mathbf{c}) = 0 & \text{in } \Omega \times (0,T), \\[2mm]
\mathbf{n}^T D_{i,e} \nabla u_{i,e} = 0 & \text{in } \Omega \times (0,T),
\end{cases}
\tag{2.3}
$$

given $I_{\text{app}}^{i,e}$: $\Omega \times (0,T) \to \mathbb{R}$ intra- and extracellular applied currents and initial values $v_0 : \Omega \to \mathbb{R}$, $\mathbf{w}_0 : \Omega \to \mathbb{R}^M$ and $\mathbf{c}_0 : \Omega \to (0, +\infty)^S$

$$v(\mathbf{x}, 0) = v_0(\mathbf{x}), \quad \mathbf{w}(\mathbf{x}, 0) = \mathbf{w}_0(\mathbf{x}), \quad \mathbf{c}(\mathbf{x}, 0) = \mathbf{c}_0(\mathbf{x}) \qquad \text{in } \Omega.$$

The zero-flux boundary conditions in the system (2.3, last row) mathematically represent the assumption that the heart is immersed in a non-conductive medium. The non-linear rection term I_{ion} and the ODEs system for the gatings $\mathbf{w}$ and the ionic concentrations $\mathbf{c}$ are given by the chosen ionic membrane model.

Parabolic-elliptic formulation. It is possible to re-write the system (2.3) in terms of the transmembrane potential $v(\mathbf{x}, t)$ and the extracellular potential $u_e(\mathbf{x}, t)$

$$
\begin{cases}
\chi C_m \dfrac{\partial v}{\partial t} - \text{div}\,(D_i \nabla v) + \text{div}\,(D_i \nabla u_e) + I_{\text{ion}}(v, \mathbf{w}, \mathbf{c}) = I_{\text{app}}^i & \text{in } \Omega \times (0,T), \\[2mm]
-\text{div}\,(D_i \nabla v) - \text{div}\,((D_i + D_e) \nabla u_e) = I_{\text{app}}^i + I_{\text{app}}^e & \text{in } \Omega \times (0,T), \\[2mm]
\dfrac{\partial \mathbf{w}}{\partial t} - \mathbf{R}(v, \mathbf{w}) = 0 & \text{in } \Omega \times (0,T), \\[2mm]
\dfrac{\partial \mathbf{c}}{dt} - \mathbf{C}(v, \mathbf{w}, \mathbf{c}) = 0 & \text{in } \Omega \times (0,T), \\[2mm]
\mathbf{n}^T D_i \nabla(v + u_e) = 0 & \text{in } \Omega \times (0,T), \\[2mm]
\mathbf{n}^T (D_i + D_e) \nabla u_e + \mathbf{n}^T D_i \nabla v = 0 & \text{in } \Omega \times (0,T),
\end{cases}
\tag{2.4}
$$

and same initial conditions as in the parabolic-parabolic formulation.

Results on existence, uniqueness and regularity of the solution of the parabolic-parabolic system (2.3) have been extensively studied, see for example References [27, 29, 124], while the well-posedness of the parabolic-elliptic formulation (2.4) has been studied for example in Refs [12, 27].

2.3 The Monodomain model

The numerical solution of the Bidomain system is computationally demanding: in order to accurately reproduce the steep potential propagation throughout the myocardium, very fine time and

spatial scales are needed. Moreover, due to the pure Neumann boundary conditions, the discretized linear system is ill-conditioned and iterative solvers such as the Conjugate Gradient (CG) method preconditioned by standard preconditioning technique (for example, like ILU or Block Jacobi) are not effective, thus motivating the development of more robust and efficient preconditioned solvers.

For this reason, for large scale simulations, it is often convenient to simplify the problem by assuming equal anisotropy rate between the internal and external diffusion coefficient - *i.e.* by taking $D_e = \lambda D_i$ with λ constant, where the system (2.3) is equivalent to a single parabolic reaction-diffusion equation describing the evolution of the transmembrane potential $v = u_i - u_e$, coupled to the microscopic model through the gating variable w.

The system we consider is then the following:

$$
\begin{cases}
\chi C_m \dfrac{\partial v}{\partial t} - \dfrac{\lambda}{1+\lambda} \mathrm{div}\,(D_i \nabla v) + I_{\mathrm{ion}}(v,w) = I_{\mathrm{app}} & \text{in } \Omega \times (0,T) \\[2mm]
\dfrac{\partial \mathbf{w}}{\partial t} - \mathbf{R}(v,\mathbf{w}) = 0 & \text{in } \Omega \times (0,T), \\[2mm]
\dfrac{\partial \mathbf{c}}{dt} - \mathbf{C}(v,\mathbf{w},\mathbf{c}) = 0 & \text{in } \Omega \times (0,T), \\[2mm]
\mathbf{n}^T D_i \nabla v = 0 & \text{in } \Omega \times (0,T),
\end{cases}
\tag{2.5}
$$

where $I_{\mathrm{app}}(\mathbf{x},t) = \dfrac{I_{\mathrm{app}}^i \sigma_l^e - I_{\mathrm{app}}^e \sigma_l^i}{\sigma_l^e + \sigma_l^i}$ is the applied current.

From the mathematical and numerical analysis point of view, this is certantly a useful reduction. However, it has some limitations directly related to the choose of equal anisotropy: experimental measurements of intracellular and extracellular conductivities show that this assumption is not realistic and it is really difficult to set the parameter λ in order to obtain physiological conductivities.

2.4 Space and time discretizations

In the following Section, we provide a Finite Element discretization for the spatial variable, and two different solution strategies for the time numerical discretization, based on a decoupling strategy (such as the one proposed in Refs. [36, 88, 89, 109]) and on a coupled fully implicit time discretization (see e.g. Ref. [90]). Common alternatives in the literature use semi-implicit time discretizations [26, 127] and/or operator splitting [22, 23, 111], since fully implicit schemes are usually more expensive from a computational point of view if complex and high-dimensional non-linear ionic (e.g. [35, 80, 114]) models are coupled with the Bidomain system. However, as the scope of this Thesis is to design an efficient class of preconditioners for fully implicit time discretizations of the Bidomain system and to avoid numerical stability constraints, both approaches (decoupled and coupled) will be considered.

To this end, our theoretical analysis will be carried on the parabolic-parabolic formulation of the Bidomain model (2.3) and will consider the class of phenomenological ionic model (by neglecting the ionic concentration variables), while ionic models such as the Luo-Rudy phase one [80] and the ten-Tusscher models [114, 115] will be only included in parallel numerical experiments in Chapter 6.

2.4.1 Weak formulation and space discretization

The current state-of-the-art on space discretization of the Bidomain model is very extensive: finite difference methods have been investigated in Refs. [15, 94, 101, 120] as well as finite volume methods (Refs. [8, 33, 58, 66, 119]). In this Thesis we focus on Finite Element (FE) discretizations of the Bidomain equations, in the same fashion as in [25, 26, 50, 107, 109].

We remark that, for our theoretical purposes, we consider here a simplified ionic model, where we denote with w both gating and ionic concentration variables.

Let the cardiac domain $\Omega \subset \mathbb{R}^3$ be a bounded open Lipschitz set with Lipschitz continuous boundary. We derive a variational formulation of the Bidomain model in the following way: consider the functional spaces $V = H^1(\Omega)$, $\widetilde{V} = \left\{ v \in V : \int_\Omega v = 0 \right\}$ and define the usual L^2-inner product

$$(u, v) = \int_\Omega uv dx \qquad \forall u, v \in L^2(\Omega)$$

and the elliptic bilinear form associated with the intra- and extracellular conductivity tensors

$$a_{i,e}(u, v) = \int_\Omega (\nabla u)^T D_{i,e} \nabla v dx, \qquad \forall u, v \in V.$$

Then, find $u_i \in L^2(0, T; V)$, $u_e \in L^2(0, T; \widetilde{V})$ and $w \in L^2(0, T; L^2(\Omega)^{N_w})$ such that for $v \in L^2(0, T; V)$, $\dfrac{\partial w}{\partial t} \in L^2(0, T; L^2(\Omega)^{N_w})$ and $\forall t \in (0, T)$ it holds

$$\begin{cases} \chi C_m \dfrac{\partial}{\partial t}(v, \varphi_i) + a_i(u_i, \varphi_i) + (I_{\text{ion}}(v, w), \varphi_i) = \left(I_{\text{app}}^i, \varphi_i\right) \\ -\chi C_m \dfrac{\partial}{\partial t}(v, \varphi_e) + a_e(u_e, \varphi_e) - (I_{\text{ion}}(v, w), \varphi_e) = \left(I_{\text{app}}^e, \varphi_e\right) \\ \dfrac{\partial}{\partial t}(w, \varphi_w) - (R(v, w), \varphi_w) = 0 \end{cases} \tag{2.6}$$

$\forall \varphi_i, \varphi_w \in V$, $\forall \varphi_e \in \widetilde{V}$, where N_w is the total number of gating and ionic concentration variables.

In a similar fashion, the Monodomain model can be written as: find $v \in L^2(0, T; V)$ and $w \in L^2(0, T; L^2(\Omega)^{N_w})$ such that for $v \in L^2(0, T; V)$, $\dfrac{\partial w}{\partial t} \in L^2(0, T; L^2(\Omega)^{N_w})$ and $\forall t \in (0, T)$ it holds

$$\begin{cases} \chi C_m \dfrac{\partial}{\partial t}(v, \varphi) + a(v, \varphi) + (I_{\text{ion}}(v, w), \varphi) = (I_{\text{app}}, \varphi) \\ \dfrac{\partial}{\partial t}(w, \varphi_w) - (R(v, w), \varphi_w) = 0, \end{cases} \tag{2.7}$$

$\forall \varphi \in V$ and $\forall \varphi_w \in V$, where the bilinear form is $a(u, v) = \int_\Omega (\nabla u)^T D \nabla v$.

The models (2.6) and (2.7) are approximated in space by the finite element method (see e.g. Ref. [14]), where the domain Ω is discretized by a structured quasi-uniform grid of hexaedral isoparametric Q_1 elements. Let $V_h \subset V$ be the associated finite element space, with the same basis functions $\{\varphi_p\}_{p=1}^{N_h}$ for all variables $u_{i,e}$ and w and let $A_{i,e}$ and M be the stiffness and mass matrices with entries

$$\{A_{i,e}\}_{nm} = \int_\Omega (\nabla \varphi_n)^T D_{i,e} \nabla \varphi_m, \qquad \{M\}_{nm} = \int_\Omega \varphi_n \varphi_m.$$

By denoting with φ_l the l-th nodal basis function, the nonlinear reaction term in (2.7) is approximated by

$$(I_{\text{ion}}(v, w), \varphi_p) = \sum_{l=1}^{N_h} I_{\text{ion}}(v_l, w_l) (\varphi_l, \varphi_p).$$

With a standard Galerkin procedure, we thus need to solve at each time step, the semidiscrete Bidomain model

$$\begin{cases} \chi C_m \mathcal{M} \dfrac{\partial}{\partial t}\begin{pmatrix} \boldsymbol{u}_i \\ \boldsymbol{u}_e \end{pmatrix} + \mathcal{A}\begin{pmatrix} \boldsymbol{u}_i \\ \boldsymbol{u}_e \end{pmatrix} + \begin{pmatrix} M\, I_{\text{ion}}(\boldsymbol{v}, \boldsymbol{w}) \\ -M\, I_{\text{ion}}(\boldsymbol{v}, \boldsymbol{w}) \end{pmatrix} = \begin{pmatrix} M\, I_{\text{app}}^i \\ -M\, I_{\text{app}}^e \end{pmatrix}, \\ \dfrac{\partial \boldsymbol{w}}{\partial t} = R(\boldsymbol{v}, \boldsymbol{w}), \end{cases}$$

where

$$\mathcal{A} = \begin{bmatrix} A_i & 0 \\ 0 & A_e \end{bmatrix}, \qquad \mathcal{M} = \begin{bmatrix} M & -M \\ -M & M \end{bmatrix}. \tag{2.8}$$

Similarly, given the stiffness matrix A associated with the bilinear form $a\left(\cdot,\cdot\right)$, the semidiscrete Monodomain system reads

$$\begin{cases} \chi C_m M \dfrac{\partial \boldsymbol{v}}{\partial t} + A\boldsymbol{v} + M I_{\text{ion}}(\boldsymbol{v}, \boldsymbol{w}) = M I_{\text{app}} \\ \dfrac{\partial \boldsymbol{w}}{\partial t} = R\left(\boldsymbol{v}, \boldsymbol{w}\right). \end{cases}$$

For simplicity, from now on we write

$$\sum_l := \sum_{l=1}^{N_h}$$

assuming that we are adding contributions from all the N_h nodes of the discretization.

2.4.2 Time decoupling strategy

In the literature, one of the most common procedure for the time discretization is the implicit-explicit (IMEX) scheme, where the diffusion term is treated implicitly while the remaining terms are treated explicitly [22, 23, 26, 127]. On the other side, a fully implicit discretization in time of the Bidomain system coupled with the gating equation while using physiological coefficients, leads to the solution of a very nonlinear problem at each time step, which can be very expensive from a computational point of view. The first approach we would like to present here is a decoupling strategy, where we decouple the gating variable w from the intra and extracellular potential u_i and u_e in the following manner: at the n-th time step

1. given $u_e = u_e^n$ and $u_i = u_i^n$ (hence v), compute w^{n+1} by solving the membrane model

$$\left(w^{n+1}, \varphi_w\right) - \tau \left(R(v, w^{n+1}), \varphi_w\right) = \left(w^n, \varphi_w\right),$$

   with time step $\tau := t_{n+1} - t_n$.

2. given $w = w^{n+1}$, calculate u_e^{n+1} and u_i^{n+1} by solving the nonlinear equation $F_{bido}(u_i^{n+1}, u_e^{n+1}) = 0$ derived from the Backward Euler scheme applied to the Bidomain equations, where

$$F_{bido}(u_i^{n+1}, u_e^{n+1}) := \begin{pmatrix} F_{bido,1}(u_i^{n+1}, u_e^{n+1}) \\ F_{bido,2}(u_i^{n+1}, u_e^{n+1}) \end{pmatrix} \tag{2.9}$$

$$= \begin{pmatrix} \chi C_m \left(v^{n+1}, \varphi_i\right) + \tau a_i \left(u_i^{n+1}, \varphi_i\right) + \tau \left(I_{\text{ion}}(v^{n+1}, w), \varphi_i\right) - \left[\chi C_m \left(u_i^n, \varphi_i\right) + \tau \left(I_{\text{app}}^i, \varphi_i\right)\right] \\ -\chi C_m \left(v^{n+1}, \varphi_e\right) + \tau a_e \left(u_e^{n+1}, \varphi_e\right) - \tau \left(I_{\text{ion}}(v^{n+1}, w), \varphi_e\right) - \left[\chi C_m \left(u_e^n, \varphi_e\right) + \tau \left(I_{\text{app}}^e, \varphi_e\right)\right] \end{pmatrix}.$$

   From now on, we will omit the dependence of I_{ion} on the gating variable w, as it is given from the previous step.

2.1 Use a Newton method to solve the nonlinear system (2.9); starting from the Newton intial value (u_i^0, u_e^0), at the kth iteration of the Newton loop, we solve the linear system of equations

$$\begin{cases} \sum_l \dfrac{\partial F_{bido,1}}{\partial u_{i,l}}(u_i^k, u_e^k) s_{i,l}^{k+1} + \sum_l \dfrac{\partial F_{bido,1}}{\partial u_{e,l}}(u_i^k, u_e^k) s_{e,l}^{k+1} = -F_{bido,1}(u_i^k, u_e^k) \\ \sum_l \dfrac{\partial F_{bido,2}}{\partial u_{i,l}}(u_i^k, u_e^k) s_{i,l}^{k+1} + \sum_l \dfrac{\partial F_{bido,2}}{\partial u_{e,l}}(u_i^k, u_e^k) s_{e,l}^{k+1} = -F_{bido,2}(u_i^k, u_e^k) \end{cases}, \tag{2.10}$$

which can be explicitly written as

$$\begin{cases} \chi C_m \left(s_i^{k+1} - s_e^{k+1}, \varphi_i \right) + \tau a_i \left(s_i^{k+1}, \varphi_i \right) + \\ \qquad\qquad + \tau \left(\sum_l \dfrac{\partial I_{\text{ion}}}{\partial v_l}(v^k) \left(s_{i,l}^{k+1} - s_{e,l}^{k+1} \right) \varphi_l, \varphi_i \right) = -F_{bido,1}(u_i^k, u_e^k) \\ -\chi C_m \left(s_i^{k+1} - s_e^{k+1}, \varphi_e \right) + \tau a_e \left(s_{e,l}^{k+1}, \varphi_e \right) + \\ \qquad\qquad - \tau \left(\sum_l \dfrac{\partial I_{\text{ion}}}{\partial v_l}(v^k) \left(s_{i,l}^{k+1} - s_{e,l}^{k+1} \right) \varphi_l, \varphi_e \right) = -F_{bido,2}(u_i^k, u_e^k) \end{cases}$$

where

$$s_i^{k+1} = \delta u_i^{k+1} \qquad s_e^{k+1} = \delta u_e^{k+1}$$

are the increments at time step k, and I_{ion} is only dependent on u_i^k and u_e^k.

In matricial form, this means solving

$$\left[\left(\chi C_m + \tau \begin{pmatrix} \dfrac{\partial I_{\text{ion}}}{\partial v}(v^k, w^k) \\ -\dfrac{\partial I_{\text{ion}}}{\partial v}(v^k, w^k) \end{pmatrix} \right) \mathcal{M} + \tau \mathcal{A} \right] \begin{pmatrix} s_i^{k+1} \\ s_e^{k+1} \end{pmatrix} = \begin{pmatrix} -MF_{bido,1}(u_i^k, u_e^k) \\ -MF_{bido,2}(u_i^k, u_e^k) \end{pmatrix},$$

(2.11)

with the same stiffness and mass matrices defined in (2.8).

2.2 Update
$$u_i^{k+1} = u_i^k + s_i^{k+1}, \qquad u_e^{k+1} = u_e^k + s_e^{k+1}.$$

In the Monodomain case, the workflow is analogous: at the n-th time step

1. given $v = v^n$, compute w^{n+1} by solving the membrane model

$$\left(w^{n+1}, \varphi_w \right) - \tau \left(R(v, w^{n+1}), \varphi_w \right) = (w^n, \varphi_w)$$

2. given $w = w^{n+1}$, calculate v^{n+1} by solving the nonlinear equation $F(v^{n+1}) = 0$ derived from the Backward Euler scheme applied to the Monodomain equation, where

$$F_{mono}(v^{n+1}) := \chi C_m \left(v^{n+1}, \varphi \right) + \tau a \left(v^{n+1}, \varphi \right) + \tau \left(I_{\text{ion}}(v^{n+1}, w), \varphi \right) + \\ - \left[\chi C_m \left(v^n, \varphi \right) + \tau \left(I_{\text{app}}, \varphi \right) \right]$$

(2.12)

2.1 Use an exact Newton method to solve the nonlinear system (2.9); at the kth iteration of the Newton loop, we solve the linear equation

$$\sum_l \frac{\partial F_{mono}}{\partial v_l}(v^k) \, s_l^{k+1} = -F_{mono}(v^k),$$

(2.13)

i.e.

$$\chi C_m \left(s^{k+1}, \varphi \right) + \tau a \left(s^{k+1}, \varphi \right) + \tau \left(\sum_l \frac{\partial I_{\text{ion}}}{\partial v_l}(v^k) s_l^{k+1} \varphi_l, \varphi \right) = -F_{mono}(v^k) \,,$$

where

$$s^{k+1} = \delta v^{k+1}$$

is the increment at time step k. In matricial form, we have

$$\left[\left(\chi C_m + \tau \frac{\partial I_{\text{ion}}}{\partial v}(v^k, w^k) \right) M + \tau A \right] s^{k+1} = -MF_{mono,1}(v^k)$$

(2.14)

2.2 Update
$$v^{k+1} = v^k + s^{k+1}.$$

Properties of the bilinear form associated with the decoupled Bidomain and Monodomain Jacobian systems

We reformulate problem (2.10) in variational form: find $s^{k+1} = \left(s_i^{k+1}, s_e^{k+1}\right) \in \mathbf{V_h} = V_h \times V_h$ such that

$$a_{bido}(s^{k+1}, \phi) = -F_{bido,1}(s^k) - F_{bido,2}(s^k), \qquad \forall \phi = (\varphi_i, \varphi_e) \in \mathbf{V_h}, \tag{2.15}$$

where

$$a_{bido}(s^{k+1}, \phi) = \chi C_m \left(s_i^{k+1} - s_e^{k+1}, \varphi_i - \varphi_e\right) + \tau a_i \left(s_i^{k+1}, \varphi_i\right) + \tau a_e \left(s_e^{k+1}, \varphi_e\right)$$
$$+ \tau \left(\sum_l \frac{\partial I_{\text{ion}}}{\partial v_l}(v^k) \left(s_{i,l}^{k+1} - s_{e,l}^{k+1}\right) \varphi_l, \varphi_i - \varphi_e\right).$$

For our theoretical analysis, we need to study some properties of this bilinear form. We will need the following lemma from Ref. [116]:

Proposition 2.1. *Let Ω be a domain in $\mathbb{R}^d$ and $\mathcal{N}_h$ the set of vertices of the triangulation. Then there exists two positive constants C and c such that*

$$ch^d \sum_{x_j \in \mathcal{N}_h} v^2(x_j) \le ||v||_{L^2(\Omega)}^2 \le Ch^d \sum_{x_j \in \mathcal{N}_h} v^2(x_j).$$

We proceed first by showing that the bilinear form (2.15) is continuous and coercive with respect to the following norm defined $\forall u = (u_i, u_e) \in \mathbf{V_h}$

$$|||u|||_\tau^2 := (1 + \tau)||u_i - u_e||_{L^2(\Omega)}^2 + \tau a_i (u_i, u_i) + \tau a_e (u_e, u_e).$$

Lemma 2.1. *Assume that*

$$\chi C_m + \tau \frac{\partial I_{ion}}{\partial v_l}(v^k) \ge c > 0, \qquad c \in \mathbb{R}^+,$$

$\forall l = 1, \ldots, N_h$ and for all k. Then the bilinear form $a_{bido}(\cdot, \cdot)$ defined in (2.15) is continuous and coercive with respect to the norm $||| \cdot |||_\tau$.

Proof. We divide the proof in two parts.

(i) *Continuity.* Let $s^{k+1} = \sum_l s_l^{k+1} \varphi_l$, with φ_l being the l-th nodal basis function. We observe that using the Cauchy-Schwarz inequality, we have

$$\left(\underbrace{\sum_l \frac{\partial I_{\text{ion}}}{\partial v_l}(v^k)(s_{i,l}^{k+1} - s_{e,l}^{k+1})\varphi_l}_{=:f(x)}, \varphi_i - \varphi_e\right) = (f(x), \varphi_i(x) - \varphi_e(x))$$
$$= \int_\Omega f(x) (\varphi_i(x) - \varphi_e(x)) \, d\Omega$$
$$\le ||f(x)||_{L^2(\Omega)} ||\varphi_i(x) - \varphi_e(x)||_{L^2(\Omega)}.$$

By using Proposition (2.1) and the triangle inequality, we get

$$||f||^2_{L^2(\Omega)} \le Ch^d \sum_{x_j \in \mathcal{N}_h} \left(\sum_l \frac{\partial I_{\text{ion}}}{\partial v_l}(v^k)(s_{i,l}^{k+1} - s_{e,l}^{k+1})\varphi_l(x_j) \right)^2$$

$$= Ch^d \sum_{x_j \in \mathcal{N}_h} \left(\frac{\partial I_{\text{ion}}}{\partial v_j}(v^k)(s_{i,j}^{k+1} - s_{e,j}^{k+1}) \right)^2$$

$$\le Ch^d \sum_{x_j \in \mathcal{N}_h} \left(\frac{\partial I_{\text{ion}}}{\partial v_j}(v^k) \right)^2 \sum_{x_j \in \mathcal{N}_h} \left(s_{i,j}^{k+1} - s_{e,j}^{k+1} \right)^2 \qquad (2.16)$$

$$= Ch^d \sum_{x_j \in \mathcal{N}_h} \underbrace{\left(\sum_l \frac{\partial I_{\text{ion}}}{\partial v_l}(v^k)\varphi_l(x_j) \right)^2}_{=:f_1(x) \text{ independent of } s^{k+1}} \sum_{x_j \in \mathcal{N}_h} \left(\sum_l (s_{i,l}^{k+1} - s_{e,l}^{k+1})\varphi_l(x_j) \right)^2$$

$$\le C||f_1||^2_{L^2(\Omega)}||s^{k+1}||^2_{L^2(\Omega)} = K_M||s^{k+1}||^2_{L^2(\Omega)},$$

for a positive constant K_M, from which we can conclude

$$\left(\sum_l \frac{\partial I_{\text{ion}}}{\partial v_l}(v^k)(s_{i,l}^{k+1} - s_{e,l}^{k+1})\varphi_l, \varphi_i - \varphi_e \right) \le ||f||_{L^2(\Omega)}||\varphi_i - \varphi_e||_{L^2(\Omega)} \overset{(2.16)}{\le} K_M||s_i^{k+1} - s_e^{k+1}||_{L^2(\Omega)}||\varphi_i - \varphi_e||_{L^2(\Omega)}.$$

The continuity simply follows

$$a_{bido}(s^{k+1}, \phi) = \chi C_m \left(s_i^{k+1} - s_e^{k+1}, \varphi_i - \varphi_e \right) + \tau a_i \left(s_i^{k+1}, \varphi_i \right) + \tau a_e \left(s_e^{k+1}, \varphi_e \right) +$$

$$+ \tau \left(\sum_l \frac{\partial I_{\text{ion}}}{\partial v_l}(v^k)(s_{i,l}^{k+1} - s_{e,l}^{k+1})\varphi_l, \varphi_i - \varphi_e \right)$$

$$\le \chi C_m||s_i^{k+1} - s_e^{k+1}||_{L^2(\Omega)}||\varphi_i - \varphi_e||_{L^2(\Omega)} + \tau a_i \left(s_i^{k+1}, s_i^{k+1} \right)^{\frac{1}{2}} a_i \left(\varphi_i, \varphi_i \right)^{\frac{1}{2}} +$$

$$+ \tau a_e \left(s_e^{k+1}, s_e^{k+1} \right)^{\frac{1}{2}} a_e \left(\varphi_e, \varphi_e \right)^{\frac{1}{2}} + \tau||s_i^{k+1} - s_e^{k+1}||_{L^2(\Omega)}||\varphi_i - \varphi_e||_{L^2(\Omega)}$$

$$\le C|||s^{k+1}|||_\tau |||\phi|||_\tau.$$

(ii) *Coercivity.* Thanks to the hypothesis, we observe that

$$\chi C_m||s_i^{k+1} - s_e^{k+1}||^2_{L^2(\Omega)} + \tau \left(\sum_l \frac{\partial I_{\text{ion}}}{\partial v_l}(v^k)(s_{i,l}^{k+1} - s_{e,l}^{k+1})\varphi_l, s_i^{k+1} - s_e^{k+1} \right)$$

$$= \left(\sum_l \left(\chi C_m + \tau \frac{\partial I_{\text{ion}}}{\partial v_l}(v^k) \right)(s_{i,l}^{k+1} - s_{e,l}^{k+1})\varphi_l, \sum_p (s_{i,p}^{k+1} - s_{e,p}^{k+1})\varphi_p \right)$$

$$= \sum_l \sum_p \left(\chi C_m + \tau \frac{\partial I_{\text{ion}}}{\partial v_l}(v^k) \right)(s_{i,l}^{k+1} - s_{e,l}^{k+1})(s_{i,p}^{k+1} - s_{e,p}^{k+1})(\varphi_l, \varphi_p)$$

$$= (1 + \tau)\sum_l \sum_p \frac{1}{1+\tau} \left(\chi C_m + \tau \frac{\partial I_{\text{ion}}}{\partial v_l}(v^k) \right)(s_{i,l}^{k+1} - s_{e,l}^{k+1})(s_{i,p}^{k+1} - s_{e,p}^{k+1})(\varphi_l, \varphi_p)$$

$$\ge (1 + \tau)\min_l \left[\frac{1}{1+\tau} \left(\chi C_m + \tau \frac{\partial I_{\text{ion}}}{\partial v_l}(v^k) \right) \right]$$

$$\left(\sum_l (s_{i,l}^{k+1} - s_{e,l}^{k+1})\varphi_l, \sum_p (s_{i,p}^{k+1} - s_{e,p}^{k+1})\varphi_p \right)$$

$$\ge (1 + \tau)||s_i^{k+1} - s_e^{k+1}||^2_{L^2(\Omega)}.$$

We can conclude that

$$a_{bido}(s^{k+1}, s^{k+1}) = \chi C_m \left(s_i^{k+1} - s_e^{k+1}, s_i^{k+1} - s_e^{k+1} \right) + \tau a_i \left(s_i^{k+1}, s_i^{k+1} \right) + \tau a_e \left(s_e^{k+1}, s_e^{k+1} \right) +$$

$$+ \tau \left(\sum_l \frac{\partial I_{\text{ion}}}{\partial v_l}(v^k)(s_{i,l}^{k+1} - s_{e,l}^{k+1})\varphi_l, s_i^{k+1} - s_e^{k+1} \right)$$

$$\geq (1 + \tau)||s_i^{k+1} - s_e^{k+1}||_{L^2(\Omega)}^2 + \tau a_i \left(s_i^{k+1}, s_i^{k+1} \right) + \tau a_e \left(s_e^{k+1}, s_e^{k+1} \right)$$

$$= |||s^{k+1}|||_\tau^2.$$

$\square$

Remark 2.1. We do observe that the hyptothesis of non-negativity of Lemma 2.1 is always satisfied for any time step $\tau \leq 0.37$ ms, using the Rogers-McCulloch ionic model. Indeed, numerical computations of $\chi C_m + \tau \frac{\partial I_{\text{ion}}}{\partial v}$ validate this assumption (see Fig. 2.9). Although we have not verified the validity of the non-negativity assumption for more general membrane models, we have numerically tested the convergence rate estimate of Section 4.1 also with the Luo-Rudy phase 1 and Ten-Tusscher ionic models (see Chap. 6).

Remark 2.2. The hypothesis of non-negativity also guarantees that the matrix of the system (2.11) is non singular. Hence, this ensures that the local problems are well-posed.
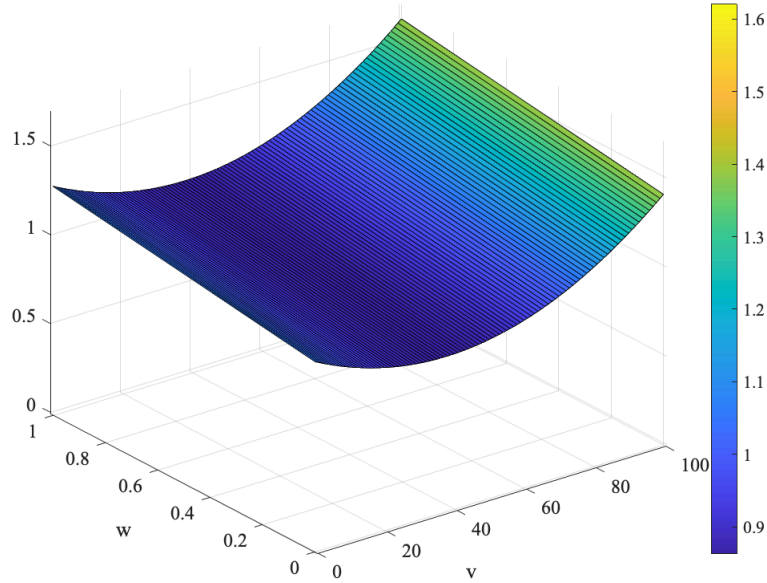
Figure 2.9: Surface plot of $\chi C_m + \tau \frac{\partial I_{\text{ion}}}{\partial v}$, with $C_m = 1 \frac{mF}{cm^3}$, $\chi = 1$ and $\tau = 0.05$ ms, which are values usually employed in numerical experiments.

As an immediate consequence of the continuity and coercivity of the bilinear form a_{bido}, it is possible to prove the following bounds, which will be useful in the convergence rate estimate.

We can drop the index k from now on, unless an explicit ambiguity occurs.

Lemma 2.2. *Assuming that the conductivity coefficients are constant in space, the bilinear form a_{bido} (2.15) satisfies the bounds*

$$a_{bido}(s, s) \leq (\chi C_m + \tau K_M) ||s_i - s_e||_{L^2(\Omega)}^2 + \tau \sigma_M^i |s_i|_{H^1(\Omega)}^2 + \tau \sigma_M^e |s_e|_{H^1(\Omega)}^2,$$

$$a_{bido}(s, s) \geq (\chi C_m + \tau K_m) ||s_i - s_e||_{L^2(\Omega)}^2 + \tau \sigma_m^i |s_i|_{H^1(\Omega)}^2 + \tau \sigma_m^e |s_e|_{H^1(\Omega)}^2,$$

where

$$\sigma_M^{i,e} = \max_{\bullet = \{l,t,n\}} \sigma_\bullet^{i,e}, \qquad \sigma_m^{i,e} = \min_{\bullet = \{l,t,n\}} \sigma_\bullet^{i,e},$$

and K_M, K_m are constants independent of the mesh size h.

Proof. Using the same arguments as in the continuity proof, it holds

$$a_{bido}(s,s) \leq \chi C_m ||s_i - s_e||^2_{L^2(\Omega)} + \tau \sigma^i_M |s_i|^2_{H^1(\Omega)} + \tau \sigma^e_M |s_e|^2_{H^1(\Omega)} +$$

$$+ \tau \left(\sum_l \frac{\partial I_{\text{ion}}}{\partial v_l}(v)\,(s_{i,l} - s_{e,l})\,\varphi_l, s_i - s_e \right)$$

$$\leq (\chi C_m + \tau K_M) \, ||s_i - s_e||^2_{L^2(\Omega)} + \tau \sigma^i_M |s_i|^2_{H^1(\Omega)} + \tau \sigma^e_M |s_e|^2_{H^1(\Omega)},$$

where K_M is the constant related to the upper bound of the reaction term, see inequalities (2.16).

Concerning the second bound, it is straightforward to show that

$$\left(\sum_l \frac{\partial I_{\text{ion}}}{\partial v_l}(v)(s_{i,l} - s_{e,l})\varphi_l, s_i - s_e \right) = \left(\sum_l \frac{\partial I_{\text{ion}}}{\partial v_l}(v)(s_{i,l} - s_{e,l})\varphi_l, \sum_p (s_{i,p} - s_{e,p})\varphi_p \right)$$

$$= \sum_l \sum_p \frac{\partial I_{\text{ion}}}{\partial v_l}(v)(s_{i,l} - s_{e,l})(s_{i,p} - s_{e,p}) \, (\varphi_l, \varphi_p)$$

$$\geq \min_l \frac{\partial I_{\text{ion}}}{\partial v_l}(v) \left(\sum_l (s_{i,l} - s_{e,l})\varphi_l, \sum_p (s_{i,p} - s_{e,p})\varphi_p \right)$$

$$\geq K_m ||s_i - s_e||^2_{L^2(\Omega)}.$$

It follows

$$a_{bido}(s,s) \geq \chi C_m ||s_i - s_e||^2_{L^2(\Omega)} + \tau \sigma^i_m |s_i|^2_{H^1(\Omega)} + \tau \sigma^e_m |s_e|^2_{H^1(\Omega)} +$$

$$+ \tau \left(\sum_l \frac{\partial I_{\text{ion}}}{\partial v_l}(v)\,(s_{i,l} - s_{e,l})\,\varphi_l, s_i - s_e \right)$$

$$\geq (\chi C_m + \tau K_m) \, ||s_i - s_e||^2_{L^2(\Omega)} + \tau \sigma^i_m |s_i|^2_{H^1(\Omega)} + \tau \sigma^e_m |s_e|^2_{H^1(\Omega)}.$$

$\square$

Remark 2.3. This result can be easily extended to the case of conductivity coefficients almost constant over each subdomain.

In the same fashion, we can prove analogous properties for the Monodomain Jacobian system. Define a variational formulation of the problem (2.13): find $s^{k+1} \in V_h$ such that

$$a_{mono}(s^{k+1}, \varphi) = -F_{mono} \qquad \forall \varphi \in V_h,$$

where

$$a_{mono}(s^{k+1}, \varphi) = \chi C_m \left(s^{k+1}, \varphi \right) + \tau a \left(s^{k+1}, \varphi \right) + \tau \left(\sum_l \frac{\partial I_{\text{ion}}}{\partial v_l}(v^k) s^{k+1}_l \varphi_l, \varphi \right).$$

We again define a norm $||| \cdot |||_{\tau, mono}$,

$$\forall u \in V_h \qquad |||u|||^2_{\tau, mono} := (1 + \tau)||u||^2_{L^2(\Omega)} + \tau a \, (u, u) \,,$$

and we can prove that the bilinear form a_{mono} is continuous and coercive w.r.t. this norm. Also in this case, the hypothesis of non negativity is fullfilled (see Remark 2.1).

Lemma 2.3. *Assume that*

$$\chi C_m + \tau \frac{\partial I_{ion}}{\partial v_l}(v^k) \geq c > 0, \qquad\qquad c \in \mathbb{R}^+,$$

$\forall l = 1, \dots, N$ *and for all k. Then the bilinear form $a_{mono}(\cdot, \cdot)$ defined in (2.4.2) is continuous and coercive with respect to the norm $||| \cdot |||_{\tau, mono}$.*

Proof. As in the Bidomain case, we divide the proof in two parts.

(i) *Continuity.* Let $s^{k+1} = \sum_l s_l^{k+1} \varphi_l$. Using Cauchy-Schwarz inequality, we have

$$\left(\underbrace{\sum_l \frac{\partial I_{\text{ion}}}{\partial v_l}(v^k) s_l^{k+1} \varphi_l}_{=:f(x)}, \varphi \right) = (f(x), \varphi(x)) = \int_\Omega f(x)\varphi(x) \, d\Omega \le ||f||_{L^2(\Omega)}||\varphi||_{L^2(\Omega)}.$$

By using Proposition (2.1) and the triangle inequality, we get

$$\begin{aligned}
||f||_{L^2(\Omega)}^2 &\le C h^d \sum_{x_j \in \mathcal{N}_h} \left(\sum_l \frac{\partial I_{\text{ion}}}{\partial v_l}(v^k) s_l^{k+1} \varphi_l(x_j) \right)^2 \\
&\le C h^d \sum_{x_j \in \mathcal{N}_h} \left(\frac{\partial I_{\text{ion}}}{\partial v_j}(v^k) \right)^2 \sum_{x_j \in \mathcal{N}_h} \left(s_j^{k+1} \right)^2 \\
&= C h^d \sum_{x_j \in \mathcal{N}_h} \underbrace{\left(\sum_l \frac{\partial I_{\text{ion}}}{\partial v_l}(v^k) \varphi_l(x_j) \right)^2}_{=:f_1(x) \text{ independent of } s^{k+1}} \sum_{x_j \in \mathcal{N}_h} \sum_l s_l^{k+1} \varphi_l(x_j) \\
&\le ||f_1||_{L^2(\Omega)}^2 ||s^{k+1}||_{L^2(\Omega)}^2 = K_M ||s^{k+1}||_{L^2(\Omega)}^2,
\end{aligned} \quad (2.17)$$

from which we can conclude

$$\left(\sum_l \frac{\partial I_{\text{ion}}}{\partial v_l}(v^k) s_l^{k+1} \varphi_l, \varphi \right) \le ||f||_{L^2(\Omega)}||\varphi||_{L^2(\Omega)} \overset{(2.17)}{\le} K_M ||s^{k+1}||_{L^2(\Omega)}||\varphi||_{L^2(\Omega)}.$$

The continuity simply follows

$$\begin{aligned}
a_{mono}(s^{k+1}, \varphi) &= \chi C_m \left(s^{k+1}, \varphi \right) + \tau a \left(s^{k+1}, \varphi \right) + \tau \left(\sum_l \frac{\partial I_{\text{ion}}}{\partial v_l}(v^k) s_l^{k+1} \varphi_l, \varphi \right) \\
&\le (1 + \tau) ||s^{k+1}||_{L^2(\Omega)}||\varphi||_{L^2(\Omega)} + \tau a \left(s^{k+1}, s^{k+1} \right)^{\frac{1}{2}} a \left(\varphi, \varphi \right)^{\frac{1}{2}} \\
&\le C |||s^{k+1}|||_{\tau,mono} |||\varphi|||_{\tau,mono}.
\end{aligned}$$

(ii) *Coercivity.* Thanks to the hypothesis, we observe that

$$\begin{aligned}
\chi C_m &\left(s^{k+1}, s^{k+1} \right) + \tau \left(\sum_l \frac{\partial I_{\text{ion}}}{\partial v_l}(v^k) s_l^{k+1} \varphi_l, s^{k+1} \right) \\
&= \left(\sum_l \left(\chi C_m + \tau \frac{\partial I_{\text{ion}}}{\partial v_l}(v^k) \right) s_l^{k+1} \varphi_l, \sum_p s_p^{k+1} \varphi_p \right) \\
&= \sum_l \sum_p \left(\chi C_m + \tau \frac{\partial I_{\text{ion}}}{\partial v_l}(v^k) \right) s_l^{k+1} s_p^{k+1} (\varphi_l, \varphi_p) \\
&= (1 + \tau) \sum_l \sum_p \frac{1}{1+\tau} \left(\chi C_m + \tau \frac{\partial I_{\text{ion}}}{\partial v_l}(v^k) \right) s_l^{k+1} s_p^{k+1} (\varphi_l, \varphi_p) \\
&\ge (1 + \tau) \min_l \left[\frac{1}{1+\tau} \left(\chi C_m + \tau \frac{\partial I_{\text{ion}}}{\partial v_l}(v^k) \right) \right] \left(\sum_l s_l^{k+1} \varphi_l, \sum_p s_p^{k+1} \varphi_p \right) \\
&\ge (1 + \tau) ||s^{k+1}||_{L^2(\Omega)}^2.
\end{aligned}$$

We can conclude that

$$a_{mono}(s^{k+1}, s^{k+1}) = \chi C_m \left(s^{k+1}, s^{k+1}\right) + \tau a \left(s^{k+1}, s^{k+1}\right) + \tau \left(\sum_l \frac{\partial I_{\text{ion}}}{\partial v_l}(v^k)s_l^{k+1}\varphi_l, s^{k+1}\right)$$

$$\geq (1+\tau)||s^{k+1}||_{L^2(\Omega)}^2 + \tau a \left(s^{k+1}, s^{k+1}\right) = |||s^{k+1}|||_{\tau, mono}^2.$$

$\square$

It is then easy to show the Monodomain bounds analogous to the bounds of Lemma 2.2.

Lemma 2.4. *The bilinear form a_{mono} satisfy the bounds*

$$a_{mono}(s, s) \leq (\chi C_m + \tau K_M) ||s||_{L^2(\Omega)}^2 + \tau \sigma_M |s|_{H^1(\Omega)}^2,$$

$$a_{mono}(s, s) \geq (\chi C_m + \tau K_m) ||s||_{L^2(\Omega)}^2 + \tau \sigma_m |s|_{H^1(\Omega)}^2,$$

where

$$\sigma_M = \max_{\bullet = \{l, t, n\}} \sigma_\bullet, \qquad \sigma_m = \min_{\bullet = \{l, t, n\}} \sigma_\bullet,$$

and K_M, K_m are constant independent of the mesh size h.

2.4.3 Fully implicit time schemes

As alternative to the decoupling strategy proposed in the previous section as well as in References [88, 89, 109], the second approach we propose is a fully implicit time discretization of the Bidomain system, in the same fashion as in Ref. [90], where we deal with a monolithic nonlinear system. At the n-th time step,

1. compute the intra- and extracellular potentials as well as the gating variables by solving the nonlinear system $F(u_i^{n+1}, u_e^{n+1}, w^{n+1}) = 0$ derived from the Backward Euler scheme applied to the Bidomain system,

$$F(u_i^{n+1}, u_e^{n+1}, w^{n+1}) := \begin{pmatrix} F_1(u_i^{n+1}, u_e^{n+1}, w^{n+1}) \\ F_2(u_i^{n+1}, u_e^{n+1}, w^{n+1}) \\ F_3(u_i^{n+1}, u_e^{n+1}, w^{n+1}) \end{pmatrix} \tag{2.18}$$

$$= \begin{pmatrix} \chi C_m \left(v^{n+1}, \varphi_i\right) + \tau a_i \left(u_i^{n+1}, \varphi_i\right) + \tau \left(I_{\text{ion}}(v^{n+1}, w), \varphi_i\right) - \left[\chi C_m \left(v^n, \varphi_i\right) + \tau \left(I_{\text{app}}^i, \varphi_i\right)\right] \\ -\chi C_m \left(v^{n+1}, \varphi_e\right) + \tau a_e \left(u_e^{n+1}, \varphi_e\right) - \tau \left(I_{\text{ion}}(v^{n+1}, w), \varphi_e\right) - \left[\chi C_m \left(v^n, \varphi_e\right) + \tau \left(I_{\text{app}}^e, \varphi_e\right)\right] \\ \left(w^{n+1}, \varphi_w\right) - \tau \left(R(v^{n+1}, w^{n+1}), \varphi_w\right) - \left(w^n, \varphi_w\right) \end{pmatrix},$$

    where φ_i, φ_e and φ_w are the test functions related to u_i, u_e and w respectively.

2.1 Apply an exact Newton method for the solution of the nonlinear system (2.18); given the initial guess (u_i^0, u_e^0, w^0), at the kth iteration of the Newton loop, solve the linear system of equations

$$\begin{cases} \sum_l \dfrac{\partial F_1}{\partial u_{i,l}}(u_i^k, u_e^k, w^k)s_{i,l}^{k+1} + \sum_l \dfrac{\partial F_1}{\partial u_{e,l}}(u_i^k, u_e^k, w^k)s_{i,l}^{k+1} + \\ \qquad\qquad + \sum_l \dfrac{\partial F_1}{\partial w_l}(u_i^k, u_e^k, w^k)s_{i,l}^{k+1} = -F_1(u_i^k, u_e^k, w^k) \\[2mm] \sum_l \dfrac{\partial F_2}{\partial u_{i,l}}(u_i^k, u_e^k, w^k)s_{e,l}^{k+1} + \sum_l \dfrac{\partial F_2}{\partial u_{e,l}}(u_i^k, u_e^k, w^k)s_{e,l}^{k+1} + \\ \qquad\qquad + \sum_l \dfrac{\partial F_2}{\partial w_l}(u_i^k, u_e^k, w^k)s_{e,l}^{k+1} = -F_2(u_i^k, u_e^k, w^k) \\[2mm] \sum_l \dfrac{\partial F_3}{\partial u_{i,l}}(u_i^k, u_e^k, w^k)s_{w,l}^{k+1} + \sum_l \dfrac{\partial F_3}{\partial u_{e,l}}(u_i^k, u_e^k, w^k)s_{w,l}^{k+1} + \\ \qquad\qquad + \sum_l \dfrac{\partial F_3}{\partial w_l}(u_i^k, u_e^k, w^k)s_{w,l}^{k+1} = -F_3(u_i^k, u_e^k, w^k) \end{cases}, \tag{2.19}$$

explicitly written as

$$
\begin{cases}
\chi C_m \left(s_i^{k+1} - s_e^{k+1}, \varphi_i\right) + \tau a_i \left(s_i^{k+1}, \varphi_i\right) + \tau \left(\sum_l \frac{\partial I_{\text{ion}}}{\partial v_l}(v^k, w^k) \left(s_{i,l}^{k+1} - s_{e,l}^{k+1}\right) \psi_l, \varphi_i\right) \\
\qquad + \tau \left(\sum_l \frac{\partial I_{\text{ion}}}{\partial w_l}(v^k, w^k) s_{w,l}^{k+1} \; \psi_l, \varphi_i\right) = -F_1(u_i^k, u_e^k, w^k) \\
-\chi C_m \left(s_i^{k+1} - s_e^{k+1}, \varphi_e\right) + \tau a_e \left(s_e^{k+1}, \varphi_e\right) - \tau \left(\sum_l \frac{\partial I_{\text{ion}}}{\partial v_l}(v^k, w^k) \left(s_{i,l}^{k+1} - s_{e,l}^{k+1}\right) \psi_l, \varphi_e\right) \\
\qquad - \tau \left(\sum_l \frac{\partial I_{\text{ion}}}{\partial w_l}(v^k, w^k) s_{w,l}^{k+1} \; \psi_l, \varphi_e\right) = -F_2(u_i^k, u_e^k, w^k) \\
\left(s_w^{k+1}, \varphi_k\right) - \tau \left(\sum_l \frac{\partial R}{\partial v_l}(v^k, w^k) \left(s_{i,l}^{k+1} - s_{e,l}^{k+1}\right) \psi_l, \varphi_w\right) \\
\qquad - \tau \left(\sum_l \frac{\partial R}{\partial w_l}(v^k, w^k) s_w^{k+1} \; \psi_l, \varphi_w\right) = -F_3(u_i^k, u_e^k, w^k),
\end{cases}
$$

where

$$
s_i^{k+1} = \sum_l s_{i,l}^{k+1} = \delta u_i^{k+1}, \qquad s_e^{k+1} = \sum_l s_{e,l}^{k+1} = \delta u_e^{k+1}, \qquad s_w^{k+1} = \sum_l s_{w,l}^{k+1} = \delta w^{k+1}
$$

are the increments at time step k and ψ_l the l-th nodal basis function. In matricial form, this means solving the linear system

$$
\mathbf{JF}^k \mathbf{s}^{k+1} = -\mathbf{F}(\mathbf{u}^k), \tag{2.20}
$$

where

$$
\mathbf{JF}^k = \begin{bmatrix}
\chi C_m M + \tau A_i + \tau M \frac{\partial I_{\text{ion}}}{\partial v}(\mathbf{v}^k, \mathbf{w}^k) & -\chi C_m M - \tau M \frac{\partial I_{\text{ion}}}{\partial v}(\mathbf{v}^k, \mathbf{w}^k) & \tau M \frac{\partial I_{\text{ion}}}{\partial w}(\mathbf{v}^k, \mathbf{w}^k) \\
-\chi C_m M - \tau M \frac{\partial I_{\text{ion}}}{\partial v}(\mathbf{v}^k, \mathbf{w}^k) & \chi C_m M + \tau A_e + \tau M \frac{\partial I_{\text{ion}}}{\partial v}(\mathbf{v}^k, \mathbf{w}^k) & -\tau M \frac{\partial I_{\text{ion}}}{\partial w}(\mathbf{v}^k, \mathbf{w}^k) \\
-\tau M \frac{\partial R}{\partial v}(\mathbf{v}^k, \mathbf{w}^k) & \tau M \frac{\partial R}{\partial v}(\mathbf{v}^k, \mathbf{w}^k) & \left(1 - \tau \frac{\partial R}{\partial w}(\mathbf{v}^k, \mathbf{w}^k)\right) M
\end{bmatrix}
$$

$$
\mathbf{s}^{k+1} = \begin{pmatrix} \mathbf{s_i}^{k+1} \\ \mathbf{s_e}^{k+1} \\ \mathbf{w}^{k+1} \end{pmatrix}, \qquad \mathbf{F}(\mathbf{u}^k) = \begin{pmatrix} -M F_1(\mathbf{u}_i^k, \mathbf{u}_e^k, \mathbf{w}^k) \\ -M F_2(\mathbf{u}_i^k, \mathbf{u}_e^k, \mathbf{w}^k) \\ -M F_3(\mathbf{u}_i^k, \mathbf{u}_e^k, \mathbf{w}^k) \end{pmatrix},
$$

with the same stiffness and mass matrices defined in (2.8).

2.2 Update

$$
u_i^{k+1} = u_i^k + s_i^{k+1}, \qquad u_e^{k+1} = u_e^k + s_e^{k+1}, \qquad w^{k+1} = w^k + s_w^{k+1}.
$$

Again, we drop the index k from now on, unless an explicit ambiguity occurs.

Properties of the symmetric part of the bilinear form associated with the Bidomain Jacobian system

The Jacobian linear system $\mathbf{JF}$ in 2.20 is non-symmetric, due to the inclusion of the ionic model. For this reason, the iterative solver we adopt must address the solution of such type of system, such as the Generalized Minimal Residual (GMRES) method (see Ref. [106]).
Following the work in Ref. [121] (where BDDC preconditioners are applied to the solution of non-symmetric problems arising from the discretization of advection-diffusion PDEs) in order to

properly prove the convergence rate estimate of the solver, we need to associate to the Jacobian system (2.20) a bilinear form and to analyze its symmetric and skew-symmetric parts.

We reformulate problem (2.19) in variational form: find $s = (s_i, s_e, s_w) \in \mathbf{V_h} = V_h \times V_h \times V_h$ such that

$$a(s, \phi) = -F_1(s) - F_2(s) - F_3(s) \qquad \forall \phi = (\varphi_i, \varphi_e, \varphi_w) \in \mathbf{V_h}, \tag{2.21}$$

where

$$
\begin{aligned}
a(s, \phi) = {} & \chi C_m \left(s_i - s_e, \varphi_i - \varphi_e \right) + (s_w, \varphi_w) + \tau a_i \left(s_i, \varphi_i \right) + \tau a_e \left(s_e, \varphi_e \right) \\
& + \tau \left(\sum_l \frac{\partial I_{\text{ion}}}{\partial v_l}(v, w)\, (s_{i,l} - s_{e,l})\, \psi_l, \varphi_i - \varphi_e \right) + \tau \left(\sum_l \frac{\partial I_{\text{ion}}}{\partial w_l}(v, w) s_{w,l}\ \psi_l, \varphi_i - \varphi_e \right) \\
& - \tau \left(\sum_l \frac{\partial R}{\partial v_l}(v, w)\, (s_{i,l} - s_{e,l})\, \psi_l, \varphi_w \right) - \tau \left(\sum_l \frac{\partial R}{\partial w_l}(v, w) s_{w,l}\ \psi_l, \varphi_w \right),
\end{aligned}
$$

being ψ_l the l-th nodal basis function. The symmetric and skew-symmetric parts of $a(s, \phi)$ respectively are denoted by

$$
\begin{aligned}
q(s, \phi) = {} & 2\chi C_m \left(s_i - s_e, \varphi_i - \varphi_e \right) + 2 \left(s_w, \varphi_w \right) + 2\tau a_i \left(s_i, \varphi_i \right) + 2\tau a_e \left(s_e, \varphi_e \right) \\
& + 2\tau \left(\sum_l \frac{\partial I_{\text{ion}}}{\partial v_l}(v, w)\, (s_{i,l} - s_{e,l})\, \psi_l, \varphi_i - \varphi_e \right) - 2\tau \left(\sum_l \frac{\partial R}{\partial w_l}(v, w) s_{w,l}\ \psi_l, \varphi_w \right) \\
& + \tau \left(\sum_l \frac{\partial I_{\text{ion}}}{\partial w_l}(v, w)\, (s_{i,l} - s_{e,l})\, \psi_l, \varphi_w \right) + \tau \left(\sum_l \frac{\partial I_{\text{ion}}}{\partial w_l}(v, w) s_{w,l}\ \psi_l, \varphi_i - \varphi_e \right) \\
& - \tau \left(\sum_l \frac{\partial R}{\partial v_l}(v, w)\, (s_{i,l} - s_{e,l})\, \psi_l, \varphi_w \right) - \tau \left(\sum_l \frac{\partial R}{\partial v_l}(v, w) s_{w,l}\ \psi_l, \varphi_i - \varphi_e \right)
\end{aligned}
$$

and

$$
\begin{aligned}
z(s, \phi) = {} & -\tau \left(\sum_l \frac{\partial I_{\text{ion}}}{\partial w_l}(v, w)\, (s_{i,l} - s_{e,l})\, \psi_l, \varphi_w \right) + \tau \left(\sum_l \frac{\partial I_{\text{ion}}}{\partial w_l}(v, w) s_{w,l}\ \psi_l, \varphi_i - \varphi_e \right) \\
& - \tau \left(\sum_l \frac{\partial R}{\partial v_l}(v, w)\, (s_{i,l} - s_{e,l})\, \psi_l, \varphi_w \right) + \tau \left(\sum_l \frac{\partial R}{\partial v_l}(v, w) s_{w,l}\ \psi_l, \varphi_i - \varphi_e \right)
\end{aligned}
$$

In the same way, the system of linear equations (2.19) correspond to the finite element problem (2.21), we can denote by Q and Z the symmetric and skew-symmetric parts of $\mathbf{JF}$, which correspond to the bilinear forms $q(\cdot, \cdot)$ and $z(\cdot, \cdot)$ respectively:

$$
Q = \begin{bmatrix}
2\left(\chi C_m M + \tau A_i + \tau M \dfrac{\partial I_{\text{ion}}}{\partial v} \right) & 2\left(-\chi C_m M - \tau M \dfrac{\partial I_{\text{ion}}}{\partial v} \right) & \tau M \left(\dfrac{\partial I_{\text{ion}}}{\partial w} - \dfrac{\partial R}{\partial v} \right) \\[2ex]
2\left(-\chi C_m M - \tau M \dfrac{\partial I_{\text{ion}}}{\partial v} \right) & 2\left(\chi C_m M + \tau A_e + \tau M \dfrac{\partial I_{\text{ion}}}{\partial v} \right) & -\tau M \left(\dfrac{\partial I_{\text{ion}}}{\partial w} - \dfrac{\partial R}{\partial v} \right) \\[2ex]
\tau M \left(\dfrac{\partial I_{\text{ion}}}{\partial w} - \dfrac{\partial R}{\partial v} \right) & -\tau M \left(\dfrac{\partial I_{\text{ion}}}{\partial w} - \dfrac{\partial R}{\partial v} \right) & 2\left(1 - \tau \dfrac{\partial R}{\partial w} \right) M
\end{bmatrix},
$$

$$
Z = \begin{bmatrix}
0 & 0 & \tau M \left(\dfrac{\partial I_{\text{ion}}}{\partial w} + \dfrac{\partial R}{\partial v} \right) \\[2ex]
0 & 0 & -\tau M \left(\dfrac{\partial I_{\text{ion}}}{\partial w} + \dfrac{\partial R}{\partial v} \right) \\[2ex]
-\tau M \left(\dfrac{\partial I_{\text{ion}}}{\partial w} + \dfrac{\partial R}{\partial v} \right) & \tau M \left(\dfrac{\partial I_{\text{ion}}}{\partial w} + \dfrac{\partial R}{\partial v} \right) & 0
\end{bmatrix},
$$

where we simplify the notation by writing $\dfrac{\partial g}{\partial \bullet} := \dfrac{\partial g}{\partial \bullet}(\mathbf{v}, \mathbf{w})$, with $g = \{I_{\text{ion}}, R\}$ and $\bullet = \{v, w\}$.

In the same spirit as in the decoupled approach, it is possible to show that the symmetric bilinear form $q(\cdot, \cdot)$ is continuous and coercive with respect to the following norm defined as

$$|||u|||^2_{\tau,coup} := (1 + \tau)||u_1 - u_2||^2_{L^2(\Omega)} + (1 - \tau)||u_3||^2_{L^2(\Omega)} + \tau a_i(u_1, u_1) + \tau a_e(u_2, u_2)$$

$\forall u = (u_1, u_2, u_3) \in \mathbf{V_h}$.

Lemma 2.5. *Assume that*

$$\chi C_m + \tau \frac{\partial I_{ion}}{\partial v_l}(v, w) \geq c_1 > 0, \quad 1 - \tau \frac{\partial R}{\partial w_l}(v, w) \geq c_2 > 0, \quad \frac{\partial I_{ion}}{\partial w_l}(v, w) - \frac{\partial R}{\partial v_l}(v, w) \geq 0,$$

$c_{1,2} \in \mathbb{R}^+$ *and* $\forall l = 1, \ldots, N$. *Then the bilinear form* $q(\cdot, \cdot)$ *is continuous and coercive with respect to the norm* $||| \cdot |||_{\tau,coup}$.

Proof. (i) **Continuity**. Let $s = \sum_l s_l \psi_l$. By using the Cauchy-Schwarz inequality, we have

$$\left(\underbrace{\sum_l \frac{\partial I_{\text{ion}}}{\partial v_l}(v, w)(s_{i,l} - s_{e,l})\psi_l}_{=:f(x)}, \varphi_i - \varphi_e \right) = (f(x), \varphi_i(x) - \varphi_e(x))$$

$$= \int_\Omega f(x)(\varphi_i(x) - \varphi_e(x))\, d\Omega$$

$$\leq ||f(x)||_{L^2(\Omega)}||\varphi_i(x) - \varphi_e(x)||_{L^2(\Omega)}.$$

By using Proposition 2.1 and the triangle inequality, we get

$$||f||^2_{L^2(\Omega)} \leq Ch^d \sum_{x_j \in \mathcal{N}_h} \left(\sum_l \frac{\partial I_{\text{ion}}}{\partial v_l}(v, w)(s_{i,l} - s_{e,l})\psi_l(x_j) \right)^2$$

$$= Ch^d \sum_{x_j \in \mathcal{N}_h} \left(\frac{\partial I_{\text{ion}}}{\partial v_j}(v, w)(s_{i,j} - s_{e,j}) \right)^2$$

$$\leq Ch^d \sum_{x_j \in \mathcal{N}_h} \left(\frac{\partial I_{\text{ion}}}{\partial v_j}(v, w) \right)^2 \sum_{x_j \in \mathcal{N}_h} (s_{i,j} - s_{e,j})^2$$

$$= Ch^d \sum_{x_j \in \mathcal{N}_h} \underbrace{\left(\sum_l \frac{\partial I_{\text{ion}}}{\partial v_l}(v, w)\psi_l(x_j) \right)^2}_{=:f_1(x) \text{ independent from } s_i, s_e} \sum_{x_j \in \mathcal{N}_h} \left(\sum_l (s_{i,l} - s_{e,l})\psi_l(x_j) \right)^2$$

$$\leq ||f_1||^2_{L^2(\Omega)}||s_i - s_e||^2_{L^2(\Omega)} = C_{I_v}||s_i - s_e||^2_{L^2(\Omega)},$$

from which we can conclude

$$\left(\sum_l \frac{\partial I_{\text{ion}}}{\partial v_l}(v, w)(s_{i,l} - s_{e,l})\psi_l, \varphi_i - \varphi_e \right) \leq C_{I_v}||s_i - s_e||_{L^2(\Omega)}||\varphi_i - \varphi_e||_{L^2(\Omega)}.$$

Following the same arguments, it is possible to see that similar bounds hold:

$$\left(\sum_l \frac{\partial R}{\partial w_l}(v, w)s_{w,l}\ \psi_l, \varphi_w \right) \leq C_{R_w}||s_w||_{L^2(\Omega)}||\varphi_w||_{L^2(\Omega)},$$

$$\left(\sum_l \frac{\partial I_{\text{ion}}}{\partial w_l}(v, w)(s_{i,l} - s_{e,l})\ \psi_l, \varphi_w \right) \leq C_{I_w}||s_i - s_e||_{L^2(\Omega)}||\varphi_w||_{L^2(\Omega)},$$

$$\left(\sum_l \frac{\partial R}{\partial v_l}(v, w)(s_{i,l} - s_{e,l})\ \psi_l, \varphi_w \right) \leq C_{R_v}||s_i - s_e||_{L^2(\Omega)}||\varphi_w||_{L^2(\Omega)},$$

$$\left(\sum_l \frac{\partial I_{\text{ion}}}{\partial w_l}(v,w)s_{w,l}\ \psi_l, \varphi_i - \varphi_e \right) \le C_{I_w}||s_w||_{L^2(\Omega)}||\varphi_i - \varphi_e||_{L^2(\Omega)},$$

$$\left(\sum_l \frac{\partial R}{\partial v_l}(v,w)s_{w,l}\ \psi_l, \varphi_i - \varphi_e \right) \le C_{R_v}||s_w||_{L^2(\Omega)}||\varphi_i - \varphi_e||_{L^2(\Omega)},$$

where C_{R_w}, C_{I_w}, C_{R_v} come out from the computation of the counterpart of the norm. The continuity follows easily:

$$q(s,\phi) \le 2\left(\chi C_m + \tau C_{I_v}\right)||s_i - s_e||_{L^2(\Omega)}||\varphi_i - \varphi_e||_{L^2(\Omega)} + 2\left(1 - \tau C_{R_w}\right)||s_w||_{L^2(\Omega)}||\varphi_w||_{L^2(\Omega)}$$

$$+ 2\tau a_i \left(s_i, s_i\right)^{\frac{1}{2}} a_i \left(\varphi_i, \varphi_i\right)^{\frac{1}{2}} + 2\tau a_e \left(s_e, s_e\right)^{\frac{1}{2}} a_e \left(\varphi_e, \varphi_e\right)^{\frac{1}{2}}$$

$$+ \tau \left(C_{I_w} - C_{R_v}\right)\left[||s_i - s_e||_{L^2(\Omega)}||\varphi_w||_{L^2(\Omega)} + ||s_w||_{L^2(\Omega)}||\varphi_i - \varphi_e||_{L^2(\Omega)} \right]$$

$$\le C|||s|||_{\tau,coup}|||\phi|||_{\tau,coup},$$

provided that $(C_{I_w} - C_{R_v}) \le 0$.

(ii) **Coercivity**. Thanks to the hypothesis, we observe

- $\chi C_m ||s_i - s_e||^2_{L^2(\Omega)} + \tau\left(\sum_l \frac{\partial I_{\text{ion}}}{\partial v_l}(v,w)(s_{i,l} - s_{e,l})\psi_l, s_i - s_e \right)$

$$= \left(\sum_l \left(\chi C_m + \tau\frac{\partial I_{\text{ion}}}{\partial v_l}(v,w) \right)(s_{i,l} - s_{e,l})\psi_l, \sum_p (s_{i,p} - s_{e,p})\psi_p \right)$$

$$= \sum_l \sum_p \left(\chi C_m + \tau\frac{\partial I_{\text{ion}}}{\partial v_l}(v,w) \right)(s_{i,l} - s_{e,l})(s_{i,p} - s_{e,p})(\psi_l, \psi_p)$$

$$= (1+\tau)\sum_l \sum_p \frac{1}{1+\tau}\left(\chi C_m + \tau\frac{\partial I_{\text{ion}}}{\partial v_l}(v,w) \right)(s_{i,l} - s_{e,l})(s_{i,p} - s_{e,p})(\psi_l, \psi_p)$$

$$\ge (1+\tau)\min_l\left[\frac{1}{1+\tau}\left(\chi C_m + \tau\frac{\partial I_{\text{ion}}}{\partial v_l}(v,w) \right) \right]\left(\sum_l (s_{i,l} - s_{e,l})\psi_l, \sum_p (s_{i,p} - s_{e,p})\psi_p \right)$$

$$\ge (1+\tau)||s_i - s_e||^2_{L^2(\Omega)}$$

- $||s_w||^2_{L^2(\Omega)} - \tau\left(\sum_l \frac{\partial R}{\partial w_l}(v,w)s_{w,l}\ \psi_l, s_w \right)$

$$= \left(\sum_l \left(1 - \tau\frac{\partial R}{\partial w_l}(v,w) \right)s_{w,l}\ \psi_l, \sum_p s_{w,p}\ \psi_p \right)$$

$$= \sum_l \sum_p \left(1 - \tau\frac{\partial R}{\partial w_l}(v,w) \right)s_{w,l}\ s_{w,p}\ (\psi_l, \psi_p)$$

$$= (1-\tau)\sum_l \sum_p \frac{1}{1-\tau}\left(1 - \tau\frac{\partial R}{\partial w_l}(v,w) \right)s_{w,l}\ s_{w,p}\ (\psi_l, \psi_p)$$

$$\ge (1-\tau)\min_l\left[\frac{1}{1-\tau}\left(1 - \tau\frac{\partial R}{\partial w_l}(v,w) \right) \right]\left(\sum_l s_{w,l}\ \psi_l, \sum_p s_{w,p}\ \psi_p \right)$$

$$\ge (1-\tau)||s_w||^2_{L^2(\Omega)}$$

- $\tau\left(\sum_l \frac{\partial I_{\text{ion}}}{\partial w_l}(v,w)(s_{i,l} - s_{e,l})\ \psi_l, s_w \right) - \tau\left(\sum_l \frac{\partial R}{\partial v_l}(v,w)(s_{i,l} - s_{e,l})\ \psi_l, s_w \right)$

$$= \tau\left(\sum_l \left(\frac{\partial I_{\text{ion}}}{\partial w_l}(v,w) - \frac{\partial R}{\partial v_l}(v,w) \right)(s_{i,l} - s_{e,l})\ \psi_l, \sum_p s_{w,p}\ \psi_p \right)$$

$$= \tau \sum_l \sum_p \left(\frac{\partial I_{\text{ion}}}{\partial w_l}(v,w) - \frac{\partial R}{\partial v_l}(v,w) \right)(s_{i,l} - s_{e,l}) \, s_{w,p} \, (\psi_l, \psi_p)$$

$$\geq \tau \min_l \left(\frac{\partial I_{\text{ion}}}{\partial w_l}(v,w) - \frac{\partial R}{\partial v_l}(v,w) \right)(s_i - s_e, s_w) \geq 0.$$

We conclude that

$$q(s,s) = 2\chi C_m \left(s_i - s_e, s_i - s_e \right) + 2 \left(s_w, s_w \right) + 2\tau a_i \left(s_i, s_i \right) + 2\tau a_e \left(s_e, s_e \right)$$

$$+ 2\tau \left(\sum_l \frac{\partial I_{\text{ion}}}{\partial v_l}(v,w)(s_{i,l} - s_{e,l}) \, \psi_l, s_i - s_e \right) - 2\tau \left(\sum_l \frac{\partial R}{\partial w_l}(v,w) s_{w,l} \, \psi_l, s_w \right)$$

$$+ \tau \left(\sum_l \frac{\partial I_{\text{ion}}}{\partial w_l}(v,w)(s_{i,l} - s_{e,l}) \, \psi_l, s_w \right) + \tau \left(\sum_l \frac{\partial I_{\text{ion}}}{\partial w_l}(v,w) s_{w,l} \, \psi_l, s_i - s_e \right)$$

$$- \tau \left(\sum_l \frac{\partial R}{\partial v_l}(v,w)(s_{i,l} - s_{e,l}) \, \psi_l, s_w \right) - \tau \left(\sum_l \frac{\partial R}{\partial v_l}(v,w) s_{w,l} \, \psi_l, s_i - s_e \right)$$

$$\geq 2(1+\tau) \|s_i - s_e\|^2_{L^2(\Omega)} + 2(1-\tau) \|s_w\|^2_{L^2(\Omega)} + 2\tau a_i \left(s_i, s_i \right) + 2\tau a_e \left(s_e, s_e \right)$$

$$\geq \||s|\|^2_{\tau,coup}.$$

$\square$

Remark 2.4. The norm $\||\cdot|\|_{\tau,coup}$ is well defined, as the quantity $1-\tau$ is always positive (typical computational values for τ are less than 10^{-2}).

Remark 2.5. The request $(C_{I_w} - C_{R_v}) \leq 0$ is justified in Lemma 2.6.

Remark 2.6. As in the case of the decoupled strategy described in the previous Section, the hypothesis of non-negativity of the above Lemma is always satisfied for any time step $\tau \leq 0.37$ ms if we consider the Rogers-McCulloch ionic model. Indeed, numerical computations of $\chi C_m + \tau \frac{\partial I_{\text{ion}}}{\partial v}$ validate this assumption (see Fig. (2.10), left). Regarding the other two hypothesis, it is easy to compute analytically that $1 - \tau \frac{\partial R}{\partial w_l} = 1 + \eta_2 \tau \geq 0$ for any value of τ, being η_2 a physiological parameter, while the last inequality is always satisfied for any $v \geqslant 2 \cdot 10^{-4}$. This request is not restrictive, as for those values of the transmembrane potential the tissue is almost at rest. Also in this case we have not verified the non-negativity hypothesis of Lemma 2.5 for more complex ionic models: possible future works should be devoted to the theoretical and numerical study of human ventricular ionic models in this coupled solution strategy.
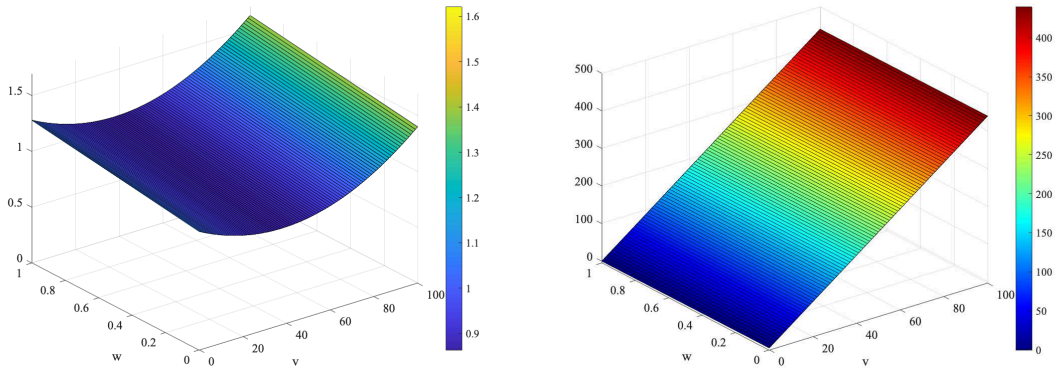
Figure 2.10: Surface plots of $\chi C_m + \tau \frac{\partial I_{\text{ion}}}{\partial v}$ (left) and $\frac{\partial I_{\text{ion}}}{\partial w} - \frac{\partial R}{\partial v}$ (right), with $C_m = 1 \frac{mF}{cm^3}$, $\chi = 1$ and $\tau = 0.05$ ms, which are values usually employed in numerical experiments.

As an immediate consequence of the continuity and coercivity of the symmetric bilinear form $q(\cdot, \cdot)$, it is possible to prove the following bounds.

Lemma 2.6. *Assuming that the conductivity coefficients are constant in space, the symmetric bilinear form $q(\cdot,\cdot)$ satisfies the bounds*

$$q(s,s) \leq 2\left[(\chi C_m + \tau K_{M,I})\,||s_i - s_e||^2_{L^2(\Omega)} + (1-\tau K_{M,R})||s_w||^2_{L^2(\Omega)} + \tau\sigma^i_M|s_i|^2_{H^1(\Omega)} + \tau\sigma^e_M|s_e|^2_{H^1(\Omega)}\right],$$

$$q(s,s) \geq 2\left[(\chi C_m + \tau K_{m,I})\,||s_i - s_e||^2_{L^2(\Omega)} + (1-\tau K_{m,R})||s_w||^2_{L^2(\Omega)} + \tau\sigma^i_m|s_i|^2_{H^1(\Omega)} + \tau\sigma^e_m|s_e|^2_{H^1(\Omega)}\right]$$

where

$$\sigma^{i,e}_M = \max_{\bullet=\{l,t,n\}}\sigma^{i,e}_\bullet, \qquad \sigma^{i,e}_m = \min_{\bullet=\{l,t,n\}}\sigma^{i,e}_\bullet,$$

and $K_{M,*}$, $K_{m,*}$ are constants, independent of the subdomain diameter H and the mesh size h.

Proof. By proceeding as in the proof for the continuity, we obtain

$$q(s,s) \leq 2\chi C_m||s_i - s_e||^2_{L^2(\Omega)} + 2\tau||s_w||^2_{L^2(\Omega)} + 2\tau\sigma^i_M|s_i|^2_{H^1(\Omega)} + 2\tau\sigma^e_M|s_e|^2_{H^1(\Omega)} +$$

$$+ 2\tau\left(\sum_l \frac{\partial I_{\text{ion}}}{\partial v_l}(v,w)\,(s_{i,l} - s_{e,l})\,\psi_l, s_i - s_e\right) - 2\tau\left(\sum_l \frac{\partial R}{\partial w_l}(v,w)s_{w,l}\;\psi_l, s_w\right)$$

$$+ \tau\left(\sum_l \frac{\partial I_{\text{ion}}}{\partial w_l}(v,w)\,(s_{i,l} - s_{e,l})\,\psi_l, s_w\right) - \tau\left(\sum_l \frac{\partial R}{\partial v_l}(v,w)\,(s_{i,l} - s_{e,l})\,\psi_l, s_w\right)$$

$$+ \tau\left(\sum_l \frac{\partial I_{\text{ion}}}{\partial w_l}(v,w)s_{w,l}\;\psi_l, s_i - s_e\right) - \tau\left(\sum_l \frac{\partial R}{\partial v_l}(v,w)s_{w,l}\;\psi_l, s_i - s_e\right)$$

$$\leq 2\chi C_m||s_i - s_e||^2_{L^2(\Omega)} + 2\tau||s_w||^2_{L^2(\Omega)} + 2\tau\sigma^i_M|s_i|^2_{H^1(\Omega)} + 2\tau\sigma^e_M|s_e|^2_{H^1(\Omega)} +$$

$$+ 2\tau K_{M,I}||s_i - s_e||^2_{L^2(\Omega)} - 2\tau K_{M,R}||s_w||^2_{L^2(\Omega)} + 2\tau\left(C_{I_w} - C_{R_v}\right)||s_i - s_e||_{L^2(\Omega)}||s_w||_{L^2(\Omega)}$$

$$\leq 2\left[\chi C_m||s_i - s_e||^2_{L^2(\Omega)} + \tau||s_w||^2_{L^2(\Omega)} + \tau\sigma^i_M|s_i|^2_{H^1(\Omega)} + \tau\sigma^e_M|s_e|^2_{H^1(\Omega)}\right.$$

$$\left.+ \tau K_{M,I}||s_i - s_e||^2_{L^2(\Omega)} - \tau K_{M,R}||s_w||^2_{L^2(\Omega)}\right],$$

where $K_{M,*}$ are the constants related to the upper bound of the reaction term and where in the last inequality we use the hypothesis of non-positivity of the quantity $C_{I_w} - C_{R_v}$ made in the previous proof.

Concerning the second bound, it is straightforward to show that

$$\left(\sum_l \frac{\partial I_{\text{ion}}}{\partial v_l}(v,w)(s_{i,l} - s_{e,l})\psi_l, s_i - s_e\right) = \left(\sum_l \frac{\partial I_{\text{ion}}}{\partial v_l}(v,w)(s_{i,l} - s_{e,l})\psi_l, \sum_p (s_{i,p} - s_{e,p})\psi_p\right)$$

$$= \sum_l \sum_p \frac{\partial I_{\text{ion}}}{\partial v_l}(v,w)(s_{i,l} - s_{e,l})(s_{i,p} - s_{e,p})\,(\psi_l, \psi_p)$$

$$\geq \min_l \frac{\partial I_{\text{ion}}}{\partial v_l}(v,w)\left(\sum_l (s_{i,l} - s_{e,l})\psi_l, \sum_p (s_{i,p} - s_{e,p})\psi_p\right)$$

$$= K_{m,I}||s_i - s_e||^2_{L^2(\Omega)}$$

and, in a similar way, that

$$\left(\sum_l \frac{\partial R}{\partial w_l}(v,w)(s_{i,l} - s_{e,l})\psi_l, s_i - s_e\right) \geq K_{m,R}||s_w||^2_{L^2(\Omega)},$$

with $K_{m,R} = \min_l \frac{\partial R}{\partial w_l}(v,w)$. Then the bound follows from the coercivity.

$\square$

Remark 2.7. This result can be extended to the case of conductivity coefficients almost constant over each subdomain.

Chapter 3

Dual-Primal Iterative Substructuring Methods

The notion of Domain Decomposition (DD) methods (DDMs) is often referred to the splitting and approximation of Partial Differential Equations (PDEs) into coupled subproblems each defined on smaller subdomains, which form a partition of the original domain.

The subdivision can be usually performed at three different stages: at continuous level, if several physical models are defined in different regions of the domain; at the discretization level, by employing different approximation methods in different portion of the domain; otherwise, the splitting can be done in the solution of algebraic systems.

As a matter of fact, in general, when modeling real life problems arising in Physics, Engineering and Biology, it is not always possible to define an exact analytic solution of these equations: thus it becomes necessary to adopt discrete formulations of the original problem. This leads to algebraic systems of equations that in case of real applications might be very large (more than 10^6 unknowns): in this sense, direct methods run into memory, complexity and scalability problems and basic iterative methods can have slow convergence.

In this framework, DDMs can be viewed as iterative algorithms to find approximate solutions of a large problem, by solving many smaller subproblems defined on single subdomains. The main effort regards the selection of subproblems that ensure a fast rate of convergence, providing preconditioners that can be accelerated by Krylov space methods. Another important feature of DDMs is their easy applicability for development of efficient codes, which nowadays are essential on modern supercomputers, since the divide-and-conquer approach used in DDMs makes them particularly suitable for parallel computing. For an extensive discussion, we refer to References [39, 110, 116].

The aim of this Chapter is to introduce the basic ideas of DDMs, focusing on non-overlapping methods; in particular on dual-primal algorithms, since the solvers proposed in this Thesis are preconditioned by the Dual-Primal Finite Element Tearing and Interconnecting (FETI-DP) (Section 3.2) and Balancing Domain Decomposition by Constraints (BDDC) (Section 3.3) algorithms. These two preconditioners will be then applied to the solvers introduced in the previous Chapter and, as they have been shown to be spectrally equivalent in Refs. [78, 83], it will be possible to derive only one convergence rate analysis for both the proposed solvers (see next Chapters). A closing section with useful technical tools that will be needed in the core of this Thesis ends this Chapter.

3.1   Non-overlapping Dual-Primal Algorithms

Let Ω_j, $j = 1, \ldots, N$, be a decomposition of the cardiac domain Ω, into non-overlapping subdomains:

$$\overline{\Omega} = \bigcup_{j=1}^{N} \overline{\Omega}_j \qquad \Omega_j \cap \Omega_k = \emptyset \quad \text{if} \quad j \neq k,$$

$$\partial\Omega_j \cap \partial\Omega_k = \begin{cases} \emptyset \\ \text{a vertex} \\ \text{an edge} \\ \text{a face} \end{cases} \quad \text{if} \quad j \neq k.$$

Each subdomain is a union of shape-regular finite elements, with matching finite element nodes on the boundaries of neighboring subdomains across the interface Γ. The interface Γ is the set of points that belong to at least two subdomains,

$$\Gamma := \bigcup_{j \neq k} \partial\Omega_j \cap \partial\Omega_k,$$

where $\partial\Omega_j$, $\partial\Omega_k$ are the boundaries of Ω_j and Ω_k respectively.

We assume that subdomains are shape regular and have a typical diameter of size H whereas the finite elements are of diameter h.

Let us denote the set of nodes on $\partial\Omega$, $\partial\Omega_j$ and Γ by $\partial\Omega^h$, $\partial\Omega_j^h$ and Γ^h, respectively. For any interface nodal point $x \in \Gamma^h$, we can use Definition 4.1 in Ref. [116]

$$\mathcal{N}_x := \{j \in \{1, \ldots, N\} |\ x \in \overline{\Omega}_j^h\}, \tag{3.1}$$

i.e. $\mathcal{N}_x$ is the set of indices of all subdomains with x in the closure of the subdomain. If x is in the interior of a subdomain, then $\mathcal{N}_x$ contains only the index of that subdomain.

For any pair of interface points $x, y \in \Gamma^h$, we introduce an equivalence relation defined by

$$x \sim y \Leftrightarrow \mathcal{N}_x = \mathcal{N}_y,$$

meaning that two nodes x, y belong to the same open set if and only if they share the same index set. We can now describe the sets of nodes on edges $\mathcal{E}$, on faces $\mathcal{F}$, on vertices $\mathcal{V}$ and in the interior $\mathcal{I}$, using their equivalence classes:[1].

Definition 3.1. *Let $x \in \partial\Omega^h \cup \partial\Omega_N^h$, then*

- *$x \in \mathcal{I}$, interior $\Longleftrightarrow |\mathcal{N}| = 1$;*
- *$x \in \mathcal{F}$, faces $\Longleftrightarrow |\mathcal{N}| = 2$;*
- *$x \in \mathcal{E}$, edges $\Longleftrightarrow |\mathcal{N}| > 2$ or $|\mathcal{N}| = 2$ and $x \in \partial\Omega$;*

and $x \in \mathcal{V}$, vertices, defined as endpoints of edges.

We denote the associated local finite element spaces by W_j. It is therefore helpful to partition W_j into the interior part $W_I^{(j)}$ and the finite element trace space $W_\Gamma^{(j)}$, such that

$$W_j = W_I^{(j)} \oplus W_\Gamma^{(j)}.$$

Note that we consider variables on the Neumann boundaries $\partial\Omega_N$ as interior to a subdomain. We introduce the product spaces by

$$W := W_1 \times \cdots \times W_N = \prod_{j=1}^{N} W_j \qquad \text{and} \qquad W_\Gamma := \prod_{j=1}^{N} W_\Gamma^{(j)}.$$

---

[1] In the definition, $|\mathcal{N}|$ denotes the cardinality of the set $\mathcal{N}$.

Therefore we define $\widehat{W} \subset W$ as the subspace of functions of W, which are continuous in all interface variables between subdomains and similarly we denote by $\widehat{W}_\Gamma \subset W_\Gamma$, the subspace formed by the continuous elements of W_Γ.

In dual-primal methods, we iterate in the space W while requiring certain constraints to hold throughout the iterations. In this case, these constraints are continuity constraints (named *primal constraints*), that have to be chosen such that each subdomain problem becomes invertible and such that a good convergence bound can be obtained [104].

We denote by $\widetilde{W}$ the space of finite element functions in W, which are continuous in all primal variables; clearly we have $\widehat{W} \subset \widetilde{W} \subset W$ and likewise $\widehat{W}_\Gamma \subset \widetilde{W}_\Gamma \subset W_\Gamma$.

We define $W_\Pi^{(j)} \subset W_\Gamma^{(j)}$ the subspace of functions which are continuous across the interface and that will be subassembled between the subdomains that share $\Gamma^{(j)}$; this subspace (and its elements) will be called *primal*. Additionally, let $W_\Delta^{(j)} \subset W_\Gamma^{(j)}$ contain the finite element functions that can be discontinuous across the interface and which vanish at the primal degrees of freedom; it will be denoted as *dual*.

In this work we will denote with subscripts I, Δ and Π the interior, the dual and the primal variables respectively.

We introduce two subspaces, W_Π and W_Δ, such that

$$W_\Pi = \prod_{j=1}^{N} W_\Pi^{(j)}, \qquad W_\Delta = \prod_{j=1}^{N} W_\Delta^{(j)}$$

and

$$W_\Gamma = W_\Pi \oplus W_\Delta.$$

Using this notation, we can decompose $\widetilde{W}_\Gamma$ into a primal subspace $\widehat{W}_\Pi$ which has continuous elements only and a dual subspace W_Δ which contains finite element functions which are not continuous, i.e. we have

$$\widetilde{W}_\Gamma = \widehat{W}_\Pi \oplus W_\Delta,$$

and similarly we can write

$$\widehat{W} = \widehat{W}_\Pi \oplus \widehat{W}_\Delta \oplus W_I.$$

This space subdivision induces a reordering of the degrees of freedom (dofs), which will be divided into those internal and those on the interface (further classified into dual and primal dofs) of each subdomain, see Fig. 3.1. From now on, we will refer interchangeably to dofs and nodal points, as we assume they coincide.

In dual-primal methods, this reordering leads to consider a reordered system matrix. Define the local stiffness matrices

$$K^{(j)} = \begin{bmatrix} K_{II}^{(j)} & K_{\Gamma I}^{(j)T} \\ K_{\Gamma I}^{(j)} & K_{\Gamma \Gamma}^{(j)} \end{bmatrix} = \begin{bmatrix} K_{II}^{(j)} & K_{I\Delta}^{(j)} & K_{\Pi I}^{(j)T} \\ K_{\Delta I}^{(j)} & K_{\Delta \Delta}^{(j)} & K_{\Pi \Delta}^{(j)T} \\ K_{\Pi I}^{(j)} & K_{\Pi \Delta}^{(j)} & K_{\Pi \Pi}^{(j)} \end{bmatrix}.$$

and

$$K_{II} = \mathrm{diag}_{j=1,\ldots,N} K_{II}^{(j)}, \qquad K_{\Delta I} = \mathrm{diag}_{j=1,\ldots,N} K_{\Delta I}^{(j)}, \qquad K_{\Delta \Delta} = \mathrm{diag}_{j=1,\ldots,N} K_{\Delta \Delta}^{(j)},$$

$$K_{\Pi I} = \mathrm{diag}_{j=1,\ldots,N} K_{\Pi I}^{(j)}, \qquad K_{\Pi \Delta} = \mathrm{diag}_{j=1,\ldots,N} K_{\Pi \Delta}^{(j)}, \qquad K_{\Pi \Pi} = \mathrm{diag}_{j=1,\ldots,N} K_{\Pi \Pi}^{(j)}.$$

Then the linear system $Ku = f$ can be written as

$$K = \begin{bmatrix} K_{II} & K_{\Delta I}^{T} & K_{\Pi \Delta}^{T} \\ K_{\Delta I} & K_{\Delta \Delta} & K_{\Delta \Pi}^{T} \\ K_{\Pi I} & K_{\Pi \Delta} & K_{\Pi \Pi} \end{bmatrix}.$$
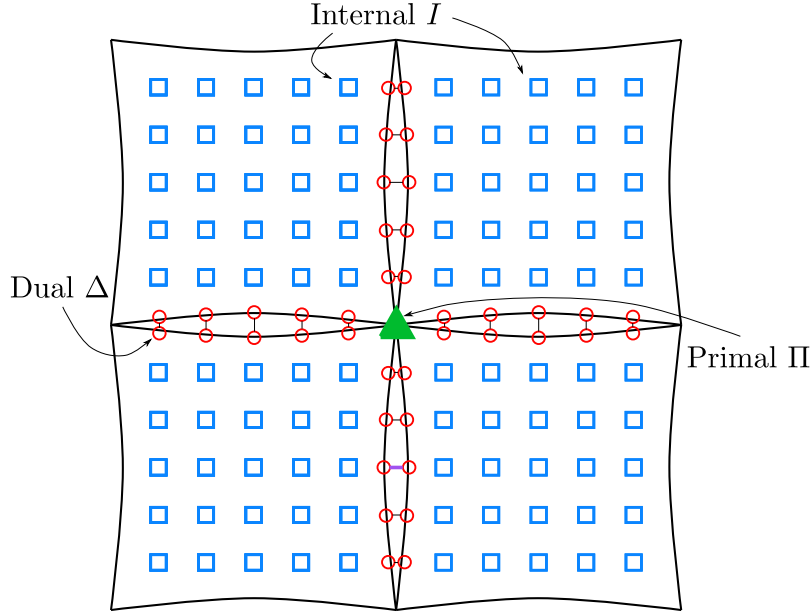
Figure 3.1: A schematic diagram of domain subdivision into four subdomains and splitting of degrees of freedom (dofs): interior (blue squares), dual (red circles) and primal (green triangles) dofs.

As in many iterative substructuring algorithms, the first step is to eliminate all the interior variables, obtaining the unassembled Schur complement S_Γ

$$S_\Gamma = K_{\Gamma\Gamma} - K_{\Gamma I} K_{II}^{-1} K_{\Gamma I}^T = \begin{bmatrix} K_{\Delta\Delta} & K_{\Delta\Pi}^T \\ K_{\Pi\Delta} & K_{\Pi\Pi} \end{bmatrix} - \begin{bmatrix} K_{\Delta I} \\ K_{\Pi I} \end{bmatrix} K_{II}^{-1} \begin{bmatrix} K_{\Delta I}^T K_{\Pi I}^T \end{bmatrix}. \tag{3.2}$$

Then, we can write $\widehat{S}_\Gamma = R_\Gamma^T S_\Gamma R_\Gamma^T$, with R_Γ being the direct sum of local restriction operators $R_\Gamma^{(j)}$ (which returns the local interface components). Applying the same idea to the right hand-side f,

$$\widehat{g}_\Gamma = \widehat{f}_\Gamma - K_{\Gamma I} K_{II}^{-1} f_I, \qquad f = \begin{bmatrix} f_I \\ \widehat{f}_\Gamma \end{bmatrix}, \qquad \widehat{f}_\Gamma = R_\Gamma^T f_\Gamma,$$

the resulting system which we need to solve is

$$\widehat{S}_\Gamma u_\Gamma = \widehat{g}_\Gamma. \tag{3.3}$$

Once this problem is solved, the solution u_Γ on the interface is used to recover the solution on the internal degrees of freedom by

$$u_I = K_{II}^{-1} \left(g_I - K_{I\Gamma} u_\Gamma \right).$$

Restriction operators and scaling.   Before going into the details of the proposed preconditioners, we need to introduce some operators needed for their definition. In particular, when working with these methods, an interface averaging is needed in order to ensure a correct continuity of the global solution. Let us define the restriction operators

$$R_\Delta^{(j)} : W_\Delta \to W_\Delta^{(j)}, \quad R_{\Gamma\Delta} : W_\Gamma \to W_\Delta,$$
$$R_\Pi^{(j)} : \widehat{W}_\Pi \to W_\Pi^{(j)}, \quad R_{\Gamma\Pi} : W_\Gamma \to \widehat{W}_\Pi,$$

and the direct sums $R_\Delta = \oplus R_\Delta^{(j)}$, $R_\Pi = \oplus R_\Pi^{(j)}$ and $\widetilde{R}_\Gamma = R_{\Gamma\Pi} \oplus R_{\Gamma\Delta}$, which maps W_Γ into $\widetilde{W}_\Gamma$.

In this Thesis we will consider mainly two types of scaling, the ρ-scaling and the *deluxe* scaling; for further details see References [7, 38, 116].

The ρ-scaling takes into account the standard counting functions of the Neumann-Neumann methods and in particular their pseudoinverses, which can be defined for the Bidomain model as, $\forall x \in \Gamma^{(j)}$

$$\delta_j^{i,e \, \dagger}(x) = \frac{\sigma_M^{i,e^{(j)}}}{\sum_{k \in \mathcal{N}_x} \sigma_M^{i,e^{(k)}}}, \qquad \sigma_M^{i,e^{(j)}} = \max_{\bullet = \{l,t,n\}} \sigma_\bullet^{i,e^{(j)}}, \qquad \delta_j^{w, \, \dagger}(x) = \frac{1}{|\mathcal{N}_x|}, \qquad (3.4)$$

where $\mathcal{N}_x$ is the set of indices of all subdomains with x in the closure of the subdomain, defined in Eq. (3.1). The following property (see [116]) holds

$$\sigma_M^{i,e^{(j)}} \left(\delta_k^{i,e \, \dagger} \right)^2 \leq \min \left\{ \sigma_M^{i,e^{(j)}}, \sigma_M^{i,e^{(k)}} \right\}.$$

Conversely the deluxe scaling, recently introduced by [38], defines the average $\bar{w} = E_D w$ differently for the equivalence classes of faces or edges.
We define the deluxe scaling for classes $\mathcal{F}$ and $\mathcal{E}$ in the following way. We recall that the class of faces $\mathcal{F}$ contains all the nodes shared by two elements. Suppose that $\mathcal{F}$ is shared by Ω_j and Ω_k; let $S_{\mathcal{F}}^{(j)}$ and $S_{\mathcal{F}}^{(k)}$ be the principal minors obtained from $S_{\Gamma}^{(j)}$ and $S_{\Gamma}^{(k)}$ by removing all the contributions that are not related to the degrees of freedom of the face $\mathcal{F}$.
Let $u_{j,\mathcal{F}} = R_{\mathcal{F}} u_j$ be the restriction of u_j to the face $\mathcal{F}$ through the restriction operator $R_{\mathcal{F}}$; the deluxe average across $\mathcal{F}$ is then defined as (see [7])

$$\bar{u}_{\mathcal{F}} = \left(S_{\mathcal{F}}^{(j)} + S_{\mathcal{F}}^{(k)} \right)^{-1} \left(S_{\mathcal{F}}^{(j)} u_{j,\mathcal{F}} + S_{\mathcal{F}}^{(k)} u_{k,\mathcal{F}} \right).$$

Note that we have denoted with $\bar{u}_{j,\mathcal{F}}$ the mean value of u_j over the face $\mathcal{F}$, while, if we omit the index j, we denote the deluxe average.
The action of $(S_{\mathcal{F}}^{(j)} + S_{\mathcal{F}}^{(k)})^{-1}$ can be computed by solving a Dirichlet problem over the two subdomains, by extending to zero the right-hand side entries associated with the interior nodes.

If we consider an edge $\mathcal{E}$, where a node is common to at least two elements, the deluxe average across $\mathcal{E}$ is defined in a similar manner.
Suppose for simplicity that $\mathcal{E}$ is shared by only three subdomains with indices j_1, j_2 and j_3; the extension to more than three subdomains is immediate. Let $u_{j,\mathcal{E}} = R_{\mathcal{E}} u_j$ be the restriction of u_j to the edge $\mathcal{E}$ through the restriction operator $R_{\mathcal{E}}$ and define

$$S_{\mathcal{E}}^{(j_{123})} = S_{\mathcal{E}}^{(j_1)} + S_{\mathcal{E}}^{(j_2)} + S_{\mathcal{E}}^{(j_3)};$$

the deluxe average across an edge $\mathcal{E}$ is given by

$$\bar{u}_{\mathcal{E}} = \left(S_{\mathcal{E}}^{(j_{123})} \right)^{-1} \left(S_{\mathcal{E}}^{(j_1)} u_{j_1,\mathcal{E}} + S_{\mathcal{E}}^{(j_2)} u_{j_2,\mathcal{E}} + S_{\mathcal{E}}^{(j_3)} u_{j_3,\mathcal{E}} \right).$$

The relevant equivalence classes, involving the substructure Ω_j, will contribute to the values of $\bar{u}$. These contributions will belong to $\widehat{W}_\Gamma$, after being extended by zero to $\Gamma \backslash \mathcal{F}$ or $\Gamma \backslash \mathcal{E}$; the sum of all contributions will result in $R_*^T \bar{u}_*$. We then add the contributions from the different equivalence classes to obtain

$$\bar{u} = E_D u = u_\Pi + \sum_{* = \{\mathcal{F}, \mathcal{E}\}} R_*^T \bar{u}_*,$$

where E_D is a projection. Its complementary projection is given by

$$P_D : \widetilde{W}_\Gamma \to \widetilde{W}_\Gamma \qquad P_D u := (I - E_D) u = u_\Delta - \sum_{* = \{\mathcal{F}, \mathcal{E}\}} R_*^T \bar{u}_*. \qquad (3.5)$$

Lastly, for each subdomain Ω_j we define the scaling matrix

$$D^{(j)} = \begin{bmatrix} D_{*k_1}^{(j)} & & \\ & \ddots & \\ & & D_{*k_j}^{(j)} \end{bmatrix}, \qquad * = \{\mathcal{F}, \mathcal{E}\} \qquad (3.6)$$

with $k_1, \ldots, k_j \in \Xi_j^*$ set containing the indices of the subdomains that share the face $\mathcal{F}$ or the edge $\mathcal{E}$ and where the diagonal blocks are given by

$$D_{\mathcal{F}}^{(j)} = (S_{\mathcal{F}}^{(j)} + S_{\mathcal{F}}^{(k)})^{-1} S_{\mathcal{F}}^{(j)} \qquad \text{or} \qquad D_{\mathcal{E}}^{(j)} = (S_{\mathcal{E}}^{(j_1)} + S_{\mathcal{E}}^{(j_2)} + S_{\mathcal{E}}^{(j_3)})^{-1} S_{\mathcal{E}}^{(j_1)}.$$

Thanks to the definition of the scaling matrix, we define the scaled local restriction operators

$$R_{D,\Gamma}^{(j)} = D^{(j)} R_{\Gamma}^{(j)}, \qquad\qquad R_{D,\Delta}^{(j)} = R_{\Gamma\Delta}^{(j)} R_{D,\Gamma}^{(j)},$$

$R_{D,\Delta}$ as direct sum of $R_{D,\Delta}^{(j)}$ and the global scaled operator $\widetilde{R}_{D,\Gamma} = R_{\Gamma\Pi} \oplus R_{D,\Delta} R_{\Gamma\Delta}$.

3.2   Dual-Primal Finite Element Tearing and Interconnecting (FETI-DP)

The Finite Element Tearing and Interconnecting Dual-Primal preconditioner was proposed first in Ref. [48] with vertex constraints as an alternative to one-level and two-level FETI, introduced in References [42, 43, 45–47]. It has been then extended to 3D in Reference [46]; References [85] provide a convergence bound in 2D, while a complete 3D dissertation of both algorithm and bound are provided in Refs. [69, 72–74].

   This class of methods is based on the transposition from the Schur problem on $\widehat{W}_\Gamma$ to a minimization problem on $\widetilde{W}_\Gamma$, with continuity constraints on dual degrees of freedom. They have been applied in several contexts, from three-dimensional elliptic problems with heterogeneous coefficients [73] to linear elasticity problems [72, 104]. In the biomechanics field, applications of FETI and FETI-DP have been extensively studied in Refs. [2, 13, 71, 127].

   We present here an algebraic formulation of FETI-DP algorithm, following Refs. [72, 104].

   Starting from the algebraic system $Ku = f$, we denote the unknowns on each subdomain by $u^{(j)}$. For each subdomain Ω_i for j = 1, . . . , N, we can distinguish between interior, dual and primal contribution in the stiffness matrix, the unknowns and the right-hand side vectors:

$$K^{(j)} = \begin{bmatrix} K_{II}^{(j)} & K_{\Delta I}^{(j)T} & K_{\Pi I}^{(j)T} \\ K_{\Delta I}^{(j)} & K_{\Delta\Delta}^{(j)} & K_{\Pi\Delta}^{(j)T} \\ K_{\Pi I}^{(j)} & K_{\Pi\Delta}^{(j)} & K_{\Pi\Pi}^{(j)} \end{bmatrix}, \qquad u^{(j)} = \begin{bmatrix} u_I^{(j)} \\ u_\Delta^{(j)} \\ u_\Pi^{(j)} \end{bmatrix}, \qquad f^{(j)} = \begin{bmatrix} f_I^{(j)} \\ f_\Delta^{(j)} \\ f_\Pi^{(j)} \end{bmatrix}.$$

Note that any variable on the Neumann boundary $\partial\Omega_N$ is considered to be interior to a subdomain. Unknowns on the Dirichlet boundary $\partial\Omega_D$ are usually eliminated upfront and do not need to be considered. We observe that in a structured decomposition (as considered in this Thesis), the vertex unknowns are all degrees of freedom which are associated with nodes shared by four or eight subdomains, as in Fig. 3.1.

We introduce the following notation

$$u_B = \begin{bmatrix} u_I \\ u_\Delta \end{bmatrix}, \qquad u_B^{(j)} = \begin{bmatrix} u_I^{(j)} \\ u_\Delta^{(j)} \end{bmatrix}, \qquad f_B = \begin{bmatrix} f_I \\ f_\Delta \end{bmatrix}, \qquad f_B^{(j)} = \begin{bmatrix} f_I^{(j)} \\ f_\Delta^{(j)} \end{bmatrix}.$$

Let us now partition the stiffness matrix K, the right-hand side f and the unknowns vector u according to the different sets of unknowns:

$$K_{BB} = \begin{bmatrix} K_{BB}^{(1)} & & \\ & \ddots & \\ & & K_{BB}^{(N)} \end{bmatrix}, \qquad K_{BB}^{(j)} = \begin{bmatrix} K_{II}^{(j)} & K_{\Delta I}^{(j)T} \\ K_{\Delta I}^{(j)} & K_{\Delta\Delta}^{(j)} \end{bmatrix},$$

$$K_{\Pi B} = \begin{bmatrix} K_{\Pi B}^{(1)} & \ldots & K_{\Pi B}^{(N)} \end{bmatrix}, \qquad K_{\Pi B}^{(j)} = \begin{bmatrix} K_{\Pi I}^{(j)} & K_{\Pi\Delta}^{(j)} \end{bmatrix}.$$

Observe that K_{BB} is a block-diagonal matrix. If we subassembly with respect to the primal displacement vectors, we obtain

$$\widetilde{K} = \begin{bmatrix} K_{BB} & \widetilde{K}_{\Pi B}^T \\ \widetilde{K}_{\Pi B}^T & \widetilde{K}_{\Pi\Pi}^T \end{bmatrix}, \qquad \widetilde{K}_{\Pi B} = \begin{bmatrix} \widetilde{K}_{\Pi B}^{(1)}, \dots, \widetilde{K}_{\Pi B}^{(N)} \end{bmatrix},$$

where, for $j = 1, \dots, N$,

$$\widetilde{K}_{\Pi B}^{(j)} = R_{\Pi}^{(j)T} K_{\Pi B}^{(j)}, \qquad \widetilde{K}_{\Pi\Pi} = \sum_{j=1}^{N} R_{\Pi}^{(j)T} K_{\Pi\Pi}^{(j)} R_{\Pi}^{(j)}.$$

We note that $\widetilde{K}$ is block diagonal and coupling is introduced only through the primal variables. To enforce continuity on the remaining interface variables $u_{\Delta}^{(j)}$, we define a discrete jump operator $B = [0 \quad B_{\Delta}]$ and a set of Lagrange multipliers $\lambda \in \Lambda = \text{range}(B)$ such that

$$B \, u_B = B_{\Delta} u_{\Delta} 0. \tag{3.7}$$

Since we assume that finite element nodes match across the interface Γ, the entries of the matrix B will be chosen between 0, 1 and -1.

For example, consider the domain Ω in Fig. 3.2: a suitable choice for the entries of B is to assign

| Ω_3 $B_3 = -1$ | Ω_4 $B_4 = 1$ |
| Ω_1 $B_1 = 1$ | Ω_2 $B_2 = -1$ |

Figure 3.2: A generic domain subdivided into 4 subdomains.

values 1, -1, -1 and 1 for subdomains Ω_1, Ω_2, Ω_3 and Ω_4 respectively.

The starting algebraic system $Ku = f$ can be reformulated as the following saddle point problem: find $(u, \lambda_K) \in \widetilde{W} \times \Lambda$, such that

$$\begin{bmatrix} K_{BB} & \widetilde{K}_{\Pi B}^T & B^T \\ \widetilde{K}_{\Pi B} & \widetilde{K}_{\Pi\Pi} & 0 \\ B & 0 & 0 \end{bmatrix} \begin{bmatrix} u_B \\ \widetilde{u}_{\Pi} \\ \lambda_K \end{bmatrix} = \begin{bmatrix} f_B \\ \widetilde{f}_{\Pi} \\ 0 \end{bmatrix}. \tag{3.8}$$

We emphasize that $Bu_B = 0$ holds if and only if $u_B \in \widehat{W}$, which means that the columns of B associated with primal degrees of freedom are null. As $\widetilde{K}$ is invertible on Λ, the degrees of freedom in $\widetilde{W}_{\Gamma}$ can be eliminated by a block-Cholesky factorization, reducing the above system to a problem only in the Lagrange multipliers unknowns

$$F_K \lambda_K = d_K, \tag{3.9}$$

where

$$F_K = BK_{BB}^{-1} \left(B^T + \widetilde{K}_{\Pi B}^T \widetilde{S}_{\Pi\Pi}^{-1} \widetilde{K}_{\Pi B} K_{BB}^{-1} B^T \right),$$

$$d_K = BK_{BB}^{-1} \left(f_B + \widetilde{K}_{\Pi B}^T \widetilde{S}_{\Pi\Pi}^{-1} \left(\widetilde{f}_{\Pi} - \widetilde{K}_{\Pi B} K_{BB}^{-1} f_B \right) \right),$$

$$\widetilde{S}_{\Pi\Pi} = \widetilde{K}_{\Pi\Pi} - \widetilde{K}_{\Pi B} K_{BB}^{-1} \widetilde{K}_{\Pi B}^T.$$

The symmetric positive definite Schur complement $\widetilde{S}_{\Pi\Pi}$ represents the FETI-DP coarse problem and it introduces the global coupling across the subdomains. For computational purposes, we note that the matrix F_K is never computed explicitly, as it can be retrieved from the solution of two linear systems; moreover, the inverse matrices that appear are never calculated, as they are only needed in terms of matrix action on a vector, and direct solvers such as Cholesky or LU factorization are used. After the solution λ_K is found, we can retrieve the solution on $\widetilde{W}_\Gamma$ as

$$u = \widetilde{K}^{-1} \left(\widetilde{f} - B^T \lambda_K \right).$$

Usually, Eq. (3.9) is preconditioned by the FETI-DP preconditioner M^{-1}: in order to properly define this preconditioner, we introduce a scaled jump operator B_D.
This operator is obtained by applying $D^{(j)} : \Lambda \to \Lambda$ scaling matrices that act on the space of the Lagrange multipliers, which are given by matrix (3.6) if the deluxe scaling is used or by the pseudoinverses Eq. (3.4) if the standard ρ-scaling is used. In both cases, the scaling is chosen such that the linear mapping $P_D = B_D^T B$ becomes a projection.

Then, a quasi-optimal preconditioner for the FETI-DP algorithm is given by

$$M^{-1} = B_D \; \widetilde{K} \; B_D^T.$$

In this way, FETI-DP method can be considered as a standard preconditioned conjugate gradient algorithm for solving the preconditioned system

$$M^{-1} F_K \lambda_K = M^{-1} d_K,$$

see Ref. [116]. It can be implemented with the recursive Algorithm (1).
In order to be consistent with the notation in the next Chapter, we reformulate the FETI-DP

Algorithm 1 FETI-DP method as a PCG method

Require: $r^0 = d - F\lambda^0$;
   for $k = 1, \ldots$ until convergence **do**
      Precondition $z^{k-1} = M^{-1} r^{k-1}$, then
      $\beta^k = \dfrac{< z^{k-1}, \; r^{k-1} >}{< z^{k-2}, \; r^{k-2} >}, \qquad [\beta^1 = 0]$
      $p^k = z^{k-1} + \beta^k p^{k-1}, \qquad [p^1 = z^0]$
      $\alpha^k = \dfrac{< z^{k-1}, \; r^{k-1} >}{< p^k, \; Fp^k >}$
      $\lambda^k = \lambda^{k-1} + \alpha^k p^k$
      $r^k = r^{k-1} - \alpha^k Fp^k$
   end for

---

preconditioner for the Schur complement problem $\widetilde{S}_\Gamma u_\Gamma = \widetilde{g}_\Gamma$.
By eliminating the interior unknowns, system (3.8) is equivalent to

$$\begin{bmatrix} \widetilde{S}_\Gamma & B_\Gamma^T \\ B_\Gamma & 0 \end{bmatrix} \begin{bmatrix} u_\Gamma \\ \lambda \end{bmatrix} = \begin{bmatrix} \widetilde{g}_\Gamma \\ 0 \end{bmatrix}, \qquad u_\Gamma \in \widetilde{W}_\Gamma, \tag{3.10}$$

where $\widetilde{S}_\Gamma$ is the partially assembled Schur complement matrix, B_Γ is the restriction to the interface of the jump operator B

$$B_\Gamma = \begin{bmatrix} B_\Delta & 0_\Pi \end{bmatrix}.$$

This saddle point problem can be also viewed as a reformulation of the minimization problem on $\widetilde{W}_\Gamma$

$$\text{find } u_\Gamma \in \widetilde{W}_\Gamma \qquad \begin{cases} \dfrac{1}{2} u_\Gamma^T \widetilde{S}_\Gamma u_\Gamma - u_\Gamma^T \widetilde{g}_\Gamma \\ B_\Gamma u_\Gamma = 0 \end{cases}.$$

In the same manner, the system (3.10) can be reduced to a problem only in the Lagrange multipliers by eliminating the interface dofs by a block-Cholesky factorization: this leads to the algebraic system

$$F\,\lambda = d, \qquad F = B_\Gamma \widetilde{S}_\Gamma^{-1} B_\Gamma^T, \quad d = B_\Gamma \widetilde{S}_\Gamma^{-1} \widetilde{g}_\Gamma,$$

and the FETI-DP preconditioner for the system above is given by

$$M_{\text{FETI-DP}}^{-1} = B_{D,\Gamma} \widetilde{S}_\Gamma B_{D,\Gamma}^T,$$

where $B_{D,\Gamma}$ is the scaled restricted jump operator.

3.3 Balancing Domain Decomposition with Constraints (BDDC)

The Balancing Domain Decomposition with Constraints (BDDC) procedure is a two-level preconditioner for the Schur complement system (3.3) $\widehat{S}_\Gamma u_\Gamma = \widehat{g}_\Gamma$.
BDDC algorithms were initially proposed by [37] for the solution of symmetric, positive definite problems, but its formulation can be equally applied to non-symmetric problems, as done in [121] for advection-diffusion equations. This preconditioner has been applied to a large variety of problems, such as 3D problems in $H(curl)$ (see e.g. [38]), Raviart-Thomas vector fields ([93]) and more recently to Isogeometric Analysis ([5–7]) and Virtual Elements Method (Refs. [10, 78]).

A very interesting feature which has been proved in References [78, 83] is the spectral equivalence with FETI-DP: if the same primal space is considered, it has been demonstrated that both preconditioners share the same eigenvalues, except for those equal to 0 and 1. This means that the rate of convergence is essentially the same, allowing us to carry out only one convergence analysis.

As previously done for FETI-DP, we partition the degrees of freedom of the interface Γ into those internal (I), dual (Δ) and primal (Π) dofs, and partition the local stiffness matrices as

$$K^{(j)} = \begin{bmatrix} K_{II}^{(j)} & K_{\Gamma I}^{(j)T} \\ K_{\Gamma I}^{(j)} & K_{\Gamma\Gamma}^{(j)} \end{bmatrix} = \begin{bmatrix} K_{II}^{(j)} & K_{I\Delta}^{(j)} & K_{\Pi I}^{(j)T} \\ K_{\Delta I}^{(j)} & K_{\Delta\Delta}^{(j)} & K_{\Pi\Delta}^{(j)T} \\ K_{\Pi I}^{(j)} & K_{\Pi\Delta}^{(j)} & K_{\Pi\Pi}^{(j)} \end{bmatrix}.$$

Let $\widetilde{S}_\Gamma$ be the partially assembled Schur complement obtained from Eq. (3.2) $\widetilde{S}_\Gamma = \widetilde{R}_\Gamma S_\Gamma \widetilde{R}_\Gamma^T$; then we define the BDDC preconditioner using the scaled restriction operators as

$$M_{\text{BDDC}}^{-1} = \widetilde{R}_{D,\Gamma}^T \widetilde{S}_\Gamma^{-1} \widetilde{R}_{D,\Gamma}.$$

The action of $\widetilde{S}_\Gamma$ on any vector u_Γ of $\widetilde{W}_\Gamma$ can be computed as

$$\begin{bmatrix} K_{II}^{(1)} & K_{\Delta I}^{(1)T} & & & & & \widetilde{K}_{\Pi I}^{(1)T} \\ K_{\Delta I}^{(1)} & K_{\Delta\Delta}^{(1)} & & & & & \widetilde{K}_{\Pi\Delta}^{(1)T} \\ & & \ddots & & & & \vdots \\ & & & K_{II}^{(N)} & K_{\Delta I}^{(N)T} & & \widetilde{K}_{\Pi I}^{(N)T} \\ & & & K_{\Delta I}^{(N)} & K_{\Delta\Delta}^{(N)} & & \widetilde{K}_{\Pi I}^{(N)T} \\ \widetilde{K}_{\Pi I}^{(1)} & \widetilde{K}_{\Pi\Delta}^{(1)} & \cdots & \widetilde{K}_{\Pi I}^{(N)} & \widetilde{K}_{\Pi I}^{(N)} & & \widetilde{K}_{\Pi\Pi} \end{bmatrix} \begin{bmatrix} u_I^{(1)} \\ u_\Delta^{(1)} \\ \vdots \\ u_I^{(N)} \\ u_\Delta^{(N)} \\ u_\Gamma \end{bmatrix} = \begin{bmatrix} 0 \\ R_\Delta^{(1)} R_{\Gamma\Delta} \widetilde{S}_\Gamma u_\Gamma \\ \vdots \\ 0 \\ R_\Delta^{(N)} R_{\Gamma\Delta} \widetilde{S}_\Gamma u_\Gamma \\ R_{\Gamma\Pi} \widetilde{S}_\Gamma w_\Gamma \end{bmatrix}.$$

The inverse of the partially assembled Schur complement $\widetilde{S}_\Gamma$ can be evaluated with a block-Cholesky elimination procedure

$$\widetilde{S}_\Gamma^{-1} = \widetilde{R}_{\Gamma\Delta}^T \left(\sum_{j=1}^N \begin{bmatrix} 0 & R_\Delta^{(j)T} \end{bmatrix} \begin{bmatrix} K_{II}^{(j)} & K_{I\Delta}^{(j)} \\ K_{I\Delta}^{(j)T} & K_{\Delta\Delta}^{(j)} \end{bmatrix}^{-1} \begin{bmatrix} 0 \\ R_\Delta^{(j)} \end{bmatrix} \right) \widetilde{R}_{\Gamma\Delta} + \Phi S_{\Pi\Pi}^{-1} \Phi.$$

In this way, the first term is the sum of local solvers on each substructure Ω_j, with Neumann data on local dual edges, while the latter is a coarse solver for the primal variables where

$$S_{\Pi\Pi} = \sum_{j=1}^{N} R_{\Pi}^{(j)T} \left(K_{\Pi\Pi}^{(j)} - \begin{bmatrix} K_{I\Pi}^{(j)T} & K_{\Delta\Pi}^{(j)T} \end{bmatrix} \begin{bmatrix} K_{II}^{(j)} & K_{I\Delta}^{(j)} \\ K_{I\Delta}^{(j)T} & K_{\Delta\Delta}^{(j)} \end{bmatrix}^{-1} \begin{bmatrix} K_{I\Pi}^{(j)} \\ R_{\Delta\Pi}^{(j)} \end{bmatrix} \right) R_{\Pi}^{(j)},$$

is the primal problem and

$$\Phi = R_{\Gamma\Pi}^{T} - R_{\Gamma\Delta}^{T} \sum_{j=1}^{N} \begin{bmatrix} 0 & R_{\Delta}^{(j)T} \end{bmatrix} \begin{bmatrix} K_{II}^{(j)} & K_{I\Delta}^{(j)} \\ K_{I\Delta}^{(j)T} & K_{\Delta\Delta}^{(j)} \end{bmatrix}^{-1} \begin{bmatrix} K_{I\Pi}^{(j)} \\ R_{\Delta\Pi}^{(j)} \end{bmatrix} R_{\Pi}^{(j)},$$

is the matrix which maps the primal degrees of freedom to the interface variables. The columns of Φ represent the coarse basis functions defined as the minimum energy extension into the subdomains and subject to the chosen set of primal constraints.

3.4   Preliminary technical results

We assume that the cardiac domain $\Omega_j \in \mathbb{R}^3$ is a bounded domain with Lipschitz continuous boundary; moreover suppose $\Gamma^{(j)} \subseteq \partial\Omega_j$ has non-vanishing two-dimensional measure and is relatively open with respect to $\partial\Omega_j$.

We recall the following definition, see [14, Definition 7.5.25] :

Definition 3.2. *The fractional order Sobolev semi-norm* $|\cdot|_{H^{1/2}(\Gamma^{(j)})}$ *is defined by*

$$|u|_{H^{1/2}(\Gamma^{(j)})} = \iint_{\Gamma^{(j)}} \frac{|u(x) - u(y)|^2}{|x - y|^2} ds_x ds_y,$$

where ds is the differential of the arc-length. The space $H^{1/2}(\Gamma^{(j)})$ *consists of functions* $u \in L^2(\Gamma^{(j)})$ *such that* $|u|_{H^{1/2}(\Gamma^{(j)})} < \infty$, *and we define the norm*

$$||u||_{H^{1/2}(\Gamma^{(j)})}^2 = ||u||_{L^2(\Gamma^{(j)})}^2 + |u|_{H^{1/2}(\Gamma^{(j)})}^2.$$

Furthermore, we define the space

$$H_{00}^{1/2}(\Gamma^{(j)}) = \left\{ u \in H^{1/2}(\Gamma^{(j)}) : \mathcal{E}_{ext} u \in H^{1/2}(\partial\Omega_j) \right\},$$

as the set of all functions $u \in H^{1/2}(\Gamma^{(j)})$ for which the zero extension from $\Gamma^{(j)}$ to $\partial\Omega_j$ by the extension operator $\mathcal{E}_{ext}$

$$\mathcal{E}_{ext} : \Gamma^{(j)} \longrightarrow \partial\Omega_j \qquad \mathcal{E}_{ext} u = \begin{cases} 0 & \text{on } \partial\Omega_j \setminus \Gamma^{(j)}, \\ u & \text{on } \Gamma^{(j)}, \end{cases}$$

remains bounded in $||\cdot||_{H^{1/2}(\Gamma^{(j)})}$. This space is equipped with the norm

$$||u||_{H_{00}^{1/2}(\Gamma^{(j)})}^2 := ||u||_{H^{1/2}(\Gamma^{(j)})}^2 + \int_{\Gamma^{(j)}} u^2 d(x; \Gamma^{(j)})^{-1} dx,$$

where $d(x; \Gamma^{(j)})$ denotes the distance between x and the boundary $\Gamma^{(j)}$. We observe that if $u \in H^{1/2}(\partial\Omega)$ vanishes almost everywhere on $\partial\Omega \setminus \Gamma$, then $||u||_{H^{1/2}(\partial\Omega)}$ and $||u||_{H_{00}^{1/2}(\Gamma)}$ are equivalent norms.

We also need to introduce the usual Lagrangian interpolator operator

$$I^h : \mathcal{C}^0(\Omega_j) \longrightarrow V_h(\Omega_j),$$

and define the discrete harmonic extensions of the Laplacian operator on $\partial\Omega_j$

$$u = \mathcal{H}_j^\Delta u_\Gamma \qquad \Leftrightarrow \qquad \begin{cases} -\Delta u = 0 & \text{in } \partial\Omega_j, \\ u = u_\Gamma & \text{on } \Gamma^{(j)} \\ u = 0 & \text{on } \partial\Omega_j \backslash \Gamma^{(j)}. \end{cases}$$

Notation We will write with $A \lesssim B$ whenever $A \leq cB$ with c constant independent of the diameter H, the mesh size h, the time step τ and the conductivity coefficients; similarly, we will write $A \sim B$ whenever $A \lesssim B$ and $B \lesssim A$.

We recall some useful technical results that will be employed in the proofs of the convergence rate estimates. These results can be found in the appendix A of [116].

Proposition 3.1 (Poincaré-Friedrichs inequality)**.** *Let Ω be Lipschitz continuous with diameter H. Then, there exists a constant C_f, that depends only on the shape of Ω but not on its size, such that*

$$||u||^2_{L^2(\Omega)} \leq C_f H^2 |u|^2_{H^1(\Omega)},$$

for all $u \in H^1(\Omega)$ with vanishing mean value on Ω.

Lemma 3.1. *Let $\Gamma \subset \partial\Omega$. There exists two constants, such that for $u \in H^{1/2}_{00}(\Gamma)$*

$$c||\mathcal{E}_{ext}u||^2_{H^{1/2}(\partial\Omega)} \leq ||u||^2_{H^{1/2}_{00}(\Gamma)} \leq C||\mathcal{E}_{ext}u||^2_{H^{1/2}(\partial\Omega)}.$$

Theorem 3.1 (Trace theorem)**.** *Let Ω_j be a polyhedral domain, then*

$$|u|^2_{H^{1/2}(\Gamma^{(j)})} \sim |\mathcal{H}_j^\Delta u_\Gamma|^2_{H^1(\Omega_j)}.$$

Also the following Lemmas are from the same reference, [116, Lemmas 4.16, 4.17 and 4.19], [116, Lemma 4.26] and [116, Lemma 4.30].

Lemma 3.2 (Edge estimate)**.** *Let $\mathcal{E}$ be an edge of $\partial\Omega_j$ and $\theta_{\mathcal{E}}$ be the finite element function*

$$\theta_{\mathcal{E}} \in V_h(\Omega_j), \qquad \theta_{\mathcal{E}} = \begin{cases} 1 & \text{on nodal points of } \mathcal{E} \\ 0 & \text{elsewhere.} \end{cases}$$

Then, $\forall u \in V_h(\Omega_j)$,

$$|I^h(\theta_{\mathcal{E}}u)|^2_{H^{1/2}(\Gamma^{(j)})} \leq C||u||^2_{L^2(\mathcal{E})},$$

$$||u||^2_{L^2(\mathcal{E})} \leq C\left(1 + \log\frac{H}{h}\right)||u||^2_{H^1(\Omega_j)},$$

$$||u - \bar{u}_{\mathcal{E}}||^2_{L^2(\mathcal{E})} \leq C\left(1 + \log\frac{H}{h}\right)|u|^2_{H^1(\Omega_j)},$$

where $\bar{u}_{\mathcal{E}}$ is the average value of u over $\mathcal{E}$. The last two inequalities hold also in case the norm and seminorm on the right-hand side are replaced with the $H^{1/2}(\Omega_j)$ norm and seminorm respectively.

Lemma 3.3 (Face estimate)**.** *Let $\mathcal{F}$ be a face of $\partial\Omega_j$ and $\theta_{\mathcal{F}}$ be the finite element function*

$$\theta_{\mathcal{F}} \in V_h(\Omega_j), \qquad \theta_{\mathcal{F}} = \begin{cases} 1 & \text{on nodal points of } \mathcal{F} \\ 0 & \text{elsewhere.} \end{cases}$$

Then, $\forall u \in V_h(\Omega_j)$,

$$|I^h(\theta_{\mathcal{F}}(u - \bar{u}_{\mathcal{F}}))|^2_{H^{1/2}(\mathcal{F})} \leq C\left(1 + \log\frac{H}{h}\right)^2 |u|^2_{H^{1/2}(\partial\Omega_j)}.$$

where $\bar{u}_{\mathcal{F}}$ is the average value of u over $\mathcal{F}$. The same bound holds if the seminorm on the left-hand side is replaced by the norm of $H_{00}^{1/2}(\mathcal{F})$. It follows [116, Lemma 6.36]

$$||\theta_{\mathcal{F}}(\bar{u}_{i,\mathcal{F}} - \bar{u}_{j,\mathcal{F}})||^2_{H_{00}^{1/2}(\mathcal{F})} \leq C \left(1 + \log \frac{H}{h}\right)^2 \left(|u_i|^2_{H^{1/2}(\mathcal{F})} + |u_j|^2_{H^{1/2}(\mathcal{F})}\right).$$

Lemma 3.4. *Let $\bar{u}_{\mathcal{F}}$ and $\bar{u}_{\mathcal{E}}$ be the average of u over $\mathcal{F}$ and $\mathcal{E}$ respectively. Then,*

$$(\bar{u}_{\mathcal{F}})^2 \leq CH^{-2}||u||^2_{L^2(\mathcal{F})}$$
$$(\bar{u}_{\mathcal{E}})^2 \leq CH^{-1}||u||^2_{L^2(\mathcal{E})}$$

where H is the subdomain diameter.

Chapter 4

Newton-Krylov Dual-Primal methods for the Decoupled Bidomain problem

As already introduced at the end of Chapter 2, two strategies arise when dealing with fully implicit time discretizations: a staggered, or decoupled, approach, where for each time step the ionic model is solved first and then its solution is used for solving and updating the Bidomain system; a monolithic, or coupled, approach, where the nonlinear system (including the ionic variables) is solved as a unique problem. In the same Chapter, we proved Lemma 2.2, which provides an upper and a lower bound for the bilinear form associated with the decoupled Jacobian Bidomain system. This Lemma is fundamental for the theoretical estimate for the condition number of the operator proposed in Chap. 2, preconditioned by FETI-DP and BDDC preconditioners (Chap. 3).

In this Chapter, after the introduction of local bilinear forms defined on each subdomain, we prove an upper bound for the projection operator, both scaled by the standard ρ-scaling and by the deluxe scaling. Then, we conclude the Chapter with the estimate of the condition number, both in case of FETI-DP and BDDC preconditioners, showing that the same bound holds, as they have been proved to be spectrally equivalent in Refs. [78, 83].

The main results of this Chapter have been submitted for publication and a preprint version can be found in Reference [65]. We notice that a similar bound for the projection, while using the ρ-scaling, has been developed in Reference [127], where a semi-implicit time discretization was applied: in our approach the main difficulty is given by the presence of the nonlinear reaction term I_{ion}, which influences the elliptic bound in Lemma 2.2.

Local bilinear forms. In the non-overlapping framework, the global system matrix (see Eq. (2.11) and (2.14) for the decoupled problem) is never formed explicity, but a local version with the same structure is assembled on each subdomain, by restricting the integration set from Ω to Ω_j

$$a_{i,e}^{(j)}(\varphi, \psi) = \int_{\Omega_j} D_{i,e}^{(j)} \nabla \varphi \cdot \nabla \psi,$$

and by defining the local bilinear forms (i.e. the local analog of the global forms defined in (2.15), (2.4.2))

$$a_{bido}^{(j)}(s, \phi) = \chi C_m (s_i - s_e, \varphi_i - \varphi_e)_{|\Omega_j} + \tau a_i (s_i, \varphi_i)^{(j)} + \tau a_e (s_e, \varphi_e)^{(j)}$$

$$+ \tau \left(\sum_l \frac{\partial I_{\mathrm{ion}}}{\partial v_l}(v^k)(s_{i,l} - s_{e,l}) \varphi_l, \varphi_i - \varphi_e \right)_{|\Omega_j},$$

$$a_{mono}^{(j)}(s, \varphi) = \chi C_m (s, \varphi)_{|\Omega_j} + \tau a (s, \varphi)^{(j)} + \tau \left(\sum_l \frac{\partial I_{\mathrm{ion}}}{\partial v_l}(v^k) s_l \varphi_l, \varphi \right)_{|\Omega_j},$$

51

where $(\,\cdot\,,\cdot\,)_{|\Omega_j}$ denotes the restriction of the L^2-inner product on the j-th subdomain.

These definitions are admissible here, as the proposed theory allows constant non-negative distribution of the conductivity coefficients among all subdomains, with large jumps aligned to the interfaces.

Since the Jacobian Bidomain (Monodomain) system 2.11 (2.14) is symmetric positive semidefinite (definite), the Schur complement matrix $\widehat{S}_\Gamma$ is also symmetric positive semidefinite (definite). Thus, it is possible to apply iterative methods for symmetric positive definite systems, such as the Conjugate Gradient method, taking care to start and keep the iteration in the orthogonal space of the possible operator kernel.

The following results will be stated in terms of the Jacobian Bidomain problem, as the case of the Jacobian Monodomain problem is analogous.

We define the Jacobian Bidomain local discrete harmonic extension operators as follows:

$$\mathcal{H}_j : W_\Gamma^{(j)} \longrightarrow W^{(j)}, \qquad \mathcal{H}_j w_\Gamma^{(j)} = \begin{cases} -K_{II}^{(j)-1} K_{I\Gamma}^{(j)} w_\Gamma^{(j)} & \text{on } W_I^{(j)} \\ w_\Gamma^{(j)} & \text{on } W_\Gamma^{(j)} \end{cases}.$$

It is appropriate to notice that the local discrete harmonic extension of a constant vector is the vector itself. From now on, we will use the componentwise notation

$$\mathcal{H}_j w_\Gamma^{(j)} = \left(\mathcal{H}_j^i w_\Gamma^{(j)}, \mathcal{H}_j^e w_\Gamma^{(j)} \right),$$

where the superscripts i, e denote the usual intra- and extracellular component.

Moreover, it would be useful to remark some useful properties between this object and the Schur complement matrices (see [116]). First, the Schur bilinear form can be defined through the action of the Schur complement matrix and the Jacobian bilinear form

$$a_{bido}^{(j)}(\mathcal{H}_j u_\Gamma^{(j)}, \mathcal{H}_j v_\Gamma^{(j)}) = v_\Gamma^{(j)} S_\Gamma^{(j)} u_\Gamma^{(j)} = s^{(j)}(u_\Gamma^{(j)}, v_\Gamma^{(j)}).$$

From the definition of $S_\Gamma^{(j)}$, it follows immediately that the bilinear form $s^{(j)}(\cdot, \cdot)$ is symmetric and coercive. Thanks to Lemma 2.2 it is possible to bound the energies related to the local Schur complements and prove that

$$s^{(j)}(u_\Gamma^{(j)}, u_\Gamma^{(j)}) = \min_{u_\Gamma^{(j)}} a_{bido}^{(j)}(\mathcal{H}_j u_\Gamma^{(j)}, \mathcal{H}_j u_\Gamma^{(j)}), \tag{4.1}$$

which allows us to consider the corresponding discrete harmonic extensions, instead of working with functions defined on Γ.

4.1 Convergence rate estimate for the decoupled Bidomain and Monodomain systems

Here we first prove our main result for the projection operator while using the standard ρ-scaling, then we show the analogous result for the deluxe scaling.

Lemma 4.1. *Assume that the primal space is spanned by the vertex nodal finite element functions and the edge cutoff functions. Let the Bidomain projection operator be scaled by either the standard ρ-scaling or the deluxe scaling. Then*

$$|P_D u|_{S_\Gamma}^2 \lesssim \max_{\substack{k=1,\ldots,N \\ \star=i,e}} \frac{\tau \sigma_M^{\star(k)} + H^2 \left(\chi C_M + \tau K_M \right)}{\tau \sigma_m^{\star(k)}} \left(1 + \log \frac{H}{h} \right)^n |u|_{S_\Gamma}^2,$$

$\forall u \in \widetilde{W}_\Gamma$, with $n = 2$ in case of ρ-scaling, $n = 3$ in case of deluxe-scaling.

By using the same arguments as in the Bidomain case, it is easy to extend this result also to the Monodomain Jacobian system.

Lemma 4.2. *Assume that the primal space is spanned by the vertex nodal finite element functions and the edge cutoff functions. Let the Monodomain projection operator be scaled by the standard ρ-scaling or the deluxe scaling. Then*

$$|P_D u|_{S_\Gamma}^2 \lesssim \max_{k=1,\dots,N} \frac{\tau \sigma_M^{(k)} + H^2 \left(\chi C_M + \tau K_M\right)}{\tau \sigma_m^{(k)}} \left(1 + \log \frac{H}{h}\right)^n |u|_{S_\Gamma}^2$$

holds $\forall u \in \widetilde{W}_\Gamma$, with $n = 2$ in case of ρ-scaling, $n = 3$ in case of deluxe-scaling.

4.1.1 Proof of Lemma 4.1 with ρ-scaling

Using the ρ-scaling, we will need the standard counting functions of the Neumann-Neumann methods and in particular their pseudoinverses, which can be defined for the Bidomain model as follows: $\forall x \in \Gamma^{(j)}$

$$\delta_j^{i,e\ \dagger}(x) = \frac{\sigma_M^{i,e^{(j)}}}{\sum_{k \in \mathcal{N}_x} \sigma_M^{i,e^{(k)}}}, \qquad \sigma_M^{i,e^{(j)}} = \max_{\bullet=\{l,t,n\}} \sigma_\bullet^{i,e^{(j)}},$$

and the following property (see [116]) holds

$$\sigma_M^{i,e^{(j)}} \left(\delta_k^{i,e\ \dagger}\right)^2 \leq \min\left\{\sigma_M^{i,e^{(j)}}, \sigma_M^{i,e^{(k)}}\right\}.$$

In this case, the action of the scaling operator on a given function $w \in \widetilde{W}_\Gamma$ is locally defined for the decoupled Jacobian Bidomain model as

$$(P_D w(x))_j = \left(\sum_{k \in \mathcal{N}_x} \delta_k^{i\ \dagger}(w_j^i(x) - w_k^i(x)), \sum_{k \in \mathcal{N}_x} \delta_k^{e\ \dagger}(w_j^e(x) - w_k^e(x))\right).$$

By eliminating all internal variables of Ω_j, we denote by $S_\Gamma^{(j)}$ the local Schur complement matrix and S_Γ the global unassembled Schur complement matrix:

$$S_\Gamma^{(j)} = \begin{bmatrix} S_{\Delta\Delta}^{(j)} & S_{\Delta\Pi}^{(j)} \\ S_{\Pi\Delta}^{(j)} & S_{\Pi\Pi}^{(j)} \end{bmatrix}, \qquad S_\Gamma = \operatorname*{diag}_j S_\Gamma^{(j)}.$$

Let $\Theta_{\mathcal{E}^{jk}}$, $\Theta_{\mathcal{F}^{jk}}$ and $\Theta_{\mathcal{V}^{jk}}$ be the characteristic finite element functions associated with and edge $\mathcal{E}^{jk}$, a face $\mathcal{F}^{jk}$ and a vertex $\mathcal{V}^{jk}$ between two substructures Ω_j and Ω_k. Those functions form a partition-of-unity associated with the decomposition of Γ into edges, faces and vertices. For brevity, we will write $\Theta_* = \left(\theta_*^i, \theta_*^e\right)$, with $* = \{\mathcal{E}, \mathcal{F}, \mathcal{V}\}$, and drop the index jk, unless an explicit ambiguity occurs.

In the substructuring framework, the global estimate on P_D can be established by bounds calculated locally: indeed, by introducing the operator $R_{\partial\Omega_j}$ that restricts the finite element function w to the subdomain boundary $\partial\Omega_j$, it is straightforward to observe that

$$|w|_{S_\Gamma}^2 = \langle w, w \rangle_{S_\Gamma} = \sum_{j=1}^{N} \langle w^{(j)}, w^{(j)} \rangle_{S_\Gamma^{(j)}}$$

$$= \sum_{j=1}^{N} \langle R_{\partial\Omega_j} w^{(j)}, R_{\partial\Omega_j} w^{(j)} \rangle_{S_\Gamma^{(j)}} = \sum_{j=1}^{N} |R_{\partial\Omega_j} w|_{S_\Gamma^{(j)}}^2$$

for all $w \in \widetilde{W}_\Gamma$. Thus, the thesis becomes

$$|P_D u|_{S_\Gamma}^2 = \sum_{j=1}^{N} |R_{\partial\Omega_j} P_D u|_{S_\Gamma^{(j)}}^2.$$

We denote by I^h the finite element interpolant,

$$v_j(x) = (P_D u(x))_j = \left(\sum_{k \in \mathcal{N}_x} I^h(\delta_k^{i\;\dagger}(u_j^i(x) - u_k^i(x))), \sum_{k \in \mathcal{N}_x} I^h(\delta_k^{e\;\dagger}(u_j^e(x) - u_k^e(x))) \right)$$
$$= \sum_{\mathcal{E}} I^h(\Theta_{\mathcal{E}} v_j) + \sum_{\mathcal{F}} I^h(\Theta_{\mathcal{F}} v_j) + \sum_{\mathcal{V}} I^h(\Theta_{\mathcal{V}} v_j).$$

We note that with our assumption on the primal space, the vertex contribution vanishes, as

$$v_j(x) = v_k(x) \qquad \forall x \in V_h, \quad j, k \in \mathcal{N}_x,$$

thus we only need to estimate the edge and face contributions.
Since each local Schur complement is positive semidefinite, it holds

$$|v_j|_{S_\Gamma^{(j)}}^2 \lesssim \sum_{\mathcal{E}} |I^h(\Theta_{\mathcal{E}} v_j)|_{S_\Gamma^{(j)}}^2 + \sum_{\mathcal{F}} |I^h(\Theta_{\mathcal{F}} v_j)|_{S_\Gamma^{(j)}}^2.$$

Since the Schur seminorm realizes the minimum of the bilinear form (Eq (4.1)), each component of the above sum can be bounded from above by using Lemma 2.2:

$$|I^h(\Theta_* v_j)|_{S_\Gamma^{(j)}}^2 = s_j \left(I^h(\Theta_* v_j), I^h(\Theta_* v_j) \right)$$
$$= a_j \left(\mathcal{H}_j^{i,e} I^h(\Theta_* v_j), \; \mathcal{H}_j^{i,e} I^h(\Theta_* v_j) \right)$$
$$\leq (\chi C_m + \tau K_M) \, \|\mathcal{H}_j^{\Delta} I^h(\Theta_*(v_j^i - v_j^e))\|_{L^2(\Omega_j)}^2 +$$
$$+ \tau \sigma_M^i |\mathcal{H}_j^{\Delta} I^h(\Theta_* v_j^i)|_{H^1(\Omega_j)}^2 + \tau \sigma_M^e |\mathcal{H}_j^{\Delta} I^h(\Theta_* v_j^e)|_{H^1(\Omega_j)}^2.$$

As the argument of the L^2-norm vanishes on a two-dimensional subset of $\Gamma^{(j)}$, we can use the Poincaré-Friedrichs inequality (Prop. 3.1) and the Trace theorem (Thm. 3.1) as follows:

$$\|\mathcal{H}_j^{\Delta} I^h(\Theta_* v_j)\|_{L^2(\Omega_j)}^2 \overset{Prop.3.1}{\lesssim} H^2 |\mathcal{H}_j^{\Delta} I^h(\Theta_* v_j)|_{H^1(\Omega_j)}^2 \overset{Thm3.1}{\sim} H^2 |I^h(\Theta_* v_j)|_{H^{1/2}(\Gamma^{(j)})}^2,$$

$$|\mathcal{H}_j^{\Delta} I^h(\Theta_* v_j)|_{H^1(\Omega_j)}^2 \overset{Thm3.1}{\sim} |I^h(\Theta_* v_j)|_{H^{1/2}(\Gamma^{(j)})}^2,$$

to obtain

$$|v_j|_{S_\Gamma^{(j)}}^2 \lesssim \sum_{\substack{*=\mathcal{E}, \mathcal{F} \\ \star = i, e}} \left[\tau \sigma_M^{\star(j)} + H^2 \left(\chi C_m + \tau K_M \right) \right] |I^h(\Theta_* v_j^\star)|_{H^{1/2}(\Gamma^{(j)})}^2. \tag{4.2}$$

We now proceed to estimate the contribution from edges and faces separately.

Edge contribution We recall that in dual-primal construction,

$$\forall v_j^{i,e} \in \widetilde{W}_\Gamma, \qquad v_j^{i,e} = \sum_{k \in \mathcal{K}_{\mathcal{E}}} \delta_j^{i,e\;\dagger}(u_j^{i,e} - u_k^{i,e}), \tag{4.3}$$

where $\mathcal{K}_{\mathcal{E}} = \mathcal{N}_{\mathcal{E}} \setminus \{j\}$ is the index set of subdomains sharing $\mathcal{E}$. Therefore, thanks to Lemma 3.2, Equation (4.3) and the triangle inequality, we have

$$|I^h(\Theta_{\mathcal{E}} v_j^{i,e})|_{H^{1/2}(\Gamma^{(j)})}^2 \lesssim \|v_j^{i,e}\|_{L^2(\mathcal{E})}^2$$
$$= \| \sum_{k \in \mathcal{K}_{\mathcal{E}}} \delta_k^{i,e\;\dagger} \left(u_j^{i,e} - u_k^{i,e} \right) \|_{L^2(\mathcal{E})}^2$$
$$\lesssim \sum_{k \in \mathcal{K}_{\mathcal{E}}} \left(\delta_k^{i,e\;\dagger} \right)^2 \|u_j^{i,e} - \bar{u}_{\mathcal{E}}^{i,e}\|_{L^2(\mathcal{E})}^2 + \sum_{k \in \mathcal{K}_{\mathcal{E}}} \left(\delta_k^{i,e\;\dagger} \right)^2 \|u_k^{i,e} - \bar{u}_{\mathcal{E}}^{i,e}\|_{L^2(\mathcal{E})}^2$$

$$\lesssim \left(1 + \log \frac{H}{h}\right) \left[\sum_{k \in \mathcal{K}_{\mathcal{E}}} \left(\delta_k^{i,e \dagger}\right)^2\right] |\mathcal{H}_j^{i,e} u_j|_{H^1(\Omega_j)}^2 + \left(1 + \log \frac{H}{h}\right) \sum_{k \in \mathcal{K}_{\mathcal{E}}} \left(\delta_k^{i,e \dagger}\right)^2 |\mathcal{H}_k^{i,e} u_k|_{H^1(\Omega_k)}^2$$

$$= \left(1 + \log \frac{H}{h}\right) \left[\sum_{k \in \mathcal{K}_{\mathcal{E}}} \left(\delta_k^{i,e \dagger}\right)^2 |\mathcal{H}_j^{i,e} u_j|_{H^1(\Omega_j)}^2 + \sum_{k \in \mathcal{K}_{\mathcal{E}}} \left(\delta_k^{i,e \dagger}\right)^2 |\mathcal{H}_k^{i,e} u_k|_{H^1(\Omega_k)}^2\right].$$

Note that, by definition of pseudoinverses,

$$\sum_l \left(\delta_l^{i,e \dagger}\right)^2 \leq \left(\sum_l \delta_l^{i,e \dagger}\right)^2 = \left(\sum_l \frac{\sigma_M^{i,e^{(l)}}}{\sum_{k \in \mathcal{N}_x} \sigma_M^{i,e^{(k)}}}\right) \leq 1$$

yelding $\sum_{k \in \mathcal{K}_{\mathcal{E}}} \left(\delta_k^{i,e \dagger}\right)^2 \leq 1$. Moreover, we recall the following property

$$\sigma_M^{i,e^{(j)}} \left(\delta_k^{i,e \dagger}\right)^2 \leq \min\left\{\sigma_M^{i,e^{(j)}}, \sigma_M^{i,e^{(k)}}\right\},$$

from which we can conclude that either

$$\sigma_M^{i,e^{(j)}} \left(\delta_k^{i,e \dagger}\right)^2 \leq \sigma_M^{i,e^{(j)}} \qquad \text{or} \qquad \sigma_M^{i,e^{(j)}} \left(\delta_k^{i,e \dagger}\right)^2 \leq \sigma_M^{i,e^{(k)}}. \tag{4.4}$$

Consequently, the edge terms in inequality (4.2) can be bounded as follows, using inequalities (4.4) and Lemma 2.2:

$$|P_D u_j|_{S_\Gamma^{(j)}}^2 = |v_j|_{S_\Gamma^{(j)}}^2$$

$$\lesssim \sum_{\star=i,e} \left[\tau \sigma_M^{\star(j)} + H^2 \left(\chi C_m + \tau K_M\right)\right] \left(1 + \log \frac{H}{h}\right) \times$$

$$\times \left[\sum_{k \in \mathcal{K}_{\mathcal{E}}} \left(\delta_k^{\star \dagger}\right)^2 |\mathcal{H}_j^\star u_j|_{H^1(\Omega_j)}^2 + \sum_{k \in \mathcal{K}_{\mathcal{E}}} \left(\delta_k^{\star \dagger}\right)^2 |\mathcal{H}_k^\star u_k|_{H^1(\Omega_k)}^2\right]$$

$$= \sum_{\star=i,e} \left[\tau \sigma_M^{\star(j)} + H^2 \left(\chi C_m + \tau K_M\right)\right] \left(1 + \log \frac{H}{h}\right) \underbrace{\sum_{k \in \mathcal{K}_{\mathcal{E}}} \left(\delta_k^{\star \dagger}\right)^2}_{\leq 1} |\mathcal{H}_j^\star u_j|_{H^1(\Omega_j)}^2 +$$

$$+ \sum_{\star=i,e} \left[\tau \sigma_M^{\star(j)} + H^2 \left(\chi C_m + \tau K_M\right)\right] \left(1 + \log \frac{H}{h}\right) \sum_{k \in \mathcal{K}_{\mathcal{E}}} \left(\delta_k^{\star \dagger}\right)^2 |\mathcal{H}_k^\star u_k|_{H^1(\Omega_k)}^2$$

$$\lesssim \sum_{\star=i,e} \left[\tau \sigma_M^{\star(j)} + H^2 \left(\chi C_m + \tau K_M\right)\right] \left(1 + \log \frac{H}{h}\right) |\mathcal{H}_j^\star u_j|_{H^1(\Omega_j)}^2 +$$

$$+ \sum_{\star=i,e} \sum_{k \in \mathcal{K}_{\mathcal{E}}} \left[\tau \sigma_M^{\star(j)} + H^2 \left(\chi C_m + \tau K_M\right)\right] \left(1 + \log \frac{H}{h}\right) \left(\delta_k^{\star \dagger}\right)^2 |\mathcal{H}_k^\star u_k|_{H^1(\Omega_k)}^2$$

$$\lesssim \sum_{\star=i,e} \left[\tau \sigma_M^{\star(j)} + H^2 \left(\chi C_m + \tau K_M\right)\right] \left(1 + \log \frac{H}{h}\right) |\mathcal{H}_j^\star u_j|_{H^1(\Omega_j)}^2 +$$

$$+ \sum_{\star=i,e} \sum_{k \in \mathcal{K}_{\mathcal{E}}} \left[\tau \underbrace{\sigma_M^{\star(j)} \left(\delta_k^{\star \dagger}\right)^2}_{\substack{\text{for Ineq. (4.4)} \\ \leq \sigma_M^{\star(k)}}} + H^2 \left(\chi C_m + \tau K_M\right) \underbrace{\left(\delta_k^{\star \dagger}\right)^2}_{\leq 1}\right] \left(1 + \log \frac{H}{h}\right) |\mathcal{H}_k^\star u_k|_{H^1(\Omega_k)}^2$$

$$\lesssim \sum_{\star=i,e} \left[\tau \sigma_M^{\star(j)} + H^2 \left(\chi C_m + \tau K_M\right)\right] \left(1 + \log \frac{H}{h}\right) |\mathcal{H}_j^\star u_j|_{H^1(\Omega_j)}^2 +$$

$$+ \sum_{\star=i,e} \sum_{k\in\mathcal{K}_\mathcal{E}} \left[\tau\sigma_M^{\star(k)} + H^2\left(\chi C_m + \tau K_M\right) \right] \left(1 + \log\frac{H}{h}\right) |\mathcal{H}_k^\star u_k|^2_{H^1(\Omega_k)}$$

$$= \sum_{\star=i,e} \frac{\tau\sigma_M^{\star(j)} + H^2\left(\chi C_m + \tau K_M\right)}{\tau\sigma_m^{\star(j)}} \left(1 + \log\frac{H}{h}\right) \sigma_m^{\star(j)}|\mathcal{H}_j^\star u_j|^2_{H^1(\Omega_j)} +$$

$$+ \sum_{\star=i,e} \sum_{k\in\mathcal{K}_\mathcal{E}} \frac{\tau\sigma_M^{\star(k)} + H^2\left(\chi C_m + \tau K_M\right)}{\tau\sigma_m^{\star(k)}} \left(1 + \log\frac{H}{h}\right) \sigma_m^{\star(k)}|\mathcal{H}_k^\star u_k|^2_{H^1(\Omega_k)}$$

$$\leq \max_{\star=i,e} \frac{\tau\sigma_M^{\star(j)} + H^2\left(\chi C_m + \tau K_M\right)}{\tau\sigma_m^{\star(j)}} \left(1 + \log\frac{H}{h}\right) |u_j|^2_{S_\Gamma^{(j)}} +$$

$$+ \sum_{k\in\mathcal{K}_\mathcal{E}} \max_{\star=i,e} \frac{\tau\sigma_M^{\star(j)} + H^2\left(\chi C_m + \tau K_M\right)}{\tau\sigma_m^{\star(k)}} \left(1 + \log\frac{H}{h}\right) |u_k|^2_{S_\Gamma^{(k)}}$$

$$= \left(1 + \log\frac{H}{h}\right) \max_{\star=i,e} \sum_{k\in\mathcal{N}_\mathcal{E}} \left(\frac{\tau\sigma_M^{\star(k)} + H^2\left(\chi C_m + \tau K_M\right)}{\tau\sigma_m^{\star(k)}} \right) |u|^2_{S_\Gamma^{(k)}},$$

since the number of subdomains sharing an edge is finite. In conclusion,

$$|P_D u|^2_{S_\Gamma^{(j)}} \lesssim \left(1 + \log\frac{H}{h}\right) \max_{\substack{k\in\mathcal{N}_\mathcal{E} \\ \star=i,e}} \frac{\tau\sigma_M^{\star(k)} + H^2\left(\chi C_m + \tau K_M\right)}{\tau\sigma_m^{\star(k)}} \sum_{k\in\mathcal{N}_\mathcal{E}} |u|^2_{S_\Gamma^{(k)}}.$$

Face contribution   The procedure is essentially the same as the edge term estimate, but we need to treat differently the addition of the average values: since we have not included the face averages in the primal space, it could happen that the mean on the face $\mathcal{F}^{jk}$ takes different values from the substructure j and from k. Therefore,

$$|I^h(\Theta_\mathcal{F} v_j^{i,e})|^2_{H^{1/2}(\Gamma^{(j)})} \lesssim |I^h(\Theta_\mathcal{F} \delta_j^{i,e\,\dagger}(u_j^{i,e} - u_k^{i,e}))|^2_{H^{1/2}(\Gamma^{(j)})}$$

$$\lesssim ||I^h(\Theta_\mathcal{F} \delta_j^{i,e\,\dagger}(u_j^{i,e} - u_k^{i,e}))||^2_{H_{00}^{1/2}(\mathcal{F})}$$

$$\leq \left(\delta_j^{i,e\,\dagger}\right)^2 ||I^h(\Theta_\mathcal{F}(u_j^{i,e} - u_k^{i,e}))||^2_{H_{00}^{1/2}(\mathcal{F})}$$

$$\leq \left(\delta_j^{i,e\,\dagger}\right)^2 ||I^h(\Theta_\mathcal{F}\left(u_j^{i,e} - \bar{u}_{j,\mathcal{F}}^{i,e}\right))||^2_{H_{00}^{1/2}(\mathcal{F})} + \left(\delta_j^{i,e\,\dagger}\right)^2 ||I^h(\Theta_\mathcal{F}\left(u_k^{i,e} - \bar{u}_{k,\mathcal{F}}^{i,e}\right))||^2_{H_{00}^{1/2}(\mathcal{F})} +$$

$$+ \left(\delta_j^{i,e\,\dagger}\right)^2 ||I^h(\Theta_\mathcal{F}\left(\bar{u}_{j,\mathcal{F}}^{i,e} - \bar{u}_{k,\mathcal{F}}^{i,e}\right))||^2_{H_{00}^{1/2}(\mathcal{F})}$$

$$= \left(\delta_j^{i,e\,\dagger}\right)^2 ||I^h(\Theta_\mathcal{F}\left(u_j^{i,e} - \bar{u}_{j,\mathcal{F}}^{i,e}\right))||^2_{H_{00}^{1/2}(\mathcal{F})} + \left(\delta_j^{i,e\,\dagger}\right)^2 ||I^h(\Theta_\mathcal{F}\left(u_k^{i,e} - \bar{u}_{k,\mathcal{F}}^{i,e}\right))||^2_{H_{00}^{1/2}(\mathcal{F})} +$$

$$+ \left(\delta_j^{i,e\,\dagger}\right)^2 ||\Theta_\mathcal{F}\left(\bar{u}_{j,\mathcal{F}}^{i,e} - \bar{u}_{k,\mathcal{F}}^{i,e}\right)||^2_{H_{00}^{1/2}(\mathcal{F})}$$

$$\lesssim \left(1 + \log\frac{H}{h}\right)^2 \left(\delta_j^{i,e\,\dagger}\right)^2 |u_j^{i,e}|^2_{H^{1/2}(\Gamma^{(j)})} + \left(1 + \log\frac{H}{h}\right)^2 \left(\delta_j^{i,e\,\dagger}\right)^2 |u_k^{i,e}|^2_{H^{1/2}(\Gamma^{(k)})} +$$

$$+ \left(1 + \log\frac{H}{h}\right)^2 \left(\delta_j^{i,e\,\dagger}\right)^2 \left[|u_j^{i,e}|^2_{H^{1/2}(\mathcal{F})} + |u_k^{i,e}|^2_{H^{1/2}(\mathcal{F})} \right]$$

$$\lesssim 2\left(1 + \log\frac{H}{h}\right)^2 \left(\delta_j^{i,e\,\dagger}\right)^2 \left[|\mathcal{H}_j^{i,e}u_j|^2_{H^1(\Omega_j)} + |\mathcal{H}_k^{i,e}u_k|^2_{H^1(\Omega_k)} \right]$$

$$\leq 2\left(1 + \log\frac{H}{h}\right)^2 \left(\delta_j^{i,e\,\dagger}\right)^2 \left[\frac{1}{\tau\sigma_m^{i,e(j)}} a_j\left(\mathcal{H}_j^{i,e}u_j,\ \mathcal{H}_j^{i,e}u_j\right) + \frac{1}{\tau\sigma_m^{i,e(k)}} a_k\left(\mathcal{H}_k^{i,e}u_k,\ \mathcal{H}_k^{i,e}u_k\right) \right]$$

$$= 2\left(1 + \log\frac{H}{h}\right)^2 \left(\delta_j^{i,e\,\dagger}\right)^2 \left[\frac{1}{\tau\sigma_m^{i,e(j)}} |u_j|^2_{S_\Gamma^{(j)}} + \frac{1}{\tau\sigma_m^{i,e(k)}} |u_k|^2_{S_\Gamma^{(k)}} \right],$$

by applying Lemmas 3.1 and 3.3, the Trace theorem (Thm 3.1) and the ellipticity property (Prop. 2.2). In the same fashion as with the edge term, we can conclude our proof with the estimate of

the face term

$$|P_D u|^2_{S_\Gamma^{(j)}} \lesssim \left(1 + \log \frac{H}{h}\right)^2 \max_{\substack{t=j,k \\ \star=i,e}} \frac{\tau\sigma_M^{\star(k)} + H^2\left(\chi C_m + \tau K_M\right)}{\tau\sigma_m^{\star(t)}} \left[|u_j|^2_{S_\Gamma^{(j)}} + |u_k|^2_{S_\Gamma^{(k)}}\right].$$

4.1.2 Proof of Lemma 4.1 with *deluxe* scaling

We now show that, for the Jacobian Bidomain linear system, the same bound holds when the deluxe scaling is used. This particular scaling (see Chapter 3) is based on the solution of local problems built from local Schur complements associated with the dual unknowns. In this particular application, the bound is essentially the same as for the ρ-scaling, but it can be potentially more efficient when applied to other systems or discretizations.

As in the previous proof, instead of proving the bound for the projection operator E_D, we prove it for the complementary projection P_D (3.5). Moreover, in the same fashion, it is sufficient to compute only the local bounds, since $|P_D u|^2_{S_\Gamma} = \sum_{j=1}^N |R_{\partial\Omega_j} P_D u|^2_{S_\Gamma^{(j)}}$. Thus, for all $u \in \widetilde{W}_\Gamma$

$$R_{\partial\Omega_j} P_D u = R_{\partial\Omega_j}\left(u_\Delta - \sum_{*=\{\mathcal{F},\mathcal{E}\}} R_*^T \bar{u}_*\right),$$

that leads to

$$|R_{\partial\Omega_j} P_D u|^2_{S_\Gamma^{(j)}} \leq |\Xi_j^*| \sum_{\substack{*=\{\mathcal{F},\mathcal{E}\} \\ *\in\Xi_j^*}} |R_*^T\left(u_{j,*}^{i,e} - \bar{u}_*^{i,e}\right)|^2_{S_\Gamma^{(j)}},$$

where Ξ_j^* is the index set containing the indices of the subdomains that share the face $\mathcal{F}$ or the edge $\mathcal{E}$. Let us distinguish between face and edge contributions.

Face contribution Suppose that the face $\mathcal{F}$ is shared by subdomains Ω_j and Ω_k. Then, by simple algebra, it follows

$$
\begin{aligned}
u_{j,\mathcal{F}}^{i,e} - \bar{u}_\mathcal{F}^{i,e} &= u_{j,\mathcal{F}}^{i,e} - \left(S_\mathcal{F}^{(j)} + S_\mathcal{F}^{(k)}\right)^{-1}\left(S_\mathcal{F}^{(j)} u_{j,\mathcal{F}}^{i,e} + S_\mathcal{F}^{(k)} u_{k,\mathcal{F}}^{i,e}\right) \\
&= \left(S_\mathcal{F}^{(j)} + S_\mathcal{F}^{(k)}\right)^{-1} S_\mathcal{F}^{(k)}\left(u_{j,\mathcal{F}}^{i,e} - u_{k,\mathcal{F}}^{i,e}\right) \\
&= \left(S_\mathcal{F}^{(j)} + S_\mathcal{F}^{(k)}\right)^{-1} S_\mathcal{F}^{(k)}\left[\left(u_{j,\mathcal{F}}^{i,e} - \bar{u}_{j,\mathcal{F}}^{i,e}\right) - \left(u_{k,\mathcal{F}}^{i,e} - \bar{u}_{k,\mathcal{F}}^{i,e}\right) + \left(\bar{u}_{j,\mathcal{F}}^{i,e} - \bar{u}_{k,\mathcal{F}}^{i,e}\right)\right],
\end{aligned}
$$

where we add and subtract the mean values $\bar{u}_{j,\mathcal{F}}^{i,e}$ and $\bar{u}_{k,\mathcal{F}}^{i,e}$ of u over the face $\mathcal{F}$ of subdomains j and k respectively. Therefore, it follows

$$
\begin{aligned}
|R_\mathcal{F}^T\left(u_{j,\mathcal{F}}^{i,e} - \bar{u}_\mathcal{F}^{i,e}\right)|^2_{S_\Gamma^{(j)}} &= \left(u_{j,\mathcal{F}}^{i,e} - \bar{u}_\mathcal{F}^{i,e}\right)^T \underbrace{R_\mathcal{F} S_\Gamma^{(j)} R_\mathcal{F}^T}_{S_\mathcal{F}^{(j)}} \left(u_{j,\mathcal{F}}^{i,e} - \bar{u}_\mathcal{F}^{i,e}\right) = \left(u_{j,\mathcal{F}}^{i,e} - \bar{u}_\mathcal{F}^{i,e}\right)^T S_\mathcal{F}^{(j)}\left(u_{j,\mathcal{F}}^{i,e} - \bar{u}_\mathcal{F}^{i,e}\right) \\
&= \left(u_{j,\mathcal{F}}^{i,e} - u_{k,\mathcal{F}}^{i,e}\right)^T S_\mathcal{F}^{(k)}\left(S_\mathcal{F}^{(j)} + S_\mathcal{F}^{(k)}\right)^{-1} S_\mathcal{F}^{(j)}\left(S_\mathcal{F}^{(j)} + S_\mathcal{F}^{(k)}\right)^{-1} S_\mathcal{F}^{(k)}\left(u_{j,\mathcal{F}}^{i,e} - u_{k,\mathcal{F}}^{i,e}\right) \\
&\leq \left(u_{j,\mathcal{F}}^{i,e} - \bar{u}_{j,\mathcal{F}}^{i,e}\right)^T S_\mathcal{F}^{(k)}\left(S_\mathcal{F}^{(j)} + S_\mathcal{F}^{(k)}\right)^{-1} S_\mathcal{F}^{(j)}\left(S_\mathcal{F}^{(j)} + S_\mathcal{F}^{(k)}\right)^{-1} S_\mathcal{F}^{(k)}\left(u_{j,\mathcal{F}}^{i,e} - \bar{u}_{j,\mathcal{F}}^{i,e}\right) + \\
&\quad + \left(u_{k,\mathcal{F}}^{i,e} - \bar{u}_{k,\mathcal{F}}^{i,e}\right)^T S_\mathcal{F}^{(k)}\left(S_\mathcal{F}^{(j)} + S_\mathcal{F}^{(k)}\right)^{-1} S_\mathcal{F}^{(j)}\left(S_\mathcal{F}^{(j)} + S_\mathcal{F}^{(k)}\right)^{-1} S_\mathcal{F}^{(k)}\left(u_{k,\mathcal{F}}^{i,e} - \bar{u}_{k,\mathcal{F}}^{i,e}\right) + \\
&\quad + \left(\bar{u}_{j,\mathcal{F}}^{i,e} - \bar{u}_{k,\mathcal{F}}^{i,e}\right)^T S_\mathcal{F}^{(k)}\left(S_\mathcal{F}^{(j)} + S_\mathcal{F}^{(k)}\right)^{-1} S_\mathcal{F}^{(j)}\left(S_\mathcal{F}^{(j)} + S_\mathcal{F}^{(k)}\right)^{-1} S_\mathcal{F}^{(k)}\left(\bar{u}_{j,\mathcal{F}}^{i,e} - \bar{u}_{k,\mathcal{F}}^{i,e}\right) \\
&\leq 2|u_{j,\mathcal{F}}^{i,e} - \bar{u}_{j,\mathcal{F}}^{i,e}|^2_{S_\mathcal{F}^{(j)}} + 2|u_{k,\mathcal{F}}^{i,e} - \bar{u}_{k,\mathcal{F}}^{i,e}|^2_{S_\mathcal{F}^{(k)}} + |\left(S_\mathcal{F}^{(j)} + S_\mathcal{F}^{(k)}\right)^{-1} S_\mathcal{F}^{(k)}\left(\bar{u}_{j,\mathcal{F}}^{i,e} - \bar{u}_{k,\mathcal{F}}^{i,e}\right)|^2_{S_\mathcal{F}^{(j)}},
\end{aligned}
$$

$\forall u_{j,\mathcal{F}}^{i,e} \in \widetilde{W}_\Gamma$, where in the last line we use the two inequalities

$$S_{\mathcal{F}}^{(k)} \left(S_{\mathcal{F}}^{(j)} + S_{\mathcal{F}}^{(k)}\right)^{-1} S_{\mathcal{F}}^{(j)} \left(S_{\mathcal{F}}^{(j)} + S_{\mathcal{F}}^{(k)}\right)^{-1} S_{\mathcal{F}}^{(k)} \le S_{\mathcal{F}}^{(j)}$$
$$S_{\mathcal{F}}^{(k)} \left(S_{\mathcal{F}}^{(j)} + S_{\mathcal{F}}^{(k)}\right)^{-1} S_{\mathcal{F}}^{(j)} \left(S_{\mathcal{F}}^{(j)} + S_{\mathcal{F}}^{(k)}\right)^{-1} S_{\mathcal{F}}^{(k)} \le S_{\mathcal{F}}^{(k)}. \tag{4.5}$$

These relations follows from the generalized eigenvalue problem $S_{\mathcal{F}}^{(j)}\phi = \lambda S_{\mathcal{F}}^{(k)}\phi$ and by observing that all eigenvalues are strictly positive [7].

It is sufficient now to estimate $|u_{j,\mathcal{F}}^{i,e} - \bar{u}_{j,\mathcal{F}}^{i,e}|_{S_{\mathcal{F}}^{(j)}}^2$ and $|\left(S_{\mathcal{F}}^{(j)} + S_{\mathcal{F}}^{(k)}\right)^{-1} S_{\mathcal{F}}^{(k)}\left(\bar{u}_{j,\mathcal{F}}^{i,e} - \bar{u}_{k,\mathcal{F}}^{i,e}\right)|_{S_{\mathcal{F}}^{(j)}}^2$; we note that, when the subdomain faces averages are included in the primal space, the last term is zero. Let us start from the first term, which we can bound by

$$|u_{j,\mathcal{F}}^{i,e} - \bar{u}_{j,\mathcal{F}}^{i,e}|_{S_{\mathcal{F}}^{(j)}}^2 = s_j\left(u_{j,\mathcal{F}} - \bar{u}_{j,\mathcal{F}}^{i,e}, u_{j,\mathcal{F}} - \bar{u}_{j,\mathcal{F}}^{i,e}\right)$$
$$\le (\chi C_m + \tau K_M) \|\mathcal{H}_j^\Delta\left(u_j - \bar{u}_{j,\mathcal{F}}^{i,e}\right)\|_{L^2(\Omega_j)}^2 +$$
$$+ \tau \sum_{\star=i,e} \sigma_M^\star |\mathcal{H}_j^\Delta\left(u_{j,\mathcal{F}} - \bar{u}_{j,\mathcal{F}}^\star\right)|_{H^1(\Omega_j)}^2$$
$$\lesssim \left[\tau\sigma_M^{i,e} + H^2\left(\chi C_m + \tau K_M\right)\right]|u_{j,\mathcal{F}} - \bar{u}_{j,\mathcal{F}}^{i,e}|_{H^{1/2}(\Gamma^{(j)})}^2,$$

by using the ellipticity Lemma 2.2, and the Poincaré-Friedrichs inequality (Prop. 3.1) combined with the Trace theorem (Thm. 3.1). In contrast to the previous Lemma, here we are already taking in consideration the discrete restriction of a function $u_j \in \widetilde{W}_\Gamma$ to the face $\mathcal{F}$. In this way the notations $u_j - \bar{u}_{j,\mathcal{F}}^{i,e}$ and $I^h(\Theta_{\mathcal{F}}(u_j - \bar{u}_{j,\mathcal{F}}^{i,e}))$ are essentially the same. Therefore, it is possible to apply Lemma 3.3 and the Trace theorem (Thm. 3.1) to obtain

$$|u_{j,\mathcal{F}}^{i,e} - \bar{u}_{j,\mathcal{F}}^{i,e}|_{S_\Gamma^{(j)}}^2 \lesssim \left[\tau\sigma_M^{i,e} + H^2\left(\chi C_m + \tau K_M\right)\right]\left(1 + \log\frac{H}{h}\right)^2 |u_j|_{H^{1/2}(\partial\Omega_j)}^2$$
$$\sim \left[\tau\sigma_M^{i,e} + H^2\left(\chi C_m + \tau K_M\right)\right]\left(1 + \log\frac{H}{h}\right)^2 |\mathcal{H}_j^\Delta u_j|_{H^1(\Omega_j)}^2.$$

Regarding the term $|\left(S_{\mathcal{F}}^{(j)} + S_{\mathcal{F}}^{(k)}\right)^{-1} S_{\mathcal{F}}^{(k)}\left(\bar{u}_{j,\mathcal{F}}^{i,e} - \bar{u}_{k,\mathcal{F}}^{i,e}\right)|_{S_{\mathcal{F}}^{(j)}}^2$, let $\mathcal{E} \subset \partial\mathcal{F}$ be a primal edge, such that $\bar{u}_{j,\mathcal{E}}^{i,e} = \bar{u}_{k,\mathcal{E}}^{i,e}$. Then, by using the two inequalities in (4.5)

$$|\left(S_{\mathcal{F}}^{(j)} + S_{\mathcal{F}}^{(k)}\right)^{-1} S_{\mathcal{F}}^{(k)}\left(\bar{u}_{j,\mathcal{F}}^{i,e} - \bar{u}_{k,\mathcal{F}}^{i,e}\right)|_{S_{\mathcal{F}}^{(j)}}^2 \le 2\,|\left(S_{\mathcal{F}}^{(j)} + S_{\mathcal{F}}^{(k)}\right)^{-1} S_{\mathcal{F}}^{(k)}\left(\bar{u}_{j,\mathcal{E}}^{i,e} - \bar{u}_{j,\mathcal{F}}^{i,e}\right)|_{S_{\mathcal{F}}^{(j)}}^2 +$$
$$+ 2\,|\left(S_{\mathcal{F}}^{(j)} + S_{\mathcal{F}}^{(k)}\right)^{-1} S_{\mathcal{F}}^{(k)}\left(\bar{u}_{k,\mathcal{E}}^{i,e} - \bar{u}_{k,\mathcal{F}}^{i,e}\right)|_{S_{\mathcal{F}}^{(j)}}^2$$
$$\le 2\,|\bar{u}_{j,\mathcal{E}}^{i,e} - \bar{u}_{j,\mathcal{F}}^{i,e}|_{S_{\mathcal{F}}^{(j)}}^2 + 2\,|\bar{u}_{k,\mathcal{E}}^{i,e} - \bar{u}_{k,\mathcal{F}}^{i,e}|_{S_{\mathcal{F}}^{(k)}}.$$

It is sufficient now to estimate the first term on the right-hand side, as we can deal with the other in the same fashion. Combining the result of ellipticity (Lemma 2.2), the Poincaré-Friedrichs inequality (Prop. 3.1) and the Trace theorem (Thm. 3.1), we have

$$|\bar{u}_{j,\mathcal{E}}^{i,e} - \bar{u}_{j,\mathcal{F}}^{i,e}|_{S_{\mathcal{F}}^{(j)}}^2 = a_j\left(\mathcal{H}_j^{i,e}\left(\bar{u}_{j,\mathcal{E}}^{i,e} - \bar{u}_{j,\mathcal{F}}^{i,e}\right),\ \mathcal{H}_j^{i,e}\left(\bar{u}_{j,\mathcal{E}}^{i,e} - \bar{u}_{j,\mathcal{F}}^{i,e}\right)\right)$$
$$= a_j\left(\mathcal{H}_j^{i,e}\overline{\left(u_j - \bar{u}_{j,\mathcal{F}}^{i,e}\right)}_{j,\mathcal{E}},\ \mathcal{H}_j^{i,e}\overline{\left(u_j - \bar{u}_{j,\mathcal{F}}^{i,e}\right)}_{j,\mathcal{E}}\right)$$
$$\le (\chi C_m + \tau K_M)\|\mathcal{H}_j^\Delta\overline{\left(u_j - \bar{u}_{j,\mathcal{F}}^{i,e}\right)}_{j,\mathcal{E}}\|_{L^2(\Omega_j)}^2 + \tau\sum_{\star=i,e}\sigma_M^\star|\mathcal{H}_j^\Delta\overline{\left(u_j - \bar{u}_{j,\mathcal{F}}^{i,e}\right)}_{j,\mathcal{E}}|_{H^1(\Omega_j)}^2$$

$$\lesssim \sum_{\star=i,e} \left[\tau\sigma_M^\star + H^2\left(\chi C_m + \tau K_M\right)\right] |\overline{\left(u_j - \bar{u}_{j,\mathcal{F}}^{i,e}\right)}_{j,\mathcal{E}}|_{H^1(\Omega_j)}.$$

Using Lemmas 3.2 and 3.4, it follows

$$\|\overline{\left(u_j - \bar{u}_{j,\mathcal{F}}^{i,e}\right)}_{j,\mathcal{E}}\|^2 \leq CH^{-1}\|u_j - \bar{u}_{j,\mathcal{F}}^{i,e}\|_{L^2(\mathcal{E})}^2$$

$$\leq C\left(1 + \log\frac{H}{h}\right)|u_j - \bar{u}_{j,\mathcal{F}}^{i,e}|_{H^{1/2}(\partial\Omega_j)}^2$$

$$\leq C\left(1 + \log\frac{H}{h}\right)^3|u_j|_{H^{1/2}(\partial\Omega_j)}^2.$$

This means that

$$|\bar{u}_{j,\mathcal{E}}^{i,e} - \bar{u}_{j,\mathcal{F}}^{i,e}|_{S_\mathcal{F}^{(j)}}^2 \leq C\left(1 + \log\frac{H}{h}\right)^3 \sum_{\star=i,e}\left[\tau\sigma_M^\star + H^2\left(\chi C_m + \tau K_M\right)\right]|u_j|_{H^{1/2}(\partial\Omega_j)}^2$$

$$\sim C\left(1 + \log\frac{H}{h}\right)^3 \sum_{\star=i,e}\left[\tau\sigma_M^\star + H^2\left(\chi C_m + \tau K_M\right)\right]|\mathcal{H}_j^\Delta u_j|_{H^1(\Omega_j)}^2.$$

To conclude, thanks again to Lemma 2.2, the face contribution is analogous to the ρ-scaling case:

$$|P_D u|_{S_\Gamma^{(j)}}^2 \lesssim \sum_{\star=i,e}\sum_{\mathcal{F}\in\Xi_j^\mathcal{F}}\left[\tau\sigma_M^\star + H^2\left(\chi C_m + \tau K_M\right)\right]\left(1 + \log\frac{H}{h}\right)^3|\mathcal{H}_j^\star u_j|_{H^1(\Omega_j)}^2$$

$$= \sum_{\star=i,e}\sum_{\mathcal{F}\in\Xi_j^\mathcal{F}}\frac{\tau\sigma_M^\star + H^2\left(\chi C_m + \tau K_M\right)}{\tau\sigma_m^\star}\left(1 + \log\frac{H}{h}\right)^3\sigma_m^\star|\mathcal{H}_j^\star u_j|_{H^1(\Omega_j)}^2$$

$$\leq \max_{\star=i,e}\sum_{\mathcal{F}\in\Xi_j^\mathcal{F}}\frac{\tau\sigma_M^\star + H^2\left(\chi C_m + \tau K_M\right)}{\tau\sigma_m^\star}\left(1 + \log\frac{H}{h}\right)^3|u_j|_{S_\Gamma^{(j)}}^2.$$

Edge contribution   For simplicity, suppose that an edge $\mathcal{E}$ is shared only by three subdomains associated with indexes j_1, j_2 and j_3. The extension to the case of more subdomains is then similar. Define $S_\mathcal{E}^{(j_{123})}$ as

$$S_\mathcal{E}^{(j_{123})} := S_\mathcal{E}^{(j_1)} + S_\mathcal{E}^{(j_2)} + S_\mathcal{E}^{(j_3)}.$$

Then, the average operator is given by

$$\bar{u}_\mathcal{E}^{i,e} := \left(S_\mathcal{E}^{(j_{123})}\right)^{-1}\left(S_\mathcal{E}^{(j_1)}u_{j_1,\mathcal{E}} + S_\mathcal{E}^{(j_2)}u_{j_2,\mathcal{E}} + S_\mathcal{E}^{(j_3)}u_{j_3,\mathcal{E}}\right).$$

Proceeding in the same fashion as for the face contribution, we find

$$u_{j_1,\mathcal{E}} - \bar{u}_\mathcal{E}^{i,e} = \left(S_\mathcal{E}^{(j_{123})}\right)^{-1}\left[\left(S_\mathcal{E}^{(j_2)} + S_\mathcal{E}^{(j_3)}\right)u_{j_1,\mathcal{E}} - S_\mathcal{E}^{(j_2)}u_{j_2,\mathcal{E}} - S_\mathcal{E}^{(j_3)}u_{j_3,\mathcal{E}}\right],$$

which leads to

$$|R_\mathcal{E}^T\left(u_{j_1,\mathcal{E}} - \bar{u}_\mathcal{E}^{i,e}\right)|_{S_\Gamma^{(j_1)}}^2 = \left(u_{j_1,\mathcal{E}} - \bar{u}_\mathcal{E}^{i,e}\right)^T R_\mathcal{E} \, S_\Gamma^{(j_1)}R_\mathcal{E}^T\left(u_{j_1,\mathcal{E}} - \bar{u}_\mathcal{E}^{i,e}\right)$$

$$= \left(u_{j_1,\mathcal{E}} - \bar{u}_\mathcal{E}^{i,e}\right)^T S_\mathcal{E}^{(j_1)}\left(u_{j_1,\mathcal{E}} - \bar{u}_\mathcal{E}^{i,e}\right)$$

$$\leq 3u_{j_1,\mathcal{E}}^T\left(S_\mathcal{E}^{(j_2)} + S_\mathcal{E}^{(j_3)}\right)^T\left(S_\mathcal{E}^{(j_{123})}\right)^{-1}S_\mathcal{E}^{(j_1)}\left(S_\mathcal{E}^{(j_{123})}\right)^{-1}\left(S_\mathcal{E}^{(j_2)} + S_\mathcal{E}^{(j_3)}\right)u_{j_1,\mathcal{E}} +$$

$$+ 3u_{j_2,\mathcal{E}}^T S_\mathcal{E}^{(j_2)T}\left(S_\mathcal{E}^{(j_{123})}\right)^{-1}S_\mathcal{E}^{(j_1)}\left(S_\mathcal{E}^{(j_{123})}\right)^{-1}S_\mathcal{E}^{(j_2)}u_{j_2,\mathcal{E}} +$$

$$+ 3u_{j_3,\mathcal{E}}^T S_{\mathcal{E}}^{(j_3)T} \left(S_{\mathcal{E}}^{(j_{123})} \right)^{-1} S_{\mathcal{E}}^{(j_1)} \left(S_{\mathcal{E}}^{(j_{123})} \right)^{-1} S_{\mathcal{E}}^{(j_3)} u_{j_3,\mathcal{E}}$$

$$\leq 3u_{j_1,\mathcal{E}}^T S_{\mathcal{E}}^{(j_1)} u_{j_1,\mathcal{E}} + 3u_{j_2,\mathcal{E}}^T S_{\mathcal{E}}^{(j_2)} u_{j_2,\mathcal{E}} + u_{j_3,\mathcal{E}}^T S_{\mathcal{E}}^{(j_3)} u_{j_3,\mathcal{E}}$$

where we use analogous inequalities as in the face case. The first term can be bounded by taking into account the matrices $S_{\mathcal{E}}^{(j_1)}$ and $S_{\mathcal{E}}^{(j_2)} + S_{\mathcal{E}}^{(j_3)}$ in the generalized eigenvalue problem

$$S_{\mathcal{E}}^{(j_1)} \phi = \lambda \left(S_{\mathcal{E}}^{(j_2)} + S_{\mathcal{E}}^{(j_3)} \right) \phi.$$

The second and third terms follow similarly, by first bounding them from above with (see for example the second term)

$$3u_{j_2,\mathcal{E}}^T S_{\mathcal{E}}^{(j_2)T} \left(S_{\mathcal{E}}^{(j_{123})} \right)^{-1} \left(S_{\mathcal{E}}^{(j_1)} + S_{\mathcal{E}}^{(j_2)} \right) \left(S_{\mathcal{E}}^{(j_{123})} \right)^{-1} S_{\mathcal{E}}^{(j_2)} u_{j_2,\mathcal{E}},$$

and then considering the generalized eigenvalue problem

$$S_{\mathcal{E}}^{(j_2)} \phi = \lambda \left(S_{\mathcal{E}}^{(j_1)} + S_{\mathcal{E}}^{(j_3)} \right) \phi.$$

By adding and subtracting the mean value $\bar{u}_{j_1,\mathcal{E}}^{i,e}$ over the edges (which assume the same value over the three subdomain, as we have included the edge averages into the primal space) we obtain the analogous estimate for the egdes:

$$u_{j_1,\mathcal{E}}^T S_{\mathcal{E}}^{(j_1)} u_{j_1,\mathcal{E}} \leq |u_{j_1,\mathcal{E}} - \bar{u}_{j_1,\mathcal{E}}^{i,e}|_{S_{\Gamma}^{(j_1)}}^2 \lesssim \left[\tau \sigma_M^{i,e} + H^2 \left(\chi C_m + \tau K_M \right) \right] |u_{j_1,\mathcal{E}} - \bar{u}_{j_1,\mathcal{E}}^{i,e}|_{H^{1/2}(\Gamma^{(j)})}^2$$

$$\leq \left[\tau \sigma_M^{i,e} + H^2 \left(\chi C_m + \tau K_M \right) \right] ||u_{j_1,\mathcal{E}} - \bar{u}_{j_1,\mathcal{E}}^{i,e}||_{L^2(\mathcal{E})}^2$$

$$\leq \left[\tau \sigma_M^{i,e} + H^2 \left(\chi C_m + \tau K_M \right) \right] \left(1 + \log \frac{H}{h} \right) |\mathcal{H}_{j_1}^{\Delta} u_{j_1,\mathcal{E}}|_{H^1(\Omega_j)}^2$$

by applying Lemma 3.2. In conclusion, using Lemma 2.2, the edge estimate gives us

$$|P_D u|_{S_{\Gamma}^{(j)}}^2 \lesssim \sum_{\star = i,e} \sum_{\mathcal{E} \in \Xi_j^{\mathcal{E}}} \left[\tau \sigma_M^{i,e} + H^2 \left(\chi C_m + \tau K_M \right) \right] \left(1 + \log \frac{H}{h} \right) |\mathcal{H}_j^{\Delta} u_j|_{H^1(\Omega_j)}^2$$

$$= \sum_{\star = i,e} \sum_{\mathcal{E} \in \Xi_j^{\mathcal{E}}} \frac{\tau \sigma_M^{i,e} + H^2 \left(\chi C_m + \tau K_M \right)}{\sigma_m^{\star}} \left(1 + \log \frac{H}{h} \right) \sigma_m^{\star} |\mathcal{H}_j^{\Delta} u_j|_{H^1(\Omega_j)}^2$$

$$\leq \max_{\star = i,e} \sum_{\mathcal{E} \in \Xi_j^{\mathcal{E}}} \frac{\tau \sigma_M^{i,e} + H^2 \left(\chi C_m + \tau K_M \right)}{\sigma_m^{\star}} \left(1 + \log \frac{H}{h} \right) |u_j|_{S_{\Gamma}^{(j_1)}}^2,$$

where the index j collects all contributions from the subdomains that share the edge $\mathcal{E}$.

4.2 Condition number bound for FETI-DP and BDDC preconditioners

Lemma 4.1 is used for estimate the condition number in the FETI-DP and in BDDC methods. As the constants are the same whether we use the ρ-scaling or the deluxe one, we can state the following result.

Theorem 4.1. *The condition number of the Bidomain FETI-DP and BDDC operators satisfies*

$$cond \ (M_*^{-1} A) \leq C \left(1 + \log \left(\frac{H}{h} \right) \right)^n,$$

with $n = 2, 3$ depending on the scaling, where M_*^{-1} denotes the FETI-DP or the BDDC preconditioner, A is the Bidomain system matrix and the constant C is computed from the above Lemmas,

$$C = \max_{\substack{k=1,\dots,N \\ \star = i,e}} \frac{\tau \sigma_M^{\star(k)} + H^2 \left(\chi C_m + \tau K_M\right)}{\tau \sigma_m^{\star(k)}}.$$

It is possible to see that (see e.g. [116, Appendix A])

$$cond\ (M_*^{-1}A) = \frac{\lambda_{\max}(M_*^{-1}A)}{\lambda_{\min}(M_*^{-1}A)},$$

so we have to estimate the smallest eigenvalue $\lambda_{\min}(M_*^{-1}A)$ from below and the largest eigenvalue $\lambda_{\max}(M_*^{-1}A)$ form above. In this case, this means to show that

$$\langle x, x \rangle_A \leq \langle M_*^{-1}Ax, x \rangle_A \leq C \left(1 + \log\left(\frac{H}{h}\right)\right)^n \langle x, x \rangle_A, \qquad n = 2, 3,$$

holds for all $x \in V$, with $\langle \mathbf{a}, \mathbf{b} \rangle_A = \mathbf{b}^T A \mathbf{a}$.

This result holds for both preconditioners, since they have been proven in Refs. [78, 83] to be spectrally equivalent. Anyway, we distinguish the proofs for the two preconditioners, showing indeed their equivalence.

4.2.1 FETI-DP preconditioner

Before going into details of the proof for FETI-DP, it is convenient to rewrite algebrically the projection P_D.
Given the operator $\widetilde{R}_{\Gamma\Delta}$ which restricts partially assembled interface variables to their dual parts

$$\widetilde{R}_{\Gamma\Delta} u_\Gamma = u_\Delta, \qquad \forall u_\Gamma \in \widetilde{W}_\Gamma,$$

we recall the definition of the interface jump operator B_Γ

$$B_\Gamma = B_\Delta \widetilde{R}_{\Gamma\Delta} = \begin{bmatrix} B_\Delta & 0_\Pi \end{bmatrix},$$

as the matrix which extends the enforced continuity on dual variables (through the Lagrangian multipliers) to the interface Γ. Lastly, it is possible to define the scaled jump operator, obtained by scaling the submatrices of B_Δ

$$B_{D,\Gamma} = B_{D,\Delta} \widetilde{R}_{\Gamma\Delta}.$$

In the FETI-DP case, the projection can be algebrically written as $P_D := B_{D,\Gamma}^T B_\Gamma$. Moreover, it is possible to show, from projection properties, that

1. P_D preserves the jump of any function $u \in \widetilde{W}_\Gamma$ with respect to the jump operator B_Γ, i.e. $B_\Gamma P_D u = B_\Gamma u$;

2. P_D^T preserves the scaled jump of any function $u \in \widetilde{W}_\Gamma$, i. e. $B_{D,\Gamma} P_D^T u = B_{D,\Gamma} u$;

3. $P_D u = 0, \forall u \in \widehat{W}$.

Lower bound. Observe that from property (2) of the projection P_D, it follows

$$B_{D,\Gamma} P_D^T u = B_{D,\Gamma} B_\Gamma^T B_{D,\Gamma} u \overset{(2)}{=} B_{D,\Gamma} u, \tag{4.6}$$

so that

$$B_{D,\Gamma} B_\Gamma^T = I. \tag{4.7}$$

So $\forall \lambda \in \text{range}(M_{\text{FETI-DP}}^{-1}) \subset \text{range}(B_{D,\Gamma})$ thanks to Eq. (4.7), it follows

$$
\begin{aligned}
\langle \lambda, \lambda \rangle_F^2 &= \langle \lambda, B_{D,\Gamma} B_\Gamma^T \lambda \rangle_F^2 \\
&= \langle \lambda, B_{D,\Gamma} \widetilde{S}_\Gamma^{1/2} \widetilde{S}_\Gamma^{-1/2} B_\Gamma^T \lambda \rangle_F^2 \\
&= \langle F\lambda, B_{D,\Gamma} \widetilde{S}_\Gamma^{1/2} \widetilde{S}_\Gamma^{-1/2} B_\Gamma^T \lambda \rangle^2.
\end{aligned}
$$

Using the inner product definition and keeping in mind that $\widetilde{S}_\Gamma$ is a block-diagonal and symmetric matrix (i.e. $\widetilde{S}_\Gamma = \widetilde{S}_\Gamma^T$), we can write

$$
\begin{aligned}
\langle F\lambda, B_{D,\Gamma} \widetilde{S}_\Gamma^{1/2} \widetilde{S}_\Gamma^{-1/2} B_\Gamma^T \lambda \rangle &= \left(B_{D,\Gamma} \widetilde{S}_\Gamma^{1/2} \widetilde{S}_\Gamma^{-1/2} B_\Gamma^T \lambda \right)^T (F\lambda) \\
&= \left(\widetilde{S}_\Gamma^{-1/2} B_\Gamma^T \lambda \right)^T \left(\widetilde{S}_\Gamma^{1/2} B_{D,\Gamma}^T F\lambda \right) \\
&= \langle \widetilde{S}_\Gamma^{1/2} B_{D,\Gamma}^T F\lambda, \widetilde{S}_\Gamma^{-1/2} B_\Gamma^T \lambda \rangle.
\end{aligned}
$$

Applying the Cauchy-Schwartz inequality, we get

$$
\begin{aligned}
\langle \lambda, \lambda \rangle_F^2 &= \langle F\lambda, B_{D,\Gamma} \widetilde{S}_\Gamma^{1/2} \widetilde{S}_\Gamma^{-1/2} B_\Gamma^T \lambda \rangle^2 \\
&\leq \langle \widetilde{S}_\Gamma^{1/2} B_{D,\Gamma}^T F\lambda, \widetilde{S}_\Gamma^{1/2} B_{D,\Gamma}^T F\lambda \rangle \langle \widetilde{S}_\Gamma^{-1/2} B_\Gamma^T \lambda, \widetilde{S}_\Gamma^{-1/2} B_\Gamma^T \lambda \rangle \\
&= \langle \widetilde{S}_\Gamma B_{D,\Gamma}^T F\lambda, B_{D,\Gamma}^T F\lambda \rangle \langle \widetilde{S}_\Gamma^{-1} B_\Gamma^T \lambda, B_\Gamma^T \lambda \rangle \\
&= \left[(B_{D,\Gamma}^T F\lambda)^T \left(\widetilde{S}_\Gamma B_{D,\Gamma}^T F\lambda \right) \right] \left[(B_\Gamma^T \lambda)^T \left(\widetilde{S}_\Gamma^{-1} B_\Gamma^T \lambda \right) \right] \\
&= \left[(F\lambda)^T \left(\underbrace{B_{D,\Gamma} \widetilde{S}_\Gamma B_{D,\Gamma}^T}_{M_{\text{FETI-DP}}^{-1}} F\lambda \right) \right] \left[\lambda^T \left(\underbrace{B_\Gamma \widetilde{S}_\Gamma^{-1} B_\Gamma^T}_{F} \lambda \right) \right] \\
&= \langle M_{\text{FETI-DP}}^{-1} F\lambda, \lambda \rangle_F \langle \lambda, \lambda \rangle_F.
\end{aligned}
$$

In conclusion we have, by cancelling the common factor $\langle \lambda, \lambda \rangle_F$,

$$
\langle \lambda, \lambda \rangle_F \leq \langle M_{\text{FETI-DP}}^{-1} F\lambda, \lambda \rangle_F.
$$

Upper bound. We observe now that for $\lambda \in \text{range}(M_{\text{FETI-DP}}^{-1})$, we have $\widetilde{S}_\Gamma B_\Gamma^T \lambda \in \widetilde{W}$. Using Lemma 4.1 from the previous Section, we otain $\forall \lambda \in \text{range}(M_{\text{FETI-DP}}^{-1})$,

$$
\begin{aligned}
\langle M_{\text{FETI-DP}}^{-1} F\lambda, \lambda \rangle_F &= \langle M_{\text{FETI-DP}}^{-1} F\lambda, F\lambda \rangle \\
&= \langle \underbrace{B_{D,\Gamma}^T B_\Gamma \widetilde{S}_\Gamma^{-1} B_\Gamma^T \lambda}_{P_D}, \underbrace{B_{D,\Gamma}^T B_\Gamma \widetilde{S}_\Gamma^{-1} B_\Gamma^T \lambda}_{P_D} \rangle_{\widetilde{S}_\Gamma} = |P_D \widetilde{S}_\Gamma^{-1} B_\Gamma^T \lambda|_{\widetilde{S}_\Gamma}^2 \\
&\leq C \left(1 + \log \left(\frac{H}{h} \right) \right)^n |\widetilde{S}_\Gamma^{-1} B_\Gamma^T \lambda|_{\widetilde{S}_\Gamma}^2 \\
&= C \left(1 + \log \left(\frac{H}{h} \right) \right)^n \langle \widetilde{S}_\Gamma^{-1} B_\Gamma^T \lambda, \widetilde{S}_\Gamma \widetilde{S}_\Gamma^{-1} B_\Gamma^T \lambda \rangle \\
&= C \left(1 + \log \left(\frac{H}{h} \right) \right)^n \langle \widetilde{S}_\Gamma^{-1} B_\Gamma^T \lambda, B_\Gamma^T \lambda \rangle \\
&= C \left(1 + \log \left(\frac{H}{h} \right) \right)^n \langle \underbrace{B_\Gamma \widetilde{S}_\Gamma^{-1} B_\Gamma^T}_{F} \lambda, \lambda \rangle \\
&= C \left(1 + \log \left(\frac{H}{h} \right) \right)^n \langle F\lambda, \lambda \rangle \\
&= C \left(1 + \log \left(\frac{H}{h} \right) \right)^n \langle \lambda, \lambda \rangle_F,
\end{aligned}
$$

where C is given by

$$C = \max_{\substack{k=1,\ldots,N \\ \star=i,e}} \frac{\tau \sigma_M^{\star(k)} + H^2 \left(\chi C_M + \tau K_M\right)}{\tau \sigma_m^{\star(k)}},$$

and $n = 2$ in case the ρ-scaling is applied and $n = 3$ if the deluxe scaling is used. Therefore,
$\langle M_{\text{FETI-DP}}^{-1} F \lambda, \lambda \rangle_F \leq C \left(1 + \log\left(\frac{H}{h}\right)\right)^2 \langle \lambda, \lambda \rangle_F$.
Eventually, we estimate the condition number $cond\,(M_{\text{FETI-DP}}^{-1} F)$ by

$$cond\,(M_{\text{FETI-DP}}^{-1} F) = \frac{\lambda_{\max}(M_{\text{FETI-DP}}^{-1} F)}{\lambda_{\min}(M_{\text{FETI-DP}}^{-1} F)}$$

$$\leq C \frac{\left(1 + \log\left(\frac{H}{h}\right)\right)^2 \langle \lambda, \lambda \rangle_F}{\langle \lambda, \lambda \rangle_F}$$

$$= \max_{\substack{k=1,\ldots,N \\ \star=i,e}} \frac{\tau \sigma_M^{\star(k)} + H^2 \left(\chi C_M + \tau K_M\right)}{\tau \sigma_m^{\star(k)}} \left(1 + \log\left(\frac{H}{h}\right)\right)^n,$$

which ends our proof for the FETI-DP preconditioner.

4.2.2 BDDC preconditioner

In the same fashion as for the FETI-DP operator, we need to estimate the smallest and the largest eigenvalues $\lambda_{\min}$ and $\lambda_{\max}$ related to the BDDC operator $M_{\text{BDDC}}^{-1} \widehat{S}_\Gamma$ from below and above respectively:

$$\langle u, u \rangle_{\widehat{S}_\Gamma} \leq \langle M_{\text{BDDC}}^{-1} \widehat{S}_\Gamma u, u \rangle_{\widehat{S}_\Gamma} \leq C \left(1 + \log\left(\frac{H}{h}\right)\right)^n \langle u, u \rangle_{\widehat{S}_\Gamma}, \qquad \forall u \in \widetilde{W}_\Gamma,$$

with $n = 2, 3$ depending on the applied scaling (ρ or deluxe scaling, respectively). In this case, it is more convenient to work directly on the projection $E_D := \widetilde{R}_\Gamma \widetilde{R}_{D,\Gamma}^T$.

Lower bound. Analogously to Eq. (4.6), it holds

$$\widetilde{R}_\Gamma^T \widetilde{R}_{D,\Gamma} = I. \tag{4.8}$$

We can evaluate the bound from below in the same manner, by using the Cauchy-Schwarz inequality:

$$\langle u, u \rangle_{\widehat{S}_\Gamma}^2 = \langle u, \widehat{S}_\Gamma u \rangle^2 = \langle u, \widetilde{R}_\Gamma^T \widetilde{R}_{D,\Gamma} \widehat{S}_\Gamma u \rangle^2$$

$$= \langle \widetilde{S}_\Gamma^{1/2} \widetilde{R}_\Gamma u, \widetilde{S}_\Gamma^{-1/2} \widetilde{R}_{D,\Gamma} \widehat{S}_\Gamma u \rangle^2$$

$$\leq \langle \widetilde{S}_\Gamma^{1/2} \widetilde{R}_\Gamma u, \widetilde{S}_\Gamma^{1/2} \widetilde{R}_\Gamma u \rangle \langle \widetilde{S}_\Gamma^{-1/2} \widetilde{R}_{D,\Gamma} \widehat{S}_\Gamma u, \widetilde{S}_\Gamma^{-1/2} \widetilde{R}_{D,\Gamma} \widehat{S}_\Gamma u \rangle$$

$$= \left[\left(\widetilde{S}_\Gamma^{1/2} \widetilde{R}_\Gamma u\right)^T \left(\widetilde{S}_\Gamma^{1/2} \widetilde{R}_\Gamma u\right)\right] \left[\left(\widetilde{S}_\Gamma^{-1/2} \widetilde{R}_{D,\Gamma} \widehat{S}_\Gamma u\right)^T \left(\widetilde{S}_\Gamma^{-1/2} \widetilde{R}_{D,\Gamma} \widehat{S}_\Gamma u\right)\right]$$

$$= \left[u^T (\underbrace{\widetilde{R}_\Gamma^T \widetilde{S}_\Gamma \widetilde{R}_\Gamma}_{\widehat{S}_\Gamma} u)\right] \left[\left(\widehat{S}_\Gamma u\right)^T (\underbrace{\widetilde{R}_{D,\Gamma}^T \widetilde{S}_\Gamma^{-1} \widetilde{R}_{D,\Gamma}}_{M_{\text{BDDC}}^{-1}} \widehat{S}_\Gamma u)\right]$$

$$= \left(u^T \widehat{S}_\Gamma u\right) \left[\left(\widehat{S}_\Gamma u\right)^T \left(M_{\text{BDDC}}^{-1} \widehat{S}_\Gamma u\right)\right]$$

$$= \langle \widehat{S}_\Gamma u, u \rangle \langle M_{\text{BDDC}}^{-1} \widehat{S}_\Gamma u, \widehat{S}_\Gamma u \rangle = \langle u, u \rangle_{\widehat{S}_\Gamma} \langle M_{\text{BDDC}}^{-1} \widehat{S}_\Gamma u, u \rangle_{\widehat{S}_\Gamma}.$$

Therefore,

$$\langle u, u \rangle_{\widehat{S}_\Gamma} \leq \langle M_{\text{BDDC}}^{-1} \widehat{S}_\Gamma u, u \rangle_{\widehat{S}_\Gamma}.$$

Upper bound. Thanks to the bound on the projection operator in Lemma 4.1, we can compute the upper bound as follows,

$$
\begin{aligned}
\langle M_{\mathrm{BDDC}}^{-1}\widehat{S}_\Gamma u, u\rangle_{\widehat{S}_\Gamma}^2 &= \langle M_{\mathrm{BDDC}}^{-1}\widehat{S}_\Gamma u, \widehat{S}_\Gamma u\rangle^2 \\
&= \langle \widetilde{R}_{D,\Gamma}^T \widetilde{S}_\Gamma^{-1} \widetilde{R}_{D,\Gamma} \widetilde{R}_\Gamma^T \widetilde{S}_\Gamma \widetilde{R}_\Gamma u, \widetilde{R}_\Gamma^T \widetilde{S}_\Gamma \widetilde{R}_\Gamma u\rangle^2 \\
&= \langle \underbrace{\widetilde{R}_\Gamma \widetilde{R}_{D,\Gamma}^T}_{E_D} \widetilde{S}_\Gamma^{-1} \widetilde{R}_{D,\Gamma} \underbrace{\widetilde{R}_\Gamma^T \widetilde{S}_\Gamma \widetilde{R}_\Gamma u}_{\widehat{S}_\Gamma}, \widetilde{S}_\Gamma \widetilde{R}_\Gamma u\rangle^2 \\
&= \langle E_D \widetilde{S}_\Gamma^{-1} \widetilde{R}_{D,\Gamma} \widehat{S}_\Gamma u, \widetilde{R}_\Gamma u\rangle_{\widetilde{S}_\Gamma}^2 \\
&\leq \langle E_D \widetilde{S}_\Gamma^{-1} \widetilde{R}_{D,\Gamma} \widehat{S}_\Gamma u, E_D \widetilde{S}_\Gamma^{-1} \widetilde{R}_{D,\Gamma} \widehat{S}_\Gamma u\rangle_{\widetilde{S}_\Gamma} \langle \widetilde{R}_\Gamma u, \widetilde{R}_\Gamma u\rangle_{\widetilde{S}_\Gamma} \\
&= |E_D \widetilde{S}_\Gamma^{-1} \widetilde{R}_{D,\Gamma} \widehat{S}_\Gamma u|_{\widetilde{S}_\Gamma}^2 |\widetilde{R}_\Gamma u|_{\widetilde{S}_\Gamma}^2 \\
&\leq C\left(1+\log\left(\frac{H}{h}\right)\right)^n |\widetilde{S}_\Gamma^{-1} \widetilde{R}_{D,\Gamma} \widehat{S}_\Gamma u|_{\widetilde{S}_\Gamma}^2 |\widetilde{R}_\Gamma u|_{\widetilde{S}_\Gamma}^2 \\
&= C\left(1+\log\left(\frac{H}{h}\right)\right)^n \langle \widetilde{S}_\Gamma^{-1} \widetilde{R}_{D,\Gamma} \widehat{S}_\Gamma u, \widetilde{S}_\Gamma^{-1} \widetilde{R}_{D,\Gamma} \widehat{S}_\Gamma u\rangle_{\widetilde{S}_\Gamma} \langle \widetilde{R}_\Gamma u, \widetilde{R}_\Gamma u\rangle_{\widetilde{S}_\Gamma} \\
&= C\left(1+\log\left(\frac{H}{h}\right)\right)^n \langle \underbrace{\widetilde{R}_{D,\Gamma}^T \widetilde{S}_\Gamma^{-1} \widetilde{R}_{D,\Gamma}}_{M_{\mathrm{BDDC}}^{-1}} \widehat{S}_\Gamma u, \widehat{S}_\Gamma u\rangle \langle \underbrace{\widetilde{R}_\Gamma^T \widetilde{S}_\Gamma \widetilde{R}_\Gamma}_{\widehat{S}_\Gamma} u, u\rangle \\
&= C\left(1+\log\left(\frac{H}{h}\right)\right)^n \langle M_{\mathrm{BDDC}}^{-1} \widehat{S}_\Gamma u, \widehat{S}_\Gamma u\rangle \langle \widehat{S}_\Gamma u, u\rangle \\
&= C\left(1+\log\left(\frac{H}{h}\right)\right)^n \langle M_{\mathrm{BDDC}}^{-1} \widehat{S}_\Gamma u, u\rangle_{\widehat{S}_\Gamma} \langle u, u\rangle_{\widehat{S}_\Gamma},
\end{aligned}
$$

where we used first the Cauchy-Schwarz inequality, then one of the estimates for the projection operator and C is given as above by

$$
C = \max_{\substack{k=1,\dots,N \\ \star=i,e}} \frac{\tau\sigma_M^{\star(k)} + H^2\left(\chi C_m + \tau K_M\right)}{\tau\sigma_m^{\star(k)}},
$$

with $n = 2,3$ depending on the type of scaling applied (ρ or deluxe scaling, respectively). So

$$
\langle M_{\mathrm{BDDC}}^{-1}\widehat{S}_\Gamma u, u\rangle_{\widehat{S}_\Gamma} \leq C\left(1+\log\left(\frac{H}{h}\right)\right)^n \langle u, u\rangle_{\widehat{S}_\Gamma}.
$$

In conclusion, the condition number $cond\,(M_{\mathrm{BDDC}}^{-1}\widehat{S}_\Gamma)$ is bounded by

$$
cond\,(M_{\mathrm{BDDC}}^{-1}\widehat{S}_\Gamma) \leq \max_{\substack{k=1,\dots,N \\ \star=i,e}} \frac{\tau\sigma_M^{\star(k)} + H^2\left(\chi C_m + \tau K_M\right)}{\tau\sigma_m^{\star(k)}} \left(1+\log\left(\frac{H}{h}\right)\right)^n,
$$

which proves that the FETI-DP and BDDC preconditioners have the same condition number bound, provided that the same primal set is taken in consideration.

Chapter 5

Newton-Krylov Dual-Primal methods for the Coupled Bidomain problem

The aim of this Chapter is to develop a theoretical convergence analysis of the preconditioned operator for the coupled Jacobian Bidomain system (2.20). Since this system is non-symmetric, due to the inclusion of the ionic model in the monolithic solution strategy, the iterative solver that we consider is the Generalised Minimal Residual (GMRES) method. In the literature, so far, the BDDC preconditioner has been applied to non-symmetric problems only in few cases and the relative convergence analysis is not widely available: in References [121, 122] BDDC application to the solution of non-symmetric algebraic problems arising from the stabilized finite element discretization of advection-diffusion problems has been studied and theoretically analyzed; in the recent work in Ref. [97], the strategy proposed by Tu and Li is extended by designing an adaptive strategy for choosing the primal constraints, while in Ref. [123] an investigation of the problem discretized with hybridizable Discontinuous Galerkin is provided.

We combine the main result for the GMRES convergence in Reference [40] and the proof technique proposed in Ref. [121] to carry out the convergence analysis of the preconditioned operator for the coupled Jacobian Bidomain system. In Section 5.1 we provide a bound for the projection operator of the symmetric part of the bilinear form associated with the Jacobian: as in the previous Chapter, this upper bound is proven for both ρ-scaling and deluxe scaling; afterwards, in Sec. 5.2 the convergence Theorem for the BDDC preconditioned GMRES solver is provided. The content of this Chapter has been partially submitted for publication and a preprint version can be found in Ref. [64].

Local bilinear forms. As done in the previous Chapter, we define the local bilinear forms by restricting the integration set, thus allowing us to assemble a local matrix on each subdomain

$$a^{(j)}(s, \phi) = \chi C_m \left(s_i - s_e, \varphi_i - \varphi_e \right)_{|\Omega_j} + (s_w, \varphi_w)_{|\Omega_j} + \tau a_i^{(j)} \left(s_i, \varphi_i \right) + \tau a_e^{(j)} \left(s_e, \varphi_e \right)$$

$$+ \tau \left(\sum_l \frac{\partial I_{\text{ion}}}{\partial v_l}(v, w) \left(s_{i,l} - s_{e,l} \right) \psi_l, \varphi_i - \varphi_e \right)_{|\Omega_j} - \tau \left(\sum_l \frac{\partial R}{\partial w_l}(v, w) s_{w,l} \, \psi_l, \varphi_w \right)_{|\Omega_j}$$

$$+ \tau \left(\sum_l \frac{\partial I_{\text{ion}}}{\partial w_l}(v, w) s_{w,l} \, \psi_l, \varphi_i - \varphi_e \right)_{|\Omega_j} - \tau \left(\sum_l \frac{\partial R}{\partial v_l}(v, w) \left(s_{i,l} - s_{e,l} \right) \psi_l, \varphi_w \right)_{|\Omega_j}.$$

The symmetric and skew-symmetric parts of $a^{(j)}(\cdot, \cdot)$ are given by

$$q^{(j)}(s, \phi) = 2\chi C_m \left(s_i - s_e, \varphi_i - \varphi_e \right)_{\Omega_j} + 2 \left(s_w, \varphi_w \right)_{\Omega_j} + 2\tau a_i^{(j)} \left(s_i, \varphi_i \right) + 2\tau a_e^{(j)} \left(s_e, \varphi_i \right)$$

65

$$+ 2\tau \left(\sum_l \frac{\partial I_{\mathrm{ion}}}{\partial v_l}(v,w)\,(s_{i,l} - s_{e,l})\,\psi_l, \varphi_i - \varphi_e \right)_{\Omega_j} - 2\tau \left(\sum_l \frac{\partial R}{\partial w_l}(v,w)s_{w,l}\,\psi_l, \varphi_w \right)_{\Omega_j}$$

$$+ \tau \left(\sum_l \frac{\partial I_{\mathrm{ion}}}{\partial w_l}(v,w)\,(s_{i,l} - s_{e,l})\,\psi_l, \varphi_w \right)_{\Omega_j} + \tau \left(\sum_l \frac{\partial I_{\mathrm{ion}}}{\partial w_l}(v,w)s_{w,l}\,\psi_l, \varphi_i - \varphi_e \right)_{\Omega_j}$$

$$- \tau \left(\sum_l \frac{\partial R}{\partial v_l}(v,w)\,(s_{i,l} - s_{e,l})\,\psi_l, \varphi_w \right)_{\Omega_j} - \tau \left(\sum_l \frac{\partial R}{\partial v_l}(v,w)s_{w,l}\,\psi_l, \varphi_i - \varphi_e \right)_{\Omega_j},$$

$$z^{(j)}(s, \phi) =$$

$$\tau \left(\sum_l \frac{\partial I_{\mathrm{ion}}}{\partial w_l}(v,w)s_{w,l}\,\psi_l, \varphi_i - \varphi_e \right)_{\Omega_j} - \tau \left(\sum_l \frac{\partial I_{\mathrm{ion}}}{\partial w_l}(v,w)\,(s_{i,l} - s_{e,l})\,\psi_l, \varphi_w \right)_{\Omega_j}$$

$$\tau \left(\sum_l \frac{\partial R}{\partial v_l}(v,w)s_{w,l}\,\psi_l, \varphi_i - \varphi_e \right)_{\Omega_j} - \tau \left(\sum_l \frac{\partial R}{\partial v_l}(v,w)\,(s_{i,l} - s_{e,l})\,\psi_l, \varphi_w \right)_{\Omega_j},$$

where $(\cdot\,,\cdot)_{\Omega_j}$ denotes the restriction of the L^2-inner product to the j-th subdomain.

Following [121], after introducing the space $\widetilde{W}$ of partially subassembled finite element space, we define the corresponding bilinear forms by

$$\widetilde{a}(s, \phi) = \sum_{j=1}^N a^{(j)}(s, \phi), \qquad \widetilde{q}(s, \phi) = \sum_{j=1}^N b^{(j)}(s, \phi), \qquad \widetilde{z}(s, \phi) = \sum_{j=1}^N z^{(j)}(s, \phi).$$

We denote the partially subassembled matrices corresponding to the bilinear forms above with $\widetilde{A}$, $\widetilde{Q}$ and $\widetilde{Z}$, respectively, and let

$$A = \widetilde{R}^T \widetilde{A} \widetilde{R}, \qquad Q = \widetilde{R}^T \widetilde{Q} \widetilde{R}, \qquad Z = \widetilde{R}^T \widetilde{Z} \widetilde{R},$$

with $\widetilde{R}$ the injection operator from $\widehat{W}$ to $\widetilde{W}$.

In the same fashion as in [121], we define the truncated norms on the space $\widetilde{W}$

$$||w||^2_{L^2(\Omega)} = \sum_{j=1}^N ||w||^2_{L^2(\Omega_j)}, \qquad |w|^2_{H^1(\Omega)} = \sum_{j=1}^N |w|^2_{H^1(\Omega_j)}, \qquad \forall w \in \widetilde{W}.$$

In this work, $||w||_{L^2(\Omega)}$ and $|w|_{H^1(\Omega)}$ for $w \in \widetilde{W}$ always represent these truncated norms. Since for construction the bilinear forms $q^{(j)}(\cdot, \cdot)$ for $j = 1, \ldots, N$ are symmetric and positive definite on $W^{(j)}$, it is possible to define

$$|u|^2_{Q^{(j)}} = q^{(j)}(u, u), \qquad \forall u \in W^{(j)}$$

and

$$|u|^2_Q = \sum_{j=1}^N |u|^2_{Q^{(j)}}, \qquad \forall u \in \widehat{W}, \qquad\qquad |u|^2_{\widetilde{Q}} = \sum_{j=1}^N |u|^2_{Q^{(j)}}, \qquad \forall u \in \widetilde{W}.$$

For any $u_\Gamma \in \widetilde{W}_\Gamma$, we define the harmonic extension $u_{\mathcal{A},\Gamma}$ to the interior of subdomains as

$$u_{\mathcal{A},\Gamma} = \begin{bmatrix} -K_{II}^{-1} \widetilde{K}_{I\Gamma} u_\Gamma \\ u_\Gamma \end{bmatrix} \in \widetilde{W},$$

and analogously, it is possible to define its counterpart $u_{\mathcal{A},\Gamma} \in \widehat{W}$ for $u_\Gamma \in \widehat{W}_\Gamma$.

We define the following bilinear forms for vectors in $\widehat{W}_\Gamma$ and $\widetilde{W}_\Gamma$

$$\langle u_\Gamma, v_\Gamma \rangle_{Q_\Gamma} = v^T_{\mathcal{A},\Gamma} Q u_{\mathcal{A},\Gamma}, \quad \langle u_\Gamma, v_\Gamma \rangle_{Z_\Gamma} = v^T_{\mathcal{A},\Gamma} Z u_{\mathcal{A},\Gamma}, \qquad \forall u_\Gamma, v_\Gamma \in \widehat{W}_\Gamma \tag{5.1}$$

$$\langle u_\Gamma, v_\Gamma \rangle_{\widetilde{Q}_\Gamma} = v_{\mathcal{A},\Gamma}^T \widetilde{Q} u_{\mathcal{A},\Gamma}, \quad \langle u_\Gamma, v_\Gamma \rangle_{\widetilde{Z}_\Gamma} = v_{\mathcal{A},\Gamma}^T \widetilde{Z} u_{\mathcal{A},\Gamma}, \qquad \forall u_\Gamma, v_\Gamma \in \widetilde{W}_\Gamma \tag{5.2}$$

We observe that [121, Lemma 7.2] follows from these definitions and this will be needed for further calculations.

Following Reference[121], it is useful to define Q_Γ and $\widetilde{Q}_\Gamma$ norms:

$$|u_\Gamma|_{Q_\Gamma}^2 = \langle u_\Gamma, u_\Gamma \rangle_{Q_\Gamma} \;\; \text{for } u_\Gamma \in \widehat{W}_\Gamma \qquad \text{and} \qquad |u_\Gamma|_{\widetilde{Q}_\Gamma}^2 = \langle u_\Gamma, u_\Gamma \rangle_{\widetilde{Q}_\Gamma} \;\; \text{for } u_\Gamma \in \widetilde{W}_\Gamma.$$

Ultimately, we define

$$\mathcal{H}_j^c \, u = \left(\mathcal{H}_j^\Delta u^i, \mathcal{H}_j^\Delta u^e, \mathcal{E}_{ext,\Omega_j} u^w \right),$$

a discrete harmonic extension whose first two components are the discrete harmonic extension of the Laplacian operator of the intra- and extracellular component of the solution, while the last is the extension to zero of the gating components u^w to Ω_j.

5.1 A bound for the projection operator for the coupled Jacobian Bidomain system

The following Lemma can be proved for both ρ-scaling and deluxe scaling:

Lemma 5.1. *Assume that the primal space is spanned by the vertex nodal finite element functions and the edge cutoff functions. Let the Bidomain projection operator be scaled by either the standard ρ-scaling or the deluxe-scaling. Then*

$$|E_D u|_{\widetilde{Q}_\Gamma}^2 \lesssim \left[\max_{\substack{k=1,\ldots,N \\ \star=i,e}} \frac{\tau \sigma_M^{\star(k)} + H^2 \left(\chi C_m + \tau K_{M,I} \right)}{\tau \sigma_m^{\star(k)}} + \frac{1 - \tau K_{M,R}}{1 - \tau K_{m,R}} \right] \left(1 + \log \frac{H}{h} \right)^n |u|_{\widetilde{Q}_\Gamma}^2,$$

$\forall u \in \widetilde{W}_\Gamma$, *with* $n = 2$ *in case of ρ-scaling or* $n = 3$ *in case of deluxe-scaling.*

5.1.1 Proof of Lemma 5.1 with ρ-scaling

As for the decoupled case, instead of proving the bound for the projection operator E_D, we prove it for the complementary projection P_D. The action of the ρ-scaling on a given $w \in \widetilde{W}_\Gamma$ can be defined locally for the coupled Jacobian Bidomain model as

$$(P_D w(x))_j = \left(\sum_{k \in \mathcal{N}_x} \delta_k^{i \;\dagger} (w_j^i(x) - w_k^i(x)), \sum_{k \in \mathcal{N}_x} \delta_k^{e \;\dagger} (w_j^e(x) - w_k^e(x)), \sum_{k \in \mathcal{N}_x} \delta_k^{w \;\dagger} (w_j^w(x) - w_k^w(x)) \right).$$

It is sufficient to compute only the local bounds, as it holds $|P_D u|_{\widetilde{Q}_\Gamma}^2 = \sum_{j=1}^N |R_{\partial \Omega_j} P_D u|_{\widetilde{Q}_\Gamma^{(j)}}^2$.

We recall that by eliminating all internal variables of Ω_j, we obtain the local Schur complement matrix $S_\Gamma^{(j)}$ and the global unassembled Schur complement matrix S_Γ:

$$S_\Gamma^{(j)} = \begin{bmatrix} S_{\Delta\Delta}^{(j)} & S_{\Delta\Pi}^{(j)} \\ S_{\Pi\Delta}^{(j)} & S_{\Pi\Pi}^{(j)} \end{bmatrix}, \qquad S_\Gamma = \operatorname*{diag}_j S_\Gamma^{(j)}.$$

Let $\Theta_{\mathcal{E}^{jk}}$, $\Theta_{\mathcal{F}^{jk}}$ and $\Theta_{\mathcal{V}^{jk}}$ be the characteristic finite element functions associated with an edge $\mathcal{E}^{jk}$, a face $\mathcal{F}^{jk}$ and a vertex $\mathcal{V}^{jk}$ respectively, between two substructures Ω_j and Ω_k. Those functions form a partition-of-unity associated with the decomposition of Γ into edges, faces and vertices. For brevity we will write $\Theta_* = \left(\theta_*^i, \theta_*^e, \theta_*^w \right)$, with $* = \{\mathcal{E}, \mathcal{F}, \mathcal{V}\}$, and drop the index jk, unless an explicit ambiguity occurs.

Denoting by I^h the finite element interpolant, we have

$$v_j(x) = (P_D u(x))_j$$

$$= \left(\sum_{k \in \mathcal{N}_x} I^h(\delta_k^{i\,\dagger}(u_j^i(x) - u_k^i(x))), \sum_{k \in \mathcal{N}_x} I^h(\delta_k^{e\,\dagger}(u_j^e(x) - u_k^e(x))), \sum_{k \in \mathcal{N}_x} I^h(\delta_k^{w\,\dagger}(u_j^w(x) - u_k^w(x))) \right)$$

$$= \sum_{\mathcal{E}} I^h(\Theta_{\mathcal{E}} v_j) + \sum_{\mathcal{F}} I^h(\Theta_{\mathcal{F}} v_j) + \sum_{\mathcal{V}} I^h(\Theta_{\mathcal{V}} v_j).$$

We note that with our assumption on the primal space, the vertex contribution vanishes, as

$$v_j(x) = v_k(x) \qquad \forall x \in V_h, \quad j, k \in \mathcal{N}_x,$$

thus we only need to estimate the edge and face contributions.

As we proved, the symmetric bilinear form $q(\cdot, \cdot)$ is positive semidefinite, and it leads

$$|v_j|_{\widetilde{Q}_\Gamma^{(j)}}^2 \lesssim \sum_{\mathcal{E}} |I^h(\Theta_{\mathcal{E}} v_j)|_{\widetilde{Q}_\Gamma^{(j)}}^2 + \sum_{\mathcal{F}} |I^h(\Theta_{\mathcal{F}} v_j)|_{\widetilde{Q}_\Gamma^{(j)}}^2.$$

Moreover, thanks to [121, Lemma 7.2], each component of the above sum can be bounded from above by using Lemma 2.6:

$$
\begin{aligned}
|I^h(\Theta_* v_j)|_{\widetilde{Q}_\Gamma^{(j)}}^2 &= |I^h(\Theta_* v_j)|_{\widetilde{S}_\Gamma^{(j)}} \\
&= s^{(j)}\left(I^h(\Theta_* v_j), I^h(\Theta_* v_j)\right) \\
&\le q^{(j)}\left(\mathcal{H}_j^c\, I^h(\Theta_* v_j), \mathcal{H}_j^c\, I^h(\Theta_* v_j)\right) \\
&\le (\chi C_m + \tau K_{M,I})\, \|\mathcal{H}_j^\Delta I^h(\Theta_*(v_j^i - v_j^e))\|_{L^2(\Omega_j)}^2 + (1 - \tau K_{M,R})\, \|\mathcal{E}_{ext,\Omega_j} I^h(\Theta_* v_j^w)\|_{L^2(\Omega_j)}^2 \\
&\quad + \tau \sigma_M^{i(j)} |\mathcal{H}_j^\Delta I^h(\Theta_* v_j^i)|_{H^1(\Omega_j)}^2 + \tau \sigma_M^{e(j)} |\mathcal{H}_j^\Delta I^h(\Theta_* v_j^e)|_{H^1(\Omega_j)}^2.
\end{aligned}
$$

As a matter of fact, since the Schur seminorm realizes the minimum of the bilinear form $a^{(j)}$ (thus of its symmetric part $q^{(j)}$), we can bound it with any function defined on the interface Γ: we choose the discrete harmonic extension of the Laplacian operator for the intra- and extracellular $u^{i,e}$ components, while for the gating we use the discrete extension by zero of u^w to Ω_j .

In this perspective, as the argument of the L^2-norm vanishes on a two-dimensional subset of $\Gamma^{(j)}$, we can use the Poincaré-Friedrichs inequality (Prop. 3.1) and the Trace theorem (Thm 3.1) as follows

$$\|\mathcal{H}_j^\Delta I^h(\Theta_* v_j)\|_{L^2(\Omega_j)}^2 \overset{Prop.3.1}{\lesssim} H^2 |\mathcal{H}_j^\Delta I^h(\Theta_* v_j)|_{H^1(\Omega_j)}^2 \overset{Thm3.1}{\sim} H^2 |I^h(\Theta_* v_j)|_{H^{1/2}(\Gamma^{(j)})}^2,$$

$$|\mathcal{H}_j^\Delta I^h(\Theta_* v_j)|_{H^1(\Omega_j)}^2 \overset{Thm3.1}{\sim} |I^h(\Theta_* v_j)|_{H^{1/2}(\Gamma^{(j)})}^2,$$

to obtain

$$
\begin{aligned}
|v_j|_{\widetilde{Q}_\Gamma^{(j)}}^2 &\lesssim \sum_{\substack{*=\mathcal{E},\mathcal{F} \\ \star=i,e}} \left[\tau \sigma_M^{\star(j)} + H^2\left(\chi C_m + \tau K_{M,I}\right) \right] |I^h(\Theta_* v_j^\star)|_{H^{1/2}(\Gamma^{(j)})}^2 \\
&\quad + \sum_{*=\{\mathcal{E},\mathcal{F}\}} (1 - \tau K_{M,R})\, \|\mathcal{E}_{ext,\Omega_j} I^h(\Theta_* v_j^w)\|_{L^2(\Omega_j)}^2.
\end{aligned}
\tag{5.3}
$$

We now proceed to estimate the contribution from edges and faces separately.

Edge contribution   We recall that in the dual-primal construction,

$$\forall v_j^{i,e} \in \widetilde{W}_\Gamma, \qquad v_j^{i,e} = \sum_{k \in \mathcal{K}_{\mathcal{E}}} \delta_j^{i,e\,\dagger}(u_j^{i,e} - u_k^{i,e}), \tag{5.4}$$

where $\mathcal{K}_{\mathcal{E}} = \mathcal{N}_{\mathcal{E}} \setminus \{j\}$ is the index set of subdomains sharing $\mathcal{E}$. Therefore,

$$|I^h(\Theta_{\mathcal{E}} v_j^{i,e})|_{H^{1/2}(\Gamma^{(j)})}^2 \lesssim \|v_j^{i,e}\|_{L^2(\mathcal{E})}^2$$

$$= || \sum_{k \in \mathcal{K}_\mathcal{E}} \delta_k^{i,e \; \dagger} \left(u_j^{i,e} - u_k^{i,e} \right) ||_{L^2(\mathcal{E})}^2$$

$$\lesssim \sum_{k \in \mathcal{K}_\mathcal{E}} \left(\delta_k^{i,e \; \dagger} \right)^2 ||u_j^{i,e} - u_k^{i,e}||_{L^2(\mathcal{E})}^2$$

$$\lesssim \sum_{k \in \mathcal{K}_\mathcal{E}} \left(\delta_k^{i,e \; \dagger} \right)^2 ||u_j^{i,e} - \bar{u}_\mathcal{E}^{i,e}||_{L^2(\mathcal{E})}^2 + \sum_{k \in \mathcal{K}_\mathcal{E}} \left(\delta_k^{i,e \; \dagger} \right)^2 ||u_k^{i,e} - \bar{u}_\mathcal{E}^{i,e}||_{L^2(\mathcal{E})}^2$$

$$\lesssim \left(1 + \log \frac{H}{h} \right) \left[\sum_{k \in \mathcal{K}_\mathcal{E}} \left(\delta_k^{i,e \; \dagger} \right)^2 \right] |\mathcal{H}_j^{i,e} u_j|_{H^1(\Omega_j)}^2 +$$

$$+ \left(1 + \log \frac{H}{h} \right) \sum_{k \in \mathcal{K}_\mathcal{E}} \left(\delta_k^{i,e \; \dagger} \right)^2 |\mathcal{H}_k^{i,e} u_k|_{H^1(\Omega_k)}^2$$

$$= \left(1 + \log \frac{H}{h} \right) \left[\sum_{k \in \mathcal{K}_\mathcal{E}} \left(\delta_k^{i,e \; \dagger} \right)^2 |\mathcal{H}_j^{i,e} u_j|_{H^1(\Omega_j)}^2 + \sum_{k \in \mathcal{K}_\mathcal{E}} \left(\delta_k^{i,e \; \dagger} \right)^2 |\mathcal{H}_k^{i,e} u_k|_{H^1(\Omega_k)}^2 \right],$$

where we used Lemma 3.2 and Eq. (5.4). By definition of pseudoinverses,

$$\sum_l \left(\delta_l^{i,e \; \dagger} \right)^2 \le \left(\sum_l \delta_l^{i,e \; \dagger} \right)^2 = \left(\sum_l \frac{\sigma_M^{i,e^{(l)}}}{\sum_{k \in \mathcal{N}_x} \sigma_M^{i,e^{(k)}}} \right) \le 1$$

yielding $\sum_{k \in \mathcal{K}_\mathcal{E}} \left(\delta_k^{i,e \; \dagger} \right)^2 \le 1$ and also - easy to prove - $\sum_{k \in \mathcal{K}_\mathcal{E}} \left(\delta_k^{w \; \dagger} \right)^2 \le 1$. Moreover, we recall that the following property

$$\sigma_M^{i,e^{(j)}} \left(\delta_k^{i,e \; \dagger} \right)^2 \le \min \left\{ \sigma_M^{i,e^{(j)}}, \sigma_M^{i,e^{(k)}} \right\},$$

holds, from which we can conclude that either

$$\sigma_M^{i,e^{(j)}} \left(\delta_k^{i,e \; \dagger} \right)^2 \le \sigma_M^{i,e^{(j)}} \qquad \text{or} \qquad \sigma_M^{i,e^{(j)}} \left(\delta_k^{i,e \; \dagger} \right)^2 \le \sigma_M^{i,e^{(k)}}. \tag{5.5}$$

In addition, we notice that

$$||\mathcal{E}_{ext,\Omega_j} I^h(\theta_* u_j)||_{L^2(\Omega_j)}^2 \le ||u_j||_{L^2(\Omega_j)}^2,$$

i.e. the L^2-norm of the extension to zero on Ω_j of the discrete restriction of u_j to $* = \{\mathcal{E}, \mathcal{F}\}$ is bounded by the L^2-norm on Ω_j of the function u_j itself.
Therefore, using the ellipticity property (Lemma 2.6), the edge terms in (5.3) lead to

$$|P_D u_j|_{\widetilde{Q}_\Gamma^{(j)}}^2 = |v_j|_{\widetilde{Q}_\Gamma^{(j)}}^2$$

$$\lesssim \sum_{\star = i, e} \left[\tau \sigma_M^{\star(j)} + H^2 \left(\chi C_m + \tau K_{M,I} \right) \right] \left(1 + \log \frac{H}{h} \right) \left[\sum_{k \in \mathcal{K}_\mathcal{E}} \left(\delta_k^{\star \; \dagger} \right)^2 |\mathcal{H}_j^\star u_j|_{H^1(\Omega_j)}^2 + \sum_{k \in \mathcal{K}_\mathcal{E}} \left(\delta_k^{\star \; \dagger} \right)^2 |\mathcal{H}_k^\star u_k|_{H^1(\Omega_k)}^2 \right]$$

$$+ (1 - \tau K_{M,R}) ||\mathcal{E}_{ext,j} I^h(\Theta_* u_j^w)||_{L^2(\Omega_j)}^2$$

$$\lesssim \sum_{\star = i, e} \left[\tau \sigma_M^{\star(j)} + H^2 \left(\chi C_m + \tau K_{M,I} \right) \right] \left(1 + \log \frac{H}{h} \right) \underbrace{\sum_{k \in \mathcal{K}_\mathcal{E}} \left(\delta_k^{\star \; \dagger} \right)^2}_{\le 1} |\mathcal{H}_j^\star u_j|_{H^1(\Omega_j)}^2 +$$

$$+ \sum_{\star = i, e} \left[\tau \sigma_M^{\star(j)} + H^2 \left(\chi C_m + \tau K_{M,I} \right) \right] \left(1 + \log \frac{H}{h} \right) \sum_{k \in \mathcal{K}_\mathcal{E}} \left(\delta_k^{\star \; \dagger} \right)^2 |\mathcal{H}_k^\star u_k|_{H^1(\Omega_k)}^2$$

$$+ (1 - \tau K_{M,R}) ||u_j^w||_{L^2(\Omega_j)}^2$$

$$\lesssim \sum_{\star = i, e} \left[\tau \sigma_M^{\star(j)} + H^2 \left(\chi C_m + \tau K_{M,I} \right) \right] \left(1 + \log \frac{H}{h} \right) |\mathcal{H}_j^\star u_j|_{H^1(\Omega_j)}^2 +$$

$$+ \sum_{\star=i,e} \sum_{k \in \mathcal{K}_{\mathcal{E}}} \left[\tau \underbrace{\sigma_M^{\star(j)} \left(\delta_k^{\star \, \dagger} \right)^2}_{\substack{\text{for Ineq.}(5.5) \\ \leq \sigma_M^{\star(k)}}} + H^2 \left(\chi C_m + \tau K_{M,I} \right) \underbrace{\left(\delta_k^{\star \, \dagger} \right)^2}_{\leq 1} \right] \left(1 + \log \frac{H}{h} \right) |\mathcal{H}_k^\star u_k|^2_{H^1(\Omega_k)}$$

$$+ (1 - \tau K_{M,R}) \, ||u_j^w||^2_{L^2(\Omega_j)}$$

$$\lesssim \sum_{\star=i,e} \left[\tau \sigma_M^{\star(j)} + H^2 \left(\chi C_m + \tau K_{M,I} \right) \right] \left(1 + \log \frac{H}{h} \right) |\mathcal{H}_j^\star u_j|^2_{H^1(\Omega_j)} +$$

$$+ \sum_{\star=i,e} \sum_{k \in \mathcal{K}_{\mathcal{E}}} \left[\tau \sigma_M^{\star(k)} + H^2 \left(\chi C_m + \tau K_{M,I} \right) \right] \left(1 + \log \frac{H}{h} \right) |\mathcal{H}_k^\star u_k|^2_{H^1(\Omega_k)} + (1 - \tau K_{M,R}) \, ||u_j^w||^2_{L^2(\Omega_j)}$$

$$= \sum_{\star=i,e} \frac{\tau \sigma_M^{\star(j)} + H^2 \left(\chi C_m + \tau K_{M,I} \right)}{\tau \sigma_m^{\star(j)}} \left(1 + \log \frac{H}{h} \right) \tau \sigma_m^{\star(j)} |\mathcal{H}_j^\star u_j|^2_{H^1(\Omega_j)} +$$

$$+ \sum_{\star=i,e} \sum_{k \in \mathcal{K}_{\mathcal{E}}} \frac{\tau \sigma_M^{\star(k)} + H^2 \left(\chi C_m + \tau K_{M,I} \right)}{\tau \sigma_m^{\star(k)}} \left(1 + \log \frac{H}{h} \right) \tau \sigma_m^{\star(k)} |\mathcal{H}_k^\star u_k|^2_{H^1(\Omega_k)}$$

$$+ \frac{1 - \tau K_{M,R}}{1 - \tau K_{m,R}} \left(1 - \tau K_{m,R} \right) ||u_j^w||^2_{L^2(\Omega_j)}$$

$$\leq \max_{\star=i,e} \frac{\tau \sigma_M^{\star(j)} + H^2 \left(\chi C_m + \tau K_{M,I} \right)}{\tau \sigma_m^{\star(j)}} \left(1 + \log \frac{H}{h} \right) |u_j|^2_{\widetilde{Q}_\Gamma^{(j)}} +$$

$$+ \sum_{k \in \mathcal{K}_{\mathcal{E}}} \max_{\star=i,e} \frac{\tau \sigma_M^{\star(k)} + H^2 \left(\chi C_m + \tau K_{M,I} \right)}{\tau \sigma_m^{\star(k)}} \left(1 + \log \frac{H}{h} \right) |u_k|^2_{\widetilde{Q}_\Gamma^{(k)}} + \frac{1 - \tau K_{M,R}}{1 - \tau K_{m,R}} |u_j|^2_{\widetilde{Q}_\Gamma^{(j)}}$$

$$= \left(1 + \log \frac{H}{h} \right) \left[\max_{\star=i,e} \sum_{k \in \mathcal{N}_{\mathcal{E}}} \left(\frac{\tau \sigma_M^{\star(k)} + H^2 \left(\chi C_m + \tau K_{M,I} \right)}{\tau \sigma_m^{\star(k)}} \right) \right] |u|^2_{\widetilde{Q}_\Gamma^{(k)}} + \frac{1 - \tau K_{M,R}}{1 - \tau K_{m,R}} |u|^2_{\widetilde{Q}_\Gamma^{(j)}}$$

$$\leq \left(1 + \log \frac{H}{h} \right) \left[\max_{\star=i,e} \sum_{k \in \mathcal{N}_{\mathcal{E}}} \left(\frac{\tau \sigma_M^{\star(k)} + H^2 \left(\chi C_m + \tau K_{M,I} \right)}{\tau \sigma_m^{\star(k)}} \right) + \frac{1 - \tau K_{M,R}}{1 - \tau K_{m,R}} \right] |u|^2_{\widetilde{Q}_\Gamma^{(j)}}$$

by eventually noting that the number of subdomains sharing an edge is finite. In conclusion,

$$|P_D u|^2_{\widetilde{Q}_\Gamma^{(j)}} \lesssim \left(1 + \log \frac{H}{h} \right) \left[\max_{\substack{k \in \mathcal{N}_{\mathcal{E}} \\ \star=i,e}} \frac{\tau \sigma_M^{\star(k)} + H^2 \left(\chi C_m + \tau K_{M,I} \right)}{\tau \sigma_m^{\star(k)}} + \frac{1 - \tau K_{M,R}}{1 - \tau K_{m,R}} \right] \sum_{k \in \mathcal{N}_{\mathcal{E}}} |u|^2_{\widetilde{Q}_\Gamma^{(k)}}.$$

Face contribution The procedure is essentially the same as the edge term estimate, treating differently the addition of the average values: as we have not included the face terms in the primal space, it could happen that the mean on the face $\mathcal{F}^{(jk)}$ takes different values from the substructure j and from k. Therefore, for the intra- and extracellular components,

$$|I^h(\Theta_{\mathcal{F}} v_j^{i,e})|^2_{H^{1/2}(\Gamma^{(j)})} \lesssim |I^h(\Theta_{\mathcal{F}} \delta_j^{i,e \, \dagger} (u_j^{i,e} - u_k^{i,e}))|^2_{H^{1/2}(\Gamma^{(j)})}$$

$$\lesssim ||I^h(\Theta_{\mathcal{F}} \delta_j^{i,e \, \dagger} (u_j^{i,e} - u_k^{i,e}))||^2_{H_{00}^{1/2}(\mathcal{F})}$$

$$\leq \left(\delta_j^{i,e \, \dagger} \right)^2 ||I^h(\Theta_{\mathcal{F}} (u_j^{i,e} - u_k^{i,e}))||^2_{H_{00}^{1/2}(\mathcal{F})}$$

$$= \left(\delta_j^{i,e \, \dagger} \right)^2 ||I^h(\Theta_{\mathcal{F}} \left(u_j^{i,e} - u_k^{i,e} + \bar{u}_{j,\mathcal{F}}^{i,e} - \bar{u}_{j,\mathcal{F}}^{i,e} + \bar{u}_{k,\mathcal{F}}^{i,e} - \bar{u}_{k,\mathcal{F}}^{i,e} \right))||^2_{H_{00}^{1/2}(\mathcal{F})}$$

$$\leq \left(\delta_j^{i,e \, \dagger} \right)^2 ||I^h(\Theta_{\mathcal{F}} \left(u_j^{i,e} - \bar{u}_{j,\mathcal{F}}^{i,e} \right))||^2_{H_{00}^{1/2}(\mathcal{F})} + \left(\delta_j^{i,e \, \dagger} \right)^2 ||I^h(\Theta_{\mathcal{F}} \left(u_k^{i,e} - \bar{u}_{k,\mathcal{F}}^{i,e} \right))||^2_{H_{00}^{1/2}(\mathcal{F})} +$$

$$+ \left(\delta_j^{i,e \, \dagger} \right)^2 ||I^h(\Theta_{\mathcal{F}} \left(\bar{u}_{j,\mathcal{F}}^{i,e} - \bar{u}_{k,\mathcal{F}}^{i,e} \right))||^2_{H_{00}^{1/2}(\mathcal{F})}$$

$$
= \left(\delta_j^{i,e \ \dagger}\right)^2 \|I^h(\Theta_{\mathcal{F}}\left(u_j^{i,e} - \bar{u}_{j,\mathcal{F}}^{i,e}\right))\|_{H_{00}^{1/2}(\mathcal{F})}^2 + \left(\delta_j^{i,e \ \dagger}\right)^2 \|I^h(\Theta_{\mathcal{F}}\left(u_k^{i,e} - \bar{u}_{k,\mathcal{F}}^{i,e}\right))\|_{H_{00}^{1/2}(\mathcal{F})}^2 +
$$

$$
+ \left(\delta_j^{i,e \ \dagger}\right)^2 \|\Theta_{\mathcal{F}}\left(\bar{u}_{j,\mathcal{F}}^{i,e} - \bar{u}_{k,\mathcal{F}}^{i,e}\right)\|_{H_{00}^{1/2}(\mathcal{F})}^2
$$

$$
\lesssim \left(1 + \log\frac{H}{h}\right)^2 \left(\delta_j^{i,e \ \dagger}\right)^2 |u_j^{i,e}|_{H^{1/2}(\Gamma^{(j)})}^2 + \left(1 + \log\frac{H}{h}\right)^2 \left(\delta_j^{i,e \ \dagger}\right)^2 |u_k^{i,e}|_{H^{1/2}(\Gamma^{(k)})}^2 +
$$

$$
+ \left(1 + \log\frac{H}{h}\right)^2 \left(\delta_j^{i,e \ \dagger}\right)^2 \left[|u_j^{i,e}|_{H^{1/2}(\mathcal{F})}^2 + |u_k^{i,e}|_{H^{1/2}(\mathcal{F})}^2\right]
$$

$$
\lesssim 2\left(1 + \log\frac{H}{h}\right)^2 \left(\delta_j^{i,e \ \dagger}\right)^2 \left[|\mathcal{H}_j^{i,e}u_j|_{H^1(\Omega_j)}^2 + |\mathcal{H}_k^{i,e}u_k|_{H^1(\Omega_k)}^2\right]
$$

$$
\leq 2\left(1 + \log\frac{H}{h}\right)^2 \left(\delta_j^{i,e \ \dagger}\right)^2 \left[\frac{1}{\tau\sigma_m^{i,e(j)}}q^{(j)}\left(\mathcal{H}_j^{i,e}u_j, \mathcal{H}_j^{i,e}u_j\right) + \right.
$$

$$
\left. + \frac{1}{\tau\sigma_m^{i,e(k)}}q^{(k)}\left(\mathcal{H}_k^{i,e}u_k, \mathcal{H}_k^{i,e}u_k\right)\right]
$$

$$
= 2\left(1 + \log\frac{H}{h}\right)^2 \left(\delta_j^{i,e \ \dagger}\right)^2 \left[\frac{1}{\tau\sigma_m^{i,e(j)}}|u_j|_{\widetilde{Q}_\Gamma^{(j)}}^2 + \frac{1}{\tau\sigma_m^{i,e(k)}}|u_k|_{\widetilde{Q}_\Gamma^{(k)}}^2\right],
$$

by using Lemmas 3.1, 3.3, the Trace theorem (Thm 3.1) and the ellipticity Lemma 2.6. We also have to add the estimate of the L^2 norm of the gating component u^w, which can be treated in the same way as in the previous case.

In the same fashion as with the edge term, we can conclude this proof with the estimate of the face term

$$
|P_D u|_{\widetilde{Q}_\Gamma^{(j)}}^2 \lesssim \left(1 + \log\frac{H}{h}\right)^2 \left[\max_{\star=i,e}\frac{\tau\sigma_M^{\star(k)} + H^2\left(\chi C_m + \tau K_{M,I}\right)}{\tau\sigma_m^{\star(k)}} + \frac{1 - \tau K_{M,R}}{1 - \tau K_{m,R}}\right] |u|_{\widetilde{Q}_\Gamma^{(j)}}^2.
$$

5.1.2 Proof of Lemma 5.1 with *deluxe* scaling

It is possible to extend the proof of the analogous Lemma for the decoupled problem, with few modifications, for the coupled problem when the deluxe scaling is applied.

We need to define first the deluxe scaling induced by the symmetric bilinear form $q(\cdot, \cdot)$. As already done in Chapter 3, suppose that the face $\mathcal{F}$ is shared by Ω_j and Ω_k; let $Q_{\mathcal{F}}^{(j)}$ and $Q_{\mathcal{F}}^{(k)}$ be the principal minors obtained from $Q_\Gamma^{(j)}$ and $Q_\Gamma^{(k)}$ by removing all the contributions that are not related to the degrees of freedom of the face $\mathcal{F}$.

Let $u_{j,\mathcal{F}} = R_{\mathcal{F}}u_j$ be the restriction of u_j to the face $\mathcal{F}$ through the restriction operator $R_{\mathcal{F}}$; we define the deluxe average induced by the bilinear form $q(\cdot, \cdot)$ across $\mathcal{F}$ as

$$
\bar{u}_{Q,\mathcal{F}} = \left(Q_{\mathcal{F}}^{(j)} + Q_{\mathcal{F}}^{(k)}\right)^{-1}\left(Q_{\mathcal{F}}^{(j)}u_{j,\mathcal{F}} + Q_{\mathcal{F}}^{(k)}u_{k,\mathcal{F}}\right).
$$

Also in this case, we have denoted with $\bar{u}_{j,\mathcal{F}}$ the mean value of u_j over the face $\mathcal{F}$, while, if we omit the index j, we denote the deluxe average.

The action of $(Q_{\mathcal{F}}^{(j)} + Q_{\mathcal{F}}^{(k)})^{-1}$ can be computed by solving a Dirichlet problem over the two sub-domains, by extending to zero the right-hand side entries associated with the interior nodes.

In a similar fashion, if we consider an edge $\mathcal{E}$, where a node is common to at least two elements, it is possible to define the deluxe average induced by the symmetric bilinear form $q(\cdot, \cdot)$ across $\mathcal{E}$. Suppose for simplicity that $\mathcal{E}$ is shared by only three subdomains with indices j_1, j_2 and j_3; the extension to more than three subdomains is immediate. Let $u_{j,\mathcal{E}} = R_{\mathcal{E}}u_j$ be the restriction of u_j to the edge $\mathcal{E}$ through the restriction operator $R_{\mathcal{E}}$ and define

$$
Q_{\mathcal{E}}^{(j_{123})} = Q_{\mathcal{E}}^{(j_1)} + Q_{\mathcal{E}}^{(j_2)} + Q_{\mathcal{E}}^{(j_3)};
$$

then, the deluxe average induced by the bilinear form $q(\cdot, \cdot)$ across an edge $\mathcal{E}$ is given by

$$\bar{u}_{Q,\mathcal{E}} = \left(Q_{\mathcal{E}}^{(j_{123})}\right)^{-1} \left(Q_{\mathcal{E}}^{(j_1)} u_{j_1,\mathcal{E}} + Q_{\mathcal{E}}^{(j_2)} u_{j_2,\mathcal{E}} + Q_{\mathcal{E}}^{(j_3)} u_{j_3,\mathcal{E}}\right).$$

Then, like in the previous proof, instead of proving the bound for the projection operator E_D, we prove it for the complementary projection P_D and we focus on the local contributions. Thus, for all $u \in \widetilde{W}_\Gamma$

$$R_{\partial\Omega_j} P_D u = R_{\partial\Omega_j} \left(u_\Delta - \sum_{*=\{\mathcal{F},\mathcal{E}\}} R_*^T \bar{u}_*\right),$$

that leads to

$$|R_{\partial\Omega_j} P_D u|^2_{Q_\Gamma^{(j)}} \leq |\Xi_j^*| \sum_{\substack{*=\{\mathcal{F},\mathcal{E}\} \\ *\in\Xi_j^*}} |R_*^T \left(u_{j,*}^{i,e,w} - \bar{u}_{Q,*}^{i,e,w}\right)|^2_{Q_\Gamma^{(j)}},$$

where Ξ_j^* is the index set containing the indices of the subdomains that share the face $\mathcal{F}$ or the edge $\mathcal{E}$. We will denote by $\bar{u}_{\cdot,\mathcal{G}}^{i,e,w} = \left(\bar{u}_{\cdot,\mathcal{G}}^i, \bar{u}_{\cdot,\mathcal{G}}^e, 0\right)$ the vector containing the mean value of the intra- and extra-cellular potentials over $\mathcal{G} = \{\mathcal{F}, \mathcal{E}\}$ on the subdomain $\cdot$ and null value corresponding to the gating component. Let us distinguish between face and edge contributions.

Face contribution   Suppose that the face $\mathcal{F}$ is shared by subdomains Ω_j and Ω_k. Then, by simple algebra, it follows

$$u_{j,\mathcal{F}} - \bar{u}_{Q,\mathcal{F}} = u_{j,\mathcal{F}} - \left(Q_{\mathcal{F}}^{(j)} + Q_{\mathcal{F}}^{(k)}\right)^{-1} \left(Q_{\mathcal{F}}^{(j)} u_{j,\mathcal{F}} + Q_{\mathcal{F}}^{(k)} u_{k,\mathcal{F}}\right)$$

$$= \left(Q_{\mathcal{F}}^{(j)} + Q_{\mathcal{F}}^{(k)}\right)^{-1} Q_{\mathcal{F}}^{(k)} \left(u_{j,\mathcal{F}} - u_{k,\mathcal{F}}\right)$$

$$= \left(Q_{\mathcal{F}}^{(j)} + Q_{\mathcal{F}}^{(k)}\right)^{-1} Q_{\mathcal{F}}^{(k)} \left[\left(u_{j,\mathcal{F}} - \bar{u}_{j,\mathcal{F}}^{i,e,w}\right) - \left(u_{k,\mathcal{F}} - \bar{u}_{k,\mathcal{F}}^{i,e,w}\right) + \left(\bar{u}_{j,\mathcal{F}}^{i,e,w} - \bar{u}_{k,\mathcal{F}}^{i,e,w}\right)\right].$$

Therefore, it follows

$$|R_{\mathcal{F}}^T \left(u_{j,\mathcal{F}} - \bar{u}_{Q,\mathcal{F}}\right)|^2_{Q_\Gamma^{(j)}} = \left(u_{j,\mathcal{F}} - \bar{u}_{Q,\mathcal{F}}\right)^T Q_{\mathcal{F}}^{(j)} \left(u_{j,\mathcal{F}} - \bar{u}_{Q,\mathcal{F}}\right)$$

$$= \left(u_{j,\mathcal{F}} - u_{k,\mathcal{F}}\right)^T Q_{\mathcal{F}}^{(k)} \left(Q_{\mathcal{F}}^{(j)} + Q_{\mathcal{F}}^{(k)}\right)^{-1} Q_{\mathcal{F}}^{(j)} \left(Q_{\mathcal{F}}^{(j)} + Q_{\mathcal{F}}^{(k)}\right)^{-1} Q_{\mathcal{F}}^{(k)} \left(u_{j,\mathcal{F}} - u_{k,\mathcal{F}}\right)$$

$$\leq \left(u_{j,\mathcal{F}} - \bar{u}_{j,\mathcal{F}}^{i,e,w}\right)^T Q_{\mathcal{F}}^{(k)} \left(Q_{\mathcal{F}}^{(j)} + Q_{\mathcal{F}}^{(k)}\right)^{-1} Q_{\mathcal{F}}^{(j)} \left(Q_{\mathcal{F}}^{(j)} + Q_{\mathcal{F}}^{(k)}\right)^{-1} Q_{\mathcal{F}}^{(k)} \left(u_{j,\mathcal{F}} - \bar{u}_{j,\mathcal{F}}^{i,e,w}\right) +$$

$$+ \left(u_{k,\mathcal{F}} - \bar{u}_{k,\mathcal{F}}^{i,e,w}\right)^T Q_{\mathcal{F}}^{(k)} \left(Q_{\mathcal{F}}^{(j)} + Q_{\mathcal{F}}^{(k)}\right)^{-1} Q_{\mathcal{F}}^{(j)} \left(Q_{\mathcal{F}}^{(j)} + Q_{\mathcal{F}}^{(k)}\right)^{-1} Q_{\mathcal{F}}^{(k)} \left(u_{k,\mathcal{F}} - \bar{u}_{k,\mathcal{F}}^{i,e,w}\right) +$$

$$+ \left(\bar{u}_{j,\mathcal{F}}^{i,e,w} - \bar{u}_{k,\mathcal{F}}^{i,e,w}\right)^T Q_{\mathcal{F}}^{(k)} \left(Q_{\mathcal{F}}^{(j)} + Q_{\mathcal{F}}^{(k)}\right)^{-1} Q_{\mathcal{F}}^{(j)} \left(Q_{\mathcal{F}}^{(j)} + Q_{\mathcal{F}}^{(k)}\right)^{-1} Q_{\mathcal{F}}^{(k)} \left(\bar{u}_{j,\mathcal{F}}^{i,e,w} - \bar{u}_{k,\mathcal{F}}^{i,e,w}\right)$$

$$\leq 2|u_{j,\mathcal{F}} - \bar{u}_{j,\mathcal{F}}^{i,e,w}|^2_{Q_{\mathcal{F}}^{(j)}} + 2|u_{k,\mathcal{F}} - \bar{u}_{k,\mathcal{F}}^{i,e,w}|^2_{Q_{\mathcal{F}}^{(k)}} + |\left(S_{\mathcal{F}}^{(j)} + Q_{\mathcal{F}}^{(k)}\right)^{-1} Q_{\mathcal{F}}^{(k)} \left(\bar{u}_{j,\mathcal{F}}^{i,e,w} - \bar{u}_{k,\mathcal{F}}^{i,e,w}\right)|^2_{Q_{\mathcal{F}}^{(j)}},$$

$\forall u_{j,\mathcal{F}} \in \widetilde{W}_\Gamma$, where in the last line we use the two inequalities

$$Q_{\mathcal{F}}^{(k)} \left(Q_{\mathcal{F}}^{(j)} + Q_{\mathcal{F}}^{(k)}\right)^{-1} Q_{\mathcal{F}}^{(j)} \left(Q_{\mathcal{F}}^{(j)} + Q_{\mathcal{F}}^{(k)}\right)^{-1} Q_{\mathcal{F}}^{(k)} \leq Q_{\mathcal{F}}^{(j)}$$

$$Q_{\mathcal{F}}^{(k)} \left(Q_{\mathcal{F}}^{(j)} + Q_{\mathcal{F}}^{(k)}\right)^{-1} Q_{\mathcal{F}}^{(j)} \left(Q_{\mathcal{F}}^{(j)} + Q_{\mathcal{F}}^{(k)}\right)^{-1} Q_{\mathcal{F}}^{(k)} \leq Q_{\mathcal{F}}^{(k)}.$$

(5.6)

These relations follow from the generalized eigenvalue problem $Q_{\mathcal{F}}^{(j)} \phi = \lambda Q_{\mathcal{F}}^{(k)} \phi$ and by observing that all eigenvalues are non-negative.

It is sufficient now to estimate $|u_{j,\mathcal{F}} - \bar{u}_{j,\mathcal{F}}^{i,e,w}|^2_{Q_{\mathcal{F}}^{(j)}}$ and $|\left(Q_{\mathcal{F}}^{(j)} + Q_{\mathcal{F}}^{(k)}\right)^{-1} Q_{\mathcal{F}}^{(k)} \left(\bar{u}_{j,\mathcal{F}}^{i,e,w} - \bar{u}_{k,\mathcal{F}}^{i,e,w}\right)|^2_{Q_{\mathcal{F}}^{(j)}}$; we note that, where the subdomain faces averages are included in the primal space, the last term is zero. Thanks to the definition of $\bar{u}_{j,\mathcal{F}}^{i,e,w}$, we obtain

$$|u_{j,\mathcal{F}} - \bar{u}_{j,\mathcal{F}}^{i,e,w}|^2_{Q_{\mathcal{F}}^{(j)}} = q^{(j)}\left(\mathcal{H}_j^c\left(u_{j,\mathcal{F}} - \bar{u}_{j,\mathcal{F}}^{i,e,w}\right), \mathcal{H}_j^c\left(u_{j,\mathcal{F}} - \bar{u}_{j,\mathcal{F}}^{i,e,w}\right)\right)$$

$$\leq (\chi C_m + \tau K_{M,I})\,\|\mathcal{H}_j^{\Delta}\left(u_j^{i,e} - \bar{u}_{j,\mathcal{F}}^{i,e}\right)\|^2_{L^2(\Omega_j)} +$$

$$+ \tau \sum_{\star=i,e} \sigma_M^{\star} |\mathcal{H}_j^{\Delta}\left(u_{j,\mathcal{F}}^{\star} - \bar{u}_{j,\mathcal{F}}^{\star}\right)|^2_{H^1(\Omega_j)}$$

$$+ (1 - \tau K_{M,R})\,\|\mathcal{E}_{ext,\Omega_j} u_{j,\mathcal{F}}^w\|^2_{L^2(\Omega_j)}$$

$$\lesssim \left[\tau \sigma_M^{i,e} + H^2 (\chi C_m + \tau K_{M,I})\right] |u_{j,\mathcal{F}}^{i,e} - \bar{u}_{j,\mathcal{F}}^{i,e}|^2_{H^{1/2}(\Gamma^{(j)})}$$

$$+ (1 - \tau K_{M,R})\,\|u_j^w\|^2_{L^2(\Omega_j)},$$

by using the ellipticity Lemma 2.6, and the Poincaré-Friedrichs inequality (Prop. 3.1) combined with the Trace theorem (Thm 3.1). Here we are already taking in consideration the discrete restriction of a function $u_j \in \widetilde{W}_{\Gamma}$ on the face $\mathcal{F}$. In this way the notations $u_j - \bar{u}_{j,\mathcal{F}}^{i,e,w}$ and $I^h(\Theta_{\mathcal{F}}(u_j - \bar{u}_{j,\mathcal{F}}^{i,e,w}))$ are essentially the same. Therefore, it is possible to apply Lemma 3.3 and the Trace theorem to have

$$|u_{j,\mathcal{F}} - \bar{u}_{j,\mathcal{F}}^{i,e,w}|^2_{Q_{\Gamma}^{(j)}} \lesssim \left[\tau \sigma_M^{i,e} + H^2 (\chi C_m + \tau K_{M,I})\right] \left(1 + \log \frac{H}{h}\right)^2 |u_j^{i,e}|^2_{H^{1/2}(\partial\Omega_j)} + (1 - K_{M,R})\,\|u_j^w\|^2_{L^2(\Omega_j)}$$

$$\sim \left[\tau \sigma_M^{i,e} + H^2 (\chi C_m + \tau K_{M,I})\right] \left(1 + \log \frac{H}{h}\right)^2 |\mathcal{H}_j^{\Delta} u_j|^2_{H^1(\Omega_j)} + (1 - K_{M,R})\,\|u_j^w\|^2_{L^2(\Omega_j)},$$

$$(5.7)$$

Regarding the term $|\left(Q_{\mathcal{F}}^{(j)} + Q_{\mathcal{F}}^{(k)}\right)^{-1} Q_{\mathcal{F}}^{(k)} \left(\bar{u}_{j,\mathcal{F}}^{i,e,w} - \bar{u}_{k,\mathcal{F}}^{i,e,w}\right)|^2_{Q_{\mathcal{F}}^{(j)}}$, let $\mathcal{E} \subset \partial\mathcal{F}$ be a primal edge, such that $\bar{u}_{j,\mathcal{E}}^{i,e,w} = \bar{u}_{k,\mathcal{E}}^{i,e,w}$. Then,

$$|\left(Q_{\mathcal{F}}^{(j)} + Q_{\mathcal{F}}^{(k)}\right)^{-1} Q_{\mathcal{F}}^{(k)} \left(\bar{u}_{j,\mathcal{F}}^{i,e,w} - \bar{u}_{k,\mathcal{F}}^{i,e,w}\right)|^2_{Q_{\mathcal{F}}^{(j)}} \leq 2\,|\left(Q_{\mathcal{F}}^{(j)} + Q_{\mathcal{F}}^{(k)}\right)^{-1} Q_{\mathcal{F}}^{(k)} \left(\bar{u}_{j,\mathcal{E}}^{i,e,w} - \bar{u}_{j,\mathcal{F}}^{i,e,w}\right)|^2_{Q_{\mathcal{F}}^{(j)}} +$$

$$+ 2\,|\left(Q_{\mathcal{F}}^{(j)} + Q_{\mathcal{F}}^{(k)}\right)^{-1} Q_{\mathcal{F}}^{(k)} \left(\bar{u}_{k,\mathcal{E}}^{i,e,w} - \bar{u}_{k,\mathcal{F}}^{i,e,w}\right)|^2_{Q_{\mathcal{F}}^{(j)}}$$

$$\leq 2\,|\bar{u}_{j,\mathcal{E}}^{i,e,w} - \bar{u}_{j,\mathcal{F}}^{i,e,w}|^2_{Q_{\mathcal{F}}^{(j)}} + 2\,|\bar{u}_{k,\mathcal{E}}^{i,e,w} - \bar{u}_{k,\mathcal{F}}^{i,e,w}|_{Q_{\mathcal{F}}^{(k)}},$$

by using the two inequalities in (5.6). It is sufficient now to estimate the first term on the right-hand side, as we can deal with the other in the same fashion. Combining the result of ellipticity (Lemma (2.6)), the Poincaré-Friedrichs inequality (Prop. 3.1) and the Trace theorem (Thm. 3.1), we have

$$|\bar{u}_{j,\mathcal{E}}^{i,e,w} - \bar{u}_{j,\mathcal{F}}^{i,e,w}|^2_{Q_{\mathcal{F}}^{(j)}} = q^{(j)}\left(\mathcal{H}_j^c\left(\bar{u}_{j,\mathcal{E}}^{i,e,w} - \bar{u}_{j,\mathcal{F}}^{i,e,w}\right),\ \mathcal{H}_j^c\left(\bar{u}_{j,\mathcal{E}}^{i,e,w} - \bar{u}_{j,\mathcal{F}}^{i,e,w}\right)\right)$$

$$= q^{(j)}\left(\mathcal{H}_j^c\overline{\left(u_j - \bar{u}_{j,\mathcal{F}}^{i,e,w}\right)}_{j,\mathcal{E}},\ \mathcal{H}_j^c\overline{\left(u_j - \bar{u}_{j,\mathcal{F}}^{i,e,w}\right)}_{j,\mathcal{E}}\right)$$

$$\leq (\chi C_m + \tau K_M)\,\|\mathcal{H}_j^{\Delta}\overline{\left(u_j^{i,e} - \bar{u}_{j,\mathcal{F}}^{i,e}\right)}_{j,\mathcal{E}}\|^2_{L^2(\Omega_j)} +$$

$$+ (1 - \tau K_{M,R})\,\|\mathcal{E}_{ext,\Omega_j}\overline{\left(u_j^w - \bar{u}_{j,\mathcal{F}}^w\right)}_{j,\mathcal{E}}\|^2_{L^2(\Omega_j)}$$

$$+ \tau \sum_{\star=i,e} \sigma_M^{\star} |\mathcal{H}_j^{\Delta}\overline{\left(u_j^{i,e} - \bar{u}_{j,\mathcal{F}}^{i,e}\right)}_{j,\mathcal{E}}|^2_{H^1(\Omega_j)}$$

$$\lesssim \sum_{\star=i,e}\left[\tau \sigma_M^{\star} + H^2 (\chi C_m + \tau K_M)\right] |\overline{\left(u_j^{i,e} - \bar{u}_{j,\mathcal{F}}^{i,e}\right)}_{j,\mathcal{E}}|^2_{H^1(\Omega_j)},$$

where in the last inequality we use the fact that $\bar{u}^w_{j,\mathcal{E}}$ and $\bar{u}^w_{j,\mathcal{F}}$ are zero by construction. Regarding the intra- and extracellular components, by using Lemma (3.2) and Lemma (3.4), it follows

$$\| \overline{(u_j - \bar{u}_{j,\mathcal{F}})}_{j,\mathcal{E}} \|^2 \le CH^{-1}\|u_j - \bar{u}_{j,\mathcal{F}}\|^2_{L^2(\mathcal{E})}$$

$$\le C \left(1 + \log \frac{H}{h}\right) |u_j - \bar{u}_{j,\mathcal{F}}|^2_{H^{1/2}(\partial\Omega_j)}$$

$$\le C \left(1 + \log \frac{H}{h}\right)^3 |u_j|^2_{H^{1/2}(\partial\Omega_j)}.$$

This means that

$$|\bar{u}^{i,e,w}_{j,\mathcal{E}} - \bar{u}^{i,e,w}_{j,\mathcal{F}}|^2_{Q^{(j)}_{\mathcal{F}}} \le C \left(1 + \log \frac{H}{h}\right)^3 \sum_{\star=i,e} \left[\tau\sigma^\star_M + H^2 \left(\chi C_m + \tau K_{M,I}\right)\right] |u^{i,e}_j|^2_{H^{1/2}(\partial\Omega_j)}$$

$$\sim C \left(1 + \log \frac{H}{h}\right)^3 \sum_{\star=i,e} \left[\tau\sigma^\star_M + H^2 \left(\chi C_m + \tau K_{M,I}\right)\right] |\mathcal{H}^\Delta_j u_j|^2_{H^1(\Omega_j)}. \tag{5.8}$$

To conclude, the face contribution is given by considering the inequalities (5.7), (5.8) and Lemma 2.6:

$$|P_D u|^2_{Q^{(j)}_\Gamma} \lesssim \sum_{\star=i,e} \sum_{\mathcal{F}\in\Xi^\mathcal{F}_j} \left[\tau\sigma^\star_M + H^2 \left(\chi C_m + \tau K_{M,I}\right)\right] \left(1 + \log \frac{H}{h}\right)^3 |\mathcal{H}^\Delta_j u_j|^2_{H^1(\Omega_j)}$$

$$+ \sum_{\mathcal{F}\in\Xi^\mathcal{F}_j} (1 - \tau K_{M,R}) \|u^w_j\|^2_{L^2(\Omega_j)}$$

$$= \sum_{\star=i,e} \sum_{\mathcal{F}\in\Xi^\mathcal{F}_j} \frac{\tau\sigma^\star_M + H^2 \left(\chi C_m + \tau K_{M,I}\right)}{\sigma^\star_m} \left(1 + \log \frac{H}{h}\right)^3 \sigma^\star_m|\mathcal{H}^\Delta_j u_j|^2_{H^1(\Omega_j)}$$

$$+ \sum_{\mathcal{F}\in\Xi^\mathcal{F}_j} (1 - \tau K_{M,R}) \|u^w_j\|^2_{L^2(\Omega_j)}$$

$$\le \max_{\star=i,e} \sum_{\mathcal{F}\in\Xi^\mathcal{F}_j} \frac{\tau\sigma^\star_M + H^2 \left(\chi C_m + \tau K_{M,I}\right)}{\tau\sigma^\star_m} \left(1 + \log \frac{H}{h}\right)^3 |u^\star_j|^2_{\widetilde{Q}^{(j)}_\Gamma}$$

$$+ \sum_{\mathcal{F}\in\Xi^\mathcal{F}_j} \frac{1 - \tau K_{M,R}}{1 - \tau K_{m,R}} |u^w_j|^2_{\widetilde{Q}^{(j)}_\Gamma}$$

$$\le \sum_{\mathcal{F}\in\Xi^\mathcal{F}_j} \left[\max_{\star=i,e} \frac{\tau\sigma^\star_M + H^2 \left(\chi C_m + \tau K_{M,I}\right)}{\tau\sigma^\star_m} + \frac{1 - \tau K_{M,R}}{1 - \tau K_{m,R}}\right] \left(1 + \log \frac{H}{h}\right)^3 |u_j|^2_{\widetilde{Q}^{(j)}_\Gamma}.$$

Edge contribution   For simplicity, suppose that an edge $\mathcal{E}$ is shared only by three subdomains, with indexes j_1, j_2 and j_3. The extension to the case of more subdomains is then similar. Define $Q^{(j_{123})}_\mathcal{E}$ as

$$Q^{(j_{123})}_\mathcal{E} := Q^{(j_1)}_\mathcal{E} + Q^{(j_2)}_\mathcal{E} + Q^{(j_3)}_\mathcal{E}.$$

Then, we recall that the average operator is given by

$$\bar{u}_{Q,\mathcal{E}} := \left(Q^{(j_{123})}_\mathcal{E}\right)^{-1} \left(Q^{(j_1)}_\mathcal{E} u_{j_1,\mathcal{E}} + Q^{(j_2)}_\mathcal{E} u_{j_2,\mathcal{E}} + Q^{(j_3)}_\mathcal{E} u_{j_3,\mathcal{E}}\right).$$

Proceeding in the same fashion as for the face contribution, it follows

$$u_{j_1,\mathcal{E}} - \bar{u}_{Q,\mathcal{E}} = \left(Q^{(j_{123})}_\mathcal{E}\right)^{-1} \left[\left(Q^{(j_2)}_\mathcal{E} + Q^{(j_3)}_\mathcal{E}\right) u_{j_1,\mathcal{E}} - Q^{(j_2)}_\mathcal{E} u_{j_2,\mathcal{E}} - Q^{(j_3)}_\mathcal{E} u_{j_3,\mathcal{E}}\right],$$

which leads to

$$|R_{\mathcal{E}}^T (u_{j_1,\mathcal{E}} - \bar{u}_{Q,\mathcal{E}})|^2_{Q_{\Gamma}^{(j_1)}} = (u_{j_1,\mathcal{E}} - \bar{u}_{Q,\mathcal{E}})^T R_{\mathcal{E}} \, Q_{\Gamma}^{(j_1)} R_{\mathcal{E}}^T (u_{j_1,\mathcal{E}} - \bar{u}_{Q,\mathcal{E}})$$

$$= (u_{j_1,\mathcal{E}} - \bar{u}_{Q,\mathcal{E}})^T Q_{\mathcal{E}}^{(j_1)} (u_{j_1,\mathcal{E}} - \bar{u}_{Q,\mathcal{E}})$$

$$\leq 3 u_{j_1,\mathcal{E}}^T \left(Q_{\mathcal{E}}^{(j_2)} + Q_{\mathcal{E}}^{(j_3)} \right)^T \left(Q_{\mathcal{E}}^{(j_{123})} \right)^{-1} Q_{\mathcal{E}}^{(j_1)} \left(Q_{\mathcal{E}}^{(j_{123})} \right)^{-1} \left(Q_{\mathcal{E}}^{(j_2)} + Q_{\mathcal{E}}^{(j_3)} \right) u_{j_1,\mathcal{E}} \; +$$

$$+ 3 u_{j_2,\mathcal{E}}^T Q_{\mathcal{E}}^{(j_2)T} \left(Q_{\mathcal{E}}^{(j_{123})} \right)^{-1} Q_{\mathcal{E}}^{(j_1)} \left(Q_{\mathcal{E}}^{(j_{123})} \right)^{-1} Q_{\mathcal{E}}^{(j_2)} u_{j_2,\mathcal{E}} \; +$$

$$+ 3 u_{j_3,\mathcal{E}}^T Q_{\mathcal{E}}^{(j_3)T} \left(Q_{\mathcal{E}}^{(j_{123})} \right)^{-1} Q_{\mathcal{E}}^{(j_1)} \left(Q_{\mathcal{E}}^{(j_{123})} \right)^{-1} Q_{\mathcal{E}}^{(j_3)} u_{j_3,\mathcal{E}}$$

$$\leq 3 u_{j_1,\mathcal{E}}^T Q_{\mathcal{E}}^{(j_1)} u_{j_1,\mathcal{E}} \; + 3 u_{j_2,\mathcal{E}}^T Q_{\mathcal{E}}^{(j_2)} u_{j_2,\mathcal{E}} \; + u_{j_3,\mathcal{E}}^T Q_{\mathcal{E}}^{(j_3)} u_{j_3,\mathcal{E}}$$

where we use analogous inequalities as in the face case. The first term can be bounded by taking into account the matrices $Q_{\mathcal{E}}^{(j_1)}$ and $Q_{\mathcal{E}}^{(j_2)} + Q_{\mathcal{E}}^{(j_3)}$ in the generalized eigenvalue problem

$$Q_{\mathcal{E}}^{(j_1)} \phi = \lambda \left(Q_{\mathcal{E}}^{(j_2)} + Q_{\mathcal{E}}^{(j_3)} \right) \phi.$$

The second and third expressions follow similarly, by first bounding them from above with (see for example the second term)

$$3 u_{j_2,\mathcal{E}}^T Q_{\mathcal{E}}^{(j_2)T} \left(Q_{\mathcal{E}}^{(j_{123})} \right)^{-1} \left(Q_{\mathcal{E}}^{(j_1)} + Q_{\mathcal{E}}^{(j_2)} \right) \left(Q_{\mathcal{E}}^{(j_{123})} \right)^{-1} Q_{\mathcal{E}}^{(j_2)} u_{j_2,\mathcal{E}}$$

and then considering the generalized eigenvalue problem

$$Q_{\mathcal{E}}^{(j_2)} \phi = \lambda \left(Q_{\mathcal{E}}^{(j_1)} + Q_{\mathcal{E}}^{(j_3)} \right) \phi.$$

By adding and subtracting $\bar{u}_{j_1,\mathcal{E}}^{i,e,w}$ (which assume the same value over the three subdomain, since we have included the edge averages into the primal space) we obtain the analogous estimate for the egdes, thanks to Lemma 3.2

$$u_{j_1,\mathcal{E}}^T Q_{\mathcal{E}}^{(j_1)} u_{j_1,\mathcal{E}} \leq |u_{j_1,\mathcal{E}} - \bar{u}_{j_1,\mathcal{E}}^{i,e,w}|^2_{Q_{\Gamma}^{j_1}}$$

$$\lesssim \left[\tau \sigma_M^{i,e} + H^2 \left(\chi C_m + \tau K_{M,I} \right) \right] |u_{j_1,\mathcal{E}}^{i,e} - \bar{u}_{j_1,\mathcal{E}}^{i,e}|^2_{H^{1/2}(\Gamma^{(j)})} + (1 - \tau K_{M,R}) \, ||u_{j_1,\mathcal{E}}^w||^2_{L^2(\Omega_j)}$$

$$\leq \left[\tau \sigma_M^{i,e} + H^2 \left(\chi C_m + \tau K_{M,I} \right) \right] ||u_{j_1,\mathcal{E}}^{i,e} - \bar{u}_{j_1,\mathcal{E}}^{i,e}||^2_{L^2(\mathcal{E})} + (1 - \tau K_{M,R}) \, ||u_{j_1,\mathcal{E}}^w||^2_{L^2(\Omega_j)}$$

$$\leq \left[\tau \sigma_M^{i,e} + H^2 \left(\chi C_m + \tau K_{M,I} \right) \right] \left(1 + \log \frac{H}{h} \right) |\mathcal{H}_{j_1}^{\Delta} u_{j_1,\mathcal{E}}|^2_{H^1(\Omega_j)}$$

$$+ (1 - \tau K_{M,R}) \, ||u_{j_1,\mathcal{E}}^w||^2_{L^2(\Omega_j)}.$$

In conclusion, applying again Lemma 2.6, the edge contribution for the estimate of $|P_D u|^2_{Q_{\Gamma}^{(j)}}$ is given by

$$|P_D u|^2_{Q_{\Gamma}^{(j)}} \lesssim \sum_{\star = i,e} \sum_{\mathcal{E} \in \Xi_j^{\mathcal{E}}} \left[\tau \sigma_M^{i,e} + H^2 \left(\chi C_m + \tau K_{M,I} \right) \right] \left(1 + \log \frac{H}{h} \right) |\mathcal{H}_j^{\Delta} u_j|^2_{H^1(\Omega_j)}$$

$$+ \sum_{\mathcal{E} \in \Xi_j^{\mathcal{E}}} (1 - \tau K_{M,R}) \, ||u_j^w||^2_{L^2(\Omega_j)}$$

$$= \sum_{\star = i,e} \sum_{\mathcal{E} \in \Xi_j^{\mathcal{E}}} \frac{\tau \sigma_M^{i,e} + H^2 \left(\chi C_m + \tau K_{M,I} \right)}{\tau \sigma_m^{\star}} \left(1 + \log \frac{H}{h} \right) \sigma_m^{\star} |\mathcal{H}_j^{\Delta} u_j|^2_{H^1(\Omega_j)}$$

$$+ \sum_{\mathcal{E} \in \Xi_j^{\mathcal{E}}} \frac{1 - \tau K_{M,R}}{1 - \tau K_{m,R}} (1 - \tau K_{m,R}) \, ||u_j^w||^2_{L^2(\Omega_j)}$$

$$\leq \max_{\star = i,e} \sum_{\mathcal{E} \in \Xi_j^{\mathcal{E}}} \frac{\tau \sigma_M^{i,e} + H^2 (\chi C_m + \tau K_{M,I})}{\tau \sigma_m^{\star}} \left(1 + \log \frac{H}{h}\right) |u_j^{\star}|^2_{\widetilde{Q}_{\Gamma}^{(j)}}$$

$$+ \sum_{\mathcal{E} \in \Xi_j^{\mathcal{E}}} \frac{1 - \tau K_{M,R}}{1 - \tau K_{m,R}} |u_j^w|^2_{\widetilde{Q}_{\Gamma}^{(j)}}$$

$$\leq \sum_{\mathcal{E} \in \Xi_j^{\mathcal{E}}} \left[\max_{\star = i,e} \frac{\tau \sigma_M^{i,e} + H^2 (\chi C_m + \tau K_{M,I})}{\tau \sigma_m^{\star}} + \frac{1 - \tau K_{M,R}}{1 - \tau K_{m,R}} \right] \left(1 + \log \frac{H}{h}\right) |u_j|^2_{\widetilde{Q}_{\Gamma}^{(j)}}.$$

where the index j collects all contributions from the subdomains that share the edge $\mathcal{E}$.

5.2   Convergence rate for the coupled non-symmetric problem

The convergence rate of the preconditioned GMRES iteration can be obtained using the result in Reference [40] and following the proof techniques proposed in Ref. [121].

Theorem 5.1. *Let H be the subdomain size and let the mesh size h be small enough. Assume, for $u \in \widehat{W}_{\Gamma}$, that there exists two positive constants c and C such that*

$$\begin{aligned} c\langle u, u \rangle_{Q_{\Gamma}} &\leq \langle u, Tu \rangle_{Q_{\Gamma}} \\ \langle Tu, Tu \rangle_{Q_{\Gamma}} &\leq C\langle u, u \rangle_{Q_{\Gamma}} \end{aligned} \tag{5.9}$$

hold, with $c = \dfrac{c_0}{K^2}$ and $C = \Phi^{\star,k}(H,h)\ K^2$, where

$$c_0 = 1 - K^4 \frac{H^2}{h} \max_{\substack{k=1,\dots,N \\ \star = i,e}} \frac{\left[\sigma_M^{\star(k)} \right]^{\frac{1}{2}}}{\sqrt{\tau} \sigma_m^{\star(k)}} \Phi^{\star,k}(H,h) \left[\Phi^{\star,k}(H,h) - 1 \right]^{\frac{1}{2}},$$

$$\Phi^{\star,k}(H,h) = \left[\max_{\substack{k=1,\dots,N \\ \star = i,e}} \frac{\tau \sigma_M^{\star(k)} + H^2 (\chi C_m + \tau K_{M,I})}{\tau \sigma_m^{\star(k)}} + \frac{1 - \tau K_{M,R}}{1 - \tau K_{m,R}} \right] \left(1 + \log \frac{H}{h}\right)^n,$$

$$K^2 = \frac{1}{4} \frac{\tau^2 |C_{I_w} - C_{R_v}|^2}{(\chi C_m + \tau K_{m,I})(1 - \tau K_{m,R})},$$

where $n = 2, 3$ depends on the ρ-scaling or deluxe scaling adopted and T is the Bidomain preconditioned operator

$$T = M_{BDDC}^{-1} \widetilde{S}_{\Gamma} = \widetilde{R}_{D,\Gamma}^T \widetilde{S}_{\Gamma}^{-1} \widetilde{R}_{D,\Gamma} \widetilde{R}_{\Gamma} S_{\Gamma} \widetilde{R}_{\Gamma}^T.$$

Then

$$\frac{|r_m|_{Q_{\Gamma}}}{|r_0|_{Q_{\Gamma}}} \leq \left(1 - \frac{c^2}{C}\right)^{\frac{m}{2}},$$

where r_m is the residual at the m-th iteration.

5.2.1   Proof of the upper bound of Theorem 5.1

For the proof of the upper bound $\langle Tu, Tu \rangle_{Q_{\Gamma}} \leq C\langle u, u \rangle_{Q_{\Gamma}}$, we need the following results.

Lemma 5.2. *There exists a constant $C_1 > 0$ such that $\forall u_j, v_j \in W^{(j)}$ with $j = 1, \dots, N$,*

$$|z^{(j)}(u_j, v_j)| \leq C_1\ K |u_j|_{Q^{(j)}} |v_j|_{Q^{(j)}},$$

$$|a^{(j)}(u_j, v_j)| \leq C_1\ K |u_j|_{Q^{(j)}} |v_j|_{Q^{(j)}},$$

where

$$K^2 = \frac{1}{4} \frac{\tau^2 |C_{I_w} - C_{R_v}|^2}{(\chi C_m + \tau K_{m,I})(1 - \tau K_{m,R})}.$$

Proof. Using the ellipticity Lemma 2.6, we can bound from below the norm

$$|u_j|^2_{Q^{(j)}} = q^{(j)}(u_j, u_j)$$

$$\overset{\underset{\text{Lemma}}{2.6}}{\geq} 2 \left[(\chi C_m + \tau K_{m,I}) \, ||u_j^i - u_j^e||^2_{L^2(\Omega_j)} + \right.$$
$$+ \, (1 - \tau K_{m,R}) \, ||u_j^w||^2_{L^2(\Omega_j)} +$$
$$\left. + \, \tau \sigma_m^i |u_j^i|^2_{H^1(\Omega_j)} + \tau \sigma_m^e |u_j^e|^2_{H^1(\Omega_j)} \right]$$
$$\geq 2 \left[(\chi C_m + \tau K_{m,I}) \, ||u_j^i - u_j^e||^2_{L^2(\Omega_j)} + \right.$$
$$\left. + \, (1 - \tau K_{m,R}) \, ||u_j^w||^2_{L^2(\Omega_j)} \right].$$

Therefore, $\forall u_j, v_j \in W^{(j)}$

$$|u_j|^2_{Q^{(j)}} |v_j|^2_{Q^{(j)}} \geq 4 \, (\chi C_m + \tau K_{m,I})^2 \, ||u_j^i - u_j^e||^2_{L^2(\Omega_j)} ||v_j^i - v_j^e||^2_{L^2(\Omega_j)} +$$
$$+ \, 4 \, (1 - \tau K_{m,R})^2 \, ||u_j^w||^2_{L^2(\Omega_j)} ||v_j^w||^2_{L^2(\Omega_j)} +$$
$$+ \, 4 \, (\chi C_m + \tau K_{m,I}) \, (1 - \tau K_{m,R}) \times$$
$$\left[||u_j^i - u_j^e||^2_{L^2(\Omega_j)} ||v_j^w||^2_{L^2(\Omega_j)} + ||u_j^w||^2_{L^2(\Omega_j)} ||v_j^i - v_j^e||^2_{L^2(\Omega_j)} \right]$$
$$\geq 4 \, (\chi C_m + \tau K_{m,I}) \, (1 - \tau K_{m,R}) \times$$
$$\left[||u_j^i - u_j^e||^2_{L^2(\Omega_j)} ||v_j^w||^2_{L^2(\Omega_j)} + ||u_j^w||^2_{L^2(\Omega_j)} ||v_j^i - v_j^e||^2_{L^2(\Omega_j)} \right],$$

from which

$$|u_j|_{Q^{(j)}} |v_j|_{Q^{(j)}} \geq 2 \, (\chi C_m + \tau K_{m,I})^{\frac{1}{2}} (1 - \tau K_{m,R})^{\frac{1}{2}} \times$$
$$\sqrt{||u_j^i - u_j^e||^2_{L^2(\Omega_j)} ||v_j^w||^2_{L^2(\Omega_j)} + ||u_j^w||^2_{L^2(\Omega_j)} ||v_j^i - v_j^e||^2_{L^2(\Omega_j)}}.$$

We estimate the bound for the skew-symmetric bilinear form as

$$|z^{(j)}(u_j, v_j)| \leq \tau |C_{I_w} - C_{R_v}| \cdot |||u_j^i - u_j^e||_{L^2(\Omega_j)} ||v_j^w||_{L^2(\Omega_j)} + ||u_j^w||_{L^2(\Omega_j)} ||v_j^i - v_j^e||_{L^2(\Omega_j)}|$$
$$\leq \frac{1}{2} \frac{\tau |C_{I_w} - C_{R_v}|}{(\chi C_m + \tau K_{m,I})^{\frac{1}{2}} (1 - \tau K_{m,R})^{\frac{1}{2}}} |u_j|_{Q^{(j)}} |v_j|_{Q^{(j)}}.$$

The bound for the bilinear form $a(\cdot, \cdot)$ follows easily from its decomposition

$$a^{(j)}(u_j, v_j) = \frac{1}{2} q^{(j)}(u_j, v_j) + \frac{1}{2} z^{(j)}(u_j, v_j)$$

and from the continuity of both symmetric and skew-symmetric forms. $\qquad \square$

Lemma 5.3. *There exists a constant $C_2 > 0$ such that $\forall u, v \in \widehat{W}$*

$$|z(u, v)| \leq C_2 \, K |u|_Q ||v||_{L^2(\Omega)},$$

with K defined in Lemma 5.2.

Lemma 5.4. *Let $C_3, C_4 > 0$ be two positive constants, independent from H and h, such that $\forall u_\Gamma, v_\Gamma \in \widetilde{W}_\Gamma$*

$$(i) \qquad |\langle u_\Gamma, v_\Gamma \rangle_{\widetilde{Z}_\Gamma}| \leq C_3 \, K \, |u_\Gamma|_{\widetilde{Q}_\Gamma} |v_\Gamma|_{\widetilde{Q}_\Gamma}$$
$$(ii) \qquad |\langle u_\Gamma, v_\Gamma \rangle_{\widetilde{S}_\Gamma}| \leq C_4 \, K \, |u_\Gamma|_{\widetilde{Q}_\Gamma} |v_\Gamma|_{\widetilde{Q}_\Gamma}$$

$$(5.10)$$

where K is defined in Lemma 5.2.

Proof.   (i) From Definition 5.2 and Lemma 5.2, $\forall u_\Gamma, v_\Gamma \in \widetilde{W}_\Gamma$,

$$|\langle u_\Gamma, v_\Gamma \rangle_{\widetilde{Z}_\Gamma}| = |\langle u_{\mathcal{A},\Gamma}, v_{\mathcal{A},\Gamma} \rangle_{\widetilde{Z}}| = |\widetilde{z}\left(u_{\mathcal{A},\Gamma}, v_{\mathcal{A},\Gamma}\right)|$$
$$\leq K|u_{\mathcal{A},\Gamma}|_{\widetilde{Q}}|v_{\mathcal{A},\Gamma}|_{\widetilde{Q}} = K|u_\Gamma|_{\widetilde{Q}_\Gamma}|v_\Gamma|_{\widetilde{Q}_\Gamma}.$$

(ii) By using [121, Lemma 7.2] and 5.2, we obtain

$$|\langle u_\Gamma, v_\Gamma \rangle_{\widetilde{S}_\Gamma}| = |\langle u_{\mathcal{A},\Gamma}, v \rangle_{\widetilde{A}}| = |\widetilde{a}\left(u_{\mathcal{A},\Gamma}, v\right)|$$
$$\leq K|u_{\mathcal{A},\Gamma}|_{\widetilde{Q}}|v|_Q = K|u_\Gamma|_{\widetilde{Q}_\Gamma}|v_\Gamma|_{\widetilde{Q}_\Gamma}.$$

$\square$

We are now ready to prove the upper bound of Theorem 5.1.

Given $u_\Gamma \in \widehat{W}_\Gamma$, by defining $w_\Gamma = \widetilde{S}_\Gamma^{-1}\widetilde{R}_{D,\Gamma}u_\Gamma$ and using [121, Lemmas 7.2 and 7.9] and Lemmas 5.1, 5.4

$$\begin{aligned}
\langle Tu_\Gamma, Tu_\Gamma \rangle_{Q_\Gamma} &= \langle Tu_\Gamma, \ Tu_\Gamma \rangle_{S_\Gamma} \\
&= \langle \widetilde{R}_{D,\Gamma}^T \widetilde{S}_\Gamma^{-1} \widetilde{R}_{D,\Gamma} u_\Gamma, \ \widetilde{R}_{D,\Gamma}^T \widetilde{S}_\Gamma^{-1} \widetilde{R}_{D,\Gamma} u_\Gamma \rangle_{S_\Gamma} \\
&= \langle \widetilde{R}_{D,\Gamma}^T w_\Gamma, \ \widetilde{R}_{D,\Gamma}^T w_\Gamma \rangle_{S_\Gamma} \\
&= \langle \widetilde{R}_{D,\Gamma}^T w_\Gamma, \ S_\Gamma \widetilde{R}_{D,\Gamma}^T w_\Gamma \rangle \\
&= \langle \widetilde{R}_{D,\Gamma}^T w_\Gamma, \ \widetilde{R}_\Gamma^T \widetilde{S}_\Gamma \widetilde{R}_\Gamma \widetilde{R}_{D,\Gamma}^T w_\Gamma \rangle \\
&= \langle \widetilde{R}_\Gamma \widetilde{R}_{D,\Gamma}^T w_\Gamma, \ \widetilde{R}_\Gamma \widetilde{R}_{D,\Gamma}^T w_\Gamma \rangle_{\widetilde{S}_\Gamma} \\
&= \langle E_D w_\Gamma, \ E_D w_\Gamma \rangle_{\widetilde{S}_\Gamma} = |E_D w_\Gamma|_{\widetilde{S}_\Gamma}^2 = |E_D w_\Gamma|_{\widetilde{Q}_\Gamma}^2 \\
&\leq \Phi^{\star,k}(H,h) \ |w_\Gamma|_{\widetilde{Q}_\Gamma}^2 \\
&= \Phi^{\star,k}(H,h) \ \langle u_\Gamma, Tu_\Gamma \rangle_{S_\Gamma} \\
&\leq \Phi^{\star,k}(H,h)K \ |u_\Gamma|_{Q_\Gamma}|Tu_\Gamma|_{Q_\Gamma} \\
&= \Phi^{\star,k}(H,h)K \ \langle u_\Gamma, u_\Gamma \rangle_{Q_\Gamma}^{1/2}\langle Tu_\Gamma, Tu_\Gamma \rangle_{Q_\Gamma}^{1/2},
\end{aligned}$$

from which we conclude

$$\langle Tu_\Gamma, Tu_\Gamma \rangle_{Q_\Gamma} \leq \Phi^{\star,k}(H,h)K^2 \ \langle u_\Gamma, u_\Gamma \rangle_{Q_\Gamma},$$

where

$$\Phi^{\star,k}(H,h) = \left[\max_{\substack{k=1,\ldots,N \\ \star=i,e}} \frac{\tau\sigma_M^{\star(k)} + H^2\left(\chi C_m + \tau K_{M,I}\right)}{\tau\sigma_m^{\star(k)}} + \frac{1 - \tau K_{M,R}}{1 - \tau K_{m,R}} \right] \left(1 + \log\frac{H}{h}\right)^n, \qquad n = 2, 3$$

$$K^2 = \frac{1}{4}\frac{\tau^2 \ |C_{I_w} - C_{R_v}|^2}{\left(\chi C_m + \tau K_{m,I}\right)\left(1 - \tau K_{m,R}\right)}.$$

5.2.2   Proof of the lower bound of Theorem 5.1

Conversely, for the proof of the lower bound, we need Lemma 7.9 from Ref. [121] and the following results.

Lemma 5.5. *There exists a constant $C_5 > 0$ such that $\forall u_\Gamma, v_\Gamma \in \widehat{W}_\Gamma$,*

$$|\langle u_\Gamma, v_\Gamma \rangle_{Z_\Gamma}| \leq C_5 \ K|u_\Gamma|_{Q_\Gamma}\|v_{\mathcal{A},\Gamma}\|_{L^2(\Omega)},$$

with K defined in Lemma 5.2.

Lemma 5.6. *Given $w_\Gamma = \widetilde{S}_\Gamma^{-1} \widetilde{R}_{D,\Gamma} S_\Gamma u_\Gamma$ for $u_\Gamma \in \widehat{W}_\Gamma$, there exists a constant $C_6 > 0$ such that*

$$|w_\Gamma|_{Q_\Gamma}^2 \leq C_6 \, K^2 \Phi^{\star,k}(H,h) \, |u_\Gamma|_{Q_\Gamma}^2,$$

with K defined in Lemma 5.2 and

$$\Phi^{\star,k}(H,h) = \left[\max_{\substack{k=1,\ldots,N \\ \star=i,e}} \frac{\tau \sigma_M^{\star(k)} + H^2 \left(\chi C_m + \tau K_{M,I} \right)}{\tau \sigma_m^{\star(k)}} + \frac{1 - \tau K_{M,R}}{1 - \tau K_{m,R}} \right] \left(1 + \log \frac{H}{h} \right)^n, \qquad n = 2, 3.$$

Proof. We make use of Lemmas 5.1 and 5.4, in addition to [121, Lemmas 7.2, 7.9]:

$$
\begin{aligned}
\langle T u_\Gamma, T u_\Gamma \rangle_{Q_\Gamma} &= \langle T u_\Gamma, T u_\Gamma \rangle_{S_\Gamma} \\
&= \langle \widetilde{R}_{D,\Gamma}^T \widetilde{S}_\Gamma^{-1} \widetilde{R}_{D,\Gamma} S_\Gamma u_\Gamma, \ \widetilde{R}_{D,\Gamma}^T \widetilde{S}_\Gamma^{-1} \widetilde{R}_{D,\Gamma} S_\Gamma u_\Gamma \rangle_{S_\Gamma} \\
&= \langle \widetilde{R}_{D,\Gamma}^T w_\Gamma, \ \widetilde{R}_{D,\Gamma}^T w_\Gamma \rangle_{S_\Gamma} \\
&= |E_D w_\Gamma|_{\widetilde{S}_\Gamma}^2 \\
&= |E_D w_\Gamma|_{\widetilde{Q}_\Gamma}^2 \\
&\leq C_6 \Phi^{\star,k}(H,h) |w_\Gamma|_{\widetilde{Q}_\Gamma}^2 \\
&= C_6 \Phi^{\star,k}(H,h) \, \langle u_\Gamma, T u_\Gamma \rangle_{S_\Gamma} \\
&\leq C_6 \, K \Phi^{\star,k}(H,h) \, \langle u_\Gamma, u_\Gamma \rangle_{Q_\Gamma}^{1/2} \langle T u_\Gamma, T u_\Gamma \rangle_{Q_\Gamma}^{1/2},
\end{aligned}
$$

which means

$$\langle T u_\Gamma, T u_\Gamma \rangle_{Q_\Gamma} \leq C_6 \, K^2 \left[\Phi^{\star,k} \right]^2 (H,h) \, \langle u_\Gamma, u_\Gamma \rangle_{Q_\Gamma}.$$

It is straightforward to conclude, by applying [121, Lemma 7.9] and Lemma 5.4

$$
\begin{aligned}
|w_\Gamma|_{\widetilde{Q}_\Gamma}^2 &= \langle u_\Gamma, T u_\Gamma \rangle_{S_\Gamma} \\
&\leq K |u_\Gamma|_{Q_\Gamma} |T u_\Gamma|_{Q_\Gamma} \\
&\leq C_6 \, K^2 \Phi^{\star,k}(H,h) |u_\Gamma|_{Q_\Gamma}^2.
\end{aligned}
$$

$\square$

Lemma 5.7. *Let $w_\Gamma = \widetilde{S}_\Gamma^{-1} \widetilde{R}_{D,\Gamma} S_\Gamma u_\Gamma$, for $u_\Gamma \in \widehat{W}_\Gamma$. Then, the following property holds*

$$\langle w_{\mathcal{A},\Gamma}, v \rangle_{\widetilde{Q}} = \langle \widetilde{R} u_{\mathcal{A},\Gamma}, v \rangle_{\widetilde{Q}},$$

for all $v \in \widetilde{R}(\widehat{W})$.

Proof. Given $v \in \widetilde{R}(\widehat{W})$, we denote by $v_\Gamma \in \widetilde{R}_\Gamma(\widehat{W}_\Gamma)$ its continuous interface part. Then, given $u_\Gamma \in \widehat{W}_\Gamma$, by using Lemma 7.2 from Ref. [121] and the identity $\widetilde{R}_\Gamma \widetilde{R}_{D,\Gamma}^T v_\Gamma = v_\Gamma$, we get

$$
\begin{aligned}
\langle w_{\mathcal{A},\Gamma}, v \rangle_{\widetilde{Q}} &= \langle w_\Gamma, v_\Gamma \rangle_{\widetilde{S}_\Gamma} = v_\Gamma^T \widetilde{S}_\Gamma w_\Gamma \\
&= v_\Gamma^T \widetilde{S}_\Gamma \widetilde{S}_\Gamma^{-1} \widetilde{R}_{D,\Gamma} S_\Gamma u_\Gamma \\
&= v_\Gamma^T \widetilde{R}_{D,\Gamma} S_\Gamma u_\Gamma \\
&= v_\Gamma^T \widetilde{R}_{D,\Gamma} \widetilde{R}_\Gamma \widetilde{R}_{D,\Gamma}^T S_\Gamma u_\Gamma \\
&= v_\Gamma^T \widetilde{R}_{D,\Gamma} \widetilde{R}_\Gamma \widetilde{S}_\Gamma \widetilde{R}_\Gamma u_\Gamma \\
&= \langle \widetilde{R}_\Gamma u_\Gamma, \widetilde{R}_\Gamma \widetilde{R}_{D,\Gamma}^T v_\Gamma \rangle_{\widetilde{S}_\Gamma} \\
&= \langle \widetilde{R}_\Gamma u_\Gamma, v_\Gamma \rangle_{\widetilde{S}_\Gamma} \\
&= \langle \widetilde{R}_\Gamma u_{\mathcal{A},\Gamma}, v \rangle_{\widetilde{Q}}
\end{aligned}
$$

$\square$

Lemma 5.8. *For h sufficiently small, given $w_\Gamma = \widetilde{S}_\Gamma^{-1}\widetilde{R}_{D,\Gamma}S_\Gamma u_\Gamma$ for $u_\Gamma \in \widehat{W}_\Gamma$, there exists a positive constant $C_7 > 0$ such that $\forall u_\Gamma \in \widehat{W}_\Gamma$*

$$||w_{\mathcal{A},\Gamma} - u_{\mathcal{A},\Gamma}||^2_{L^2(\Omega)} \leq C_7\ H^2\ K^2 \max_{\substack{k=1,\dots,N \\ \star=i,e}} \frac{\Phi^{\star,k}(H,h) - 1}{\tau\sigma_m^{\star,k}}\ |u_\Gamma|_{Q_\Gamma},$$

with K and Φ defined in Lemmas 5.2 and 5.6 respectively.

Proof. It is useful to observe that, being $u_\Gamma \in \widehat{W}_\Gamma$, by defining $\widetilde{R}: \widehat{W} \longrightarrow \widetilde{W}$, then $\widetilde{R}u_\Gamma \in \widetilde{R}\left(\widehat{W}\right)$. By using the Poincaré-Friedrichs inequality (Prop. 3.1), the ellipticity Lemma 2.6 and [121, Lemma 7.2], we obtain

$$||w_{\mathcal{A},\Gamma} - u_{\mathcal{A},\Gamma}||^2_{L^2(\Omega)} \leq CH^2|w_{\mathcal{A},\Gamma} - u_{\mathcal{A},\Gamma}|^2_{H^1(\Omega)}$$
$$\leq CH^2 \max_{\substack{k=1,\dots,N \\ \star=i,e}} \frac{1}{\tau\sigma_m^{\star,k}}|w_{\mathcal{A},\Gamma} - \widetilde{R}u_{\mathcal{A},\Gamma}|^2_{\widetilde{Q}}$$

The right-hand side is:

$$|w_{\mathcal{A},\Gamma} - \widetilde{R}u_{\mathcal{A},\Gamma}|^2_{\widetilde{Q}} = \langle w_{\mathcal{A},\Gamma} - \widetilde{R}u_{\mathcal{A},\Gamma}, w_{\mathcal{A},\Gamma} - \widetilde{R}u_{\mathcal{A},\Gamma}\rangle_{\widetilde{Q}}$$
$$= \langle w_{\mathcal{A},\Gamma} - \widetilde{R}u_{\mathcal{A},\Gamma}, w_{\mathcal{A},\Gamma}\rangle_{\widetilde{Q}} - \langle w_{\mathcal{A},\Gamma} - \widetilde{R}u_{\mathcal{A},\Gamma}, \widetilde{R}u_{\mathcal{A},\Gamma}\rangle_{\widetilde{Q}}.$$

We treat separately the two terms.

(i) Using Lemma 5.6 and [121, Lemma 7.2],

$$\langle w_{\mathcal{A},\Gamma} - \widetilde{R}u_{\mathcal{A},\Gamma}, w_{\mathcal{A},\Gamma}\rangle_{\widetilde{Q}} = |w_{\mathcal{A},\Gamma}|^2_{\widetilde{Q}} - \langle \widetilde{R}u_{\mathcal{A},\Gamma}, w_{\mathcal{A},\Gamma}\rangle_{\widetilde{Q}}$$
$$= |w_\Gamma|^2_{\widetilde{Q}_\Gamma} - |\widetilde{R}u_{\mathcal{A},\Gamma}|^2_{\widetilde{Q}}$$
$$= |w_\Gamma|^2_{\widetilde{Q}_\Gamma} - |u_{\mathcal{A},\Gamma}|^2_{Q}$$
$$= |w_\Gamma|^2_{\widetilde{Q}_\Gamma} - |u_\Gamma|^2_{Q_\Gamma}$$
$$\leq C\left[K^2\Phi^{\star,k}(H,h) - 1\right]|u_\Gamma|^2_{Q_\Gamma},$$

where we observe that, for $u_{\mathcal{A},\Gamma} \in \widehat{W}$, $\widetilde{R}u_{\mathcal{A},\Gamma} \in \widetilde{R}(\widehat{W})$ and, since $\widetilde{Q}$ is symmetric, Lemma 5.7 holds:
$$\langle \widetilde{R}u_{\mathcal{A},\Gamma}, w_{\mathcal{A},\Gamma}\rangle_{\widetilde{Q}} = \langle w_{\mathcal{A},\Gamma}, \widetilde{R}u_{\mathcal{A},\Gamma}\rangle_{\widetilde{Q}} = \langle \widetilde{R}u_{\mathcal{A},\Gamma}, \widetilde{R}u_{\mathcal{A},\Gamma}\rangle_{\widetilde{Q}}.$$

(ii) From Lemma 5.7, it holds
$$\langle w_{\mathcal{A},\Gamma} - \widetilde{R}u_{\mathcal{A},\Gamma},\ \widetilde{R}u_{\mathcal{A},\Gamma}\rangle_{\widetilde{Q}} = 0,$$

since $\widetilde{R}u_{\mathcal{A},\Gamma} \in \widetilde{R}(\widehat{W})$.

Then
$$|w_{\mathcal{A},\Gamma} - \widetilde{R}u_{\mathcal{A},\Gamma}|^2_{\widetilde{Q}} \leq C\left[K^2\Phi^{\star,k}(H,h) - 1\right]|u_\Gamma|^2_{Q_\Gamma},$$

which leads to

$$||w_{\mathcal{A},\Gamma} - u_{\mathcal{A},\Gamma}||^2_{L^2(\Omega)} \leq C\ H^2\ K^2 \max_{\substack{k=1,\dots,N \\ \star=i,e}} \left[\frac{\Phi^{\star,k}(H,h) - 1}{\tau\sigma_m^{\star,k}}\right]|u_\Gamma|^2_{Q_\Gamma}.$$

$\square$

Lemma 5.9. *Given $v_\Gamma = \widetilde{R}_{D,\Gamma}^T w_\Gamma$ for $w_\Gamma \in \widetilde{W}_\Gamma$, there exists a positive constant $C > 0$ such that*

$$||v_{\mathcal{A},\Gamma}||_{L^2(\Omega)}^2 \leq C \frac{H^2}{h^2} \max_{\substack{k=1,\dots,N \\ \star=i,e}} \frac{\sigma_M^{\star,k}}{\sigma_m^{\star,k}} \left[\Phi^{\star,k}(H,h)\right]^2 ||w_{\mathcal{A},\Gamma}||_{L^2(\Omega)}^2,$$

with Φ defined in Lemma 5.6.

Proof. As the quantity $v_{\mathcal{A},\Gamma} - w_{\mathcal{A},\Gamma}$ has zero average on the interface, $\forall w_\Gamma \in \widetilde{W}_\Gamma$, then thanks to Poincaré-Friedrichs inequality, the ellipticity Lemma 2.6, Lemma 5.1 and [121, Lemma 7.2], we have

$$||v_{\mathcal{A},\Gamma} - w_{\mathcal{A},\Gamma}||_{L^2(\Omega)}^2 \leq C\, H^2 |v_{\mathcal{A},\Gamma} - w_{\mathcal{A},\Gamma}|_{H^1(\Omega)}^2$$

$$\leq \max_{\substack{k=1,\dots,N \\ \star=i,e}} C \frac{H^2}{\tau \sigma_m^{\star,k}} |v_{\mathcal{A},\Gamma} - w_{\mathcal{A},\Gamma}|_{\widehat{Q}}^2$$

$$= \max_{\substack{k=1,\dots,N \\ \star=i,e}} C \frac{H^2}{\tau \sigma_m^{\star,k}} |v_\Gamma - w_\Gamma|_{\widehat{Q}_\Gamma}^2$$

$$\leq \max_{\substack{k=1,\dots,N \\ \star=i,e}} C \frac{H^2}{\tau \sigma_m^{\star,k}} \left[\Phi^{\star,k}(H,h)\right]^2 |w_\Gamma|_{\widehat{Q}_\Gamma}^2$$

$$\leq \max_{\substack{k=1,\dots,N \\ \star=i,e}} C H^2 \frac{\tau \sigma_M^{\star,k}}{\tau \sigma_m^{\star,k}} \left[\Phi^{\star,k}(H,h)\right]^2 |w_{\mathcal{A},\Gamma}|_{H^1(\Omega)}^2$$

$$\leq \max_{\substack{k=1,\dots,N \\ \star=i,e}} C \frac{H^2}{h^2} \frac{\sigma_M^{\star,k}}{\sigma_m^{\star,k}} \left[\Phi^{\star,k}(H,h)\right]^2 ||w_{\mathcal{A},\Gamma}||_{L^2(\Omega)}^2$$

where we used the definition of projection E_D,

$$v_\Gamma - w_\Gamma = \left(I - \widetilde{R}_{D,\Gamma}^T\right) w_\Gamma = E_D w_\Gamma,$$

and an inverse inequality. $\qquad \square$

Lemma 5.10. *Set $v_\Gamma = T u_\Gamma - u_\Gamma$, for $u_\Gamma \in \widehat{W}_\Gamma$. For h sufficiently small, there exists a positive constant $C > 0$ such that for $u_\Gamma \in \widehat{W}_\Gamma$,*

$$||v_{\mathcal{A},\Gamma}||_{L^2(\Omega)}^2 \leq C\, K^2 \frac{H^4}{h^2} \max_{\substack{k=1,\dots,N \\ \star=i,e}} \frac{\sigma_M^{\star,k}}{\tau \left(\sigma_m^{\star,k}\right)^2} \left[\Phi^{\star,k}(H,h)\right]^2 \left[\Phi^{\star,k}(H,h) - 1\right] |u_\Gamma|_{Q_\Gamma}^2,$$

with K and Φ defined in Lemmas 5.2 and 5.6 respectively.

Proof. Since $T u_\Gamma = \widetilde{R}_{D,\Gamma}^T w_\Gamma$ and $\widetilde{R}_{D,\Gamma}^T \widetilde{R}_\Gamma = I$, then

$$v_\Gamma = T u_\Gamma - u_\Gamma$$
$$= \widetilde{R}_{D,\Gamma}^T w_\Gamma - \widetilde{R}_{D,\Gamma}^T \widetilde{R}_\Gamma u_\Gamma$$
$$= \widetilde{R}_{D,\Gamma}^T \left(w_\Gamma - \widetilde{R}_\Gamma u_\Gamma\right).$$

Therefore, by Lemmas 5.9 and 5.8,

$$||v_{\mathcal{A},\Gamma}||_{L^2(\Omega)}^2 \leq C \frac{H^2}{h^2} \max_{\substack{k=1,\dots,N \\ \star=i,e}} \frac{\sigma_M^{\star,k}}{\sigma_m^{\star,k}} \left[\Phi^{\star,k}(H,h)\right]^2 ||w_{\mathcal{A},\Gamma} - \widetilde{R}_\Gamma u_{\mathcal{A},\Gamma}||_{L^2(\Omega)}^2$$

$$\leq C\, K^2 \frac{H^4}{h^2} \max_{\substack{k=1,\dots,N \\ \star=i,e}} \frac{\sigma_M^{\star,k}}{\tau \left(\sigma_m^{\star,k}\right)^2} \left[\Phi^{\star,k}(H,h)\right]^2 \left[\Phi^{\star,k}(H,h) - 1\right] |u_\Gamma|_{Q_\Gamma}^2.$$

$\qquad \square$

Finally, we are able to conclude the proof of Theorem 5.1 by proving the lower bound of the inequality (5.9).

By using Lemma 5.4 and [121, lemmas 7.2 and 7.9],

$$
\begin{aligned}
\langle u_\Gamma, u_\Gamma \rangle_{Q_\Gamma} &= \langle u_\Gamma, u_\Gamma \rangle_{S_\Gamma} \\
&= u_\Gamma^T S_\Gamma u_\Gamma \\
&= u_\Gamma^T \widetilde{R}_\Gamma^T \widetilde{R}_{D,\Gamma} S_\Gamma u_\Gamma \\
&= u_\Gamma^T \widetilde{R}_\Gamma^T \widetilde{S}_\Gamma \widetilde{S}_\Gamma^{-1} \widetilde{R}_{D,\Gamma} S_\Gamma u_\Gamma \\
&= u_\Gamma^T \widetilde{R}_\Gamma^T \widetilde{S}_\Gamma w_\Gamma \\
&\leq K |w_\Gamma|_{\widetilde{Q}_\Gamma} |\widetilde{R}_\Gamma u_\Gamma|_{\widetilde{Q}_\Gamma} \\
&= K \langle u_\Gamma, T u_\Gamma \rangle_{S_\Gamma}^{1/2} \langle u_\Gamma, u_\Gamma \rangle_{Q_\Gamma}^{1/2},
\end{aligned}
$$

which means

$$
\langle u_\Gamma, u_\Gamma \rangle_{Q_\Gamma} \leq K^2 \langle u_\Gamma, T u_\Gamma \rangle_{S_\Gamma}. \tag{5.11}
$$

From [121, Lemma 7.2] and $\langle u_\Gamma, u_\Gamma \rangle_{Z_\Gamma} = 0$, we obtain

$$
\begin{aligned}
\langle u_\Gamma, T u_\Gamma \rangle_{S_\Gamma} &= \langle u_\Gamma, T u_\Gamma \rangle_{Q_\Gamma} + \langle u_\Gamma, T u_\Gamma \rangle_{Z_\Gamma} - \langle u_\Gamma, u_\Gamma \rangle_{Z_\Gamma} \\
&= \langle u_\Gamma, T u_\Gamma \rangle_{Q_\Gamma} + \langle u_\Gamma, T u_\Gamma - u_\Gamma \rangle_{Z_\Gamma}.
\end{aligned}
$$

Therefore, (5.11) becomes

$$
\langle u_\Gamma, u_\Gamma \rangle_{Q_\Gamma} \leq K^2 \langle u_\Gamma, T u_\Gamma \rangle_{Q_\Gamma} + K^2 \langle u_\Gamma, T u_\Gamma - u_\Gamma \rangle_{Z_\Gamma}.
$$

However, thanks to Lemmas 5.5 and 5.10,

$$
\begin{aligned}
\langle u_\Gamma, T u_\Gamma - u_\Gamma \rangle_{Z_\Gamma} &\leq K |u_\Gamma|_{Q_\Gamma} \|v_{\mathcal{A},\Gamma}\|_{L^2(\Omega)} \\
&\leq C\, K^2 \frac{H^2}{h} \max_{\substack{k=1,\ldots,N \\ \star=i,e}} \frac{\left[\sigma_M^{\star,k}\right]^{1/2}}{\tau^{\frac{1}{2}} \sigma_m^{\star,k}} \Phi^{\star,k}(H,h) \left[\Phi^{\star,k}(H,h)\right]^{1/2} \langle u_\Gamma, u_\Gamma \rangle_{Q_\Gamma},
\end{aligned}
$$

from which it follows

$$
\langle u_\Gamma, u_\Gamma \rangle_{Q_\Gamma} \leq K^2 \langle u_\Gamma, T u_\Gamma \rangle_{Q_\Gamma} + C\, K^4 \frac{H^2}{h} \max_{\substack{k=1,\ldots,N \\ \star=i,e}} \frac{\left[\sigma_M^{\star,k}\right]^{1/2}}{\tau^{\frac{1}{2}} \sigma_m^{\star,k}} \Phi^{\star,k}(H,h) \left[\Phi^{\star,k}(H,h)\right]^{1/2} \langle u_\Gamma, u_\Gamma \rangle_{Q_\Gamma}.
$$

In conclusion, we have the lower bound

$$
c_0 \langle u_\Gamma, u_\Gamma \rangle_{Q_\Gamma} \leq K^2 \langle u_\Gamma, T u_\Gamma \rangle_{Q_\Gamma},
$$

where

$$
c_0 = 1 - K^4 \frac{H^2}{h} \max_{\substack{k=1,\ldots,N \\ \star=i,e}} \frac{\left[\sigma_M^{\star,k}\right]^{1/2}}{\tau^{\frac{1}{2}} \sigma_m^{\star,k}} \Phi^{\star,k}(H,h) \left[\Phi^{\star,k}(H,h)\right]^{1/2}.
$$

Chapter 6

Parallel Numerical Tests

In this Chapter we present extensive parallel numerical experiments related to the solution strategies proposed in Chapters 4 and 5. The ionic model which has been considered as benchmark is the Rogers-McCulloch ionic model (see Chap. 2), but some preliminary tests using the Luo-Rudy phase 1 and the Ten Tusscher-Panfilov 2006 models (Chap. 2 and Appendix A) have been reported for the decoupled approach. Further investigations using these complex ventricular ionic models should be carried out, in order to confirm the robustness of the proposed solver.

We investigate two important properties of the proposed solvers, namely scalability and optimality (see [116, Definitions 1.3 and 1.2]).

Definition 6.1 (Scalability). *A domain decomposition iterative algorithm for the solution of a linear system is said to be scalable if its rate of convergence does not deteriorate when the number of subdomains grows. This typically means that the convergence does not deteriorate when H, the typical subdomain size, becomes small.*

Computationally, this property can be translated as, while fixing the local mesh size h (diameter of the finite elements) and increasing the number of subdomains $1/H$ (being H the diameter of a typical subdomain), the average number of linear iterations does not increase uncontrolled. In our tests, we always assign one subdomain to each processor.

Definition 6.2 (Optimality). *An iterative method for the solution of a linear system is said to be optimal if its rate of convergence to the exact solution is independent of the size of the system.*

In this sense, we have theoretically proved that the condition number of the preconditioned operator for the decoupled strategy (Thm 4.1) and the residual of the GMRES iterations in the coupled approach (Thm 5.1) are bounded by a polylogarithmic term depending from the ratio H/h. Therefore, we expect to numerically confirm scalability and quasi-optimality properties.

Lastly, we also compute and study the speedup, in order to evaluate the efficiency of the proposed solvers. The speedup usually indicates a measure of the relative performance of two systems processing the same task. Throughout this Thesis, we will refer to the speedup S_p as the ratio between the runtime needed by p processors and the average runtime needed by N processors to complete the task.

$$S_p = \frac{T_p}{T_N}.$$

All the codes are written in C, with the usage of the Portable, Extensive Toolkit for Scientific computation (PETSc), from the Argonne National Laboratory [3]. This library provides structures and many linear (KSP) and non-linear (SNES) solver routines for the parallel solution of scientific applications.

Architectures.   We describe here the hardware used for all the numerical experiments.

1. **Linux Cluster, Eos.** At the University of Pavia, a Linux Infiniband cluster with 21 nodes, each carrying 2 processors Intel Xeon Gold 6130 2.1 GHz with 16 cores each, for a total of 672 cores.

2. **Linux Cluster, Marconi.** Supercomputer of Cineca centre, an Intel OmniPath cluster with 3600 nodes, each with 68 1.40 GHz Intel Xeon Phi 7250 Knights Landing (KNL) cores and 16 GB/node, for a total 244 800 cores.

3. **Linux Cluster, Galileo.** Supercomputer of Cineca centre, a Linux Infiniband cluster equipped with 1084 nodes, each with 36 2.30 GHz Intel Xeon E5-2697 v4 cores and 128 GB/node, for a total 39 024 cores.

4. **Linux Cluster, Indaco.** At the University of Milano, a Linux infiniband cluster with 16 nodes, each carrying 2 processors Intel Xeon E5-2683 V4 2.1 GHz with 16 cores each, for a total amount of 512 cores.

For each set of experiments we will specify the cluster employed.

Domain geometry.   All numerical experiments are carried both on a thin slab and on a idealized left ventricular geometry, modeled as a half truncated ellipsoid (see Fig. 6.1). The latter is described in ellipsoidal coordinates by the parametric equations

$$\begin{cases} \mathbf{x} = a(r)\cos\theta\cos\varphi, & \theta_{\min} \leq \theta \leq \theta_{\max}, \\ \mathbf{y} = b(r)\cos\theta\sin\varphi, & \varphi_{\min} \leq \varphi \leq \varphi_{\max}, \\ \mathbf{z} = c(r)\sin\varphi, & 0 \leq r \leq 1, \end{cases}$$

where $a(r) = a_1 + r(a_2 - a_1)$, $b(r) = b_1 + r(b_2 - b_1)$ and $c(r) = c_1 + r(c_2 - c_1)$ with $a_{1,2}$, $b_{1,2}$ and $b_{1,2}$ given coefficients defining the main axes of the ellipsoid.
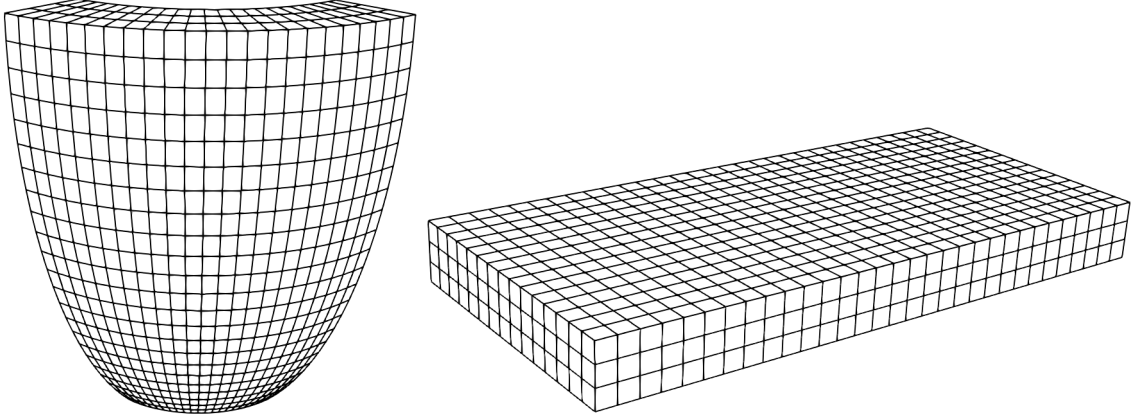
Figure 6.1: *Computational domains.* Portion of left ventricle, idealized as a truncated ellipsoid (left) and slab geometry (right).

The fibers rotate intramurally linearly with the depth for a total amount of 120° proceeding counterclockwise from epicardium ($r = 1$, outer surface of the truncated ellipsoid) to endocardium ($r = 0$, inner surface). More precisely, where not otherwise specified, the geometry is settled with the parameters reported in Table 6.1.

Conductivity coefficients and parameters.   Regarding the physiological coefficients in Table 6.2, we refer to the original paper Ref. [105] for the parameters of the Roger-McCulloch ionic membrane model, while for the Bidomain and Monodomain model to Ref. [27]. For Luo-Rudy phase one and ten Tusscher-Panfilov 2006 ionic models, we refer to References [80, 81, 114, 115] and Appendix A for the equations and constant values.

Parameter	Value	Parameter	Value
a_1	1.5	$\theta_{\min}$	$-\frac{\pi}{2}$
a_2	2.7	$\theta_{\max}$	$\frac{\pi}{2}$
b_1	1.5	$\varphi_{\min}$	$-\frac{\pi}{8}$
b_2	2.7	$\varphi_{\max}$	$\frac{\pi}{8}$
c_1	4.4		
c_2	5.0		

Table 6.1: Geometries parameters.

Bidomain conductivity coeff.		Ionic parameters	
σ_l^i	$3 \times 10^{-3} \Omega^{-1}$ cm^{-1}	G	$1.2\ \Omega^{-1}$ cm^{-2}
σ_t^i	$3.1525 \times 10^{-4} \Omega^{-1}$ cm^{-1}	η_1	$4.4\ \Omega^{-1}$ cm^{-1}
σ_n^i	$3.1525 \times 10^{-5} \Omega^{-1}$ cm^{-1}	η_2	0.012
σ_l^e	$2 \times 10^{-3} \Omega^{-1}$ cm^{-1}	v_{th}	13 mV
σ_t^e	$1.3514 \times 10^{-3} \Omega^{-1}$ cm^{-1}	v_p	100 mV
σ_n^e	$6.757 \times 10^{-4} \Omega^{-1}$ cm^{-1}	C_m	1 mF/cm^2

Table 6.2: Conductivity coefficients for the Bidomain model and physiological parameters for the Rogers-McCulloch ionic model.

Time setting and stimulation site. If otherwise not specified, the external stimulus I_{app} needed for the potential to start propagating is applied for 1 ms to the surface of the domain representing the endocardium, with intensity 100 mA/cm^3. On the other hand, if a thin slab is considered, the stimulus is applied in one corner of the domain, over a spheric (or circular) area of radius 0.1 cm. The boundary conditions are for an insulated tissue, while the initial conditions represent a resting potential.

The time step is fixed $\tau = 0.05$ ms. Indeed, increasing it might slightly affect the solver performance, but we would loose accuracy in the final solution, especially during the activation phase. On the other hand, decreasing the time step means to rise the computational costs, without a significant improvement in terms of accuracy.

Figures 6.2 and 6.3 show the time evolution of the extracellular and transmembrane potentials respectively, from the epicardial view of a portion of the idealized left ventricle when the external stimulus I_{app} is applied on the surface of the ellipsoid representing the epicardium layer.
The staggered propagating wavefront seems to indicate an insufficient mesh resolution, despite the usage of a fine mesh ($192 \times 96 \times 48$ elements): this further motivates the need of efficient solvers which can be both accurate and computationally competitive.

As another example, we report in Figures 6.4 and 6.5 the time evolution of the transmembrane and extracellular potentials respectively from the endocardial side of the portion of the half truncated ellipsoid. The external stimulus I_{app} is applied on five different sites on the endocardium layer, positioned at the apex of the idealized left ventricle.

Nonlinear solver. The outer Newton loop is implemented both:

- as an exact Newton method, with an absolute convergence test on the reduction of a weighted Euclidean norm of the residual, setting a tolerance of 10^{-4}, if not otherwise specified;

- by taking advantage of the non-linear solvers component SNES (Scalable Nonlinear Equations Solvers) from PETSc library, which by default implements an inexact Newton method with cubic backtracking linesearch. The default tolerances are reported in Table 6.3.

Linear Solver. The linear systems arising from the discretization of the Jacobian problems at each Newton step are solved with
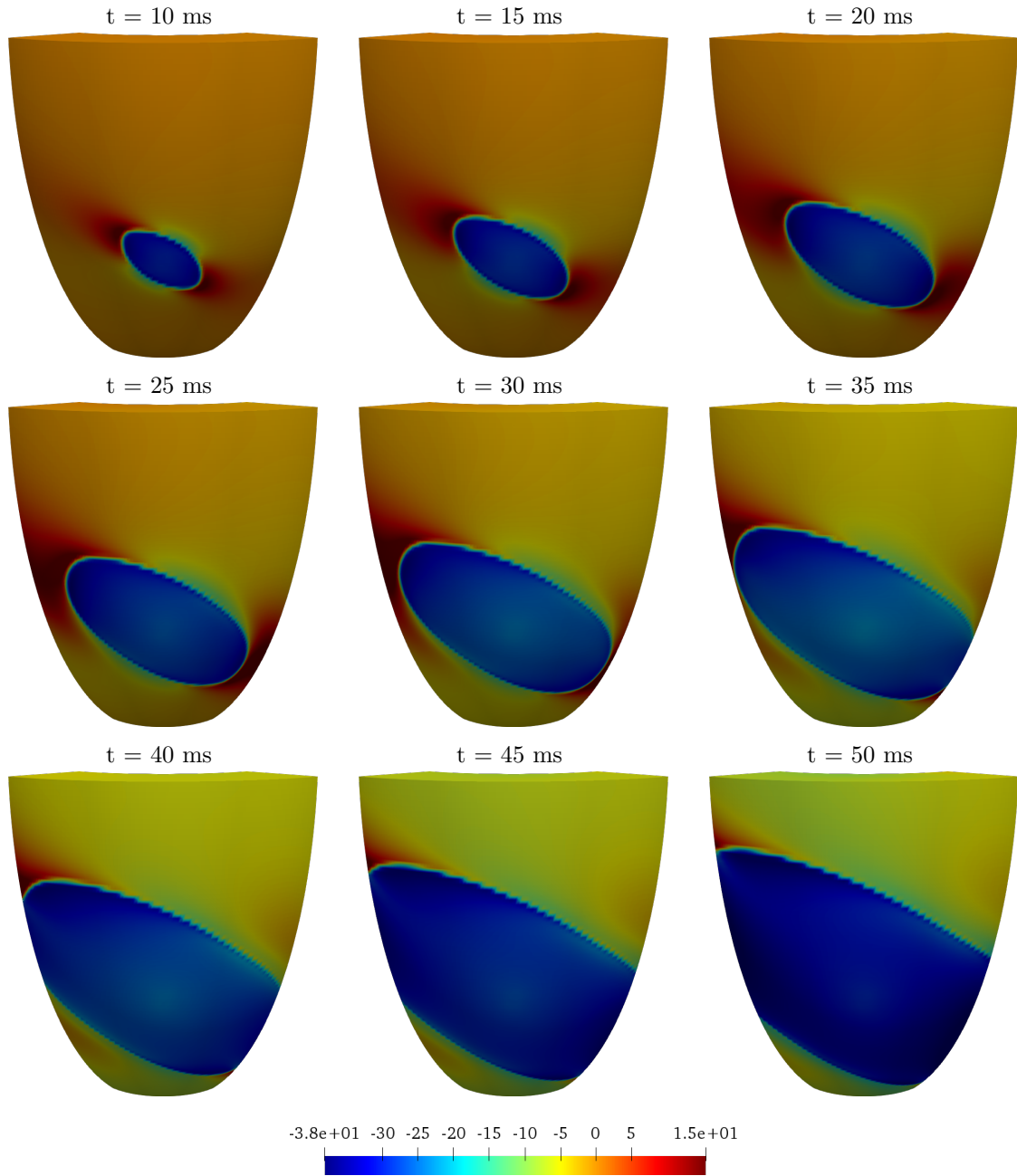
Figure 6.2: Snapshots (every 5 ms) of extracellular potential u_e time evolution. For each time frame, we report the epicardial view of a portion of the left ventricle, modeled as a truncated ellipsoid.

1. the Conjugate Gradient (CG) method, if the resulting system is symmetric (decoupled case);

2. the Generalized Minimal Residual (GMRES) or the BiConjugate Gradient Stabilized (BiCGStab) methods, if the resulting system is not symmetric (coupled case).

We employ the linear solvers component KSP from PETSc library, which provides a user-ready interface for the combination of a Krylov subspace iterative method and a preconditioning technique. CG, GMRES and BiCGStab are employed with the default values from PETSc implementation (so e.g. with restart value = 30 for GMRES). If not otherwise specified, we adopt the tolerances from Table 6.3.
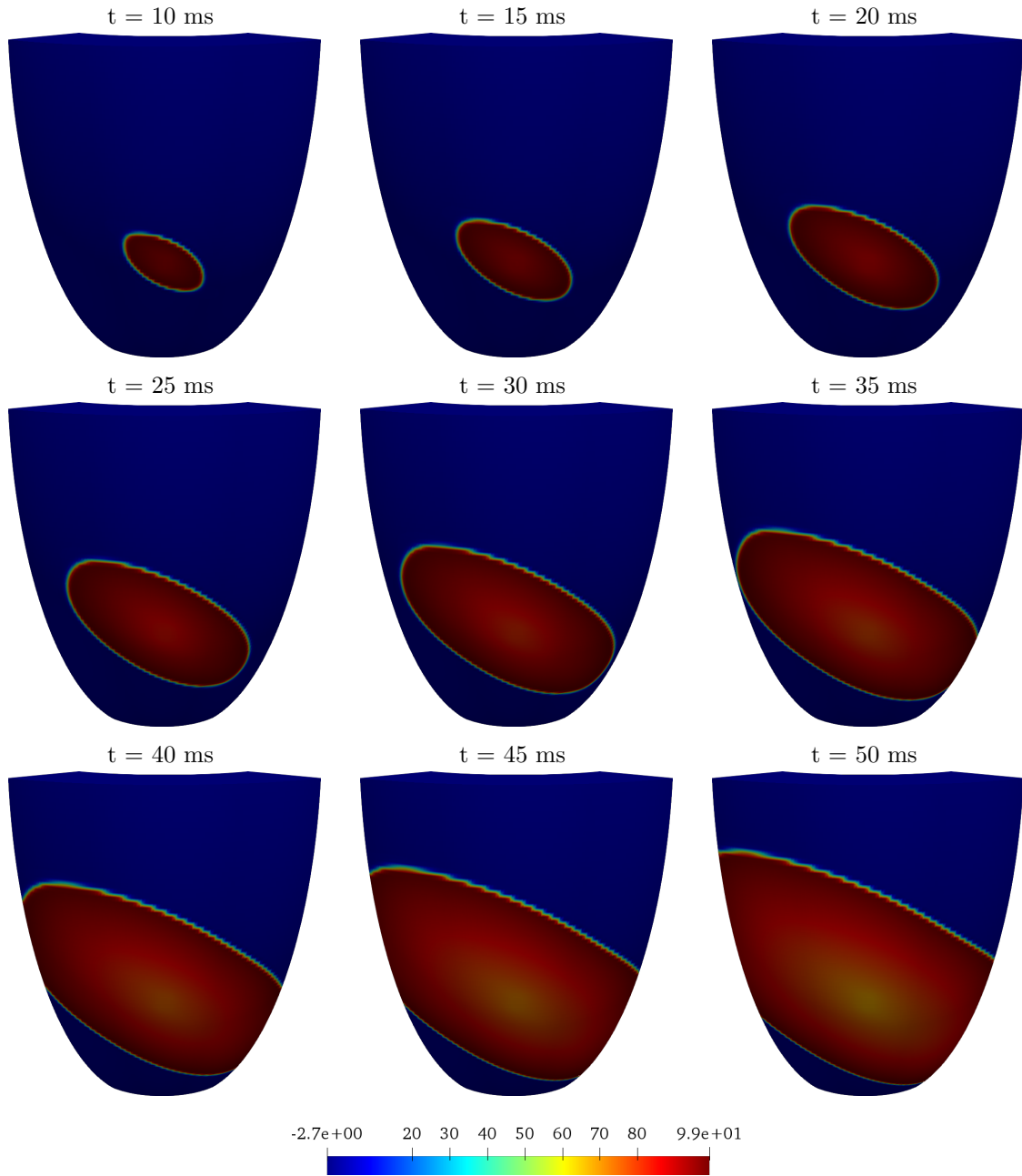
Figure 6.3: Snapshots (every 5 ms) of transmembrane potential v time evolution. For each time frame, we report the epicardial view of a portion of the left ventricle, modeled as a truncated ellipsoid.

The Jacobian matrix is always computed analytically in all the experiments, both for the decoupled and the coupled problem; we tested (but not reported in this Thesis) an approximation of the Jacobian via automatic differentiation, but without gaining substancial differences.

KSP	$r_{tol} = 1e^{-08}$	$a_{tol} = 1e^{-10}$	$d_{tol} = 1e^{+04}$
SNES	$r_{tol} = 1e^{-04}$	$a_{tol} = 1e^{-08}$	$s_{tol} = 1e^{-08}$

Table 6.3: PETSc SNES and KSP tolerances. r_{tol} is the relative convergence tolerance, a_{tol} is the absolute convergence tolerance, d_{tol} is the KSP divergence convergence tolerance and s_{tol} is the convergence tolerance related to the solution change between Newton steps.
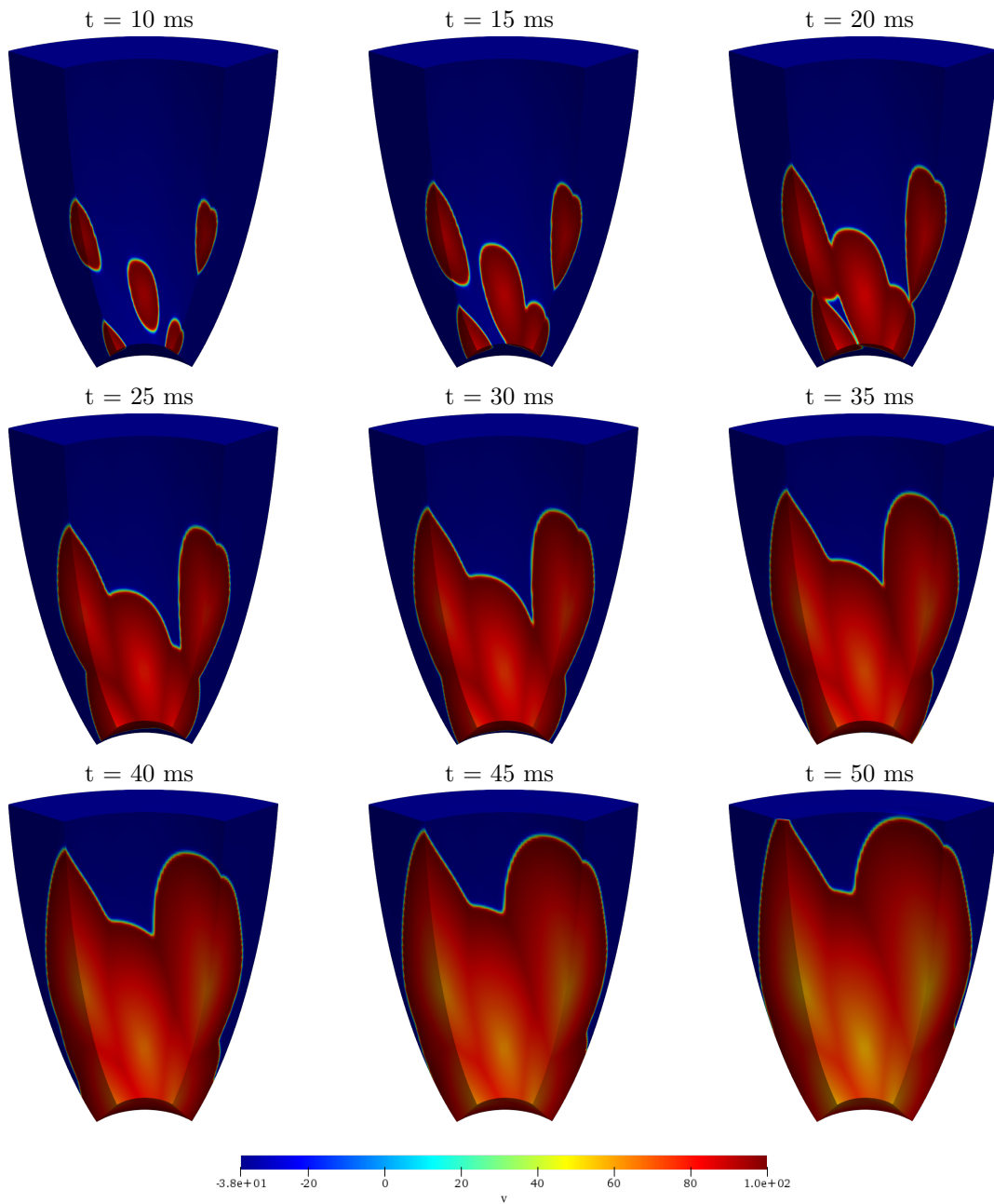
Figure 6.4: Snapshots (every 5 ms) of transmembrane potential v time evolution. For each time frame, we report the epicardial view of a portion of the left ventricle, modeled as a truncated ellipsoid.

Preconditioner.   In order to accelerate the convergence of the linear solver, a preconditioner is needed. We always compare the efficiency of our dual-primal preconditioners to more standard ones. In particular, in our tests we use

- Balancing Domain Decomposition with Constraints (BDDC) preconditioner, from PETSc implementation;

- Finite Element Tearing and Interconnecting Dual-Primal (FETI-DP) preconditioner, from PETSc implementation;

- Block Jacobi (BJ) preconditioner, from PETSc implementation;

t = 10 ms   t = 15 ms   t = 20 ms

t = 25 ms   t = 30 ms   t = 35 ms

t = 40 ms   t = 45 ms   t = 50 ms
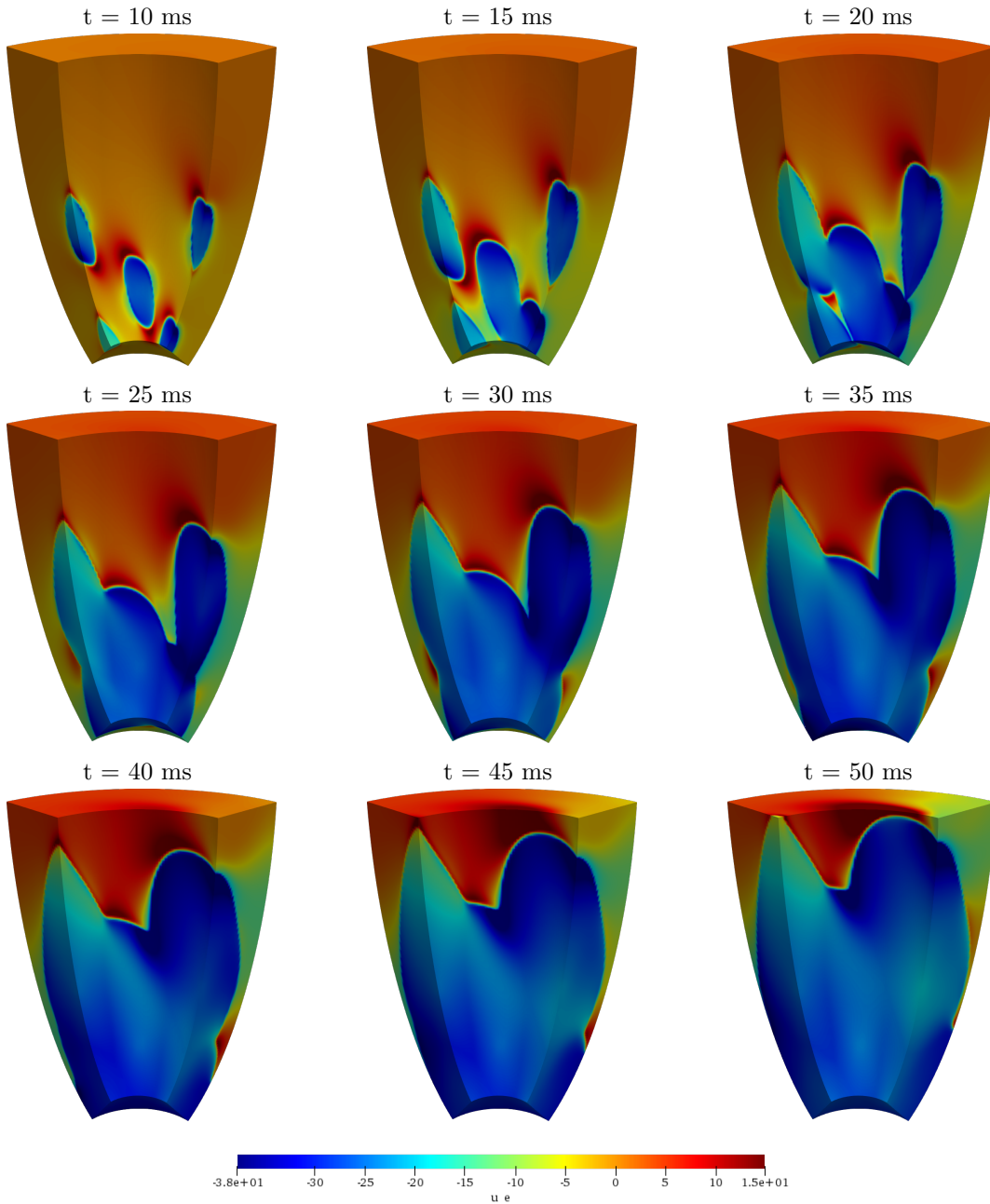
Figure 6.5: Snapshots (every 5 ms) of extra-cellular potential u_e time evolution. For each time frame, we report the epicardial view of a portion of the left ventricle, modeled as a truncated ellipsoid.

- Algebraic MultiGrid (GAMG), from PETSc implementation;

- *Boomer* Algebraic MultiGrid (bAMG), from the Hypre library [41].

In the latter, we use the default Hypre parameters, such as strong threshold 0.25, number of smoothing levels 25 and number of aggressive coarsening 0. Since the focus of this Thesis is on dual-primal Domain Decomposition preconditioners, we have not investigated the behavior of bAMG with different parameters. As concerns BDDC and FETI-DP preconditioners (as not otherwise specified) we employ the default primal space with only vertices and edge averages, and we set a direct solver for BDDC coarse problem with a LU factorization.

Since we are employing BDDC and FETI-DP with default settings from PETSc implementation, sometimes they can differ in terms of performance (both CPU time and average number of linear iterations). A further tuning of the parameters could be done in order to obtain the same behavior, but it is beyond the scope of this Thesis.

6.1   Decoupled Monodomain tests

We start by reporting here a number of parallel numerical tests that validate the decoupled bound Thm 4.1 for the Monodomain problem, solved with a decoupling strategy from the Rogers-McCulloch ionic model (see Chapter 2 and 4 for more details). As the resulting Jacobian linear system is symmetric, we can use the Preconditioned Conjugate Gradient (PCG) method for its resolution.

These preliminary tests does not show the entire potential of the proposed dual-primal solvers, as they seem to be comparable to the standard Block-Jacobi in terms of average number of nonlinear and linear iterations; actually, BDDC preconditioner presents higher timings. However, since the results show a constant behavior for the average number of nonlinear and linear iterations, these experiments can be considered as indicator of a good behavior of the proposed dual-primal solvers on more complex and singular problems, like the Bidomain problem.

All the values reported in the following Tables are an average over the time steps of the related quantity: in particular, the number of nonlinear and linear iterations are rounded to the nearest integer. Moreover, since the Monodomain problem is non-singular, when considering a simple geometry such as the slab domain, the overall system is well conditioned. This explains the reported condition number almost near 1.0: we report a mean value, but the actual range of values oscillates around that value.

Throughout these experiments for the Monodomain decoupled problem, the tolerances for KSP solver are set as follows: relative convergence tolerance 10^{-5}, absolute convergence tolerance 10^{-50} and divergence tolerance 10^4.

Scalability on slab domain

These sets of experiments are performed on the Linux cluster Eos at the University of Pavia. We focus on a thin slab domain during the initial activation phase ($[0, 2]$ ms), which is discretized with fixed time steps of 0.05 ms, for a total of 40 time steps.

Weak scalability on slab domain.   In this test, we fix the local mesh size to $32 \cdot 32 \cdot 32$ elements and we vary the number of subdomains from 8 to 256; thus, we consider increasing geometries, where the dimension of the slab increases from $0.48 \times 0.48 \times 0.48$ cm^3 to $7.68 \times 3.84 \times 0.96$ cm^3. As shown in Table 6.4, all quantities seem to be independent of the number of processors, showing that the preconditioned solver is scalable. Moreover, the average number of linear iterations per nonlinear step of the dual-primal preconditioners is lower than the standard Block-Jacobi. Reported average CPU times per time step display a faster performance of the CG solver preconditioned with Block-Jacobi as compared to BDDC or FETI-DP: this behavior may be due to the implementation of vector and matrix structures within PETSc library, which involves several communications between processors, thus slowing down the overall computational time.

Strong scalability on slab domain.   We fix the global mesh size to $256 \cdot 256 \cdot 2$ elements and we increase the number of processors from 16 to 256, thus reducing the local problem dimensions. The average CPU times and the average number of nonlinear iterations per time step for the Block-Jacobi preconditioner is now comparable to the FETI-DP; thus, focusing on the average

procs	Block-Jacobi				BDDC				FETI-DP			
	time	nlit	lit	cond	time	nlit	lit	cond	time	nlit	lit	cond
8	3.98	3	2	1.0027	297.0	2	2	1.0	6.72	2	1	1.0
16	4.17	3	2	1.0027	297.75	2	2	1.0	5.92	2	1	1.0
32	3.68	3	2	1.0027	302.25	2	2	1.0	7.1	2	1	1.0
64	4.19	3	2	1.0027	302.0	2	2	1.0	7.14	2	1	1.0
128	4.49	3	2	1.0027	310.0	2	2	1.0	7.51	2	1	1.0
256	4.47	3	2	1.0027	311.25	2	2	1.0	7.51	2	1	1.0

Table 6.4: *Weak scalability on slab domain for the Monodomain decoupled solver.* Fixed local mesh size $32 \cdot 32 \cdot 32$ and increasing number of processors from 8 to 256. Rogers-McCulloch ionic model. Comparison between average CPU time per time step in seconds (*time*), (rounded) average number of nonlinear iteration per time step (*nlit*), (rounded) average linear PCG iterations and average condition number per Newton step (*lit* and *cond*). Performed on Eos cluster.

number of linear iterations per Newton step, we can observe a better performance of the dual-primal preconditioners, confirmed by the average condition number estimate per nonlinear step (Table 6.5).

procs	Block-Jacobi				BDDC				FETI-DP			
	time	nlit	lit	cond	time	nlit	lit	cond	time	nlit	lit	cond
16	0.35	2	2	1.0004	1.25	2	2	1.0	0.36	2	1	1.0
32	0.2	2	2	1.0004	2.22	2	2	1.0	0.21	2	1	1.0
64	0.1	2	2	1.0004	1.89	2	2	1.0	0.13	2	1	1.0
128	0.06	2	2	1.0003	5.77	2	2	1.0	0.11	2	2	1.0
256	0.04	2	3	1.133	0.22	2	2	1.0	0.14	2	2	1.0

Table 6.5: *Strong scalability on slab domain for the Monodomain decoupled solver.* Fixed global mesh size $256 \cdot 256 \cdot 2$ and increasing number of processors from 16 to 256. Rogers-McCulloch ionic model. Comparison between average CPU time per time step in seconds (*time*), (rounded) average number of nonlinear iteration per time step (*nlit*), (rounded) average linear PCG iterations and average condition number per Newton step (*lit* and *cond*). Performed on Eos cluster.

Scalability on ellipsoidal domain

These sets of experiments are performed on the Linux cluster Galileo at Cineca centre. We consider a truncated ellipsoidal domain, which models an idealized left ventricular geometry during the initial activation phase ($[0, 2]$ ms), with fixed time step of 0.05 ms, for a total of 40 steps.

Weak scalability on ellipsoidal domain.   As already done for the slab domain, in this weak scaling test we fix the local mesh size to $16 \cdot 16 \cdot 16$ elements and we vary the number of subdomains from 4 to 256, thus resulting in an increasing ellipsoidal geometry.
As shown in Table 6.6, all quantities (average number of nonlinear and linear iterations, average CPU times) remain bounded independently of the number of processors, revealing that the preconditioned solvers are scalable.
In contrast to the analogous test on the slab, here we do not see any relevant improvements of the dual-primal preconditioners with respect to the Block-Jacobi, neither in terms of average number of cumulative linear iterations or average nonlinear steps.
We observe an increase in the average number of nonlinear iterations, probably due to the additional complexity of solving the problem on an ellipsoidal domain. This not so relevant, as this quantity remains bounded.

Reported average CPU times display a faster performance of the solver preconditioned with Block-Jacobi and FETI-DP as compared to BDDC (see also Fig. 6.6, left). In particular, the almost-identical timings of Block-Jacobi and FETI-DP while increasing the number of processors

is a good indicator that the preconditioned dual-primal solver may behaves well on more complex and singular problems, like the Bidomain system.

procs	Block-Jacobi				BDDC				FETI-DP			
	time	nlit	lit	cond	time	nlit	lit	cond	time	nlit	lit	cond
8	0.36	6	2	1.0034	2.53	5	2	1.0052	0.42	6	1	1.0
16	0.32	5	3	1.0315	2.35	5	2	1.1680	0.41	5	2	1.0004
32	0.31	5	3	1.0342	2.61	4	2	1.2161	0.47	5	2	1.0005
64	0.30	4	4	1.1358	2.37	4	2	1.0992	0.44	4	2	1.0061
128	0.28	4	4	1.1440	2.30	4	2	1.0078	0.48	4	2	1.0080
256	0.34	3	4	1.1428	1.96	3	2	1.0076	0.49	3	2	1.0072

Table 6.6: *Weak scalability on ellipsoidal domain for the Monodomain decoupled solver.* Fixed local mesh size $16 \cdot 16 \cdot 16$ and increasing number of processors from 8 to 256. Rogers-McCulloch ionic model. Comparison between average CPU time per time step in seconds (*time*), (rounded) average number of nonlinear iteration per time step (*nlit*), (rounded) average linear PCG iterations and average condition number per Newton step (*lit* and *cond*). Performed on Galileo cluster.

Strong scalability on ellipsoidal domain.   Lastly, we fix the global mesh size to $256 \cdot 128 \cdot 32$ elements and we increase the number of processors from 16 to 512, thus reducing the local problem dimensions.

The average number of nonlinear iterations per time step for Block-Jacobi preconditioner case is comparable to the dual-primals (Table 6.7); thus, focusing on the average number of linear iterations per Newton step, we can easily see a better performance of dual-primal preconditioners, confirmed by the average condition number estimate per nonlinear step (Table 6.7).
FETI-DP preconditioner, when increasing the number of processors, has a good performance on the computational time point of view, almost comparable to Block-Jacobi (Fig. 6.6, right).

No remarkable differences are measured between the ρ-scaling or the deluxe scaling, applied to BDDC preconditioner, which again presents higher timings with respect to the other two preconditioners.

procs	Block-Jacobi				FETI-DP			
	time	nlit	lit	cond	time	nlit	lit	cond
16	3.05	3	4	1.1202	9.18	3	2	1.0073
32	1.57	3	3	1.0714	5.22	3	2	1.0064
64	0.81	3	3	1.1341	1.64	3	2	1.0
128	0.45	3	3	1.1243	0.72	3	2	1.0073
256	0.28	3	4	1.1428	0.33	3	2	1.0072
512	0.18	3	4	1.1432	0.24	3	2	1.0079

procs	BDDC ρ scaling				BDDC deluxe scaling			
	time	nlit	lit	cond	time	nlit	lit	cond
16	436.75	3	2	1.0414	447.0	3	2	1.0400
32	247.87	3	2	1.0185	262.5	3	2	1.0186
64	41.25	3	2	1.1351	35.17	3	2	1.4206
128	9.75	3	2	1.0073	8.72	3	2	1.0072
256	2.13	3	2	1.0076	2.13	3	2	1.0076
512	out of memory				out of memory			

Table 6.7: *Strong scalability on ellipsoidal domain for the Monodomain decoupled solver.* Fixed global mesh size $256 \cdot 128 \cdot 32$ and increasing number of processors from 16 to 512. Rogers-McCulloch ionic model. Comparison between average CPU time per time step in seconds (*time*), (rounded) average number of nonlinear iteration per time step (*nlit*), (rounded) average linear PCG iterations and average condition number per Newton step (*lit* and *cond*). Performed on Galileo cluster.
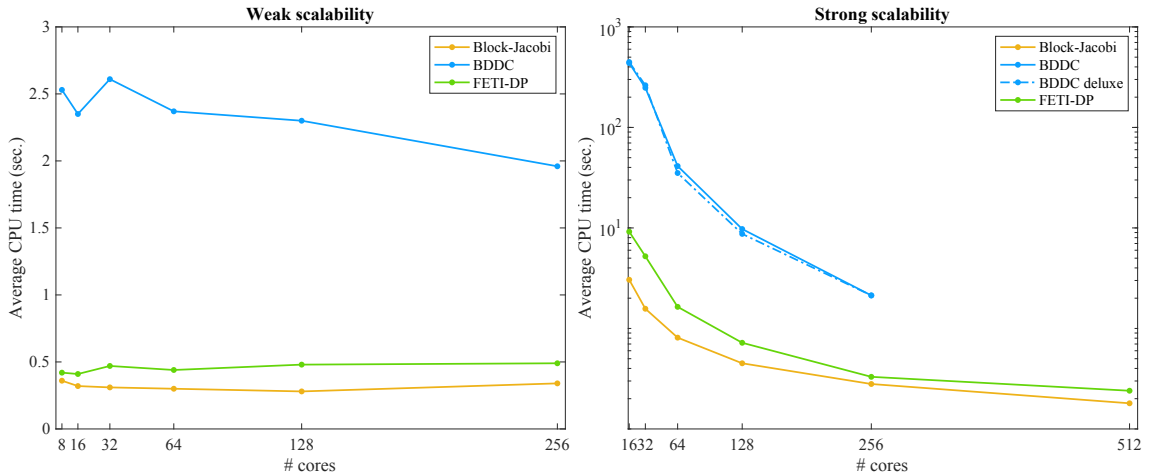
Figure 6.6: *Weak scalability (left) and strong scalability (right) on ellipsoidal domain for the Monodomain decoupled solver.* Fixed local mesh size $16 \cdot 16 \cdot 16$ and increasing number of processors from 8 to 256 for weak scaling; fixed global mesh size $256 \cdot 128 \cdot 32$ and increasing number of processors from 16 to 512 for strong scaling. Rogers-McCulloch ionic model. Average CPU time per time step in seconds. Performed on Galileo cluster.

6.2 Decoupled Bidomain tests

In this section we report extensive parallel numerical experiments related to the decoupled solution strategy presented in Chapter 2 applied to the Bidomain equations. These tests validate the theoretical bound for the condition number of the preconditioned operator (see Chap. 4).

As in the previous section, the resulting Jacobian system using the Rogers-McCulloch ionic model is symmetric and positive semi-definite, thus allowing us to solve it with the CG method, along with BDDC and FETI-DP preconditioners from PETSc library [3]. We compare their performance with the *Boomer* Algebraic Multigrid (bAMG) from the Hypre library [41].
Both weak and strong scaling tests contain also a comparison between different ionic models: the Rogers-McCulloch (which has been used so far as benchmark for our experiments), the Luo-Rudy phase 1 and the ten Tusscher-Panfilov ionic models. Since the resulting Jacobian system when using the last two ionic models is not positive semi-definite, the Generalised Minimal Residual (GMRES) method is applied instead of the CG.

We clarify that, in the Tables where the number of nonlinear iterations is 1, the actual values oscillates between 1 and 2. For simplicity, we report an average value rounded to the nearest integer.

Weak scalability on slab and ellipsoidal domains. The first set of tests we report is a weak scalability test on both slab and ellipsoidal domain, performed on Galileo cluster. For both cases, we fix the local mesh size to $16 \cdot 16 \cdot 16$ finite elements and we increase the number of processors (thus subdomains) from 32 to 2048, thus resulting in an increasing slab geometry and in an increasing portion of ellipsoid. Tables 6.8 and 6.9 show how BDDC and FETI-DP have a better performance than bAMG: the average number of linear iteration per Newton iteration (lit) is clearly lower and does not increase with the number of subdomains, except for BDDC on the slab domain, where the linear iterations increase unexpectedly. Moreover, the reported average CPU times (in seconds) per nonlinear step (see also Fig. 6.7) are slightly better for the BDDC and FETI-DP preconditioners, except for FETI-DP on the slab domain and 2048 processors. In the harder ellipsoidal tests, both BDDC and FET-DP are scalable and outperform bAMG when the number of processors increases past 128, indicating lower computational complexity and interprocessor communications.
Additionally, we perform the weak scalability test comparing the performances of the Newton-Krylov solvers in case realistic human ionic ventricle models are included. Tables 6.10 and 6.11

procs	mesh	dofs	bAMG			BDDC			FETI-DP		
			nit	lit	time	nit	lit	time	nit	lit	time
32	$64 \cdot 64 \cdot 32$	278,850	1	106	4.9	1	22	6.1	1	10	6.0
64	$128 \cdot 64 \cdot 32$	553,410	1	132	6.8	1	27	6.2	1	11	6.0
128	$128 \cdot 128 \cdot 32$	1,098,306	1	180	9.4	1	32	7.6	1	10	7.4
256	$256 \cdot 128 \cdot 32$	2,188,098	1	237	15.2	1	39	7.2	1	10	7.9
512	$256 \cdot 256 \cdot 32$	4,359,234	1	318	20.0	1	48	10.1	1	10	11.1
1024	$512 \cdot 256 \cdot 32$	8,701,506	1	405	29.6	1	63	13.8	1	10	18.7
2048	$512 \cdot 512 \cdot 32$	17,369,154	1	536	40.3	1	78	33.5	1	10	63.2

Table 6.8: *Weak scalability on slab domain for the Bidomain decoupled solver.* Local mesh of $16 \cdot 16 \cdot 16$ elements. Simulations of 2 ms of cardiac activation with $dt = 0.05$ ms, for a total amount fo 40 time steps. Comparison of Newton-Krylov solvers with boomerAMG (bAMG), BDDC and FETI-DP preconditioners. Rogers-McCulloch ionic model. Average Newton iterations per time step (nit); average conjugate gradient iterations per Newton iteration (lit); average CPU solution time per time step (time) in seconds. Performed on Galileo cluster.

procs	mesh	dofs	bAMG			BDDC			FETI-DP		
			nit	lit	time	nit	lit	time	nit	lit	time
32	$64 \cdot 32 \cdot 64$	278,850	1	86	3.3	1	30	5.4	1	20	4.7
64	$64 \cdot 64 \cdot 64$	549,250	1	124	6.0	1	37	6.2	1	20	6.5
128	$64 \cdot 128 \cdot 64$	1,090,050	1	207	11.3	1	26	7.5	1	19	6.6
256	$64 \cdot 256 \cdot 64$	2,171,650	1	348	22.2	1	25	8.7	1	17	10.7
512	$128 \cdot 256 \cdot 64$	4,309,890	1	335	21.3	1	27	10.5	1	18	11.4
1024	$256 \cdot 256 \cdot 64$	8,586,370	out of memory			1	28	12.5	1	19	11.0
2048	$512 \cdot 256 \cdot 64$	17,139,330	out of memory			1	28	26.6	1	19	21.4

Table 6.9: *Weak scalability on ellipsoidal domain for the Bidomain decoupled solver.* Local mesh of $16 \cdot 16 \cdot 16$ elements. Simulations of 2 ms of cardiac activation with $dt = 0.05$ ms, for a total amount fo 40 time steps. Comparison of Newton-Krylov solvers with boomerAMG (bAMG), BDDC and FETI-DP preconditioners. Rogers-McCulloch ionic model. Average Newton iterations per time step (nit); average conjugate gradient iterations per Newton iteration (lit); average CPU solution time per time step (time) in seconds. Performed on Galileo cluster.
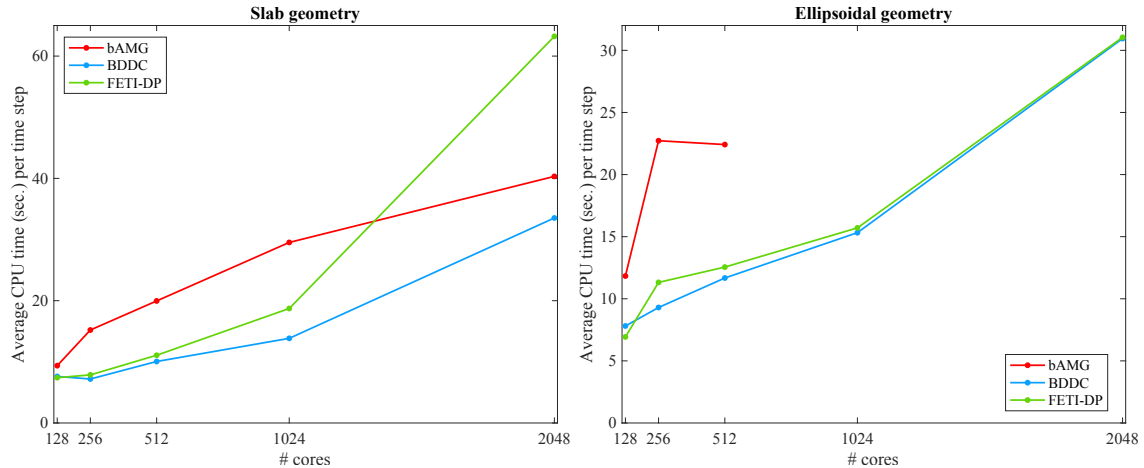
Figure 6.7: *Weak scalability on slab (left) and ellipsoidal (right) domains for the Bidomain decoupled solver.* Local mesh of $16 \cdot 16 \cdot 16$ elements. Simulations of 2 ms of cardiac activation with $dt = 0.05$ ms, for a total amount fo 40 time steps. Rogers-McCulloch ionic model. Comparison of average CPU time per time step in seconds. Performed on Galileo cluster.

report a comparison between the algebraic multigrid and the dual-primal preconditioners, while employing the Luo-Rudy phase 1 and Ten Tusscher-Panfilov ionic models (LR1 and TP06, respectively). The local mesh size is fixed to $12 \cdot 12 \cdot 12$ and the number of processors is increased from

4 to 256, thus resulting in an increasing number of dofs from 16,250 to 926,786. GMRES iterative solver is employed, due to the loss of positive semidefinite property.

We observe an overall raise in the average number of nonlinear iterations, with lower values for the TP06 case for both geometries; as above, this parameter seems to be affected by the increasing complexity of the ellipsoidal domain, as it presents slightly higher values.

The performance of BDDC and FETI-DP in terms of average CPU time show robustness of the preconditioned solver, since this quantity remains bounded while increasing the number of subdomains; this trend cannot be found for bAMG, which presents higher and increasing values, as shown in Fig. 6.8.

For what concerns the average number of linear iterations, on the slab geometry we observe the same trend as for the average CPU timings: for both ionic models, BDDC and FETI-DP's values are lower and remain almost constant, while for bAMG these values increase with the number of processors. On the ellipsoidal geometry, we have some fluctuations for BDDC and FETI-DP, although the average number of linear iterations remains bounded; the multigrid case presents higher values with respect to its corresponding cases on the slab.

Luo-Rudy phase 1

procs	mesh	dofs	bAMG			BDDC			FETI-DP		
			nit	lit	time	nit	lit	time	nit	lit	time
4	$24 \cdot 24 \cdot 12$	16,250	3.0	48.7	1.5	3.0	10.0	3.8	3.0	7.0	3.6
8	$24 \cdot 24 \cdot 24$	31,250	2.9	62.1	2.3	2.9	13.0	3.7	2.9	8.5	3.5
16	$48 \cdot 24 \cdot 24$	61,250	2.9	72.2	3.3	2.9	14.0	13.0	2.9	9.2	3.6
32	$48 \cdot 24 \cdot 48$	120,050	2.8	99.3	4.6	2.8	13.0	3.1	2.8	8.6	2.8
64	$48 \cdot 48 \cdot 48$	235,298	2.8	118.1	5.7	2.8	13.0	4.1	2.8	8.4	3.7
128	$48 \cdot 96 \cdot 48$	465,794	2.8	259.3	17.3	2.8	13.0	4.3	2.8	8.4	3.9
256	$48 \cdot 192 \cdot 48$	926,786	2.8	622.0	41.5	2.8	13.0	4.6	2.8	8.4	4.3

Ten Tusscher-Panfilov

procs	mesh	dofs	bAMG			BDDC			FETI-DP		
			nit	lit	time	nit	lit	time	nit	lit	time
4	$24 \cdot 24 \cdot 12$	16,250	1.8	49.1	0.9	1.85	10.0	1.8	1.8	7.4	1.7
8	$24 \cdot 24 \cdot 24$	31,250	1.8	62.8	1.5	1.87	12.9	2.4	1.8	8.6	2.3
16	$48 \cdot 24 \cdot 24$	61,250	1.8	73.2	2.2	1.87	14.0	2.5	1.8	9.3	2.3
32	$48 \cdot 24 \cdot 48$	120,050	1.8	98.9	2.9	1.82	13.2	1.9	1.8	8.7	1.7
64	$48 \cdot 48 \cdot 48$	235,298	1.8	119.5	3.7	1.82	13.0	2.6	1.8	8.7	2.4
128	$48 \cdot 96 \cdot 48$	465,794	1.8	261.2	11.2	1.82	13.0	2.7	1.8	8.6	2.5
256	$48 \cdot 192 \cdot 48$	926,786	1.8	629.1	26.6	1.82	13.0	2.9	1.8	8.7	2.7

Table 6.10: *Weak scalability on slab domain for the Bidomain decoupled solver.* Local mesh of $12 \cdot 12 \cdot 12$ elements. Simulations of 2 ms of cardiac activation with $dt = 0.05$ ms, for a total amount fo 40 time steps. Comparison of Newton-Krylov solvers with boomerAMG (bAMG), BDDC and FETI-DP preconditioners. Luo-Rudy phase 1 (LR1) and Ten Tusscher-Panfilov 2006 (TT06) ionic models. Average Newton iterations per time step (nit); average conjugate gradient iterations per Newton iteration (lit); average CPU solution time per time step (time) in seconds. Performed on Indaco cluster.

Strong scalability on slab and ellipsoidal domains. We now perform a strong scaling test for the two geometries on the cluster Indaco.

For the thin slab geometry, we fix the global mesh to $192 \cdot 192 \cdot 32$ elements (for a total of 2,458,434 dofs) and we increase the number of subdomains from 32 to 256. We fix the global mesh to $128 \cdot 128 \cdot 64$ elements for the portion of ellipsoid instead (thus resulting in 2,163,3360 dofs).

When the local number of dofs decreases, the preconditioner with the better balance in term of average linear iterations and CPU time per time step is FETI-DP, as reported in Tables 6.12 and 6.13.

Luo-Rudy phase 1

procs	mesh	dofs	bAMG			BDDC			FETI-DP		
			nit	lit	time	nit	lit	time	nit	lit	time
4	$24 \cdot 24 \cdot 12$	16,250	3.4	520.2	4.1	3.4	9.8	3.5	3.4	6.9	3.2
8	$24 \cdot 24 \cdot 24$	31,250	3.3	791.3	8.9	3.3	15.4	4.9	3.3	10.7	3.3
16	$48 \cdot 24 \cdot 24$	61,250	3.9	720.4	16.2	3.9	21.3	6.1	3.9	14.6	5.4
32	$48 \cdot 24 \cdot 48$	120,050	4.3	720.0	22.9	4.3	34.0	6.5	4.3	23.2	5.2
64	$48 \cdot 48 \cdot 48$	235,298	3.8	560.1	20.1	3.8	21.5	6.4	3.8	14.9	5.7
128	$48 \cdot 96 \cdot 48$	465,794	4.1	604.7	34.3	4.1	15.3	6.6	4.1	10.2	5.9
256	$48 \cdot 192 \cdot 48$	926,786	4.4	526.4	51.7	4.4	14.4	7.6	4.4	9.4	6.9

Ten Tusscher-Panfilov

procs	mesh	dofs	bAMG			BDDC			FETI-DP		
			nit	lit	time	nit	lit	time	nit	lit	time
4	$24 \cdot 24 \cdot 12$	16,250	3.3	516.5	3.8	3.3	9.8	3.4	3.3	6.9	3.1
8	$24 \cdot 24 \cdot 24$	31,250	3.0	867.2	8.4	3.0	15.7	4.7	3.0	11.1	3.0
16	$48 \cdot 24 \cdot 24$	61,250	2.8	731.1	12.5	2.8	21.8	4.5	2.8	15.9	4.1
32	$48 \cdot 24 \cdot 48$	120,050	3.1	736.5	16.9	3.1	34.4	4.6	4.3	23.2	3.7
64	$48 \cdot 48 \cdot 48$	235,298	2.9	542.1	14.7	2.9	21.7	4.8	2.9	15.1	4.3
128	$48 \cdot 96 \cdot 48$	465,794	3.0	597.0	25.2	3.0	15.4	4.9	3.0	10.1	4.5
256	$48 \cdot 192 \cdot 48$	926,786	2.9	498.0	32.8	2.9	14.6	5.1	2.9	9.5	4.7

Table 6.11: *Weak scalability on ellipsoidal domain for the Bidomain decoupled solver.* Local mesh of $12 \cdot 12 \cdot 12$ elements. Simulations of 2 ms of cardiac activation with $dt = 0.05$ ms, for a total amount fo 40 time steps. Comparison of Newton-Krylov solvers with boomerAMG (bAMG), BDDC and FETI-DP preconditioners. Luo-Rudy phase 1 (LR1) and Ten Tusscher-Panfilov 2006 (TT06) ionic models. Average Newton iterations per time step (nit); average conjugate gradient iterations per Newton iteration (lit); average CPU solution time per time step (time) in seconds. Performed on Indaco cluster.
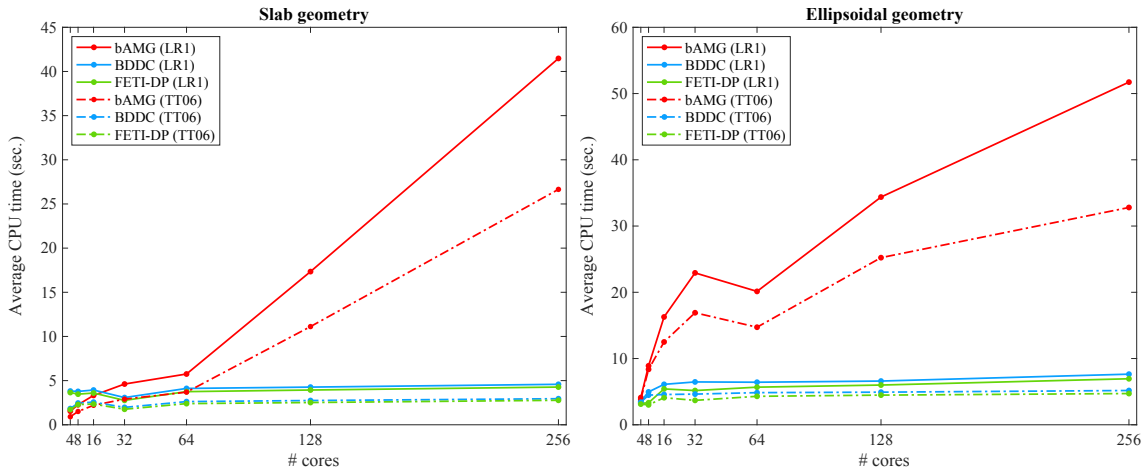
Figure 6.8: *Weak scalability on slab (left) and ellipsoidal (right) domains for the Bidomain decoupled solver.* Local mesh of $12 \cdot 12 \cdot 12$ elements. Simulations of 2 ms of cardiac activation with $dt = 0.05$ ms, for a total amount fo 40 time steps. Comparison of average CPU time per time step in seconds between Luo-Rudy phase 1 (LR1) and Ten Tusscher-Panfilov 2006 (TT06) ionic models. Performed on Indaco cluster.

However, in both cases, BDDC and FETI-DP preconditioners outperform the ideal speedup, while bAMG is sub-optimal (see Fig. 6.9). Indeed, since we are working with a low number of processors, the local problem sizes are high, thus requiring lot of time for the LU factorization of the matrices.

Moreover we compare the performance of the Newton-Krylov solver with BDDC preconditioner

using different ionic models: the Rogers-McCulloch (RMC), the Luo-Rudy phase 1 (LR1) and the Ten Tusscher-Panfilov 2006 (TP06) ionic models in Tables 6.14 and 6.15. In this case the Jacobian linear system is solved with the GMRES method, as it loses the positive semidefinite property.

By increasing the complexity of the ionic current, we observe an increasing in the average number of nonlinear iterations from 1-2 per time step using the RMC model to 2-3 per time step with LR1 and TP06 models. On the other hand, the average numbers of linear iterations per time step for the three ionic models are comparable, indicating that our dual-primal solver retains its good convergence properties even for more complex ionic models. As a consequence, the CPU times for LR1 and TP06 model increase due to the increase of nonlinear iterations, but the associated parallel speedups of the models are comparable.

procs	bAMG					BDDC					FETI-DP				
	nit	lit	time	S_{32}	S_{64}	nit	lit	time	S_{32}	S_{64}	nit	lit	time	S_{32}	S_{64}
32	1.25	250	116.0	-	-	1.0	27	348.2	-	-	1.25	11	352.2	-	-
64	1.25	252	62.7	1.8	-	1.22	32	59.5	5.8	-	1.25	17	53.0	6.6	-
128	1.25	252	33.6	3.5	1.8	1.22	37	21.9	15.8	2.7	1.25	21	19.9	17.6	2.6
256	1.25	252	18.6	6.2	3.4	1.22	22	10.4	33.5	5.7	1.25	13	8.9	39.7	5.9

Table 6.12: *Strong scalability on slab domain for the Bidomain decoupled solver.* Global mesh of $192 \cdot 192 \cdot 32$ elements, 2,458,434 dofs. Simulations of 2 ms of cardiac activation with $dt = 0.05$ ms, for a total amount fo 40 time steps. Rogers-McCulloch ionic model. Comparison of Newton-Krylov solvers with boomerAMG (bAMG), BDDC and FETI-DP preconditioners. Average Newton iterations per time step (nit); average conjugate gradient iterations per Newton iteration (lit); average CPU solution time per time step (time) in seconds; parallel speedup with respect to 32 (S_{32}) and 64 (S_{64}) processors. Performed on Indaco cluster.

procs	bAMG					BDDC					FETI-DP				
	nit	lit	time	S_{32}	S_{64}	nit	lit	time	S_{32}	S_{64}	nit	lit	time	S_{32}	S_{64}
32	1.92	311	188.4	-	-	1.92	36	571.8	-	-	1.92	14	558.2	-	-
64	1.92	310	113.4	1.7	-	1.92	30	129.1	4.4	-	1.92	19	129.7	4.3	-
128	1.92	310	60.5	3.1	1.9	1.92	40	40.2	14.2	3.2	1.92	24	42.4	13.2	3.1
256	1.92	311	32.2	5.8	3.1	1.92	23	15.1	37.9	8.5	1.92	14	19.0	29.4	6.8

Table 6.13: *Strong scalability on ellipsoidal domain for the Bidomain decoupled solver.* Global mesh of $128 \cdot 128 \cdot 64$ elements, 2,163,330 dofs. Simulations of 2 ms of cardiac activation with $dt = 0.05$ ms, for a total amount fo 40 time steps. Rogers-McCulloch ionic model. Comparison of Newton-Krylov solvers with boomerAMG (bAMG), BDDC and FETI-DP preconditioners. Average Newton iterations per time step (nit); average conjugate gradient iterations per Newton iteration (lit); average CPU solution time per time step (time) in seconds; parallel speedup with respect to 32 (S_{32}) and 64 (S_{64}) processors. Performed on Indaco cluster

procs	RMC				LR1				TP06			
	nit	lit	time	$S_{32(64)}$	nit	lit	time	$S_{32(64)}$	nit	lit	time	$S_{32(64)}$
32	1.25	16.9	220.2	- (-)	2.85	16.9	502.2	- (-)	1.85	17.0	326.2	- (-)
64	1.25	19.9	62.1	3.5 (-)	2.85	19.6	140.9	3.5 (-)	1.85	19.7	91.9	3.5 (-)
128	1.25	15.3	19.2	11.5 (3.2)	2.85	15.0	43.9	11.4 (3.2)	1.85	15.0	28.4	11.4 (3.2)
256	1.25	17.4	5.8	37.9 (10.7)	2.85	29.5	17.0	38.1 (10.6)	1.85	17.1	8.6	37.6 (10.6)

Table 6.14: *Strong scalability on slab domain for the Bidomain decoupled solver, comparison between ionic models.* Global mesh $192 \cdot 192 \cdot 32$ elements, 2,458,434 dofs. Simulations of 2 ms of cardiac activation with $dt = 0.05$ ms (40 time steps). Comparison of Newton-Krylov solvers with BDDC preconditioner using Rogers-McCulloch (RMC), Luo-Rudy phase 1 (LR1) and ten Tusscher-Panfilov 2006 (TP06) ionic models. Average Newton iterations per time step (nit); average conjugate gradient iterations per Newton iteration (lit); average CPU solution time per time step (time) in seconds; parallel speedup (S_p) computed with respect to $p = 32$ and $p = 64$ processors.

Optimality tests on slab and ellipsoidal domains. Tables 6.16 and 6.17 report the results of optimality tests employing RMC ionic model, for both slab and ellipsoid geometries, carried on Eos cluster. We fix the number of processors (subdomains) to $4 \cdot 4 \cdot 4$ and we increase the local size H/h from 8 to 24, thus reducing the finite element size h.

We focus only on the behavior of the BDDC preconditioner, as the FETI-DP has been proven to be spectrally equivalent. We consider both scalings (ρ-scaling on top, deluxe scaling at bottom of

procs	RMC				LR1				TP06			
	nit	lit	time	$S_{32(64)}$	nit	lit	time	$S_{32(64)}$	nit	lit	time	$S_{32(64)}$
32	2	21.1	436.5	- (-)	3.95	20.5	862.2	- (-)	2.5	21.1	488.0	- (-)
64	2	26.9	99.3	4.4 (-)	3.95	25.9	194.9	4.4 (-)	2.5	26.5	122.7	3.9 (-)
128	2	21.4	27.3	16.0 (3.6)	3.95	20.8	53.5	16.1 (3.6)	2.5	21.3	33.8	14.4 (3.6)
256	2	30.0	8.2	53.4 (12.1)	3.95	29.5	16.1	53.6 (12.1)	2.5	29.9	10.1	48.3 (12.1)

Table 6.15: *Strong scalability on ellipsoidal domain for the Bidomain decoupled solver, comparison between ionic models.* Global mesh $128 \cdot 128 \cdot 64$ elements, 2,163,330 dofs. Simulations of 2 ms of cardiac activation with $dt = 0.05$ ms (40 time steps). Comparison of Newton-Krylov solvers with BDDC preconditioner using Rogers-McCulloch (RMC), Luo-Rudy phase 1 (LR1) and ten Tusscher-Panfilov 2006 (TP06) ionic models. Average Newton iterations per time step (nit); average conjugate gradient iterations per Newton iteration (lit); average CPU solution time per time step (time) in seconds; parallel speedup (S_p) computed with respect to $p = 32$ and $p = 64$ processors.
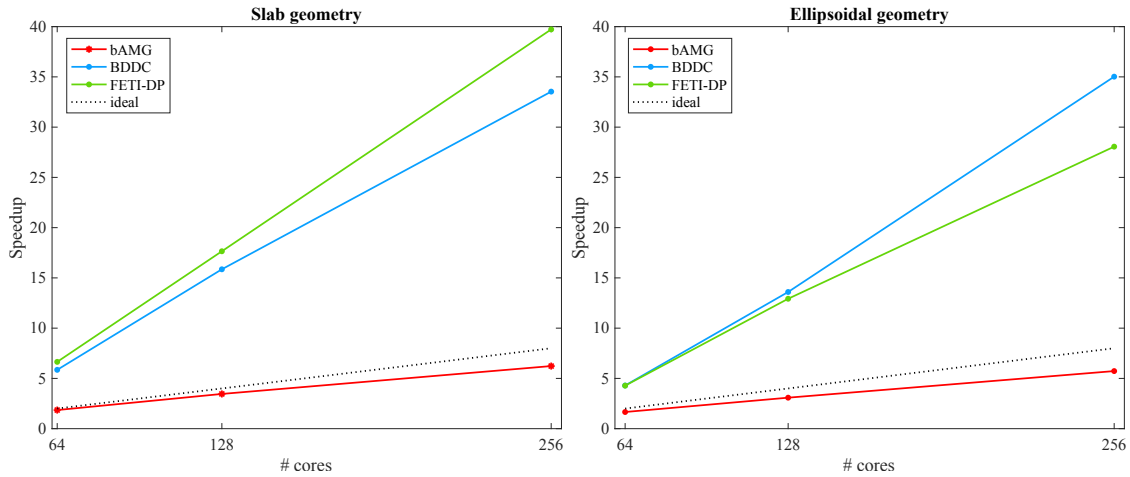
Figure 6.9: *Strong scalability for the Bidomain decoupled solver.* Left: strong scaling test on slab domain, with global mesh of $192 \cdot 192 \cdot 32$. Right: strong scaling test on ellipsoidal domain, with global mesh of $128 \cdot 128 \cdot 64$. Simulations of 2 ms of cardiac activation with $dt = 0.05$ ms, for a total amount fo 40 time steps. Rogers-McCulloch ionic model. Comparison of actual parallel speedup (ideal speedup dotted). Performed on Indaco cluster.

each table) and we test the solver for increasing primal spaces: V includes only vertex constraints, while V+E and V+E+F include vertex and edge constraints or vertex, edge and face constraints.

The simulations time is 2 ms of cardiac activation with time step $dt = 0.05$ ms, for a total amount fo 40 time steps.

Similar results hold for both geometries. Despite an higher average CPU time using the deluxe scaling, all the other parameters are quite similar between the two scalings.

We observe almost linear dependence of the condition number if the coarsest primal space (only V) is chosen (see also Figures 6.10, 6.11 bottom), while we can obtain quasi-optimality if we enrich the primal space by adding edge (V+E) and face (V+E+F) constraints.

We report in Tables 6.18 and 6.19 the optimality results in case LR1 and TP06 ionic models are employed. As for the RMC tests, these results are independent of the scaling chosen.

The average number of nonlinear iterations increases to 2-4 in case of the LR1 ionic model and to 2-3 for the TP06, with higher values for the ellipsoid, as already observed in the scalability tests. This parameter seems to be dependent only on the local size of the problems, but independent of the coarse space. As confirmed by Fig. 6.12, the average number of linear iterations per time step deteriorates while increasing the local problem size, if the coarse space is made up only of vertices. Instead, by enriching the primal space by adding edge (V+E) and face (V+E+F) constraints, this quantity remains bounded and with lower values.

The average CPU times are almost identical if we consider the richest primal spaces (V+E and V+E+F).

ρ-scaling

H/h	V				V+E				V+E+F			
	nlit	lit	time	cond	nlit	lit	time	cond	nlit	lit	time	cond
4	1	26	1.7	8.4	1	11	0.9	1.9	1	9	0.9	1.7
8	1	47	3.4	24.1	1	14	1.4	2.6	1	12	1.4	2.5
12	1	66	10.3	42.9	1	18	6.4	3.2	1	15	4.5	3.2
16	out of memory				1	20	11.9	3.7	1	20	11.6	3.7
20	out of memory				1	22	34.2	4.2	1	20	32.5	4.2
24	out of memory				1	23	83.1	4.6	1	21	80.5	4.5

deluxe scaling

H/h	V				V+E				V+E+F			
	nlit	lit	time	cond	nlit	lit	time	cond	nlit	lit	time	cond
4	1	26	1.9	8.4	1	11	0.9	1.9	1	9	1.0	1.7
8	1	47	4.1	24.0	1	14	1.7	2.6	1	12	1.8	2.5
12	1	65	14.7	42.7	1	18	5.5	3.2	1	15	7.8	3.2
16	1	80	30.0	63.7	1	20	19.1	3.7	1	20	21.4	3.7
20	1	90	93.8	86.3	1	22	73.9	4.2	1	20	70.0	4.2
24	1	99	211.9	110.1	1	24	205.8	4.5	1	21	247.3	4.5

Table 6.16: *Optimality tests on slab domain for the Bidomain decoupled solver.* Fixed number of subdomains $4 \cdot 4 \cdot 4$. Increasing local size from $4 \cdot 4 \cdot 4$ to $24 \cdot 24 \cdot 24$. Rogers-McCulloch ionic model. CG solver preconditioned by BDDC. Comparison between different scaling and different primal sets (V = vertices, E = edges, F = faces). Average non-linear iterations (nlit), average number of linear iteration, average CPU time in seconds and average condition number per time step. Performed on Eos cluster.
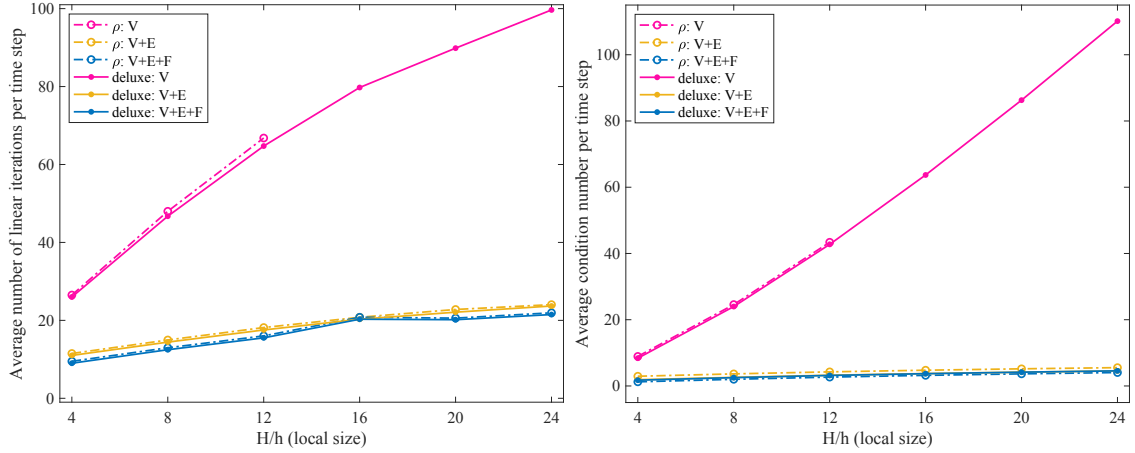
Figure 6.10: *Optimality test on slab domain for the Bidomain decoupled solver.* Fixed number of subdomains $4 \cdot 4 \cdot 4$. Increasing local size from $4 \cdot 4 \cdot 4$ to $24 \cdot 24 \cdot 24$. Rogers-McCulloch ionic model. CG solver preconditioned by BDDC. Comparison between different scaling (dash-dotted ρ-scaling, continuous *deluxe* scaling) and different primal sets (V = vertices, E = edges, F = faces). Comparison average number of linear iteration (right) and average condition number (left) per time step. Performed on Eos cluster.

Strong scaling on a full activation-recovery interval. In this last set of tests (performed on Indaco cluster), we compare the performance of our dual-primal and the multigrid preconditioner during a complete activation-recovery interval over the computational domains.

We fix the number of subdomains to $128 = 8 \cdot 8 \cdot 2$ and the global mesh size to $192 \cdot 96 \cdot 24$, thus resulting in local problems with 8,450 dofs.

We consider a time interval of $[0, 170]$ ms for a total of 3400 time steps for a portion of ellipsoid defined by $\varphi_{\min} = -\pi/2$, $\varphi_{\max} = 0$, $\theta_{\min} = -3/8\pi$ and $\theta_{\max} = \pi/8$, while on the slab of dimensions $1.92 \times 1.92 \times 0.48$ cm^3 we performed the tests for 2400 time steps, on $[0, 120]$ ms.

ρ-scaling

H/h	V				V+E				V+E+F			
	nlit	lit	time	cond	nlit	lit	time	cond	nlit	lit	time	cond
8	2	50	5.5	30.1	2	17	2.4	4.3	2	16	2.4	4.0
12	2	66	11.8	54.6	2	19	5.6	5.4	2	18	5.6	4.9
16	2	80	33.9	80.6	2	21	16.9	6.3	2	21	16.9	5.7
20	2	91	90.3	108.2	2	22	44.7	6.9	2	21	44.9	6.3
24	2	100	206.3	137.2	2	24	109.3	7.5	2	23	84.0	6.8

deluxe scaling

H/h	V				V+E				V+E+F			
	nlit	lit	time	cond	nlit	lit	time	cond	nlit	lit	time	cond
8	2	49	6.7	31.0	2	17	3.1	4.3	2	16	3.0	4.0
12	2	54	27.2	54.6	2	19	9.6	5.4	2	18	9.6	4.9
16	2	79	54.1	80.6	2	21	32.1	6.2	2	21	32.7	5.7
20	2	90	142.4	108.2	2	22	125.8	7.0	2	21	111.1	6.3
24	2	99	329.3	137.1	2	24	236.7	7.5	2	22	247.1	6.8

Table 6.17: *Optimality tests on ellipsoidal domain for the Bidomain decoupled solver.* Fixed number of subdomains $4 \cdot 4 \cdot 4$. Increasing local size from $8 \cdot 8 \cdot 8$ to $24 \cdot 24 \cdot 24$. Rogers-McCulloch ionic model. CG solver preconditioned by BDDC. Comparison between different scaling and different primal sets (V = vertices, E = edges, F = faces). Average non-linear iterations (nlit), average number of linear iteration, average CPU time in seconds and average condition number per time step. Performed on Eos cluster.
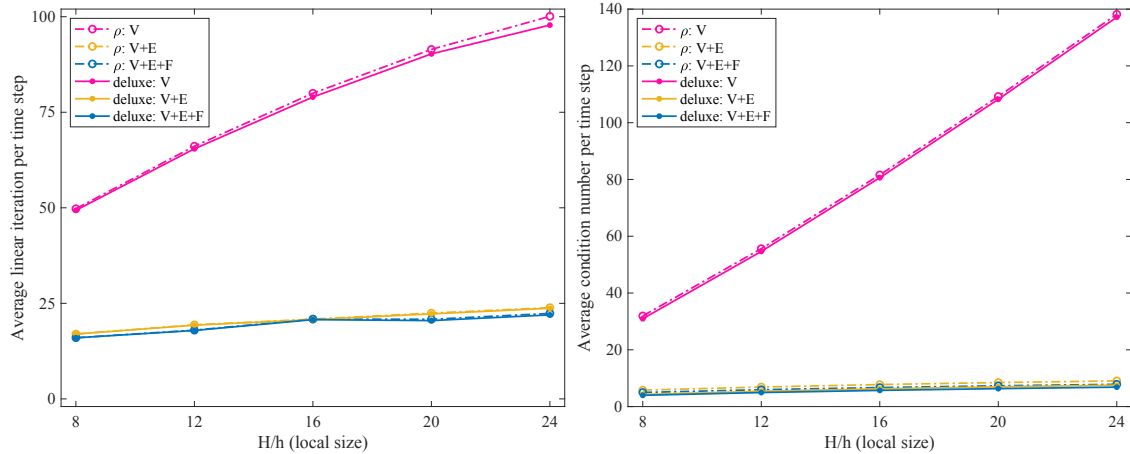
Figure 6.11: *Optimality tests on ellipsoidal domain for the Bidomain decoupled solver.* Fixed number of subdomains $4 \cdot 4 \cdot 4$. Increasing local size from $8 \cdot 8 \cdot 8$ to $24 \cdot 24 \cdot 24$. Rogers-McCulloch ionic model. CG solver preconditioned by BDDC. Comparison between different scaling (dash-dotted ρ-scaling, continuous *deluxe* scaling) and different primal sets (V = vertices, E = edges, F = faces). Comparison average number of linear iteration (right) and average condition number (left) per time step. Performed on Eos cluster.

In Figures 6.13 and 6.14 we report the trend of the average number of linear iteration per time step during the simulation. The average number of linear iterations remains bounded and almost constant during the test. Moreover, we notice a huge difference between the multigrid preconditioner and the dual-primal preconditioners, with a reduction of more than 90% for the latter.

If we focus on the trend of the dual-primal preconditioners average number of linear iterations (Figures 6.13 and 6.14, on the right), we can notice that for both domains FETI-DP is affected by the different phases of the action potential: there is an initial peak matching to the activation phase, followed by an increase in the number of linear iterations as the potential propagates in the tissue and by a slow decrease as wider portions of tissue return to resting. Similar behavior can be

LR1 ionic model, ρ-scaling

H/h	V			V+E			V+E+F		
	nlit	lit	time	nlit	lit	time	nlit	lit	time
4	2.92	70.4	0.3	2.92	29.3	0.2	2.92	26.1	0.3
8	2.85	113.8	1.1	2.85	34.9	0.6	2.85	31.1	0.8
12	2.87	147.1	4.9	2.87	37.7	3.3	2.87	34.4	3.5
16	2.90	167.7	21.5	2.90	40.6	16.1	2.90	36.8	16.6
20	2.90	195.9	67.9	2.90	42.6	51.6	2.90	38.1	52.1
24	2.92	222.9	194.6	2.92	43.9	149.5	2.92	40.8	152.0

LR1 ionic model, deluxe scaling

H/h	V			V+E			V+E+F		
	nlit	lit	time	nlit	lit	time	nlit	lit	time
4	2.92	70.2	0.5	2.92	29.2	0.2	2.92	26.0	0.3
8	2.85	112.9	2.3	2.85	34.8	1.8	2.85	30.8	1.7
12	2.87	145.5	17.3	2.87	37.5	14.3	2.87	34.5	14.6
16	2.90	167.6	88.4	2.90	40.6	79.6	2.90	37.2	79.8
20	2.90	196.8	335.7	2.90	42.2	304.5	2.90	38.3	307.0
24	2.92	221.2	1014.3	2.92	43.8	950.0	2.92	40.9	951.5

TP06 ionic model, ρ-scaling

H/h	V			V+E			V+E+F		
	nlit	lit	time	nlit	lit	time	nlit	lit	time
4	1.90	45.4	0.2	1.90	19.0	0.1	1.90	16.7	0.2
8	1.85	72.2	0.8	1.85	22.2	0.4	1.85	19.6	0.4
12	1.82	93.3	3.2	1.82	23.7	2.2	1.82	21.6	2.3
16	1.80	104.5	13.6	1.80	25.2	10.4	1.80	22.6	10.5
20	1.80	121.7	43.2	1.80	26.5	32.2	1.80	23.7	32.5
24	1.82	139.4	121.2	1.82	27.4	93.6	1.82	25.5	93.9

TP06 ionic model, deluxe scaling

H/h	V			V+E			V+E+F		
	nlit	lit	time	nlit	lit	time	nlit	lit	time
4	1.90	45.4	0.2	1.90	19.0	0.2	1.90	16.6	0.2
8	1.85	71.7	1.6	1.85	22.2	1.1	1.85	19.4	1.1
12	1.82	92.3	10.9	1.82	23.7	9.1	1.82	21.7	9.2
16	1.80	104.0	54.9	1.80	25.2	49.3	1.80	22.8	49.6
20	1.80	122.5	207.5	1.80	26.3	189.6	1.80	23.8	190.2
24	1.82	137.8	632.0	1.82	27.4	592.2	1.82	25.5	593.5

Table 6.18: *Optimality tests on slab domain for the Bidomain decoupled solver, LR1 and TP06 ionic models.* Fixed number of subdomains $4 \cdot 4 \cdot 4$. Increasing local size from $4 \cdot 4 \cdot 4$ to $24 \cdot 24 \cdot 24$. GMRES solver preconditioned by BDDC. Luo-Rudy phase 1 (LR1) and Ten Tusscher-Panfilov (TP06) ionic models. Comparison between different scaling and different primal sets (V = vertices, E = edges, F = faces). Average non-linear iterations (nlit), average number of linear iteration, average CPU time in seconds and average condition number per time step. Performed on Indaco cluster.

observed for BDDC preconditioner on the slab domain: there is an initial peak corresponding to the activation phase, followed by a constant period, as the tissue turn to resting. This trend is not appreciable for BDDC on the ellipsoidal domain, probably due to the complexity of the geometry.

We also observe a better performance of dual-primal preconditioners in terms of average CPU time per time step (see Table 6.20).

LR1 ionic model, ρ-scaling

H/h	V			V+E			V+E+F		
	nlit	lit	time	nlit	lit	time	nlit	lit	time
4	3.60	122.0	0.6	3.60	61.0	0.4	3.60	57.8	0.4
8	3.17	162.2	1.4	3.17	64.8	0.9	3.17	62.4	0.9
12	3.85	245.6	8.1	3.85	83.6	5.4	3.85	79.5	5.7
16	4.22	323.5	37.6	4.22	98.0	26.8	4.22	93.2	28.0
20	4.20	369.6	116.4	4.20	103.2	83.9	4.20	97.9	84.9
24	4.17	425.8	319.0	4.17	107.4	238.7	4.17	101.9	242.3

LR1 ionic model, deluxe scaling

H/h	V			V+E			V+E+F		
	nlit	lit	time	nlit	lit	time	nlit	lit	time
4	3.60	124.9	0.6	3.60	60.8	0.4	3.60	57.7	0.5
8	3.17	162.3	3.1	3.17	64.9	2.4	3.17	62.3	2.5
12	3.85	245.6	26.0	3.85	83.9	21.9	3.85	79.5	22.1
16	4.22	321.8	144.1	4.22	97.5	126.8	4.22	92.9	128.1
20	4.20	370.5	524.5	4.20	102.8	477.3	4.20	97.3	479.5
24	4.17	422.3	1561.3	4.17	106.8	1449.2	4.17	101.1	1453.2

TP06 ionic model, ρ-scaling

H/h	V			V+E			V+E+F		
	nlit	lit	time	nlit	lit	time	nlit	lit	time
4	3.50	117.6	0.5	3.50	58.6	0.4	3.50	56.6	0.4
8	2.82	144.8	1.2	2.82	57.6	0.7	2.82	55.3	0.8
12	2.90	185.5	6.1	2.90	63.4	4.0	2.90	60.0	4.3
16	3.05	234.7	26.9	3.05	71.3	20.1	3.05	68.0	20.8
20	2.90	257.7	80.7	2.90	71.9	58.3	2.90	68.5	59.2
24	2.45	252.5	183.9	2.45	63.9	140.8	2.45	60.6	142.4

TP06 ionic model, deluxe scaling

H/h	V			V+E			V+E+F		
	nlit	lit	time	nlit	lit	time	nlit	lit	time
4	3.50	120.8	0.6	3.50	58.7	0.4	3.50	56.0	0.5
8	2.82	144.9	2.9	2.82	57.6	2.1	2.82	55.2	2.2
12	2.90	185.7	19.5	2.90	63.6	16.5	2.90	60.0	16.5
16	3.05	233.9	104.6	3.05	71.1	91.6	3.05	67.7	92.4
20	2.90	259.6	362.2	2.90	71.7	329.7	2.90	68.1	331.0
24	2.45	249.7	918.7	2.45	63.8	997.5	2.45	60.1	852.0

Table 6.19: *Optimality tests on ellipsoidal domain for the Bidomain decoupled solver, LR1 and TP06 ionic models.* Fixed number of subdomains $4 \cdot 4 \cdot 4$. Increasing local size from $4 \cdot 4 \cdot 4$ to $24 \cdot 24 \cdot 24$. GMRES solver preconditioned by BDDC. Luo-Rudy phase 1 (LR1) and Ten Tusscher-Panfilov (TP06) ionic models. Comparison between different scaling and different primal sets (V = vertices, E = edges, F = faces). Average non-linear iterations (nlit), average number of linear iteration, average CPU time in seconds and average condition number per time step. Performed on Indaco cluster.

6.2.1   Transmural ischemic tests

In this Section, we test the robustness of our dual-primal Bidomain decoupled solver also in case of jumps in the diffusion coefficients, modelling pathological conditions such as myocardial ischemia. In particular, we consider here a transmural ischemic region located at the center of both geometries.

The ischemia is modeled by decreasing the diffusion coeffiecnts σ_l^i and σ_t^i along and across
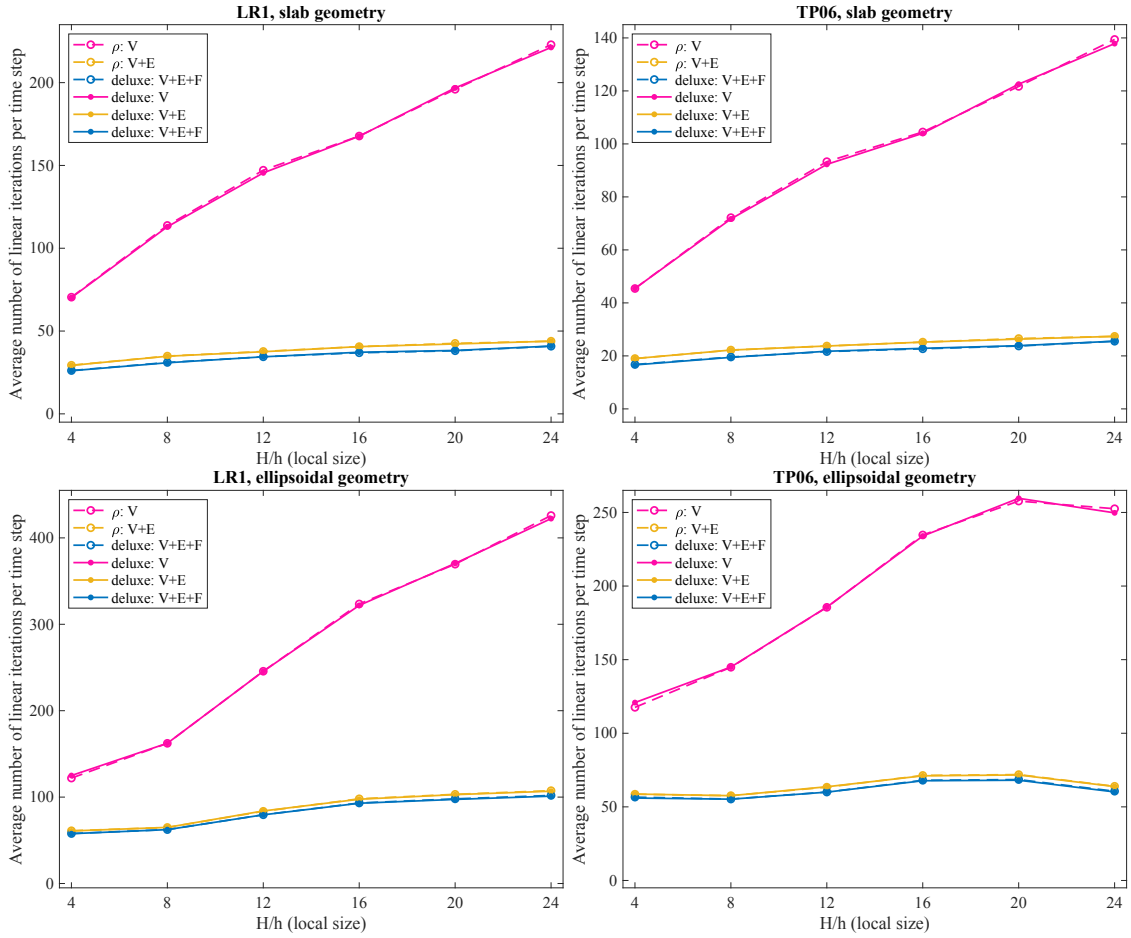
Figure 6.12: *Optimality tests on ellipsoidal domain for the Bidomain decoupled solver.* Fixed number of subdomains $4 \cdot 4 \cdot 4$. Increasing local size from $4 \cdot 4 \cdot 4$ to $24 \cdot 24 \cdot 24$. GMRES solver preconditioned by BDDC. Luo-Rudy phase 1 (LR1) and Ten Tusscher-Panfilov (TP06) ionic models. Comparison between different scaling (dash-dotted ρ-scaling, continuous *deluxe* scaling) and different primal sets (V = vertices, E = edges, F = faces). Comparison of average number of linear iteration per time step. Performed on Indaco cluster.
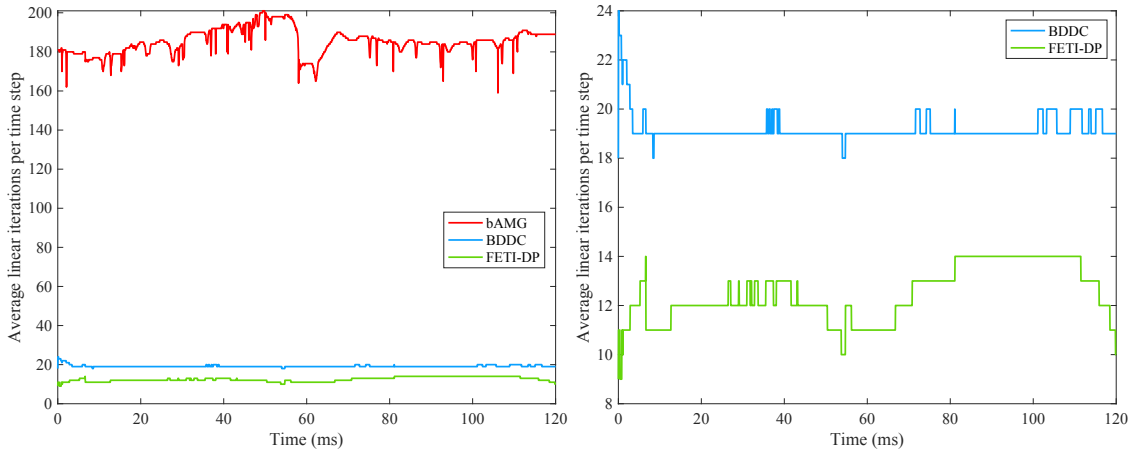
Figure 6.13: *Strong scalability on slab domain for the Bidomain decoupled solver.* Fixed number of subdomains $8 \cdot 8 \cdot 2$ and fixed global mesh of $192 \cdot 96 \cdot 24$. Simulation of a full activation-recovery cycle: time interval of $[0, 120]$ms, 2400 time steps. Rogers-McCulloch ionic model. Comparison between preconditioners of the average number of linear iterations per time step (left). Zoom over dual-primal preconditioner (right). Performed on Indaco cluster.
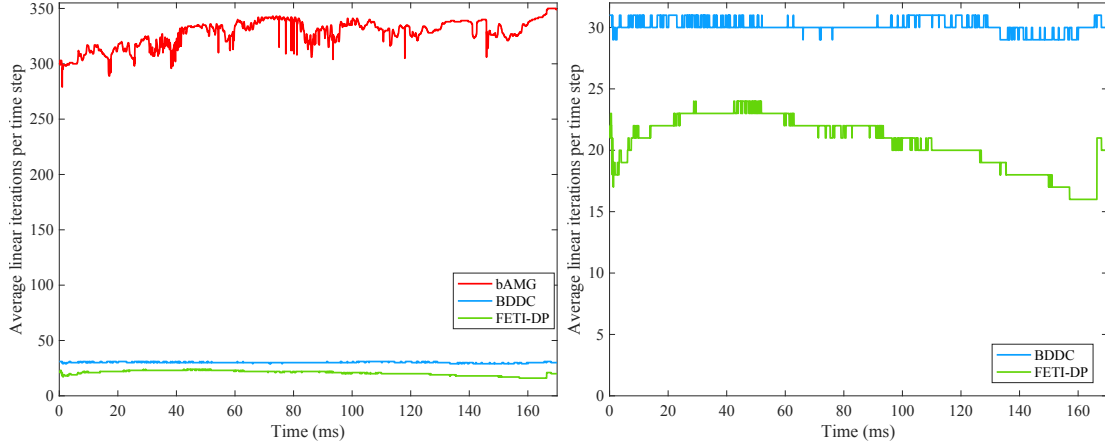
Figure 6.14: *Strong scalability on ellipsoidal domain for the Bidomain decoupled solver.* Fixed number of sub-domains $8 \cdot 8 \cdot 2$ and fixed global mesh of $192 \cdot 96 \cdot 24$. Simulation of a full activation-recovery cycle: time interval of $[0, 170]$ms, 3400 time steps. Rogers-McCulloch ionic model. Comparison between preconditioners of the average number of linear iterations per time step (left). Zoom over dual-primal preconditioner (right). Performed on Indaco cluster.

	procs	dofs	bAMG			BDDC			FETI-DP		
			nlit	lit	time	nlit	lit	time	nlit	lit	time
slab	128	8,450	2	185	11.28	2	19	8.02	2	12	7.62
ellipsoid	128	8,450	2	328	13.24	2	30	8.85	2	21	8.05

Table 6.20: *Strong scalability for the Bidomain decoupled solver.* Fixed number of subdomains $8 \cdot 8 \cdot 2$ and fixed global mesh of $192 \cdot 96 \cdot 24$. Simulation of a full activation-recovery cycle: time interval of $[0, 170]$ ms, 3400 time steps for the ellipsoidal domain and time interval of $[0, 120]$ ms, 2400 time steps for the slab. Rogers-McCulloch ionic model. Comparison of average Newton steps, average linear iterations and average CPU time (in sec.) per time step. Performed on Indaco cluster.

the fibers as shown in Table 6.21. In case the Rogers-McCulloch ionic model is employed, we reduce the ionic current by 30%; in case of the Ten Tusscher-Panfilov ionic model, we increase the extracellular concentration of potassium K_o from 5.4 mV to 8 mV, and we decrease the sodium conductance G_{Na} by 30%, simulating a mild ischemic event.

	Normal tissue	Ischemic tissue - RMC	Ischemic tissue - TP06
σ_l^i	$3 \times 10^{-3} \Omega^{-1}$ cm^{-1}	$1.5 \times 10^{-3} \Omega^{-1}$ cm^{-1}	$1.5 \times 10^{-3} \Omega^{-1}$ cm^{-1}
σ_t^i	$3.1525 \times 10^{-4} \Omega^{-1}$ cm^{-1}	$5.2541 \times 10^{-5} \Omega^{-1}$ cm^{-1}	$1.57625 \times 10^{-4} \Omega^{-1}$ cm^{-1}

Table 6.21: Conductivity coefficients for the Bidomain model: physiological and ischemic tissue for Rogers-McCulloch (RMC) and Ten Tusscher - Panfilov (TP06) ionic models.

Figures 6.15, 6.16, 6.17 and 6.18 show the time evolution of the transmembrane potential v and the extracellular potential u_e from the epicardial surfaces respectively, with a transmural ischemic region in the middle of the slab and the ellipsoidal geometries.

The simulations time is 2 ms of cardiac activation with time step $dt = 0.05$ ms, for a total amount fo 40 time steps. The external stimulus of 100 mA/cm^3 is applied for 1 ms on a small area of the endocardium.

The discontinuity of the diffusion coefficients on the boundaries of the ischemic region impairs the condition of the linear systems, thus requiring robust solvers.

We report in the following paragraphs several numerical tests investigating the scalability and optimality of the dual-primal decoupled solver. Due to the loss of positive semidefinite property in case of the inclusion of TP06 ionic model, we employ GMRES iterative solver also for RMC. In this experiments we employ PETSc implementation of algebraic multigrid (GAMG). All the tests are performed on Indaco cluster from the University of Milan.
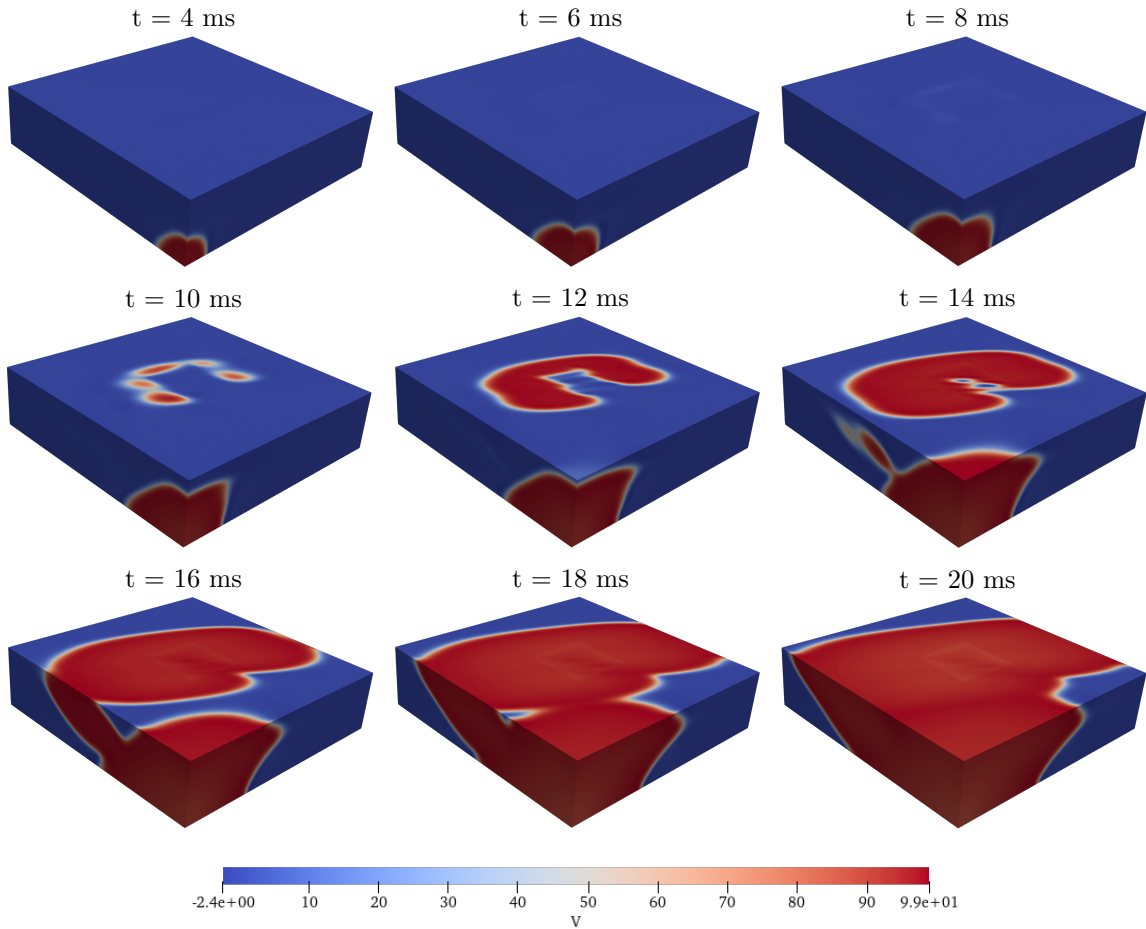
Figure 6.15: Snapshots (every 2 ms) of transmembrane potential v time evolution in presence of an ischemic transmural region. For each time frame, we report the epicardial side of slab domain.

Weak scalability on slab and ellipsoidal domains. Transmural ischemic region. We perform the weak scalability tests in presence of a transmural ischemic region by comparing the performances of the Newton-Krylov solvers in case RMC and TP06 ionic models are employed. Tables 6.22 and 6.23 report a comparison between the algebraic multigrid and the dual-primal preconditioners, with both ionic models and geometries. The local mesh size is fixed to $14 \cdot 14 \cdot 14$ and the number of processors is increased from 4 to 256, thus resulting in an increasing number of dofs from 25,230 to 1,462,050.

As expected from the previous comparison between ionic models in normal physiological cases (see for example Tables 6.10 or 6.11), for both geometries the average number of nonlinear iterations rises as the ionic model becomes more stiff; moreover also in this case, this parameter seems to be affected by the increasing complexity of the ellipsoidal domain.

As concerns the slab geometry, we observe a good behavior of BDDC and FETI-DP in terms of average number of linear iterations, since this quantity remains bounded while increasing the problem's size, while GAMG's iterations increase. The ellipsoidal geometry presents more fluctuations for all preconditioners, but the dual-primal solvers present lower values.

BDDC and FETI-DP perform slightly worse in terms of average CPU time, since their timings are higher than GAMG (probably due to the higher need of interprocessors communication). In contrast to these higher values, GAMG presents an increasing trend, while the dual-primal preconditioners remain constant.

Figure 6.16: Snapshots (every 2 ms) of extracellular potential u_e time evolution in presence of an ischemic transmural region. For each time frame, we report the epicardial side of slab domain.

Strong scalability on slab and ellipsoidal domains. Transmural ischemic region. We report here the strong scalability experiments in presence of a transmural ischemic region.

As in the normal physiological case, for the slab geometry, we fix the global mesh to $192 \cdot 192 \cdot 32$ elements (for a total of 2,458,434 dofs) and we increase the number of subdomains from 32 to 256. We fix the global mesh to $128 \cdot 128 \cdot 64$ elements for the portion of ellipsoid instead (thus resulting in 2,163,3360 dofs).

We have an increasing in the average number of nonlinear iterations by increasing the complexity of the ionic current, as happened in Table 6.14:as reported in Tables 6.24 and 6.25, this parameter increase from 1-2 per time step using the RMC model to 2-3 per time step with TP06 model.

The average number of linear iterations are comparable for all the preconditioners and for both ionic models, thus indicating robustness of the solvers and that our dual-primal solver retains its good convergence properties even for more complex ionic model. Again, as a consequence, the CPU times of TP06 model increase (with respect to RMC) due to the increase of nonlinear iterations, but the associated parallel speedups of the models are comparable. As in the previous strong scalability tests (Tables 6.12 and 6.13), since we are working with a low number of processors, BDDC and FETI-DP outperform the ideal speedup (both with respect to 32 and 64 processors).

Optimality tests on slab and ellipsoidal domains. Transmural ischemic region. Tables 6.26 and 6.27 report the results of optimality tests, for both RMC and TP06 ionic models, for both geometries. We fix the number of processors (and subdomains) to $64 = 4 \cdot 4 \cdot 4$ and we increase
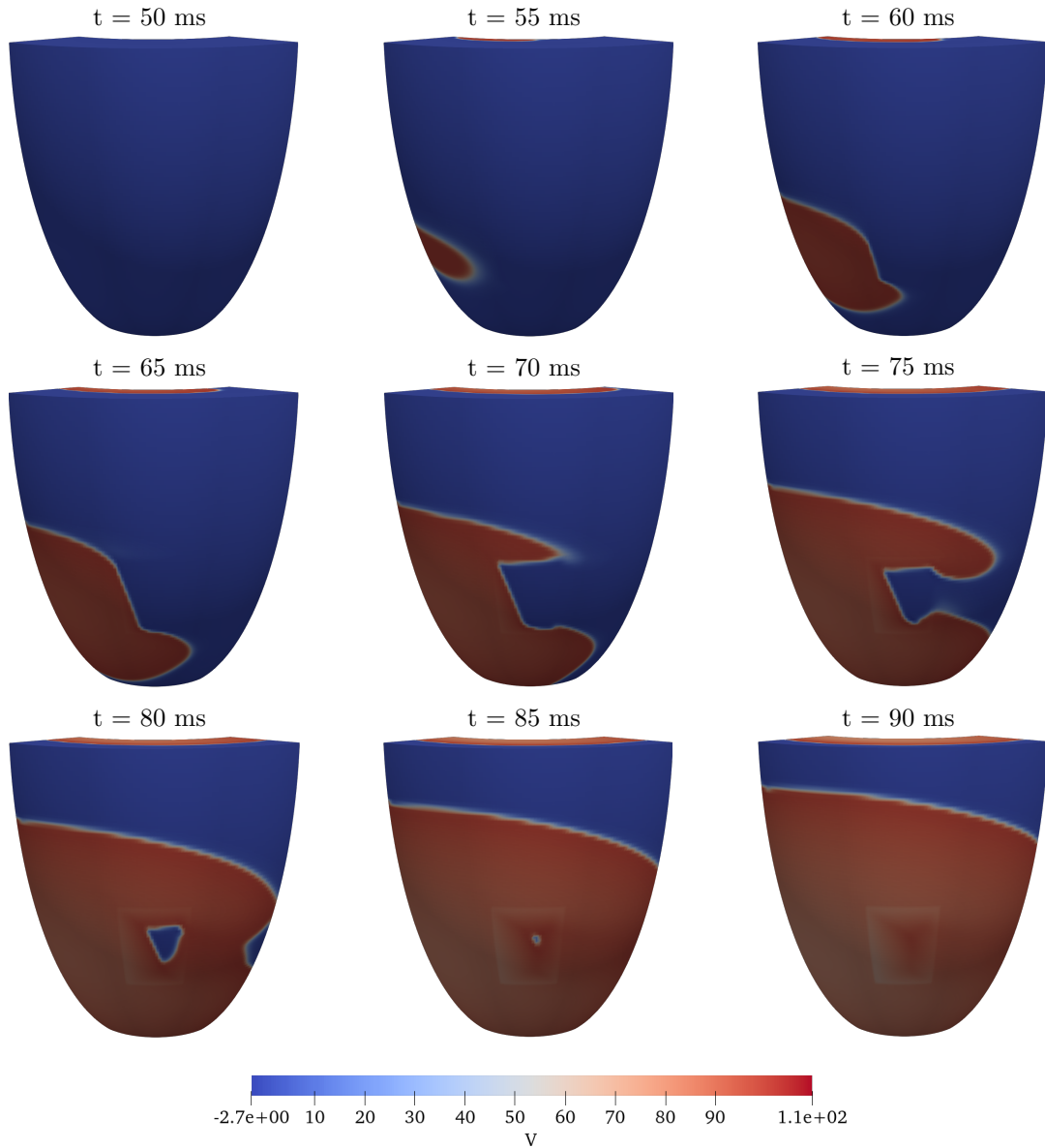
Figure 6.17: Snapshots (every 5 ms) of transmembrane potential v time evolution in presence of an ischemic transmural region. For each time frame, we report the epicardial side of a portion of half truncated ellipsoidal domain.

the local size H/h from 4 to 24, thus reducing the finite element size h.

Also in presence of the transmural ischemic region, we focus only on the behavior of the BDDC preconditioner, as the FETI-DP has been proven to be spectrally equivalent. For both ionic models, we consider both scalings (ρ-scaling on top, deluxe scaling at bottom of each table) and we test the solver for increasing primal spaces: V includes only vertex constraints, while V+E and V+E+F include vertex and edge constraints or vertex, edge and face constraints.

Similar results hold for both geometries, independently of the ionic model employed or the scaling chosen. Despite higher average CPU timings for the deluxe scaling, all the other parameters are similar between the two scalings (the average number of nonlinear iterations are the same, for each ionic model).

If we consider the coarsest space (with only vertices V), we observe that the number of linear
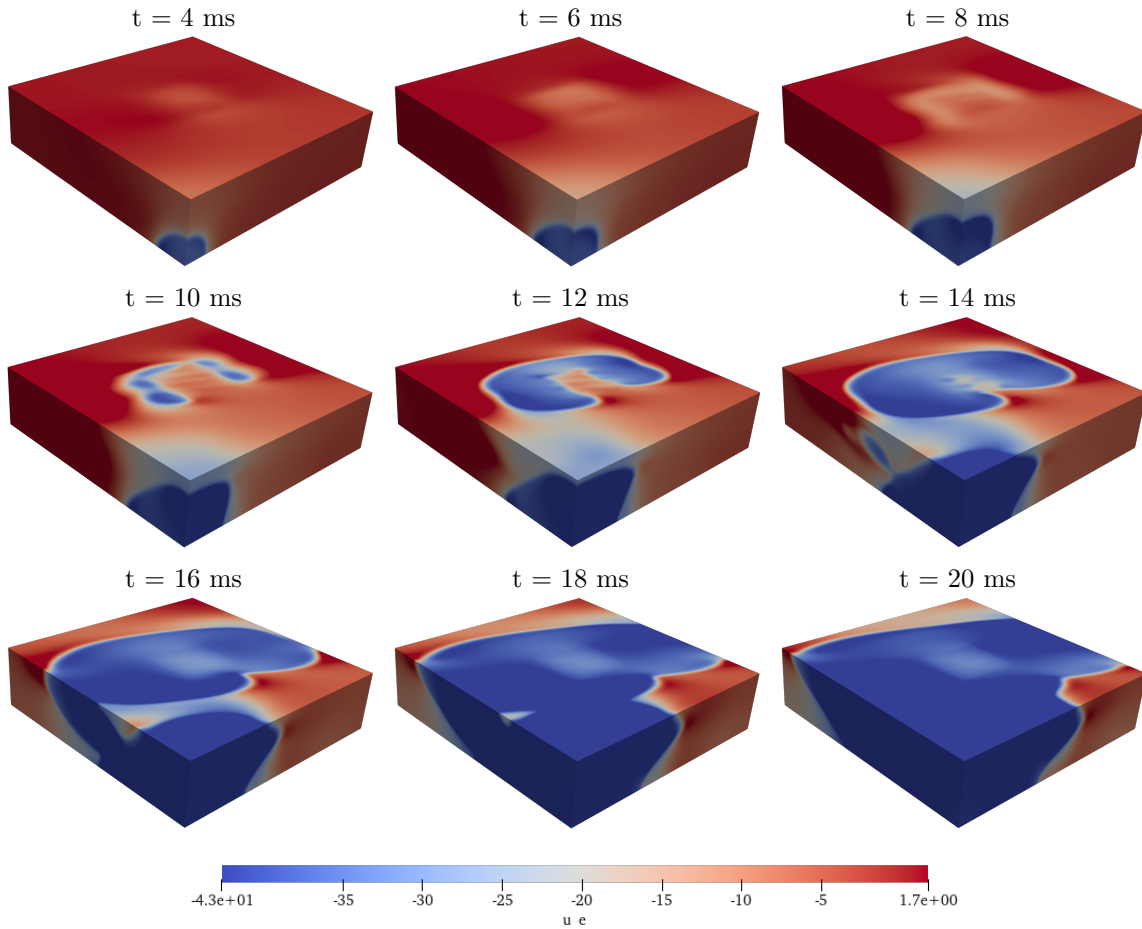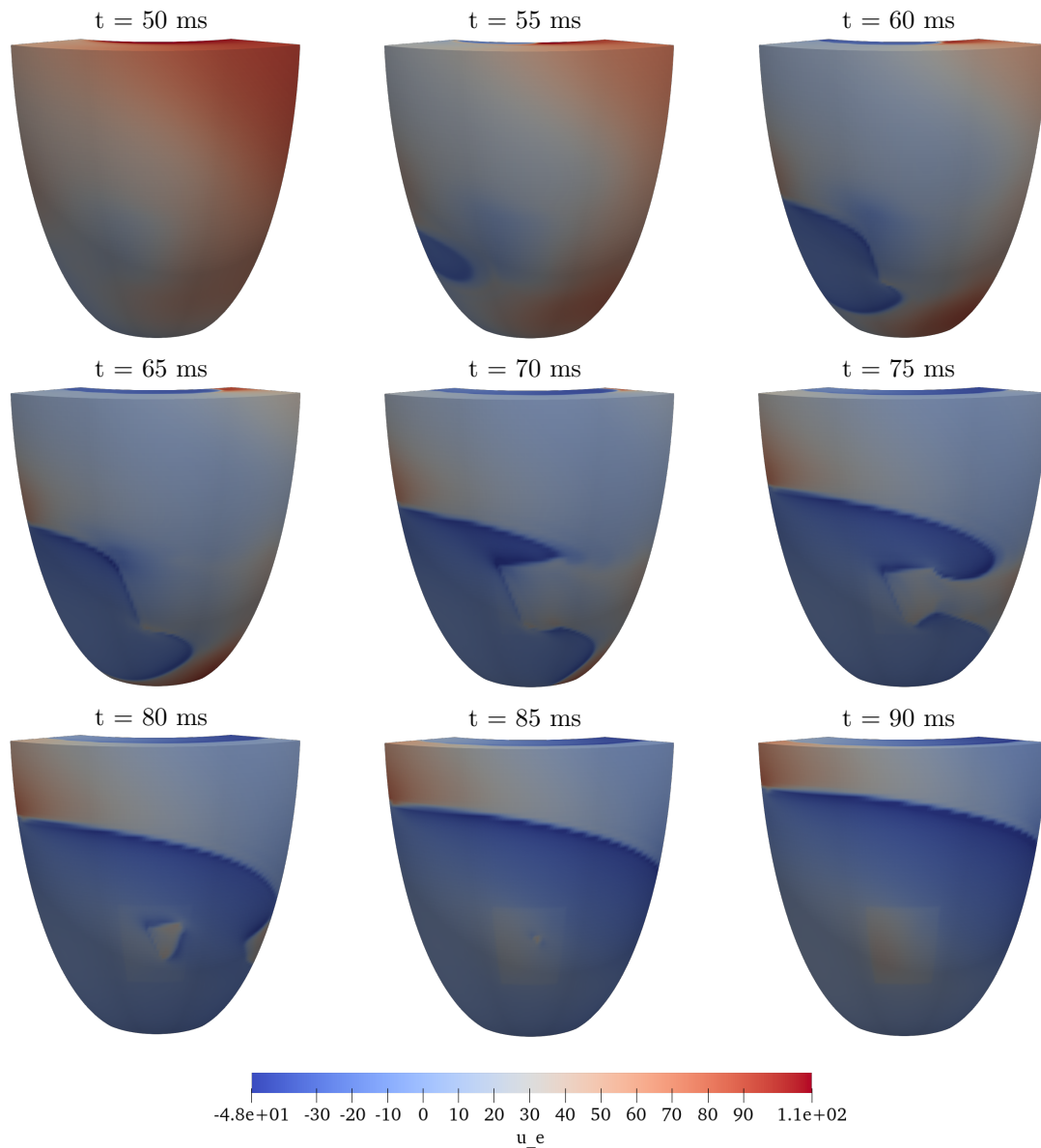
Figure 6.18: Snapshots (every 5 ms) of extracellular potential u_e time evolution in presence of an ischemic transmural region. For each time frame, we report the epicardial side of a portion of half truncated ellipsoidal domain domain.

iterations increase by increasing the local size, see Figure 6.19. On the other hand, if we enrich the primal space by adding edge and (V+E) and face (V+E+F) constraints, we can obtain quasi-optimality, where this quantity remain bounded, except for the slab geometry with TP06 ionic model, where the ρ-scaling with the full primal space (V+E+F) behaves as the coarsest (only V).

6.3   Coupled Monodomain tests

In the case of the coupled strategy, we implement "by hand" the Newton method, with stopping criterion based on the decresing of the L^{2}-norm of the residual with tolerance 10^{-4}.

The non-symmetric linear system arising from the discretization of the Jacobian problem at each Newton step is solved with the Generalized Minimal Residual (GMRES) and the stabilized

RMC ionic model, slab

procs	mesh	dofs	GAMG			BDDC			FETI-DP		
			nit	lit	time	nit	lit	time	nit	lit	time
4	$28 \cdot 28 \cdot 14$	25,230	1.2	16.4	0.35	1.2	10.5	2.03	1.2	7.8	1.92
8	$28 \cdot 28 \cdot 28$	48,778	1.2	18.9	0.41	1.2	13.8	2.09	1.2	9.6	1.93
16	$56 \cdot 28 \cdot 28$	95,874	1.2	18.5	0.63	1.2	14.8	2.34	1.2	10.4	2.12
32	$56 \cdot 28 \cdot 56$	188,442	1.2	20.8	0.72	1.2	14.7	2.63	1.2	10.4	2.38
64	$56 \cdot 56 \cdot 56$	370,386	1.2	20.9	0.89	1.2	13.9	2.88	1.2	9.7	2.64
128	$56 \cdot 112 \cdot 56$	734,274	1.2	22.0	1.09	1.2	13.7	3.09	1.2	9.6	2.84
256	$56 \cdot 224 \cdot 56$	1,462,050	1.2	22.9	1.89	1.2	13.7	3.52	1.2	9.5	3.20

TP06 ionic model, slab

procs	mesh	dofs	GAMG			BDDC			FETI-DP		
			nit	lit	time	nit	lit	time	nit	lit	time
4	$28 \cdot 28 \cdot 14$	25,230	2.0	16.1	0.67	2.0	10.2	3.46	2.0	7.2	3.27
8	$28 \cdot 28 \cdot 28$	48,778	2.1	18.0	0.68	2.1	13.4	3.69	2.1	9.1	3.42
16	$56 \cdot 28 \cdot 28$	95,874	2.2	18.0	1.17	2.2	14.6	4.19	2.2	9.7	3.78
32	$56 \cdot 28 \cdot 56$	188,442	2.2	20.1	1.34	2.2	14.7	3.93	2.2	9.6	4.28
64	$56 \cdot 56 \cdot 56$	370,386	2.2	20.8	1.56	2.2	14.1	5.06	2.2	9.4	4.72
128	$56 \cdot 112 \cdot 56$	734,274	2.2	22.0	2.13	2.2	13.8	5.48	2.2	9.4	5.07
256	$56 \cdot 224 \cdot 56$	1,462,050	2.2	22.4	3.03	2.2	13.9	6.21	2.2	9.4	5.42

Table 6.22: *Weak scalability on slab domain for the Bidomain decoupled solver, transmural ischemic region.* Local mesh of $14 \cdot 14 \cdot 14$ elements. Simulations of 2 ms of cardiac activation with $dt = 0.05$ ms, for a total amount fo 40 time steps. Comparison of Newton-Krylov solvers with GAMG, BDDC and FETI-DP preconditioners. Rogers-McCulloch (RMC) and Ten Tusscher-Panfilov (TP06) ionic models, in presence of transmural ischemic region. Average Newton iterations per time step (nit); average conjugate gradient iterations per Newton iteration (lit); average CPU solution time per time step (time) in seconds. Performed on Indaco cluster.

RMC ionic model, ellipsoid

procs	mesh	dofs	GAMG			BDDC			FETI-DP		
			nit	lit	time	nit	lit	time	nit	lit	time
4	$28 \cdot 28 \cdot 14$	25,230	2.0	26.6	0.62	2.0	9.6	2.96	2.0	6.8	3.46
8	$28 \cdot 28 \cdot 28$	48,778	2.0	41.5	0.85	2.0	16.8	3.86	2.0	12.2	3.55
16	$56 \cdot 28 \cdot 28$	95,874	2.0	59.5	1.80	2.0	23.3	4.42	2.0	17.3	3.87
32	$56 \cdot 28 \cdot 56$	188,442	2.0	78.1	2.41	2.0	39.7	5.85	2.0	26.7	4.66
64	$56 \cdot 56 \cdot 56$	370,386	2.0	56.0	2.13	2.0	22.9	5.42	2.0	16.2	4.77
128	$56 \cdot 112 \cdot 56$	734,274	1.4	34.6	1.39	1.4	16.5	3.82	1.4	12.5	3.47
256	$56 \cdot 224 \cdot 56$	1,462,050	1.1	30.5	1.24	1.1	15.6	3.77	1.4	11.7	3.13

TP06 ionic model, ellipsoid

procs	mesh	dofs	GAMG			BDDC			FETI-DP		
			nit	lit	time	nit	lit	time	nit	lit	time
4	$28 \cdot 28 \cdot 14$	25,230	3.7	25.8	1.32	3.7	9.6	7.01	3.7	6.3	6.62
8	$28 \cdot 28 \cdot 28$	48,778	3.3	45.3	1.64	3.3	17.0	6.68	3.3	11.6	6.09
16	$56 \cdot 28 \cdot 28$	95,874	3.4	57.7	2.96	3.4	22.9	7.65	3.4	16.1	6.67
32	$56 \cdot 28 \cdot 56$	188,442	3.7	81.1	4.73	3.7	37.9	10.80	3.7	24.9	8.72
64	$56 \cdot 56 \cdot 56$	370,386	3.5	54.6	3.66	3.5	23.1	9.34	3.5	15.5	8.11
128	$56 \cdot 112 \cdot 56$	734,274	3.2	35.8	3.63	3.2	16.4	8.82	3.2	10.9	7.94
256	$56 \cdot 224 \cdot 56$	1,462,050	2.9	31.5	3.85	2.9	15.7	8.95	2.9	10.3	8.11

Table 6.23: *Weak scalability on ellipsoidal domain for the Bidomain decoupled solver, transmural ischemic region.* Local mesh of $14 \cdot 14 \cdot 14$ elements. Simulations of 2 ms of cardiac activation with $dt = 0.05$ ms, for a total amount fo 40 time steps. Comparison of Newton-Krylov solvers with GAMG, BDDC and FETI-DP preconditioners. Rogers-McCulloch (RMC) and Ten Tusscher-Panfilov (TP06) ionic models, in presence of transmural ischemic region. Average Newton iterations per time step (nit); average conjugate gradient iterations per Newton iteration (lit); average CPU solution time per time step (time) in seconds. Performed on Indaco cluster.

Biconjugate Gradient (BiCGStab) method, preconditioned by BDDC preconditioner (included in the PETSC library) and *Boomer* Algebraic MultiGrid (bAMG, from the Hypre library [41]).

Since the main focus of the work is to apply the proposed solver to the Bidomain model, we provide here only few preliminary experiments for the Monodomain problem with the Rogers-McCulloch ionic model: in particular, we propose only weak scalability tests on a portion of half truncated

RMC ionic model, slab

procs	GAMG					BDDC					FETI-DP				
	nit	lit	time	S_{32}	S_{64}	nit	lit	time	S_{32}	S_{64}	nit	lit	time	S_{32}	S_{64}
16	1.2	19.9	19.28	-	-	1.2	22.7	679.75	-	-	1.2	22.7	680.00	-	-
32	1.2	19.9	10.14	-	-	1.2	16.9	220.9	-	-	1.2	16.9	220.80	-	-
64	1.2	20.0	5.17	1.96	-	1.2	20.0	62.77	3.52	-	1.2	20.0	63.22	3.49	-
128	1.2	19.9	2.93	3.46	1.76	1.2	15.3	20.06	11.01	3.13	1.2	15.3	19.90	11.09	3.17
256	1.2	19.9	1.84	5.51	2.81	1.2	17.4	6.79	32.55	9.25	1.2	17.4	6.53	33.80	9.67

TP06 ionic model, slab

procs	GAMG					BDDC					FETI-DP				
	nit	lit	time	S_{32}	S_{64}	nit	lit	time	S_{32}	S_{64}	nit	lit	time	S_{32}	S_{64}
16	2.2	20.1	35.62	-	-	out of memory					out of memory				
32	2.2	19.7	18.68	-	-	2.2	17.8	386.75	-	-	2.2	17.8	387.00	-	-
64	2.2	20.2	9.32	2.0	-	2.2	20.9	109.37	3.54	-	2.2	20.9	110.42	3.51	-
128	2.2	19.6	5.36	3.48	1.74	2.2	15.8	35.72	10.83	3.06	2.2	15.8	35.22	10.98	3.14
256	2.2	20.0	3.88	4.81	2.41	2.2	17.8	11.60	33.33	9.43	2.2	17.8	11.48	33.71	9.62

Table 6.24: *Strong scalability on slab domain for the Bidomain decoupled solver, transmural ischemic region.* Global mesh of $192 \cdot 192 \cdot 32$ elements (2,458,434 dofs). Simulations of 2 ms of cardiac activation with $dt = 0.05$ ms, for a total amount fo 40 time steps. Comparison of Newton-Krylov solvers with GAMG, BDDC and FETI-DP preconditioners. Rogers-McCulloch (RMC) and Ten Tusscher-Panfilov (TP06) ionic models, in presence of transmural ischemic region. Average Newton iterations per time step (nit); average conjugate gradient iterations per Newton iteration (lit); average CPU solution time per time step (time) in seconds; parallel speedup with respect to 32 (S_{32}) and 64 (S_{64}) processors. Performed on Indaco cluster.

RMC ionic model, ellipsoid

procs	GAMG					BDDC					FETI-DP				
	nit	lit	time	S_{32}	S_{64}	nit	lit	time	S_{32}	S_{64}	nit	lit	time	S_{32}	S_{64}
16	1.1	37.1	19.98	-	-	1.1	27.0	862.50	-	-	1.1	27.0	863.0	-	-
32	1.1	36.8	10.19	-	-	1.0	20.5	240.57	-	-	1.1	20.5	240.60	-	-
64	1.1	38.2	5.63	1.81	-	1.1	26.7	55.05	4.37	-	1.1	26.7	55.40	4.34	-
128	1.1	36.5	3.15	3.23	1.78	1.1	21.4	15.56	15.46	3.54	1.1	21.4	15.91	15.12	3.48
256	1.1	38.5	1.86	38.5	3.02	1.1	31.4	5.39	44.63	10.21	1.1	44.1	5.46	44.04	10.12

TP06 ionic model, ellipsoid

procs	GAMG					BDDC					FETI-DP				
	nit	lit	time	S_{32}	S_{64}	nit	lit	time	S_{32}	S_{64}	nit	lit	time	S_{32}	S_{64}
16	2.9	38.5	53.47	-	-	out of memory					out of memory				
32	2.9	38.3	28.45	-	-	2.9	20.2	628.75	-	-	2.9	20.2	629.00	-	-
64	2.9	39.4	15.15	1.88	-	2.9	26.3	114.47	4.35	-	2.9	26.3	144.35	4.36	-
128	2.9	37.3	8.22	3.46	1.84	2.9	20.7	40.97	15.35	3.53	2.9	20.7	41.22	15.26	3.51
256	2.9	39.8	5.69	5.0	2.66	2.9	29.7	13.54	46.44	10.67	2.9	29.7	14.07	44.9	10.31

Table 6.25: *Strong scalability on ellipsoidal domain for the Bidomain decoupled solver, transmural ischemic region.* Global mesh of $128 \cdot 128 \cdot 64$ elements (2,163,330 dofs). Simulations of 2 ms of cardiac activation with $dt = 0.05$ ms, for a total amount fo 40 time steps. Comparison of Newton-Krylov solvers with GAMG, BDDC and FETI-DP preconditioners. Rogers-McCulloch (RMC) and Ten Tusscher-Panfilov (TP06) ionic models, in presence of transmural ischemic region. Average Newton iterations per time step (nit); average conjugate gradient iterations per Newton iteration (lit); average CPU solution time per time step (time) in seconds; parallel speedup with respect to 32 (S_{32}) and 64 (S_{64}) processors. Performed on Indaco cluster.

ellipsoidal domain. The good results can be considered as a good indicator of well behavior of the solvers on the Bidomain problem.

This set of tests are run on the Linux cluster Marconi, at Cineca centre.

Weak scalability on ellipsoidal domain. We report a mean of nonlinear iteration number *nlit* over integration time, while *lit* and *cond* denote the average cumulative linear iterations and the mean condition number per Newton step respectively. *time* denotes the average CPU time per nonlinear iteration.

We fix the local mesh size to $16 \cdot 16 \cdot 16$ and we increase the number of processors from 32 to 512, thus increasing the global number of dofs from 131,072 to 2,097,152. The integration time is

RMC ionic model, ρ-scaling

H/h	V			V+E			V+E+F		
	nlit	lit	time	nlit	lit	time	nlit	lit	time
4	1.35	32.9	0.15	1.35	13.6	0.09	1.35	12.1	0.12
8	1.25	50.4	0.45	1.25	15.6	0.25	1.25	14.0	0.29
12	1.25	64.2	2.24	1.25	16.8	1.45	1.25	15.3	1.56
16	1.25	73.7	9.98	1.25	17.5	7.22	1.25	16.2	7.81
20	1.25	85.6	0.10	1.25	18.6	21.84	1.25	16.8	22.41
24	1.25	98.7	83.42	1.25	18.8	63.02	1.25	17.4	63.82

RMC ionic model, deluxe scaling

H/h	V			V+E			V+E+F		
	nlit	lit	time	nlit	lit	time	nlit	lit	time
4	1.35	32.3	0.18	1.35	13.6	0.12	1.35	12.1	0.19
8	1.25	49.7	0.99	1.25	15.4	0.74	1.25	13.8	0.84
12	1.25	64.1	7.54	1.25	16.6	6.22	1.25	15.1	6.34
16	1.25	73.5	38.27	1.25	17.5	34.17	1.25	16.2	34.32
20	1.25	86.0	143.80	1.25	18.7	131.35	1.25	17.1	132.27
24	1.25	96.9	432.70	1.25	18.8	404.75	1.25	17.5	407.25

TP06 ionic model, ρ-scaling

H/h	V			V+E			V+E+F		
	nlit	lit	time	nlit	lit	time	nlit	lit	time
4	1.9	44.2	0.22	1.9	19.0	0.13	1.9	44.2	0.20
8	2.1	83.6	0.80	2.1	26.3	0.45	2.1	83.6	0.87
12	2.1	110.0	3.81	2.1	29.1	2.55	2.1	110.0	3.79
16	2.1	129.1	16.90	2.1	31.1	12.47	2.1	129.1	16.93
20	2.1	153.0	52.40	2.1	33.6	38.40	2.1	153.1	52.37
24	2.2	174.9	147.92	2.2	35.7	113.45	2.2	174.9	149.37

TP06 ionic model, deluxe scaling

H/h	V			V+E			V+E+F		
	nlit	lit	time	nlit	lit	time	nlit	lit	time
4	1.9	43.8	0.25	1.9	18.9	0.17	1.9	15.8	0.28
8	2.1	82.9	1.79	2.1	26.1	1.36	2.1	23.1	1.36
12	2.1	108.5	12.79	2.1	29.1	10.74	2.1	26.8	10.85
16	2.1	126.6	65.27	2.1	31.1	58.52	2.1	28.2	58.82
20	2.1	151.7	248.40	2.1	33.5	227.37	2.1	30.7	227.75
24	2.2	171.2	762.50	2.2	35.8	715.50	2.2	33.6	717.00

Table 6.26: *Optimality tests on slab domain for the Bidomain decoupled solver, transmural ischemic region.* Fixed number of subdomains $4 \cdot 4 \cdot 4$. Increasing local size from $4 \cdot 4 \cdot 4$ to $24 \cdot 24 \cdot 24$. GMRES solver preconditioned by BDDC. Rogers-McCulloch (RMC) and Ten Tusscher-Panfilov (TP06) ionic models, in presence of transmural ischemic region. Comparison between different scaling and different primal sets (V = vertices, E = edges, F = faces). Average non-linear iterations (nlit), average number of linear iteration, average CPU time in seconds and average condition number per time step. Performed on Indaco cluster.

$[0, 5]$ ms, with a time step of 0.05 ms, for a total of 40 time steps.

Similar results hold independently of the employed preconditioner, as shown in Table 6.28. The average number of nonlinear iterations per time step remains bounded for both GMRES and BiCGStab methods; the average number of cumulative linear iterations per time step is slightly lower in case BiCGStab is used and, more generally, is lower for the multigrid preconditioner. This is not a limitation, as for BDDC this value remains bounded and actually it decreases while

RMC ionic model, ρ-scaling

H/h	V			V+E			V+E+F		
	nlit	lit	time	nlit	lit	time	nlit	lit	time
4	1.95	73.6	0.36	1.95	36.7	0.19	1.95	34.7	0.23
8	2.05	106.7	0.89	2.05	42.6	0.55	2.05	40.7	0.59
12	2.0	131.3	4.17	2.0	44.8	2.82	2.0	42.3	2.95
16	2.0	156.4	18.53	2.0	46.9	12.99	2.0	44.4	13.18
20	2.0	177.4	55.37	2.0	49.4	40.25	2.0	46.4	40.37
24	1.85	187.8	137.15	1.85	47.3	105.07	1.85	44.7	105.80

RMC ionic model, deluxe scaling

H/h	V			V+E			V+E+F		
	nlit	lit	time	nlit	lit	time	nlit	lit	time
4	1.95	75.6	0.37	1.95	38.6	0.26	1.95	34.7	0.26
8	2.05	104.3	1.99	2.05	42.1	1.46	2.05	40.3	1.61
12	2.0	129.1	13.62	2.0	43.7	11.42	2.0	41.4	11.45
16	2.0	153.6	58.27	2.0	45.7	60.00	2.0	43.4	60.10
20	2.0	175.8	248.97	2.0	49.2	227.17	2.0	45.4	228.00
24	1.85	185.4	692.00	1.85	46.7	641.25	1.85	43.7	643.50

TP06 ionic model, ρ-scaling

H/h	V			V+E			V+E+F		
	nlit	lit	time	nlit	lit	time	nlit	lit	time
4	3.9	140.2	0.66	3.9	69.6	0.50	3.9	65.7	0.46
8	3.4	173.9	1.54	3.4	69.5	0.92	3.4	67.3	0.98
12	3.35	246.2	6.96	3.35	74.3	4.76	3.35	71.1	4.96
16	3.25	252.9	29.65	3.25	77.3	21.10	3.25	73.2	21.89
20	3.05	271.0	84.77	3.05	76.1	61.42	3.05	71.6	62.00
24	2.8	293.2	218.90	2.8	74.5	164.32	2.8	70.3	165.95

TP06 ionic model, deluxe scaling

H/h	V			V+E			V+E+F		
	nlit	lit	time	nlit	lit	time	nlit	lit	time
4	3.9	144.8	0.80	3.9	72.3	0.55	3.9	65.8	0.59
8	3.4	173.8	3.40	3.4	70.4	2.47	3.4	66.4	2.64
12	3.35	214.8	22.80	3.35	74.8	19.12	3.35	70.7	19.16
16	3.25	249.1	111.40	3.25	76.6	97.60	3.25	72.6	98.30
20	3.05	268.1	380.00	3.05	75.1	346.25	3.05	71.2	348.25
24	2.8	291.7	1076.80	2.8	73.8	997.75	2.8	69.7	999.25

Table 6.27: *Optimality tests on ellipsoidal domain for the Bidomain decoupled solver, transmural ischemic region.* Fixed number of subdomains $4 \cdot 4 \cdot 4$. Increasing local size from $4 \cdot 4 \cdot 4$ to $24 \cdot 24 \cdot 24$. GMRES solver preconditioned by BDDC. Rogers-McCulloch (RMC) and Ten Tusscher-Panfilov (TP06) ionic models, in presence of transmural ischemic region. Comparison between different scaling and different primal sets (V = vertices, E = edges, F = faces). Average non-linear iterations (nlit), average number of linear iteration, average CPU time in seconds and average condition number per time step. Performed on Indaco cluster.

increasing the number of subdomains. The average CPU time per time step for the dual-primal preconditioner is higher, again maybe due to the higher need of communication between processors.
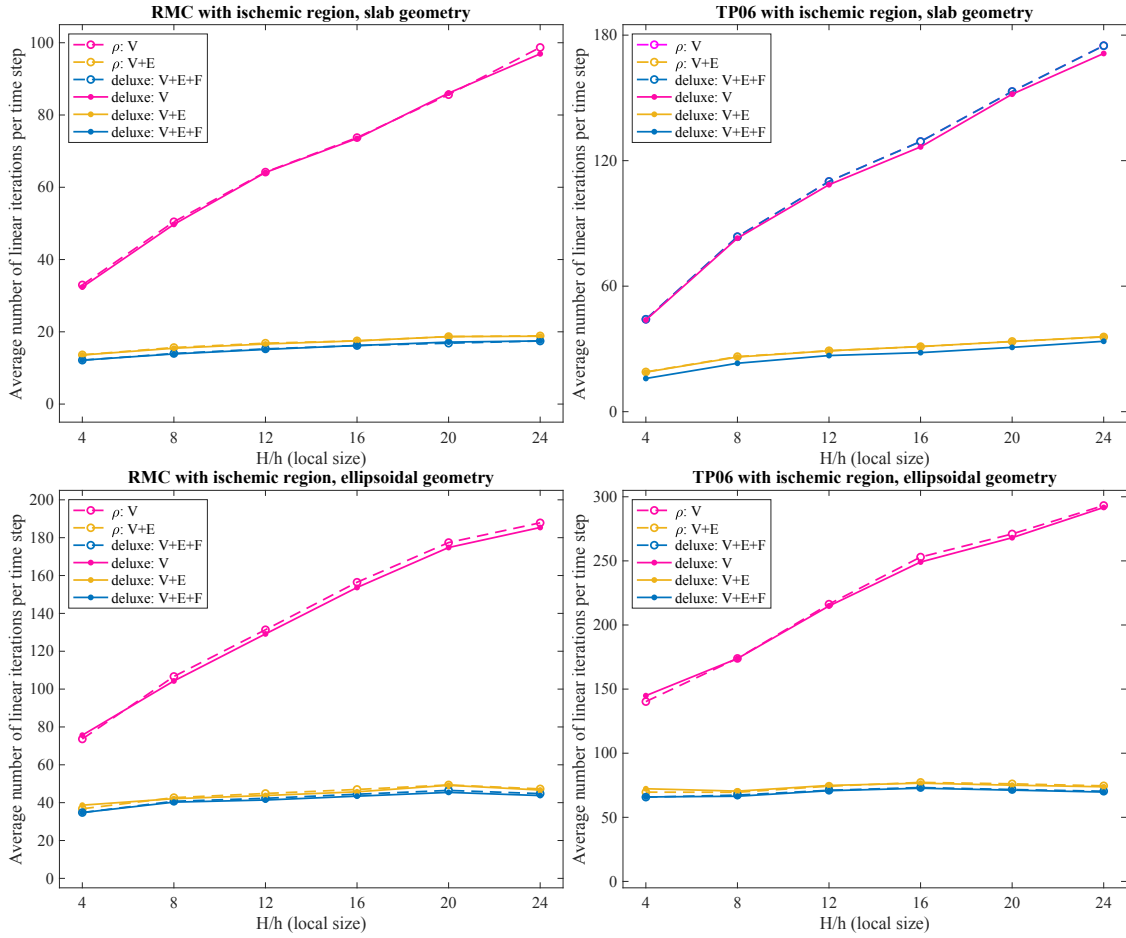
Figure 6.19: *Optimality tests on ellipsoidal domain for the Bidomain decoupled solver, transmural ischemic region.* Fixed number of subdomains $4 \cdot 4 \cdot 4$. Increasing local size from $4 \cdot 4 \cdot 4$ to $24 \cdot 24 \cdot 24$. GMRES solver preconditioned by BDDC. Rogers-McCulloch (RMC) and Ten Tusscher-Panfilov (TP06) ionic models, in presence of transmural ischemic region. Comparison between different scaling (dash-dotted ρ-scaling, continuous *deluxe* scaling) and different primal sets (V = vertices, E = edges, F = faces). Comparison of average number of linear iteration per time step. Performed on Indaco cluster.
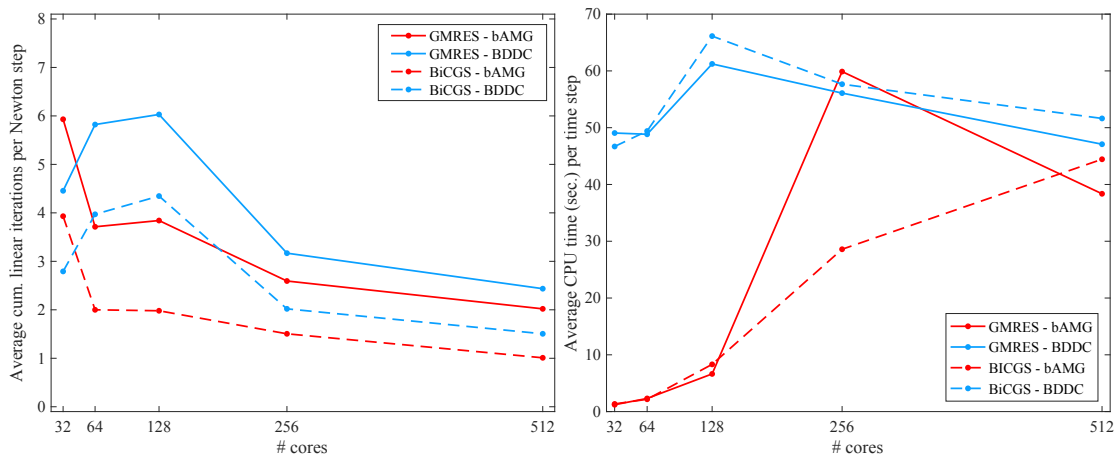
Figure 6.20: *Weak scalability on ellipsoidal domain for the Monodomain coupled solver.* Fixed local mesh size $16 \cdot 16 \cdot 16$ and increasing number of processors. Average number of cumulative linear iterations per nonlinear step (left) and average CPU time per time step in seconds (right). Performed on Marconi cluster.

procs	Glob. mesh	GMRES - bAMG				GMRES - BDDC			
		time	nlit	lit	cond	time	nlit	lit	cond
32	$64 \cdot 64 \cdot 32$	1.2	2	6	1.0	49.1	2	4	3.5
64	$64 \cdot 64 \cdot 64$	2.3	2	4	1.0	48.8	2	6	3.2
128	$128 \cdot 128 \cdot 32$	6.6	2	4	1.0	61.2	out of memory		
256	$128 \cdot 128 \cdot 64$	59.9	1	3	1.0	56.1	1	3	1.1
512	$256 \cdot 256 \cdot 32$	38.4	1	2	1.0	47.1	1	2	1.0

procs	Glob. mesh	BiCGStab - AMG				BiCGStab - BDDC			
		time	nlit	lit	cond	time	nlit	lit	cond
32	$64 \cdot 64 \cdot 32$	1.3	2	4	1.0	46.7	2	3	1.0
64	$64 \cdot 64 \cdot 64$	2.2	2	2	1.0	49.4	2	4	1.0
128	$128 \cdot 128 \cdot 32$	8.3	2	2	1.0	66.1	2	4	1.0
256	$128 \cdot 128 \cdot 64$	28.6	1	1	1.0	57.6	1	2	1.0
512	$256 \cdot 256 \cdot 32$	44.4	1	1	1.0	51.6	1	2	1.0

Table 6.28: *Weak scalability on ellipsoidal domain for the Monodomain coupled solver.* Fixed local mesh size $16 \cdot 16 \cdot 16$ and increasing number of processors. Comparison between average CPU time per nonlinear step in seconds (*time*), (rounded) average number of nonlinear iteration per time step (*nlit*), (rounded) average cumulative linear iterations and average condition number per Newton step (*lit* and *cond*). Perfomed on Marconi cluster.

6.4 Coupled Bidomain tests

As for the Monodomain coupled solver, we implement "by hand" the Newton method, with stopping criterion based on the decresing of the Euclidean norm of the residual with tolerance 10^{-4}. For the Bidomain model, we solve with the Generalized Minimal Residual (GMRES) method the non-symmetric linear system arising from the discretization of the Jacobian problem at each Newton step, preconditioned by BDDC preconditioner (included in the PETSC library) and *Boomer* Algebraic MultiGrid (bAMG, from the Hypre library [41]). The employed ionic model is the Rogers-McCulloch. All these experiments have been run on the cluster Galileo at Cineca center.

Weak scalability on slab and ellipsoidal domains. These set of tests is a weak scalability test on both slab and ellipsoidal domains. For both geometries, we fix the local mesh size to $12 \cdot 12 \cdot 12$ and we increase the number of subdomains from 32 to 256, thus resulting in an increasing slab geometry and in an increasing portion of half ellipsoid. In this way, the dofs are increasing from 180k up to 1 million and a half. Tables 6.29 and 6.30 show how the dual-primal algorithm has a better behavior respect to the bAMG: the average number of linear iteration per nonlinear step (lit) does not increase while increasing the number of subdomains and is clearly lower. Indeed, for the slab geometry we observe an increasing reduction rate from 85% up to 93% for the average number of linear iterations, while for the ellipsoidal geometry it varies between 65% and 90%. In contrast, BDDC's average CPU time is higher than bAMG CPU time (we do not have a clear explanation of this fact), maybe due to the interprocessor communications: however, we remark that BDDC timings do not increase significantly when the number of processors is increased from 32 to 256, while bAMG timings more than double.

Strong scalability on slab and ellipsoidal domains. We perform a strong scaling test for the two geometries: we fix the global mesh to $128 \cdot 128 \cdot 24$ elements (resulting in more than 1 millions of dofs) and we increase the number of subdomains from 32 to 256.

We observe from Table 6.31 that, as the number of processors increases, the local number of dofs and BDDC's average number of linear iterations decrease and the latter parameter is certainly lower than bAMG's. Timings of the multigrid preconditioner are lower than BDDC timings, even if they decrease less than expected.

We test the efficiency of the proposed solver on the parallel architecture by computing the parallel speedup $S_p = \frac{T_p}{T_N}$. In both cases, BDDC preconditioner outperforms the ideal speedup,

subds.	global mesh	dofs	bAMG			BDDC		
			nit	lit	time	nit	lit	time
32	$48 \cdot 48 \cdot 24$	180,075	1	100	0.6	1	16	3.2
64	$96 \cdot 48 \cdot 24$	356,475	1	127	0.9	1	16	3.4
128	$96 \cdot 96 \cdot 24$	705,675	1	168	1.3	1	17	3.4
256	$192 \cdot 96 \cdot 24$	1,404,075	1	243	1.9	1	17	4.3

Table 6.29: *Weak scalability on slab domain for the Bidomain coupled solver.* Local mesh of $12 \cdot 12 \cdot 12$ elements. Simulations of 2 ms of cardiac activation with $dt = 0.05$ ms (40 time steps). Comparison of Newton-Krylov solvers preconditioned by bAMG and BDDC. Average Newton iterations per time step (nit); average GMRES iterations per Newton iteration (lit); average CPU solution time per time step (time) in seconds. Performed on Galileo cluster.

subds.	global mesh	dofs	bAMG			BDDC		
			nit	lit	time	nit	lit	time
32	$48 \cdot 48 \cdot 24$	180,075	2	142	1.5	2	45	6.8
64	$96 \cdot 48 \cdot 24$	356,475	2	145	1.9	2	32	6.9
128	$96 \cdot 96 \cdot 24$	705,675	2	158	2.1	2	23	7.0
256	$192 \cdot 96 \cdot 24$	1,404,075	2	212	3.2	2	23	8.5

Table 6.30: *Weak scalability on ellipsoidal domain for the Bidomain coupled solver.* Local mesh of $12 \cdot 12 \cdot 12$ elements. Simulations of 2 ms of cardiac activation with $dt = 0.05$ ms (40 time steps). Comparison of Newton-Krylov solvers preconditioned by bAMG and BDDC. Average Newton iterations per time step (nit); average GMRES iterations per Newton iteration (lit); average CPU solution time per time step (time) in seconds. Performed on Galileo cluster.
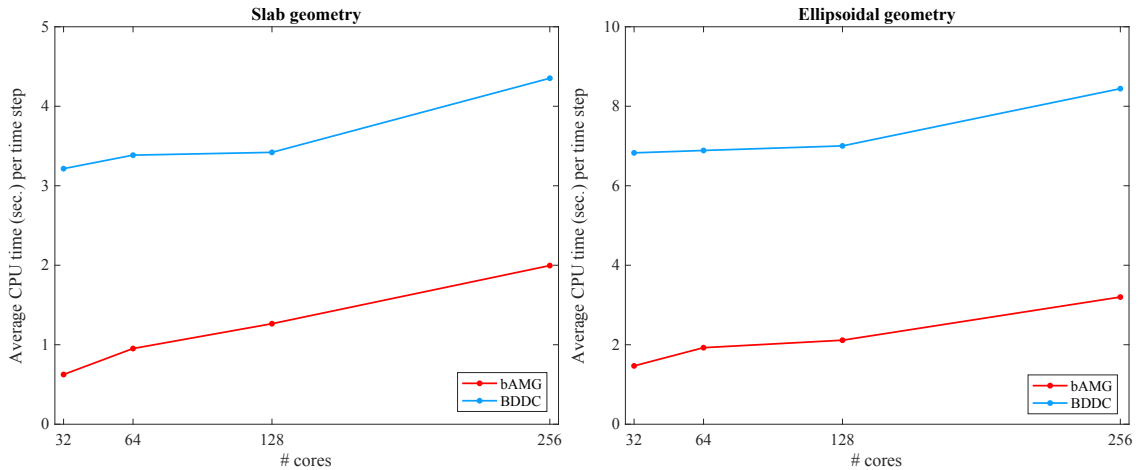
Figure 6.21: *Weak scalability on slab (left) and ellipsoidal (right) domains for the Bidomain coupled solver.* Local mesh of $12 \cdot 12 \cdot 12$ elements. Simulations of 2 ms of cardiac activation with $dt = 0.05$ ms (40 time steps). Comparison of average CPU time per time step, in seconds. Performed on Galileo cluster.

while bAMG is sub-optimal (see Fig. 6.22). Again, this can be explained by the low number of processors employed, thus by the high local problem sizes which increase the time spent for the LU factorization.

Optimality tests on slab and ellipsoidal domains. Tables 6.32 and 6.33 report the results of optimality experiments, for both slab and ellipsoid geometries.

We fix the number of subdomains to $4 \cdot 4 \cdot 4$ and we increase the local size H/h from 4 to 24, thus reducing the finite element size h. We consider both ρ-scaling (on top of each table) and deluxe scaling (at the bottom of each table) and we test the solver for increasing primal spaces: V includes only vertex constraints, V+E includes vertex and edge constraints, and V+E+F includes vertex, edge and face constraints. The deluxe scaling tests are up to a local size of $20 \cdot 20 \cdot 20$ elements, due to limited computational resources. Similar results hold for both geometries. The

Slab domain

subds.	bAMG				BDDC			
	nit	lit	time	S_{32}	nit	lit	time	S_{32}
32	1	183	9.5	-	1	20	98.7	-
64	1	196	5.4	1.7 (2)	1	23	30.8	3.2 (2)
128	1	201	2.9	3.2 (4)	1	17	10.7	9.1 (4)
256	1	232	1.9	4.9 (8)	1	19	3.7	26.3 (8)

Ellipsoidal domain

subds.	bAMG				BDDC			
	nit	lit	time	S_{32}	nit	lit	time	S_{32}
32	2	187	15.1	-	2	37	189.3	-
64	2	222	9.2	1.6 (2)	2	44	59.1	3.2 (2)
128	2	240	5.3	2.8 (4)	2	29	20.1	9.4 (4)
256	2	280	3.2	4.7 (8)	2	46	10.2	18.5 (8)

Table 6.31: *Strong scalability on slab (top) and ellipsoidal (bottom) domains for the Bidomain coupled solver.* Global mesh of $128 \cdot 128 \cdot 24$ elements, 1,248,075 dofs. Simulations of 2 ms of cardiac activation with $dt = 0.05$ ms, for a total amount fo 40 time steps. Comparison of Newton-Krylov solvers with bAMG and BDDC preconditioners. Average Newton iterations per time step (nit); average GMRES iterations per Newton iteration (lit); average CPU solution time per time step (time) in seconds; parallel speedup w.r.t. 32 processors S_{32}, with ideal speedup in brackets. Performed on Galileo cluster.
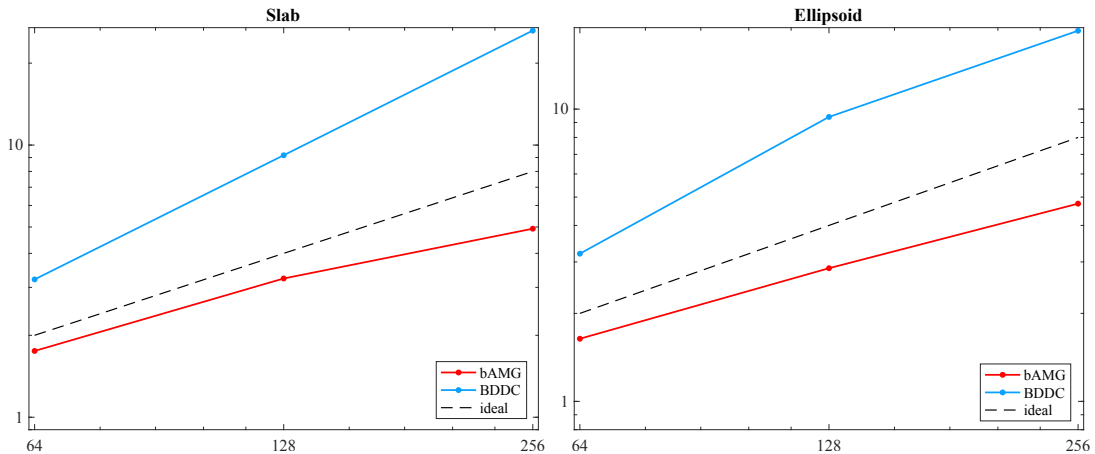
Figure 6.22: *Strong scalability on slab (left) and ellipsoidal (right) domains for the Bidomain coupled solver.* Global mesh of $128 \cdot 128 \cdot 24$, 1,248,075 dofs. Simulations of 2 ms of cardiac activation with $dt = 0.05$ ms, for a total amount fo 40 time steps. Comparison of actual parallel speedup (ideal speedup dotted). Performed on Galileo cluster.

deluxe solver seems to be more robust while increasing the local mesh size, both in terms of average linear iterations (see also Figure 6.23) and average CPU time per time step.

Strong scaling on a full activation-recovery interval.   Lastly, we compare the performance of the dual-primal and the multigrid preconditioners during a full activation-recovery interval.

We fix the number of subdomains to $128 = 8 \cdot 8 \cdot 2$ and the global mesh size to $128 \cdot 96 \cdot 24$, considering local problems of 8,619 dofs. We consider a time interval of $[0, 200]$ ms for a total of 4000 time steps for a portion of ellipsoid defined by $\varphi_{\min} = -\pi/2$, $\varphi_{\max} = \pi/2$, $\theta_{\min} = -3/8\pi$ and $\theta_{\max} = \pi/8$, while on the slab of dimensions $1.92 \times 0.96 \times 0.96$ cm^3 we perform the tests for 3000 time steps, on the time interval $[0, 150]$ ms.

Fig. 6.24 reports the trend of the average number of linear iteration per time step during the simulation. We notice a huge difference between bAMG and BDDC preconditioners, with

H/h	ρ-scaling V			V+E			V+E+F		
	nlit	lit	time	nlit	lit	time	nlit	lit	time
4	1	29	0.2	1	16	0.1	1	18	0.2
8	1	48	0.8	1	17	0.7	1	16	0.6
12	1	65	4.5	1	19	3.4	1	18	3.6
16	1	77	20.6	1	21	15.8	1	19	16.5
20	1	99	70.0	1	23	52.5	1	21	54.4
24	1	219	256.2	1	24	156.4	1	22	158.6

H/h	deluxe scaling V			V+E			V+E+F		
	nlit	lit	time	nlit	lit	time	nlit	lit	time
4	1	29	0.3	1	14	0.2	1	16	0.2
8	1	46	1.1	1	15	0.6	1	15	0.6
12	1	59	5.4	1	17	3.2	1	15	3.1
16	1	67	21.8	1	17	13.3	1	16	13.2
20	1	73	66.7	1	18	42.6	1	17	42.5

Table 6.32: *Optimality tests on slab domain for the Bidomain coupled solver.* $4 \cdot 4 \cdot 4$ subdomains, increasing local size from $4 \cdot 4 \cdot 4$ to $24 \cdot 24 \cdot 24$ (up to $20 \cdot 20 \cdot 20$ for the deluxe scaling). Comparison between different scalings and different primal sets (V = vertices, E = edge averages, F = face averages). Average non-linear iterations (nlit), average number of linear iterations (lit) and average CPU time in seconds per time step. Performed on Galileo cluster.

H/h	ρ-scaling V			V+E			V+E+F		
	nlit	lit	time	nlit	lit	time	nlit	lit	time
4	2	57	0.3	2	27	0.9	-	-	-
8	2	113	1.6	2	58	1.4	2	56	1.4
12	2	139	8.7	2	67	6.4	2	65	4.5
16	2	228	47.2	2	75	11.9	2	75	11.6
20	2	277	144.6	2	82	34.2	2	81	32.5
24	2	477	494.5	2	75	83.1	2	87	80.5

H/h	deluxe scaling V			V+E			V+E+F		
	nlit	lit	time	nlit	lit	time	nlit	lit	time
4	2	45	0.3	2	25	0.3	2	24	0.3
8	2	86	1.8	2	40	1.2	2	40	1.2
12	2	118	9.8	2	53	6.9	2	46	6.3
16	2	138	39.8	2	50	25.1	2	51	25.2
20	2	172	130.8	2	60	81.6	2	62	83.5

Table 6.33: *Optimality tests on ellipsoidal domain for the Bidomain coupled solver.* $4 \cdot 4 \cdot 4$ subdomains, increasing local size from $4 \cdot 4 \cdot 4$ to $24 \cdot 24 \cdot 24$ (up to $20 \cdot 20 \cdot 20$ for the deluxe scaling). Comparison between different scalings and different primal sets (V = vertices, E = edge averages, F = face averages). Average non-linear iterations (nlit), average number of linear iterations (lit) and average CPU time in seconds per time step. Performed on Galileo cluster.

a reduction of more than 85% for the latter. The average number of linear iterations remains bounded during the test. We observe a significant difference in performance of bAMG between Tables 6.31 and 6.34. This can be explained by the different geometry considered: in Table 6.34 we enlarge the portion of truncated ellipsoid considered, both in height and in width, and this can
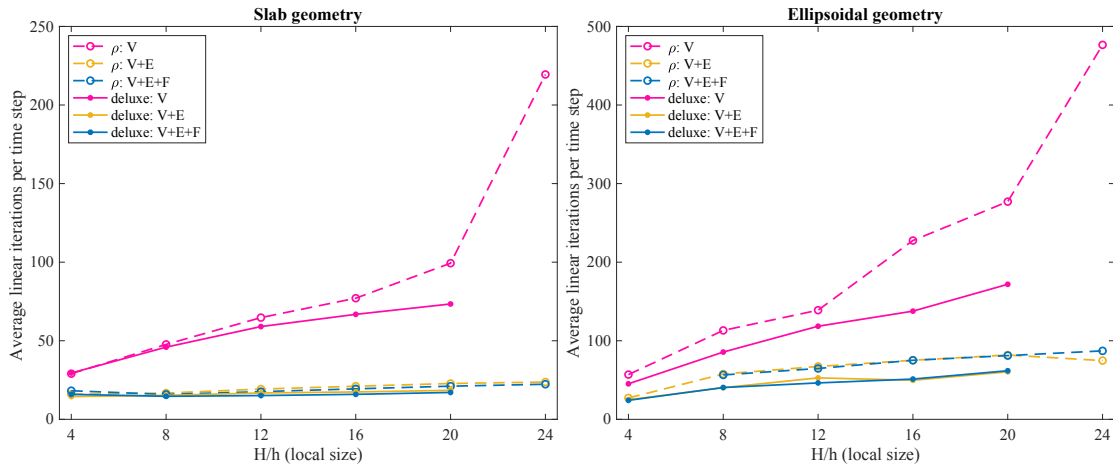
Figure 6.23: *Optimality tests on slab (left) and ellipsoidal (right) domains for the Bidomain coupled solver.* Different scalings (dash-dotted ρ-scaling, continuous *deluxe* scaling) and primal sets (V = vertices, E = edge averages, F = face averages). Slab (left) and ellipsoidal (right) domains, $4 \cdot 4 \cdot 4$ subdomains, increasing local size from $4 \cdot 4 \cdot 4$ to $24 \cdot 24 \cdot 24$. Average number of linear iterations per time step. Performed on Galileo cluster.

affect the performance of the solver.

Both preconditioned solvers seem to affected by the different stages of the action potential: an initial peak during the activation phase is followed by a constant elevated number of linear iterations as the electric signal propagates in the cardiac tissue, ending with a lower - but always constant - number of linear iterations during the resting phase.

Despite similar qualitative trends between the two geometries, it is undeniable that there are differences from the quantitative point of view, due to the complexity of the domain taken in consideration. Comparable performances in terms of average CPU time per time step (see Table 6.34) hold for both preconditioners.
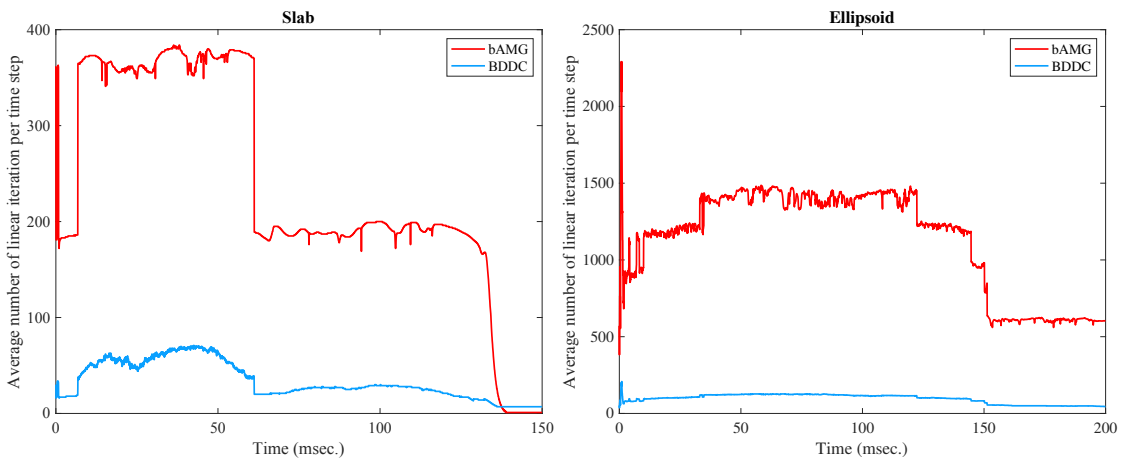
Figure 6.24: *Strong scalability for the Bidomain coupled solver.* Time interval $[0, 150]$ms, 3000 time steps for the slab (on the left) and time interval $[0, 200]$ms, 4000 time steps for the ellipsoid (on the right). Fixed number of subdomains $8 \cdot 8 \cdot 2$ and fixed global mesh $128 \cdot 96 \cdot 24$. Comparison between bAMG and BDDC average number of linear iterations per time step. Performed on Galileo cluster.

	procs	dofs	bAMG			BDDC		
			nlit	lit	time	nlit	lit	time
slab	128	8,619	1	235	3.65	1	34	20.66
ellipsoid	128	8,619	6	1,134	9.54	6	96	8.27

Table 6.34: *Strong scalability for the Bidomain coupled solver.* Time interval $[0, 150]$ ms, 3000 time steps for the slab and time interval $[0, 200]$ ms, 4000 time steps for the ellipsoidal domain. Fixed number of subdomains $8 \cdot 8 \cdot 2$ and fixed global mesh $128 \cdot 96 \cdot 24$. Comparison of average Newton steps, average linear iterations and average CPU time (in sec.) per time step. Performed on Galileo cluster.

Chapter 7

Conclusions

In this Thesis, we have presented and theoretically analyzed two different strategies for the solution of the nonlinear system arising from fully implicit time discretization of the Bidomain model. These discretization schemes avoid numerical stability issues and provide a valid alternative to operator splittings or semi-implicit time discretizations. In particular, we have explored the potential of dual-primal Domain Decomposition (DD) preconditioners in the improvement of the convergence.

The first strategy we have investigated relies on a decoupling (or segregated) approach, where at each time step the ionic model is solved first, and its solution vector is then employed within the Bidomain system. Instead of applying a nonlinear DD approach, where the decomposition is made before the linearization, we wrap the nonlinear system within a Newton method and we linearize the algebraic system, resulting in a symmetric problem. We have constructed and analyzed BDDC and FETI-DP methods for the Jacobian linear system, in order to accelerate the convergence of the Preconditioned Conjugate Gradient method. We have proved a novel theoretical bound for the projection operator, using the deluxe scaling; this bound has been employed in the proofs of the upper bound for the condition number of the preconditioned operator, for both dual-primal algorithms, showing a theoretical quasi-optimality property.

Secondly, we have explored a coupled (or monolithic) solution strategy, where the ionic model is solved all-at-once with the Bidomain system. In this case, the Jacobian system, arising from the linearization of the coupled problem, is non-symmetric and we are forced to employ the Generalized Minimal Residual (GMRES) method for its solution. In the literature, BDDC preconditioners for non-symmetric problems have not been largely studied yet: therefore we provide an *ad-hoc* theoretical analysis for the convergence of the solver. This analysis exploits a classical result for the upper bound for the residual of GMRES iterations, together with a proof technique recently proposed for BDDC applied to advection-diffusion problems.

Both these quasi-optimality conditions have been validated numerically through extensive parallel experiments. We have tested the robustness of the proposed solvers also in case of realistic human ventricular ionic models, such as LR1 and TP06, as well as in presence of an ischemic transmural region, meaning jumps in the diffusion coefficients. The results indicate scalability and robustness of the solvers, as well as optimality.

The results presented in this Thesis enlarge the class of solvers for fully implicit time discretizations of the Bidomain model; surely the nonlinear approach requires attentions, in order to reduce the computational workload. In this perspective, optimization of the codes and employment of quasi-Newton methods should improve the numerical performance.

Possible future discussions should be devoted to the development and theoretical analysis of nonlinear dual-primal DD solvers for this system, and a numerical comparison of the performances between these two nonlinear approaches, both for segregated and monolithic solution strategies.

Potential interesting applications could be the employment of these nonlinear solvers in the simulation of cardiac diseases, such as arrythmias or ischemic events.

Appendix A

Ionic models

We report here the equations and the constants values for the ionic models described in Chapter 2 and implemented in the simulations presented in Chap. 6. The original formulations and detailed explanation can be found in the works [80, 114, 115].

We remind the reader that, given a gating variable y, its dynamics is described by

$$\frac{dy}{dt} = \alpha_y(1-y) - \beta_y \, y$$

and by setting

$$y_\infty = \frac{\alpha_y}{\alpha_y + \beta_y}, \qquad \tau_y = \frac{1}{\alpha_y + \beta_y},$$

we can rewrite the gating equation as $\frac{dy}{dt} = \frac{y_\infty - y}{\tau_y}$, whose solution can be easily obtained as $y(t) = y_\infty \cdot \left(1 - e^{-t/\tau_y}\right)$. Moreover, with the notation $E_X = \frac{RT}{F} \log\left(\frac{[\text{X}]_e}{[\text{X}]_i}\right)$ we indicate the reverse potential of ion X, being R, T and F the universal gas constant, the absolute temperature and the Faraday constant respectively.

A.1 Luo-Rudy phase 1

The ionic concentrations for standard preparations are

$$[\text{K}]_e = 5.4 \text{ mM} \qquad [\text{Na}]_e = 140 \text{ mM} \qquad [\text{Ca}]_e = 1.8 \text{ mM}$$
$$[\text{K}]_i = 145 \text{ mM} \qquad [\text{Na}]_i = 18 \text{ mM} \qquad [\text{Ca}]_i = 2 \cdot 10^{-4} \text{ mM}$$

Inward currents

Fast sodium current
$$\text{I}_{\text{Na}} = 23 \, m^3 h j (v - E_{\text{Na}}).$$

For $v \geq -40$ mV

$$\alpha_h = \alpha_j = 0.0$$

$$\beta_h = \frac{1}{0.13 \left(1 + e^{(v+10.66)/-11.1}\right)}$$

$$\beta_j = \frac{0.3 \cdot e^{-2.535 \cdot 10^{-7} v}}{1 + e^{-0.1(v+32)}}$$

For $v \leq -40$ mV

$$\alpha_h = 0.135 \cdot e^{(80+v)/-6.8}$$

$$\alpha_j = \frac{\left(-1.2714 \cdot 10^5 \cdot e^{0.2444v} - 3.474 \cdot 10^{-5} \cdot e^{-0.04391v}\right)(v + 37.78)}{1 + e^{0.311(v+79.23)}}$$

$$\beta_h = 3.56 \cdot e^{0.079v} + 3.1 \cdot 10^5 \cdot e^{0.35v}$$

$$\beta_j = \frac{0.1212 \cdot e^{-0.01052v}}{1 + e^{-0.1(v+47.13)}}$$

For all range of v

$$\alpha_m = \frac{0.32(v + 47.13)}{1 - e^{-0.1(v+47.13)}} \qquad \beta_m = 0.08 \cdot e^{-v/11}$$

Slow inward current

$$\text{I}_{\text{si}} = 0.9 \ d \ f(v - E_{\text{si}}),$$

with $E_{\text{si}} = 7.7 - 13.0287 \log\left([\text{Ca}]_i\right)$

$$\alpha_d = \frac{0.095 \cdot e^{-0.01(v-5)}}{1 + e^{-0.072(v-5)}} \qquad \alpha_f = \frac{0.012 \cdot e^{-0.008(v+28)}}{1 + e^{0.15(v+28)}}$$

$$\beta_d = \frac{0.07 \cdot e^{-0.017(v+44)}}{1 + e^{0.05(v+44)}} \qquad \beta_f = \frac{0.0065 \cdot e^{-0.02(v+30)}}{1 + e^{-0.2(v+30)}}$$

Calcium uptake: $\dfrac{d[\text{Ca}]_i}{dt} = -10^{-4} \cdot \text{I}_{\text{si}} + 0.07\left(10^{-4} - [\text{Ca}]_i\right)$

Outward currents

Time-dependent potassium current

$$\text{I}_{\text{K}} = G_K \cdot X \cdot X_i \cdot (v - E_{\text{K}}), \qquad \text{with } G_K = 0.282\sqrt{\frac{[\text{K}]_e}{5.4}}.$$

$$X_i = \begin{cases} 2.837 \dfrac{e^{0.04(v+77)} - 1}{(v + 77) \cdot e^{0.04(v+35)}} & \text{for } v > -100\text{mV} \\ 1 & \text{for } v \le -100\text{mV} \end{cases}$$

$$\alpha_X = \frac{0.0005 \cdot e^{0.083(v+50)}}{1 + e^{0.057(v+50)}} \qquad \beta_X = \frac{0.0013 \cdot e^{-0.06(v+20)}}{1 + e^{-0.04(v+20)}}$$

Time-independent potassium current

$$\text{I}_{\text{K1}} = G_{K1} \cdot K1_\infty \cdot (v - E_{\text{K1}}), \qquad \text{with } G_{K1} = 0.6047\sqrt{\frac{[\text{K}]_e}{5.4}}.$$

$$\alpha_{K1} = \frac{1.02}{1 + e^{0.2385(v-E_{\text{K1}}-59.215)}} \qquad \beta_{K1} = \frac{0.49124 \cdot e^{0.08032(v-E_{\text{K1}}+5.476)} + e^{0.06175(v-E_{\text{K1}}-594.31)}}{1 + e^{-0.5143(v-E_{\text{K1}}+4.753)}}$$

Plateau potassium current

$$\text{I}_{\text{Kp}} = 0.0183 \cdot Kp \cdot (v - E_{\text{Kp}}), \qquad Kp = \frac{1}{1 + e^{(7.488-v)/5.98}} \qquad \text{with } E_{\text{Kp}} = E_{\text{K1}}.$$

Background current

$$\text{I}_b = 003921(v + 59.87).$$

A.2   Ten Tusscher - Panfilov 2006

This model is structurally the same as the model from 2004 (we refer to [114, Table 1] for all the numerical constants) with few modifications in the calcium dynamics, in the L-type Ca^{2+} and in the slow delayed rectifier currents. In this case, the reverse potential for the slow delayed rectifier current is in the form $E_{Ks} = \frac{RT}{F} \log\left(\frac{K_e + p_{KNa}Na_e}{K_i + p_{KNa}Na_i}\right)$.

.

Fast Na$^+$ current

$$I_{Na} = G_{Na}m^3hj(v - E_{Na})$$

$$m_\infty = \frac{1}{\left(1 + e^{(-56.86-v)/9.03}\right)^2}$$

$$\alpha_m = \frac{1}{1 + e^{(-60-v)/5}}$$

$$\beta_m = \frac{0.1}{1 + e^{(+35)/5}} + \frac{0.1}{1 + e^{(v-50)/200}}$$

$$\tau_m = \alpha_m\beta_m$$

$$h_\infty = \frac{1}{\left(1 + e^{(v+71.55)/7.43}\right)^2}$$

$$\alpha_h = \begin{cases} 0.0 & v \geq -40 \\ 0.057 \cdot e^{-(v+80)/6.8} & \text{otherwise} \end{cases}$$

$$\beta_m = \begin{cases} \dfrac{0.77}{0.13\left(1 + e^{-(v+10.66)/11.1}\right)} & v \geq -40 \\ 2.7 \cdot e^{0.079v} + 3.1 10^5 \cdot e^{0.3485v} \end{cases}$$

$$\tau_m = \frac{1}{\alpha_m\beta_m}$$

$$j_\infty = \frac{1}{1\left(1 + e^{(v+71.55)/7.43}\right)^2}$$

$$\alpha_j = \begin{cases} 0.0 & v \geq -40 \\ \dfrac{\left(\begin{matrix} -2.5428 \cdot 10^4 \cdot e^{0.2444v} - \\ 6.948 \cdot 10^{-6} \cdot e^{-0.04391v} \end{matrix}\right)(v + 37.78)}{1 + e^{0.311(v+79.23)}} \end{cases}$$

$$\beta_j = \begin{cases} \dfrac{0.6 \cdot e^{0.057v}}{1 + e^{-0.1(v+32)}} & v \geq -40 \\ \dfrac{0.0242 \cdot e^{-0.01052v}}{1 + e^{-0.1378(v+40.14)}} & \text{otherwise} \end{cases}$$

$$\tau_m = \frac{1}{\alpha_m\beta_m}$$

L-type Ca^{2+} current

$$I_{CaL} = G_{CaL}d\,f\,f_2\,f_{cass}4\frac{(v-15)F^2}{RT} \times$$
$$\frac{0.25Ca_{SS}e^{2(v-15)F/RT} - Ca_o}{e^{2(v-15)F/RT} - 1}$$

$$d_\infty = \frac{1}{1 + e^{(-8-v)/7.5}}$$

$$\alpha_d = \frac{1.4}{1 + e^{(-35-v)/13}} + 0.25$$

$$\beta_d = \frac{1.4}{1 + e^{(v+5)/5}}$$

$$\gamma_d = \frac{1}{1 + e^{(50-v)/20}}$$

$$\tau_d = \alpha_d\beta_d + \gamma_d$$

$$f_\infty = \frac{1}{1 + e^{(v+20)/7}}$$

$$\alpha_f = 1102.5 \cdot e^{-\left(\frac{v+27}{15}\right)^2}$$

$$\beta_f = \frac{200}{1 + e^{(13-v)/10}}$$

$$\gamma_f = \frac{180}{1 + e^{(v+30)/10}} + 20$$

$$\tau_f = \alpha_f + \beta_f + \gamma_f$$

$$f_{2\infty} = \frac{0.67}{1 + e^{(v+35)/7}} + 0.33$$

$$\alpha_{f2} = 600 \cdot e^{-\frac{(v+25)^2}{170}}$$

$$\beta_{f2} = \frac{31}{1 + e^{(25-v)/10}}$$

$$\gamma_{f2} = \frac{16}{1 + e^{(v+30)/10}}$$

$$\tau_{f2} = \alpha_{f2} + \beta_{f2} + \gamma_{f2}$$

$$f_{cass\infty} = \frac{0.6}{1 + \left(\frac{Ca_{SS}}{0.05}\right)^2} + 0.4$$

$$\tau_{fcass} = \frac{80}{1 + \left(\frac{Ca_{SS}}{0.05}\right)^2} + 2$$

Transient outward current

$$I_{to} = G_{to}rs(v - E_K)$$

For all cell types

$$r_\infty = \frac{1}{1 + e^{(20-v)/6}}$$

$$\tau_r = 9.5 \cdot e^{-(v+40)^2/1800} + 0.8$$

For epicardial and M cells

$$s_\infty = \frac{1}{1 + e^{(v+20)/5}}$$

$$\tau_s = 8.5 \cdot e^{-(v+45)^2/320} + \frac{5}{1 + e^{(v-20)/5}} + 3$$

For endocardial cells

$$s_\infty = \frac{1}{1 + e^{(v+28)/5}}$$

$$\tau_s = 10^3 \cdot e^{-(v+67)^2/1000} + 8$$

Slow delayed rectifier current

$$I_{Ks} = G_{Ks}x_s^2(v - E_{Ks})$$

$$x_{s\infty} = \frac{1}{1 + e^{(-5-v)/14}}$$

$$\alpha_{xs} = \frac{1400}{\sqrt{1 + e^{(5-v)/6}}}$$

$$\beta_{xs} = \frac{1}{1 + e^{(v-35)/15}}$$

$$\tau_{xs} = \alpha_{f2}\beta_{f2} + 80$$

Rapid delayed rectifier current

$$I_{Kr} = G_{Kr}\sqrt{\frac{K_o}{5.4}}x_{r1}x_{r2}(v - E_K)$$

$$x_{r1\infty} = \frac{1}{1 + e^{(-26-v)/7}}$$

$$\alpha_{xr1} = \frac{450}{1 + e^{(-45-v)/10}}$$

$$\beta_{xr1} = \frac{6}{1 + e^{(v+30)/11.5}}$$

$$\tau_{xr1} = \alpha_{xr1}\beta_{xr1}$$

$$x_{r2\infty} = \frac{1}{1 + e^{(v+88)/24}}$$

$$\alpha_{xr2} = \frac{3}{1 + e^{(-60-v)/20}}$$

$$\beta_{xr2} = \frac{1.12}{1 + e^{(v-60)/20}}$$

$$\tau_{xr2} = \alpha_{xr2}\beta_{xr2}$$

Inward rectifier K^+ current

$$I_{K1} = G_{K1}\sqrt{\frac{K_e}{5.4}}x_{K1\infty}(v - E_K)$$

$$\alpha_{K1} = \frac{0.1}{1 + e^{0.06(v-E_K-200)}}$$

$$\beta_{k1} = \frac{3 \cdot e^{0.0002(v-E_K+100)} + e^{0.1(v-E_K-10)}}{1 + e^{-0.5(v-E_K)}}$$

$$x_{K1\infty} = \frac{\alpha_{K1}}{\alpha_{K1} + \beta_{K1}}$$

Na^+ / Ca^{2+} echanger current

$$I_{NaCa} = k_{NaCa}\frac{e^{\gamma vF/RT}Na_i{}^3Ca_e - e^{(\gamma-1)vF/RT}Na_e{}^3Ca_i\alpha}{\left(K_{mNai}^3 + Na_e{}^3\right)\left(K_{mCa} + Ca_e\right)\left(1 + k_{sat}e^{(\gamma-1)vF/RT}\right)}$$

Na^+ / K^+ pump current

$$I_{NaK} = P_{NaK} \times$$

$$\frac{K_e Na_i}{(K_e + K_{mK})(Na_i + K_{mNa})\left(1 + 0.1245e^{-0.1vF/RT} + 0.0353e^{-vF/RT}\right)}$$

$$I_{pCa} = G_{pCa}\frac{Ca_i}{K_{pCa} + Ca_i}$$

$$I_{pK} = G_{pK}\frac{v - E_K}{1 + e^{(25-v)/5.98}}$$

Background currents

$$I_{bNa} = G_{bNa}(v - E_{Na})$$

$$I_{bCa} = G_{bCa}(v - E_{Ca})$$

Calcium dynamics

$$I_{leak} = v_{leak}(Ca_{SR} - Ca_i)$$

$$I_{up} = \frac{v_{maxup}}{1 + K_{up}^2/Ca_i{}^2}$$

$$I_{rel} = v_{rel}(Ca_{SR} - Ca_{SS})$$

$$I_{xfer} = v_{xfer}(Ca_{SS} - Ca_i)$$

$$O = \frac{k_1 Ca_{SS}{}^2\bar{R}}{k_3 + k_1 Ca_{SS}{}^2}$$

$$\frac{d\bar{R}}{dt} = -k_2 Ca_{SS}\bar{R} + k_4(1 - \bar{R})$$

$$k_1 = \frac{k_{1'}}{k_{casr}}$$

$$k_2 = k_{2'}k_{casr}$$

$$k_{casr} = \max_{sr} - \frac{\max_{sr} - \min_{sr}}{1 + (EC/Ca_{SR})^2}$$

$$Ca_{ibufc} = \frac{Ca_i \times Buf_c}{Ca_i + K_{bufc}}$$

$$\frac{d\mathrm{Ca}_{\mathrm{itotal}}}{dt} = -\frac{\mathrm{I}_{\mathrm{bCa}} + \mathrm{I}_{\mathrm{pCa}} - 2\mathrm{I}_{\mathrm{NaCa}}}{2v_c F} + \frac{v_{\mathrm{sr}}}{v_{\mathrm{c}}}\left(\mathrm{I}_{\mathrm{leak}} - \mathrm{I}_{\mathrm{up}}\right) + \mathrm{I}_{\mathrm{xfer}}$$

$$\mathrm{Ca}_{\mathrm{srbufsr}} = \frac{\mathrm{Ca}_{\mathrm{sr}} \times \mathrm{Buf}_{\mathrm{sr}}}{\mathrm{Ca}_{\mathrm{sr}} + K_{\mathrm{bufsr}}}$$

$$\frac{d\mathrm{Ca}_{\mathrm{SRtotal}}}{dt} = \mathrm{I}_{\mathrm{up}} - \mathrm{I}_{\mathrm{leak}} - \mathrm{I}_{\mathrm{rel}}$$

$$\mathrm{Ca}_{\mathrm{ssbufss}} = \frac{\mathrm{Ca}_{\mathrm{ss}} \times \mathrm{Buf}_{\mathrm{ss}}}{\mathrm{Ca}_{\mathrm{ss}} + K_{\mathrm{bufss}}}$$

$$\frac{d\mathrm{Ca}_{\mathrm{SStotal}}}{dt} = -\frac{\mathrm{I}_{\mathrm{CaL}}}{2v_{SS} F} + \frac{v_{\mathrm{sr}}}{v_{\mathrm{ss}}}\mathrm{I}_{\mathrm{rel}} - \frac{v_{\mathrm{c}}}{v_{\mathrm{ss}}}\mathrm{I}_{\mathrm{xfer}}$$

Sodium and Potassium dynamics

$$\frac{d\mathrm{Na}_i}{dt} = -\frac{\mathrm{I}_{\mathrm{Na}} + \mathrm{I}_{\mathrm{bNa}} + 3\mathrm{I}_{\mathrm{NaK}} + 3\mathrm{I}_{\mathrm{NaCa}}}{v_{\mathrm{c}} F}$$

$$\frac{d\mathrm{K}_i}{dt} = -\frac{\mathrm{I}_{\mathrm{K1}} + \mathrm{I}_{\mathrm{to}} + \mathrm{I}_{\mathrm{Kr}} + \mathrm{I}_{\mathrm{Ks}} - 2\mathrm{I}_{\mathrm{NaK}} + \mathrm{I}_{\mathrm{pK}} + \mathrm{I}_{\mathrm{stim}} - \mathrm{I}_{\mathrm{ax}}}{v_{\mathrm{c}} F}$$

Bibliography

[1] R. R. Aliev and A. V. Panfilov. "A simple two-variable model of cardiac excitation". In: *Chaos, Solitons & Fractals* 7.3 (1996), pp. 293–301.

[2] C. M. Augustin, G. A. Holzapfel, and O. Steinbach. "Classical and all-floating FETI methods for the simulation of arterial tissues". In: *International journal for numerical methods in engineering* 99.4 (2014), pp. 290–312.

[3] S. Balay et al. "PETSc users manual". In: (2019).

[4] G. W. Beeler and H. Reuter. "Reconstruction of the action potential of ventricular myocardial fibres". In: *The Journal of physiology* 268.1 (1977), pp. 177–210.

[5] L. Beirão Da Veiga et al. "Adaptive selection of primal constraints for isogeometric BDDC deluxe preconditioners". In: *SIAM Journal on Scientific Computing* 39.1 (2017), A281–A302.

[6] L. Beirão da Veiga et al. "BDDC preconditioners for isogeometric analysis". In: *Mathematical Models and Methods in Applied Sciences* 23.06 (2013), pp. 1099–1142.

[7] L. Beirão Da Veiga et al. "Isogeometric BDDC preconditioners with deluxe scaling". In: *SIAM Journal on Scientific Computing* 36.3 (2014), A1118–A1139.

[8] M. Bendahmane and K. H. Karlsen. "Convergence of a finite volume scheme for the bidomain model of cardiac tissue". In: *Applied numerical mathematics* 59.9 (2009), pp. 2266–2284.

[9] D. Bers. *Excitation-contraction coupling and cardiac contractile force*. Vol. 237. Springer Science & Business Media, 2001.

[10] S. Bertoluzza, M. Pennacchio, and D. Prada. "BDDC and FETI-DP for the virtual element method". In: *Calcolo* 54.4 (2017), pp. 1565–1593.

[11] R. Bordas et al. "Simulation of cardiac electrophysiology on next-generation high-performance computers". In: *Philosophical Transactions of the Royal Society A: Mathematical, Physical and Engineering Sciences* 367.1895 (2009), pp. 1951–1969.

[12] Y. Bourgault, Y. Coudiere, and C. Pierre. "Existence and uniqueness of the solution for the bidomain model used in cardiac electrophysiology". In: *Nonlinear analysis: Real world applications* 10.1 (2009), pp. 458–482.

[13] D. Brands et al. "Modelling and convergence in arterial wall simulations using a parallel FETI solution strategy". In: *Computer Methods in Biomechanics and Biomedical Engineering* 11.5 (2008), pp. 569–583.

[14] S. Brenner and R. Scott. *The mathematical theory of finite element methods*. Vol. 15. Springer Science & Business Media, 2007.

[15] M. Buist et al. "A deformable finite element derived finite difference method for cardiac activation problems". In: *Annals of biomedical engineering* 31.5 (2003), pp. 577–588.

[16] X.-C. Cai et al. "Newton-Krylov-Schwarz methods in CFD". In: *Numerical methods for the Navier-Stokes equations*. Springer, 1994, pp. 17–30.

[17] X.-C. Cai et al. "Parallel Newton–Krylov–Schwarz algorithms for the transonic full potential equation". In: *SIAM Journal on Scientific Computing* 19.1 (1998), pp. 246–265.

[18] A. Carusi, K. Burrage, and B. Rodríguez. "Bridging experiments, models and simulations: an integrative approach to validation in computational cardiac electrophysiology". In: *American Journal of Physiology-Heart and Circulatory Physiology* (2012).

[19] N. Chamakuri, K. Kunisch, and G. Plank. "On boundary stimulation and optimal boundary control of the bidomain equations". In: *Mathematical biosciences* 245.2 (2013), pp. 206–215.

[20] L. A. Charawi. "Isogeometric overlapping Schwarz preconditioners for the bidomain reaction–diffusion system". In: *Computer Methods in Applied Mechanics and Engineering* 319 (2017), pp. 472–490.

[21] F. Chegini et al. "Efficient identification of scars using heterogeneous model hierarchies". In: *EP Europace* 23.Supplement_1 (2021), pp. i113–i122.

[22] H. Chen, X. Li, and Y. Wang. "A splitting preconditioner for a block two-by-two linear system with applications to the bidomain equations". In: *Journal of Computational and Applied Mathematics* 321 (2017), pp. 487–498.

[23] H. Chen, X. Li, and Y. Wang. "A two-parameter modified splitting preconditioner for the Bidomain equations". In: *Calcolo* 56.2 (2019), pp. 1–24.

[24] P. Colli Franzone, L. Pavarino, and S. Scacchi. "Joint influence of transmural heterogeneities and wall deformation on cardiac bioelectrical activity: A simulation study". In: *Mathematical biosciences* 280 (2016), pp. 71–86.

[25] P. Colli Franzone and L. F. Pavarino. "A parallel solver for reaction–diffusion systems in computational electrocardiology". In: *Mathematical models and methods in applied sciences* 14.06 (2004), pp. 883–911.

[26] P. Colli Franzone, L. F. Pavarino, and S. Scacchi. "A numerical study of scalable cardiac electro-mechanical solvers on HPC architectures". In: *Frontiers in physiology* 9 (2018), p. 268.

[27] P. Colli Franzone, L. F. Pavarino, and S. Scacchi. *Mathematical cardiac electrophysiology*. Vol. 13. Springer, 2014.

[28] P. Colli Franzone, L. F. Pavarino, and S. Scacchi. "Parallel multilevel solvers for the cardiac electro-mechanical coupling". In: *Applied Numerical Mathematics* 95 (2015), pp. 140–153.

[29] P. Colli Franzone and G. Savaré. "Degenerate evolution systems modeling the cardiac electric field at micro-and macroscopic level". In: (2002), pp. 49–78.

[30] P. Colli-Franzone et al. "Role of infarct scar dimensions, border zone repolarization properties and anisotropy in the origin and maintenance of cardiac reentry". In: *Mathematical biosciences* 315 (2019), p. 108228.

[31] R. Coronel et al. "Right ventricular fibrosis and conduction delay in a patient with clinical signs of Brugada syndrome: a combined electrophysiological, genetic, histopathologic, and computational study". In: *Circulation* 112.18 (2005), pp. 2769–2777.

[32] C. Corrado et al. "A work flow to build and validate patient specific left atrium electrophysiology models from catheter measurements". In: *Medical image analysis* 47 (2018), pp. 153–163.

[33] Y. Coudière and C. Pierre. "Stability and convergence of a finite volume method for two systems of reaction-diffusion equations in electro-cardiology". In: *Nonlinear analysis: real world applications* 7.4 (2006), pp. 916–935.

[34] J. Dhamala et al. "Spatially adaptive multi-scale optimization for local parameter estimation in cardiac electrophysiology". In: *IEEE transactions on medical imaging* 36.9 (2017), pp. 1966–1978.

[35] D. Di Francesco and D. Noble. "A model of cardiac electrical activity incorporating ionic pumps and concentration changes". In: *Philosophical Transactions of the Royal Society of London. B, Biological Sciences* 307.1133 (1985), pp. 353–398.

[36] T. Dickopf et al. "Design and analysis of a lightweight parallel adaptive scheme for the solution of the monodomain equation". In: *SIAM Journal on Scientific Computing* 36.2 (2014), pp. C163–C189.

[37] C. R. Dohrmann. "A preconditioner for substructuring based on constrained energy minimization". In: *SIAM Journal on Scientific Computing* 25.1 (2003), pp. 246–258.

[38] C. R. Dohrmann and O. B. Widlund. "A BDDC Algorithm with Deluxe Scaling for Three-Dimensional H (curl) Problems". In: *Communications on Pure and Applied Mathematics* 69.4 (2016), pp. 745–770.

[39] V. Dolean, P. Jolivet, and F. Nataf. *An introduction to domain decomposition methods: algorithms, theory, and parallel implementation.* SIAM, 2015.

[40] S. C. Eisenstat, H. C. Elman, and M. H. Schultz. "Variational iterative methods for nonsymmetric systems of linear equations". In: *SIAM Journal on Numerical Analysis* 20.2 (1983), pp. 345–357.

[41] R. D. Falgout and U. M. Yang. "hypre: A library of high performance preconditioners". In: *International Conference on Computational Science.* Springer. 2002, pp. 632–641.

[42] C. Farhat. "A Lagrange multiplier based divide and conquer finite element algorithm". In: *Computing Systems in Engineering* 2.2-3 (1991), pp. 149–156.

[43] C. Farhat. "A saddle-point principle domain decomposition method for the solution of solid mechanics problems". In: *Domain Decomposition Methods for Partial Differential Equations* (1992), pp. 271–292.

[44] C. Farhat, J. Li, and P. Avery. "A FETI-DP method for the parallel iterative solution of indefinite and complex-valued solid and shell vibration problems". In: *International Journal for Numerical Methods in Engineering* 63.3 (2005), pp. 398–427.

[45] C. Farhat, J. Mandel, and F. X. Roux. "Optimal convergence properties of the FETI domain decomposition method". In: *Computer methods in applied mechanics and engineering* 115.3-4 (1994), pp. 365–385.

[46] C. Farhat, K. Pierson, and M. Lesoinne. "The second generation FETI methods and their application to the parallel solution of large-scale linear and geometrically non-linear structural analysis problems". In: *Computer methods in applied mechanics and engineering* 184.2-4 (2000), pp. 333–374.

[47] C. Farhat and F.-X. Roux. "A method of finite element tearing and interconnecting and its parallel solution algorithm". In: *International journal for numerical methods in engineering* 32.6 (1991), pp. 1205–1227.

[48] C. Farhat et al. "FETI-DP: a dual–primal unified FETI method—part I: A faster alternative to the two-level FETI method". In: *International journal for numerical methods in engineering* 50.7 (2001), pp. 1523–1544.

[49] F. Fenton and A. Karma. "Vortex dynamics in three-dimensional continuous myocardium with fiber rotation: Filament instability and fibrillation". In: *Chaos: An Interdisciplinary Journal of Nonlinear Science* 8.1 (1998), pp. 20–47.

[50] G. Fischer et al. "A bidomain model based BEM-FEM coupling formulation for anisotropic cardiac tissue". In: *Annals of biomedical engineering* 28.10 (2000), pp. 1229–1243.

[51] R. FitzHugh. "Impulses and physiological states in theoretical models of nerve membrane". In: *Biophysical journal* 1.6 (1961), pp. 445–466.

[52] R. FitzHugh. "Mathematical models of excitation and propagation in nerve". In: *Biological engineering* (1969), pp. 1–85.

[53] S. Götschel et al. "Lossy compression in optimal control of cardiac defibrillation". In: *Journal of Scientific Computing* 60.1 (2014), pp. 35–59.

[54] T. Grandits et al. "PIEMAP: personalized inverse Eikonal model from cardiac electro-anatomical maps". In: *International Workshop on Statistical Atlases and Computational Models of the Heart.* Springer. 2020, pp. 76–86.

[55]   T. Grandits et al. "Learning atrial fiber orientations and conductivity tensors from in-
        tracardiac maps using physics-informed neural networks". In: *International Conference on
        Functional Imaging and Modeling of the Heart.* Springer. 2021, pp. 650–658.

[56]   M. Hanek, J. Šístek, and P. Burda. "An application of the BDDC method to the Navier-
        Stokes equations in 3-D cavity". In: *Programs and algorithms of numerical mathematics*
        (2015), pp. 77–85.

[57]   M. Hanek, J. Šístek, and P. Burda. "Multilevel BDDC for Incompressible Navier–Stokes
        Equations". In: *SIAM Journal on Scientific Computing* 42.6 (2020), pp. C359–C383.

[58]   D. M. Harrild and C. S. Henriquez. "A finite volume model of cardiac propagation". In:
        Annals of biomedical engineering 25.2 (1997), pp. 315–334.

[59]   A. L. Hodgkin and A. F. Huxley. "A quantitative description of membrane current and
        its application to conduction and excitation in nerve". In: *The Journal of physiology* 117.4
        (1952), pp. 500–544.

[60]   A. L. Hodgkin, A. F. Huxley, and B. Katz. "Measurement of current-voltage relations in
        the membrane of the giant axon of Loligo". In: *The Journal of physiology* 116.4 (1952),
        pp. 424–448.

[61]   A. L. Hodgkin and A. F. Huxley. "Currents carried by sodium and potassium ions through
        the membrane of the giant axon of Loligo". In: *The Journal of physiology* 116.4 (1952),
        pp. 449–472.

[62]   A. L. Hodgkin and A. F. Huxley. "The components of membrane conductance in the giant
        axon of Loligo". In: *The Journal of physiology* 116.4 (1952), pp. 473–496.

[63]   A. L. Hodgkin and A. F. Huxley. "The dual effect of membrane potential on sodium con-
        ductance in the giant axon of Loligo". In: *The Journal of physiology* 116.4 (1952), pp. 497–
        506.

[64]   N. M. M. Huynh. "Newton-Krylov-BDDC deluxe solvers for non-symmetric fully implicit
        time discretizations of the Bidomain model". In: *arXiv preprint arXiv:2102.08736* (2021).

[65]   N. M. M. Huynh, L. F. Pavarino, and S. Scacchi. "Parallel Newton-Krylov-BDDC and FETI-
        DP deluxe solvers for implicit time discretizations of the cardiac Bidomain equations". In:
        to appear in SIAM J. Sci. Comp.*, arXiv preprint arXiv:2101.02959* (2021).

[66]   V. Jacquemet and C. S. Henriquez. "Finite volume stiffness matrix for solving anisotropic
        cardiac propagation in 2-D and 3-D unstructured meshes". In: *IEEE transactions on biomed-
        ical engineering* 52.8 (2005), pp. 1490–1492.

[67]   Y. Jiang, R. Chen, and X.-C. Cai. "A highly parallel implicit domain decomposition method
        for the simulation of the left ventricle on unstructured meshes". In: *Computational Mechan-
        ics* 66.6 (2020), pp. 1461–1475.

[68]   J. P. Keener and J. Sneyd. *Mathematical physiology.* Vol. 1. Springer, 1998.

[69]   A. Klawonn and O. Rheinbach. "A parallel implementation of dual-primal FETI methods
        for three-dimensional linear elasticity using a transformation of basis". In: *SIAM Journal
        on Scientific Computing* 28.5 (2006), pp. 1886–1906.

[70]   A. Klawonn and O. Rheinbach. "Robust FETI-DP methods for heterogeneous three dimen-
        sional elasticity problems". In: *Computer Methods in Applied Mechanics and Engineering*
        196.8 (2007), pp. 1400–1414.

[71]   A. Klawonn and O. Rheinbach. "Highly scalable parallel domain decomposition methods
        with an application to biomechanics". In: *ZAMM-Journal of Applied Mathematics and Me-
        chanics/Zeitschrift für Angewandte Mathematik und Mechanik: Applied Mathematics and
        Mechanics* 90.1 (2010), pp. 5–32.

[72]   A. Klawonn and O. B. Widlund. "Dual-primal FETI methods for linear elasticity". In: *Com-
        munications on Pure and Applied Mathematics: A Journal Issued by the Courant Institute
        of Mathematical Sciences* 59.11 (2006), pp. 1523–1572.

[73] A. Klawonn, O. B. Widlund, and M. Dryja. "Dual-primal FETI methods for three-dimensional elliptic problems with heterogeneous coefficients". In: *SIAM Journal on Numerical Analysis* 40.1 (2002), pp. 159–179.

[74] A. Klawonn, O. B. Widlund, and M. Dryja. "Dual-Primal FETI methods with face constraints". In: *Recent developments in domain decomposition methods*. Springer, 2002, pp. 27–40.

[75] A. Klawonn et al. "Nonlinear FETI-DP and BDDC methods: a unified framework and parallel results". In: *SIAM Journal on Scientific Computing* 39.6 (2017), pp. C417–C451.

[76] I. J. LeGrice et al. "Laminar structure of the heart: ventricular myocyte arrangement and connective tissue architecture in the dog". In: *American Journal of Physiology-Heart and Circulatory Physiology* 269.2 (1995), H571–H582.

[77] J. Li and O. B. Widlund. "BDDC algorithms for incompressible Stokes equations". In: *SIAM journal on numerical analysis* 44.6 (2006), pp. 2432–2455.

[78] J. Li and O. B. Widlund. "FETI-DP, BDDC, and block Cholesky methods". In: *International journal for numerical methods in engineering* 66.2 (2006), pp. 250–271.

[79] L. Liu, D. E. Keyes, and R. Krause. "A note on adaptive nonlinear preconditioning techniques". In: *SIAM Journal on Scientific Computing* 40.2 (2018), A1171–A1186.

[80] C.-H. Luo and Y. Rudy. "A model of the ventricular cardiac action potential. Depolarization, repolarization, and their interaction." In: *Circulation research* 68.6 (1991), pp. 1501–1526.

[81] C.-H. Luo and Y. Rudy. "A dynamic model of the cardiac ventricular action potential. I. Simulations of ionic currents and concentration changes." In: *Circulation research* 74.6 (1994), pp. 1071–1096.

[82] J. Mandel and C. R. Dohrmann. "Convergence of a balancing domain decomposition by constraints and energy minimization". In: *Numerical linear algebra with applications* 10.7 (2003), pp. 639–659.

[83] J. Mandel, C. R. Dohrmann, and R. Tezaur. "An algebraic theory for primal and dual substructuring methods by constraints". In: *Applied numerical mathematics* 54.2 (2005), pp. 167–193.

[84] J. Mandel and R. Tezaur. "Convergence of a substructuring method with Lagrange multipliers". In: *Numerische Mathematik* 73.4 (1996), pp. 473–487.

[85] J. Mandel and R. Tezaur. "On the convergence of a dual-primal substructuring method". In: *Numerische Mathematik* 88.3 (2001), pp. 543–558.

[86] C. Mendonca Costa et al. "Modeling the electrophysiological properties of the infarct border zone". In: *Frontiers in physiology* 9 (2018), p. 356.

[87] C. Morris and H. Lecar. "Voltage oscillations in the barnacle giant muscle fiber". In: *Biophysical journal* 35.1 (1981), pp. 193–213.

[88] M. Munteanu and L. F. Pavarino. "Decoupled Schwarz algorithms for implicit discretizations of nonlinear monodomain and bidomain systems". In: *Mathematical Models and Methods in Applied Sciences* 19.07 (2009), pp. 1065–1097.

[89] M. Munteanu, L. F. Pavarino, and S. Scacchi. "A scalable Newton–Krylov–Schwarz method for the Bidomain reaction-diffusion system". In: *SIAM Journal on Scientific Computing* 31.5 (2009), pp. 3861–3883.

[90] M. Murillo and X.-C. Cai. "A fully implicit parallel algorithm for simulating the non-linear electrical activity of the heart". In: *Numerical linear algebra with applications* 11.2-3 (2004), pp. 261–277.

[91] S. A. Niederer, J. Lumens, and N. A. Trayanova. "Computational models in cardiology". In: *Nature Reviews Cardiology* 16.2 (2019), pp. 100–111.

[92]   D. Nordsletten et al. "Coupling multi-physics models to cardiac mechanics". In: *Progress in biophysics and molecular biology* 104.1-3 (2011), pp. 77–88.

[93]   D.-S. Oh et al. "BDDC algorithms with deluxe scaling and adaptive selection of primal constraints for Raviart-Thomas vector fields". In: *Mathematics of Computation* 87.310 (2018), pp. 659–692.

[94]   A. V. Panfilov. "Spiral breakup as a model of ventricular fibrillation". In: *Chaos: An Interdisciplinary Journal of Nonlinear Science* 8.1 (1998), pp. 57–64.

[95]   L. F. Pavarino, S. Scacchi, and S. Zampini. "Newton–Krylov-BDDC solvers for nonlinear cardiac mechanics". In: *Computer Methods in Applied Mechanics and Engineering* 295 (2015), pp. 562–580.

[96]   L. F. Pavarino and S. Scacchi. "Multilevel additive Schwarz preconditioners for the Bidomain reaction-diffusion system". In: *SIAM Journal on Scientific Computing* 31.1 (2008), pp. 420–443.

[97]   J. Peng et al. "An adaptive BDDC preconditioner for advection-diffusion problems with a stabilized finite element discretization". In: *Applied Numerical Mathematics* 165 (2021), pp. 184–197.

[98]   M. Pennacchio, G. Savaré, and P. Colli Franzone. "Multiscale modeling for the bioelectric activity of the heart". In: *SIAM Journal on Mathematical Analysis* 37.4 (2005), pp. 1333–1370.

[99]   S. Pezzuto, J. Hake, and J. Sundnes. "Space-discretization error analysis and stabilization schemes for conduction velocity in cardiac electrophysiology". In: *International journal for numerical methods in biomedical engineering* 32.10 (2016), e02762.

[100]   S. Pezzuto et al. "Evaluation of a rapid anisotropic model for ECG simulation". In: *Frontiers in physiology* 8 (2017), p. 265.

[101]   M. Potse et al. "A comparison of monodomain and bidomain reaction-diffusion models for action potential propagation in the human heart". In: *IEEE Transactions on Biomedical Engineering* 53.12 (2006), pp. 2425–2435.

[102]   A. Quarteroni, A. Manzoni, and C. Vergara. "The cardiovascular system: mathematical modelling, numerical algorithms and clinical applications". In: *Acta Numerica* 26 (2017), pp. 365–590.

[103]   A. Quarteroni et al. "Integrated Heart—Coupling multiscale and multiphysics models for the simulation of the cardiac function". In: *Computer Methods in Applied Mechanics and Engineering* 314 (2017), pp. 345–407.

[104]   O. Rheinbach. "Parallel scalable iterative substructuring: Robust exact and inexact FETI-DP methods with applications to elasticity [PhD thesis]". In: *Essen (Germany): University of Duisburg-Essen, Essen* (2006).

[105]   J. M. Rogers and A. D. McCulloch. "A collocation-Galerkin finite element model of cardiac action potential propagation". In: *IEEE Transactions on Biomedical Engineering* 41.8 (1994), pp. 743–757.

[106]   Y. Saad and M. H. Schultz. "GMRES: A generalized minimal residual algorithm for solving nonsymmetric linear systems". In: *SIAM Journal on scientific and statistical computing* 7.3 (1986), pp. 856–869.

[107]   S. Sanfelici. "Convergence of the Galerkin approximation of a degenerate evolution problem in electrocardiology". In: *Numerical Methods for Partial Differential Equations: An International Journal* 18.2 (2002), pp. 218–240.

[108]   S. Scacchi. "A hybrid multilevel Schwarz method for the bidomain model". In: *Computer Methods in Applied Mechanics and Engineering* 197.45-48 (2008), pp. 4051–4061.

[109]   S. Scacchi. "A multilevel hybrid Newton–Krylov–Schwarz method for the bidomain model of electrocardiology". In: *Computer methods in applied mechanics and engineering* 200.5-8 (2011), pp. 717–725.

[110] B. F. Smith, P. E. Bjorstad, and W. Gropp. *Domain Decomposition: parallel multilevel methods for elliptic partial differential equations*. Cambridge University Press, 2004.

[111] J. Sundnes, G. T. Lines, and A. Tveito. "An operator splitting method for solving the bidomain equations coupled to a volume conductor model for the torso". In: *Mathematical biosciences* 194.2 (2005), pp. 233–248.

[112] J. Sundnes et al. *Computing the electrical activity in the heart*. Vol. 1. Springer Science & Business Media, 2007.

[113] T. T. P. Team. *The Trilinos Project Website*. 2020 (acccessed May 22, 2020). URL: https://trilinos.github.io.

[114] K. Ten Tusscher et al. "A model for human ventricular tissue". In: *American Journal of Physiology-Heart and Circulatory Physiology* 286.4 (2004), H1573–H1589.

[115] K. H. Ten Tusscher and A. V. Panfilov. "Alternans and spiral breakup in a human ventricular tissue model". In: *American Journal of Physiology-Heart and Circulatory Physiology* 291.3 (2006), H1088–H1100.

[116] A. Toselli and O. B. Widlund. "Domain decomposition methods-algorithms and theory". In: *Mathematical Models and Methods in Applied Sciences* 34 (2006).

[117] N. A. Trayanova. "Whole-heart modeling: applications to cardiac electrophysiology and electromechanics". In: *Circulation research* 108.1 (2011), pp. 113–128.

[118] N. A. Trayanova and J. J. Rice. "Cardiac electromechanical models: from cell to organ". In: *Frontiers in physiology* 2 (2011), p. 43.

[119] M. L. Trew et al. "A finite volume method for modeling discontinuous electrical activation in cardiac tissue". In: *Annals of biomedical engineering* 33.5 (2005), pp. 590–602.

[120] M. L. Trew et al. "A generalized finite difference method for modeling cardiac electrical activation on arbitrary, irregular computational meshes". In: *Mathematical biosciences* 198.2 (2005), pp. 169–189.

[121] X. Tu and J. Li. "A balancing domain decomposition method by constraints for advection-diffusion problems". In: *Communications in Applied Mathematics and Computational Science* 3.1 (2008), pp. 25–60.

[122] X. Tu and J. Li. "BDDC for Nonsymmetric positive definite and symmetric indefinite problems". In: *Domain Decomposition Methods in Science and Engineering XVIII*. Springer, 2009, pp. 75–86.

[123] X. Tu and J. Zhang. "BDDC Algorithms for Advection-diffusion problems with HDG Discretizations". In: *arXiv preprint arXiv:2103.09296* (2021).

[124] M. Veneroni. "Reaction–diffusion systems for the macroscopic bidomain model of the cardiac electric field". In: *Nonlinear Analysis: Real World Applications* 10.2 (2009), pp. 849–868.

[125] K. P. Vincent et al. "High-order finite element methods for cardiac monodomain simulations". In: *Frontiers in physiology* 6 (2015), p. 217.

[126] H. Yang, E. E. Prudencio, and X.-C. Cai. "Fully implicit Lagrange–Newton–Krylov–Schwarz algorithms for boundary control of unsteady incompressible flows". In: *International journal for numerical methods in engineering* 91.6 (2012), pp. 644–665.

[127] S. Zampini. "Dual-primal methods for the cardiac bidomain model". In: *Mathematical Models and Methods in Applied Sciences* 24.04 (2014), pp. 667–696.

[128] S. Zampini. "Inexact BDDC methods for the cardiac bidomain model". In: *Domain decomposition methods in science and engineering XXI*. Springer, 2014, pp. 247–255.